
Mobility and distribution of proteins in the nucleus of living cells

Robert M. Martin

**Dissertation
der Fakultät für Biologie
der Ludwig-Maximilians-Universität München**

vorgelegt am 14. August 2008

Mobility and distribution of proteins in the nucleus of living cells

Dissertation der Fakultät für Biologie

der Ludwig-Maximilians-Universität München (LMU)

vorgelegt von

Dipl.-Biol. Robert M. Martin

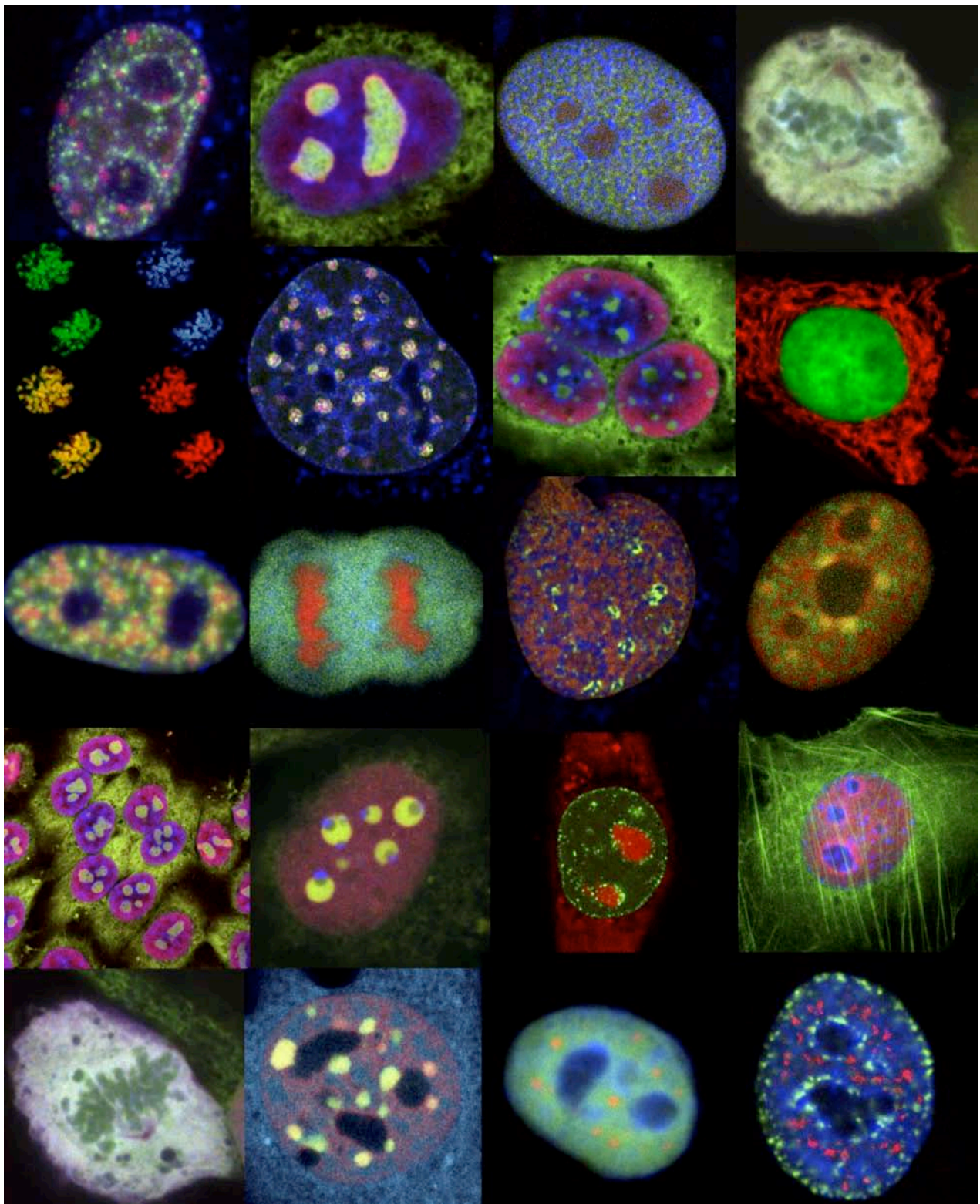
Erstgutachter: Prof Dr. Heinrich Leonhardt

Zweitgutachter: Prof. Dr. Harry MacWilliams

Tag der mündlichen Prüfung: 13.03.2009

"What gets us into trouble
is not what we don't know.
Is what we know for sure
that just ain't so"

Mark Twain



Collection of delightful confocal microscopy images

Content	I
Summary	II
Zusammenfassung	III
1 Introduction	1
1.1 Dynamic organization of nuclear structure and function	1
1.2 The molecular organization of chromatin in the cell nucleus	3
1.3 The role of epigenetic information in the formation of functional chromatin	5
1.4 Chromatin condensation	7
1.5 Nuclear bodies and nucleoplasmic proteins	11
1.6 The nucleolus	13
1.7 The consequences of the dynamic architecture of nuclear structures	14
1.8 The dynamic behavior of molecules in the cell nucleus	15
2 Questions and aims of the thesis	18
3 Results	19
3.1 DNA labeling in living cells	19
3.2 Nucleolar marker for living cells	28
3.3 Cargo-dependent mode of uptake and bioavailability of TAT-containing proteins and peptides in living cells	39
3.4 Live-cell analysis of cell penetration ability and toxicity of oligo-arginines	50
3.5 An unexpected link between energy metabolism, calcium, chromatin condensation and cell cycle	60
3.6 Chromatin condensation modulates access and binding of nuclear proteins	66
3.7 Probing intranuclear environments at the single-molecule level	88
4 Discussion and Outlook	108
4.1 The labeling of nuclear substructures in living cells	108
4.2 Delivery of macromolecules by cell penetrating peptides in live cells	110
4.3 Mechanisms and effects of chromatin condensation	113
4.4 Accessibility of chromatin in living cell nuclei	114
4.5 The effect of chromatin condensation on DNA metabolism	115
4.6 Dynamics of protein movement in the nucleus of living cells	117
4.7 The dynamics of single molecules in the nuclear interior	118
4.8 Compartmentalized microenvironments provide an additional regulation level for the nuclear metabolism	121
4.9 Outlook	122
5 Literature	124
6 Annex	136
6.1 Abbreviations	136
6.2 Publications	137
6.3 Conference contributions	138
6.4 Acknowledgments and declaration of own contributions	139
6.5 Curriculum Vitæ	143
7 Index of electronic supplementary material CD	144

Summary

The study of the structure and function of the cell nucleus has revealed a highly organized organelle that stores genetic information and in which the DNA metabolism takes place. The nuclear interior is formed by a closed membrane system that divides the nucleoplasm from the cytoplasm. Although there are no separating membranes inside, the nucleus shows a manifold compartmentalization related to different functions in nucleic acid metabolism and structural maintenance. The research of the last decade has brought great improvements in the understanding of nuclear structure and function. Yet little is known about the molecular mechanisms that establish nuclear substructures and microenvironments as well as the consequences of the compartmentalization on the nuclear metabolism of nucleic acids and proteins. In this thesis I have investigated the question of how macromolecules move through the nuclear interior and what are the effects of the nuclear subcompartments on their mobility and distribution. Specifically, I focused on analyzing the access of assorted polypeptides to different chromatin domains and subnuclear compartments. These investigations should give insight into the basic principles determining the association of proteins to functional compartments within the nucleus.

This project can be divided into three distinct parts. First, different fluorescent markers to visualize nuclear structures in living cells were generated and evaluated, including a peptide based nucleolar marker and the DNA dye DRAQ5. Secondly, techniques to deliver molecules into living cell nuclei by means of cell penetrating peptides have been developed and tested. This approach was combined with the basic principles of specific targeting of bioactive molecules to subnuclear compartments, where they exert a biological function. The *in vivo* labeling of nuclear structures was combined with imaging of fluorescently tagged proteins of increasing sizes and different charge. By inducing changes in chromatin condensation it was possible to directly determine the effect of nuclear structure changes on the protein distribution in single cells. The data acquisition was done in living cells using high resolution confocal fluorescence microscopy or very fast and sensitive detection of single molecules. Finally, image analysis was performed and combined with statistical methods to quantitatively determine molecule distributions and relate this information to different nuclear structures.

My results demonstrate that single nucleoplasmic proteins move rapidly in the nuclear interior and also in nuclear substructures. The protein movement is interrupted by short time trapping of proteins in nuclear substructures. Considering chromatin, the condensation level in respect to the cell cycle and after induced changes has a profound influence on the distribution of nuclear non chromatin proteins as well as on the mobility of chromatin bound proteins. In the mass dense nucleoli, proteins lacking specific localization signals are mostly excluded and their mobility in this compartment is characterized by reduced trapping and a fast transit. Unlike this small basic peptides with a positive charge show an accumulation in the nucleolus.

In summary, the structural framework, microenvironments and density of nuclear subcompartments have a dramatic influence on the distribution and mobility of molecules with different charges. The results elucidate basic principles and consequences of the functional nuclear organization.

Zusammenfassung

Die Erforschung der Struktur und Funktion des Zellkerns enthüllte eine hochorganisierte Zellorganelle, in welcher die genetische Information gespeichert wird und der DNS-Stoffwechsel stattfindet. Der Zellkern entsteht durch ein geschlossenes Membransystem, wodurch das Zellkernplasma vom Cytoplasma abgegrenzt wird. Obwohl sich im Inneren des Zellkerns keine weiteren abgrenzenden Membranen befinden, ist eine vielfältige Unterteilung vorhanden, die im Zusammenhang mit den verschiedenen Aufgaben im DNS-Stoffwechsel und der Aufrechterhaltung der Struktur steht. Die Forschung in der letzten Dekade erzielte große Fortschritte hinsichtlich des Verständnisses der Struktur und Funktion des Zellkerns. Doch ist noch wenig darüber bekannt, welche molekularen Mechanismen zum Aufbau von Zellkernstrukturen und Mikro-Umgebungen führen, und welchen Einfluss die Organisation des Zellkerns auf den Stoffwechsel von Nukleinsäuren und Proteinen hat. In dieser Arbeit bin ich der Fragestellung nachgegangen, wie Makromoleküle sich im Inneren des Zellkerns bewegen und welchen Einfluss die Organisation des Zellkerns auf deren Bewegung und Verteilung hat. Speziell wurde untersucht, ob und in welcher Weise ausgesuchte Poly-Peptide Zugang zu verschiedenen Chromatin-Domänen und Kompartimenten des Zellkerns haben. Die hier gezeigten Untersuchungen geben Einblick in grundlegende Prinzipien, welche die Assoziation von Proteinen mit funktionellen Strukturen des Zellkerns bestimmen.

Diese Arbeit kann in drei Unterteile gegliedert werden. Erstens wurden verschiedene fluoreszierende Markierungen für Zellkernstrukturen in lebenden Zellen hergestellt beziehungsweise charakterisiert, einschließlich einer auf Peptiden basierenden Markierung des Nukleolus und des DNA-Farbstoffes DRAQ5. Zweitens wurden Techniken entwickelt und getestet, um Moleküle mit Hilfe von membranpenetrierenden Peptiden in die Kerne von lebenden Zellen einzubringen. Das Verfahren wurde kombiniert mit den grundlegenden Prinzipien der Lokalisierung biologisch aktiver Moleküle in Zellkernstrukturen, um eine biologische Funktion zu bewirken. Anschließend wurde das *in vivo* Markieren von Zellkernstrukturen kombiniert mit dem Abbilden von fluoreszenzmarkierten Proteinen, welche unterschiedliche Größen und Ladungen besitzen. Durch die induzierte Veränderung der Chromatinkondensierung war es möglich, den direkten Einfluss von Änderungen in der Struktur des Zellkerns auf die Verteilung von Proteinen in einzelnen Zellen zu bestimmen. Die Datenaufnahme erfolgte dabei in lebenden Zellen mit Hilfe hochauflösender konfokaler Fluoreszenz-Mikroskopie oder mit sehr schneller und empfindlicher Erfassung einzelner Moleküle. Letztendlich wurde die Bildanalyse mit statistischen Methoden kombiniert, um die Verteilung der Moleküle quantitativ zu bestimmen und diese Informationen mit den verschiedenen Strukturen im Zellkern in Verbindung zu bringen.

Die hier präsentierten Ergebnisse zeigen, dass einzelne Proteine sich sehr schnell im Zellkernplasma und in den Zellkernstrukturen bewegen. Die Proteinbewegungen sind durch kurzzeitiges Verweilen und Festsetzen in Kernstrukturen unterbrochen. Berücksichtigt man das Chromatin, so hat der Grad der Kondensierung in Abhängigkeit vom Zellzyklus und nach induzierten Änderungen einen enormen Einfluss sowohl auf die Verteilung der Proteine, die nicht an Chromatin gebunden sind, als auch auf die Mobilität chromatin-gebundener Proteine. Von den massereichen Nukleoli sind Proteine ohne ein spezielles Lokalisierungssignal weitgehend ausgeschlossen und die Bewegung dort ist bestimmt durch kürzere Verweildauer und ein schnelles Hindurchbewegen. Im Gegensatz dazu sind in den Nukleoli kurze basische Peptide mit einer positiven Ladung angereichert.

Zusammenfassend kann festgestellt werden, dass das strukturelle Grundgerüst, Mikro-Umgebungen und die Dichte von Kernstrukturen einen starken Einfluss auf die Verteilung und Bewegung von Molekülen mit verschiedenen Ladungen haben. Die Ergebnisse zeigen einige grundlegende Prinzipien und Auswirkungen der funktionellen Organisation im Zellkern.

1 Introduction

1.1 Dynamic organization of nuclear structure and function

The cell is defined as an aqueous plasma separated from the environment by a lipid membrane that regulates the flow and exchange of molecules between the cytoplasm and the surrounding system. Functional substructures inside the cytoplasm are often surrounded and protected by membranes to maintain and regulate spatially separated biochemical processes e.g. mitochondria, vesicles and all vesicle derived organelles including the nucleus, endoplasmatic reticulum (ER), Golgi, lysosomes and peroxisomes.

The eukaryotic nucleus is the organelle, that contains the genetic and epigenetic information of the cell. It is the space enclosed by a double membrane system continuously connected to the endoplasmatic reticulum (Fig. 1) (Ellenberg et al., 1997; Anderson and Hetzer, 2007). In somatic cells the nucleus has usually a diameter of 2 – 10 µm with a disc like to spherical shape. Nuclear pores formed by megadalton protein complexes span the double membrane layer and enable molecule exchange with the cytoplasm (Davis, 1995; Cronshaw et al., 2002). With the help of specialized import proteins, the nuclear pores selectively regulate the concentration of proteins with a molecular weight (MW) higher than about 60 kDa (Cronshaw et al., 2002; Paschal, 2002; Stoffler et al., 2003). Although no membrane structures have been found inside the cell nucleus, its interior is characterized by highly organized subcompartments that are involved in different aspects of nucleic acid and protein metabolism (Fig. 1, 2, 3 and 4) (Cremer et al., 2000; Dunder and Misteli, 2001). Nevertheless there is a regulated crosstalk and exchange components between the nuclear substructures (Sleeman et al., 1998; Belmont, 2003). In the last decades numerous studies have identified and analyzed the molecular structure, content, function and interactions of nuclear substructures (Spector, 2001; Spector, 2006). A schematic drawing of known aspects of the steady state nuclear organization is depicted in Fig. 1.

Chromatin is the major molecular structure of the cell nucleus and is organized into chromosomes. In interphase nuclei, decondensed chromosomes occupy distinct territories and their positioning correlates with size and gene density (Tanabe et al., 2002; Mayer et al., 2005; Cremer et al., 2006). The

interchromatin space describes nuclear regions devoid of chromatin, that are often occupied by nuclear bodies like splicing speckles, cajal and promyelocytic leukemia (PML) bodies (Cremer et al., 2000; Ogg and Lamond, 2002). These nuclear bodies are accumulations of different proteins with regulatory or enzymatic function that take part in the nucleic acid metabolism (Sutherland et al., 2001). The nucleolus, the site of ribosome biogenesis, is in most cases the largest visible nuclear substructure and is often surrounded by dense chromatin (Fig. 1 and 4) (Perry, 1962; Scheer and Hock, 1999; Lam et al., 2005). The molecular organization of chromatin and nuclear bodies is discussed in more detail in the following section.

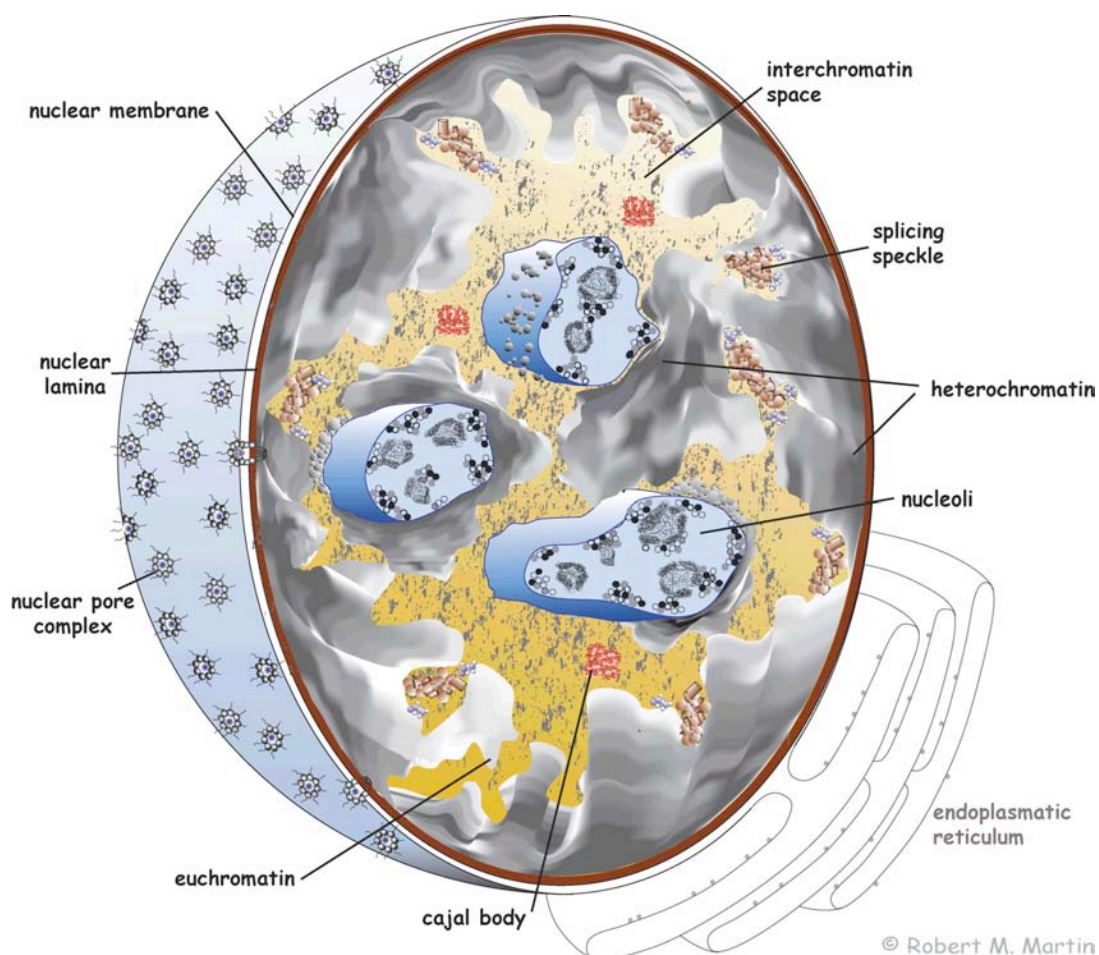


Figure 1: Law and order in the cell nucleus. The eukaryotic cell nucleus is a highly compartmentalized cell organelle. Despite the lack of separating membranes inside, a variety of subnuclear compartments, nuclear bodies and chromatin domains can be identified. The different structures are characterized by their composition of specific proteins and nucleic acids, which are involved in distinct steps and pathways of the nuclear metabolism.

1.2 The molecular organization of chromatin in the cell nucleus

The genetic information in e.g. human cells is stored within the DNA double helix consisting of $\sim 3 \times 10^9$ base pairs forming a triplet code. Additional epigenetic information regulating the expression of the genetic information is encoded in the complex assembly of chromatin including DNA, protein modifications and the formation of higher order structures. Chromatin is described as a chain like macromolecule made of connected subunits, which adopt different spacings and form higher order structures (Bednar et al., 1998; Sadoni et al., 2001). In eukaryotic cells the DNA is wrapped around histone octamers to form the nucleosomal fiber as the basic chromatin structure, illustrated in Fig. 2 (Luger et al., 1997). The nucleosomal histones H2A, H2B, H3 and H4 are assembled by chromatin chaperones like the chromatin assembly factor (CAF1) and can form 11 nm fibers already by incubation with naked DNA *in vitro* (Verreault et al., 1996; Okuwaki et al., 2005). The organization of nucleosomes as building blocks into higher order structures involves additional chromatin proteins interacting with the DNA and histones (Bednar et al., 1998). A more compact structural organization is achieved by the binding of histone H1, which leads to the formation of 30 – 40 nm sized fibers of closely packed nucleosomes arranged possibly in a zig-zag pattern (Fig. 2) (Karymov et al., 2001; Dorigo et al., 2004; Robinson et al., 2006). Subsequent level of DNA and chromatin fiber organization were suggested to involve matrix elements e.g. nuclear lamina with the formation of loops or rosette like structures (Ascoli et al., 1988; Heng et al., 2004). However, the proposed fibers of 30 nm or larger in diameter could not yet been observed in living cells (Rydberg et al., 1998; Tremethick, 2007). Finally the loops of chromatin are organized in structurally and functionally distinct chromatin domains and chromosome territories (Cremer and Cremer, 2001). Chromatin is classified according to its condensation status, metabolic activity and molecular composition as eu- and heterochromatin. Euchromatin has a decondensed open structure and is transcriptionally active (Fig. 2) (Woodcock and Dimitrov, 2001). In contrast, heterochromatin is highly condensed similar to mitotic chromosomes and transcriptionally inactive (Fig. 2) (Dillon, 2004; Dimitri et al., 2005).

- 4 -

1.3 The role of epigenetic information in the formation of functional chromatin

The eu- or heterochromatin properties of genome subsets are on a basic level defined by chemical modifications on chromatin that represent epigenetic information (Bird, 2007). These chromatin modifications include methylation of DNA at cytosines (5mC) and histone tails, which can be also acetylated, phosphorylated, ubiquitylated and sumoylated (Fig. 2) (Kouzarides, 2007). Beside this, epigenetics involves histone variants, remodeled nucleosome structures and non coding RNAs (Corona et al., 1999; Gilbert et al., 2000; Chow et al., 2005).

Euchromatin is linked to the hyperacetylation of specific lysines of histone H3 at lysine 14 or histone H4 at lysine 20 (H3K14ac / H4K20ac) (Marvin et al., 1990). The acidic charge of an acetyl group neutralizes the basic charge of the histone lysines and weakens the electrostatic binding of the DNA to histones (Higashi et al., 2007; Shahbazian and Grunstein, 2007). This results in a more open nucleosome conformation, which allows the access and assembly of the transcriptional machinery (Fig. 2). Furthermore, euchromatic nucleosomes are methylated at H3K4, K36 and K79, phosphorylated at H3S10 and additionally ubiquitylated at H2BK123 (Richards and Elgin, 2002). Transcription factors, chromatin modifying and remodeling proteins interact with these histone modifications. Once bound, they allow transcription or mediate the modification or replacement of neighboring nucleosomes to maintain the active chromatin status (Fig. 2) (McKittrick et al., 2004; Mito et al., 2007; Henikoff, 2008).

Heterochromatin was first described almost a century ago according to the condensation level reflected by the staining intensity in transmission light microscopy (Heitz, 1928; Heitz, 1929). The modern molecular definitions of heterochromatin show that it contains DNA enriched in cytosine methylation at CpG sequences, introduced by DNA methyltransferases dependent or independent of replication (Fig. 2) (Bird, 1986; Leonhardt et al., 1992; Easwaran et al., 2004; Smallwood et al., 2007). Methylated DNA is closely correlated with transcriptionally inactive, silenced or non-coding chromatin (Boyes and Bird, 1992; Ohtani-Fujita et al., 1993; Pikaart et al., 1998), and has been shown to be directly linked to histone deacetylation and heterochromatin

specific histone methylation (Fuks et al., 2000; Gregory et al., 2001; Xin et al., 2003). Symmetrically methylated CpG sequences are recognized and bound by proteins containing a **methyl cytosine binding domain** (MBD) (Lewis and Bird, 1991; Boyes and Bird, 1991; Nan et al., 1996). The proteins that bind to methylated DNA like the **methyl cytosine binding protein 2** (MeCP2) themselves act as transcriptional repressors. They further recruit enzymes that introduce modifications on neighboring histones, e.g. histone deacetylase and histone methyl transferase (Fig. 2) (Boyes and Bird, 1991; Nan et al., 1997; Nan et al., 1998; Yu et al., 2000; Fujita et al., 2003). The removal of acidic charge from histones increases their basic charge and results in a closed nucleosome conformation with strong binding to DNA via charge driven interactions. The epigenetic marks of heterochromatic nucleosomes are hypoacetylation of histones, methylation of histone H3 K9/K27 and H4K20 as well as sumoylation of H2A, H2B, H4 and ubiquitylation of H2AK119 (Kouzarides, 2007).

A large number of proteins bind to chromatin modifications and their combined action, interaction and cooperation results in chromatin subsets with different condensation level and eu- or heterochromatin character, illustrated in Fig. 2 (Gilbert et al., 2005; Schneider and Grosschedl, 2007; Taverna et al., 2007). The epigenetic states of the chromatin domains are transmitted to daughter cells in mitosis by the segregation of the sister chromatids. On the DNA level the 5mC modifications are inherited by the methylation of the newly synthesized DNA strands during replication in S-phase by the DNA methyltransferase Dnmt1 (Stein et al., 1982; Leonhardt et al., 1992). Subsequently following replication, the nucleosomes of the parental DNA molecule, that contain already modifications, are redistributed to both DNA daughter strands also involving the CAF1 histone assembly complex (Verreault et al., 1996; Taddei et al., 1999; Zhang et al., 2000). For newly incorporated histones, lacking specific modifications, a copy mechanism introduces similar modifications on neighboring nucleosomes. This mechanism can involve members of the **heterochromatin protein** (HP1) family, which bind to present H3K9me3 and recruit the histone methyl transferase Suvar 39h (Suv39h) that introduces the same modification on adjacent nucleosomes (Felsenfeld and

Groudine, 2003; Schotta et al., 2004). Similarly, Suvar 4-20h (Suv4-20h) is recruited and trimethylates H4K20 as an important heterochromatin specific histone modification (Schotta et al., 2004). By this mechanism specific chromatin modifications are self-amplified in adjacent chromatin, but can also spread into neighboring chromatin domains and establish heterochromatin formation. Insulator DNA sequence elements restrict this spreading of histone modifications between chromatin regions by blocking the interactions of chromatin modifying factors with each other and the chromatin (Pikaart et al., 1998; Felsenfeld and Groudine, 2003). Furthermore, the Suv39h mediated histone H3K9 methylation can also direct the methylation of DNA and thus target the respective genomic sequence for a stable inheritable imprinting and heterochromatin formation (Lehnertz et al., 2003). Independent of replication there are further mechanisms of assembling variant histones into nucleosomes to initially mark or maintain the epigenetic state of chromatin domains (Henikoff and Ahmad, 2005).

The change of epigenetic modifications on the DNA and nucleosome level results in structural changes, that are linked to alterations in the chromatin condensation level and transcriptional activity (Rice and Futscher, 2000; Nguyen et al., 2001). This can be the result of cell signaling or treatments with drugs inhibiting chromatin modifying enzymes and change chromatin structures and condensation (Yu, 1993; Görisch et al., 2005; Lopez-Larrazza et al., 2006).

In summary, two closely connected properties characterize the organization of DNA and proteins into chromatin: On the one hand chromatin organization involves the distribution of structural elements that form chromatin domains with different condensation level. On the other hand the establishing and maintenance of the metabolic status in a genetic region is based on the interaction of nuclear factors on chromatin. These associations are regulated to a large degree by chromatin modifications.

1.4 Chromatin condensation

As a result of the epigenetic modifications coupled to the genetic program throughout development and differentiation, the chromatin is organized into

subsets of different compaction level. Chromatin condensation starts with the aggregation of nucleosomes and the reduction of interleaving space between them, illustrated in Fig. 2 (Hammermann et al., 2000; Dorigo et al., 2004).

In heterochromatin for example, transcriptional repressors, which bind to regulatory genetic elements in the chromatin fiber, recruit enzymes that deacetylate histone tails and promote closer nucleosome stacking (Robertson et al., 2000; Terranova et al., 2005). In addition, MBD proteins like MeCP2 and polycomb group proteins can induce the formation of irregular condensed nucleosomal arrays (Georgel et al., 2003; Francis et al., 2004). Together with the formation of fibers from regularly stacked nucleosomes mentioned in section 1.3, the aggregation of complex condensed chromatin cluster can take place, although no structure has been described so far. One example for the clustering and formation of condensed chromatin domains is the pericentromeric heterochromatin in mouse cells. This specialized type of constitutive heterochromatin comprises of a 6-17 Mbp genetic region adjacent to the centromeres (Joseph et al., 1989; Garagna et al., 2002). These so called chromocenters consist of repeats of a highly 5mC enriched 234 bp major satellite sequence (Miller et al., 1974; Mitchell, 1996). Hence these chromocenters are target sites for proteins that bind to 5mC like MeCP2, MBD1, 2 and 4, which have been found to accumulate at these chromatin domains (Lewis et al., 1992; Hendrich and Bird, 1998). Furthermore the pericentromeric chromatin includes the histone modifications characteristic for heterochromatin like H3K9me₃, H3K27me₃ and H4K20me₃ and a lack of euchromatin linked modifications like methylation at H3K4 and acetylation of H4 (Peters et al., 2003; Kourmouli et al., 2004; Maison and Almouzni, 2004; Schotta et al., 2004). Accordingly, proteins that bind to these modifications can be found in the chromocenters like HP1 α and HP1 β (Maison et al., 2002; Kourmouli et al., 2005). Following this the proteins interacting with HP1 can also be associated with pericentromeric heterochromatin such as the histone methyltransferase Suv39h or the lamin B receptor (Singh and Georgatos, 2002). In mouse cells the pericentromeric heterochromatin forms round condensed chromatin domains often located at the nuclear periphery or in the perinucleolar region and has important functions in chromosome segregation

and thus genome stability (Peters et al., 2001; Taddei et al., 2001). Furthermore there are implications for a role in genetic silencing in cases of spatial gene proximity to chromocenters (Brown et al., 1997). In addition to the formation of condensed nucleosomal arrays, it has been shown that MeCP2 can induce the large scale aggregation of chromocenters during myogenic differentiation. This leads to the formation of only a few big clusters consisting of several individual pericentromeric heterochromatin domains from different chromosomes (Brero et al., 2005).

The complex interactions of chromatin binding factors with each other, the nucleosomes and structural elements in a regulatory network, specific for DNA sequences and chromatin modifications, promote, mediate and induce chromatin condensation (Fig. 2). On a larger scale, chromatin condensation results in the formation of heterochromatin compartments, mitotic chromosomes or apoptotic chromatin by the aggregation of chromatin domains (Dillon, 2004; Lu et al., 2005; Mozziconacci et al., 2006). The formation of different chromatin substructures directly influences the functional compartmentalization of the cell nucleus.

In cycling cells the chromatin undergoes regularly a global conformation and condensation change in mitosis by the formation of condensed chromosomes (Fig. 3) (Belmont, 2006). The molecular events of the formation of condensed chromosomes are driven by the complex regulatory network governing the cell cycle via the function of cyclin dependent kinases and cyclins (Maldonado-Codina and Glover, 1992).

Several processes including histone phosphorylation and the incorporation of histone variants like the different **centromere proteins** (CENP) are crucial for the complete condensation of chromatin into compact chromosomes (Crosio et al., 2002; Maddox et al., 2006). The formation of the mitotic chromosomes involves protein complexes for anchoring and compacting the chromatin (Hirano et al., 1997; Collas et al., 1999; Kimura et al., 1999). The actual condensation process is a result of folding of large scale chromatin fibers along a axial scaffold (Kireeva et al., 2004). Concomitantly the DNA metabolism like transcription is stopped during the existence of condensed chromosomes in mitosis (Johnson and Holland, 1965; Weisenberger and

Scheer, 1995; Gottesfeld and Forbes, 1997). DNA replication and repair has to be finished before the entry into mitosis is permitted (Roberge, 1992; Weinert et al., 1994). Interestingly, during mitotic chromosome compaction not only transcription factors are displaced from chromatin, but also proteins building functional interphase heterochromatin like HP1 are at least partially released (Martinez-Balbas et al., 1995; Hirota et al., 2005). The redistribution of proteins from mitotic chromatin results from altered binding kinetics by phosphorylation of the target structure, e.g. histones by Aurora B kinase, or the binding protein, e.g. **high-mobility group nucleosome binding proteins** (HMGN proteins) (Segil et al., 1991; Prymakowska-Bosak et al., 2001). The status of interphase transcription is transmitted through mitosis by specific histone modifications that mark active and silenced genomic regions. This suggests a *de novo* establishing of active and silent chromatin during chromosome decondensation by nucleosome binding factors. The different pathways of chromatin condensation for interphase heterochromatin and chromosomes in mitosis indicate a functional separation of the two types of condensed chromatin over the cell cycle. The condensation of chromatin structures is thought to have an effect on the reduction of DNA metabolism (Martinez-Balbas et al., 1995). With the beginning of interphase a partial genome decondensation takes place, where euchromatin correlates with decondensation and heterochromatin with structures remaining condensed (Fig. 3). With the formation of the nucleus and functional chromatin in early G1 the proteins involved in nucleic acid metabolism become relocated to the nucleus and bind to their respective interphase chromatin substrate (Dirks and Snaar, 1999).

It was also suggested that cellular ions may play a role in mitotic condensed chromatin with a function in maintaining the structural chromosome integrity (Strick et al., 2001). Further it is known that significant changes in the cellular ion concentration, especially calcium, have a drastic effect on chromatin structures and induce condensation (Jacobs et al., 1976; Hammermann et al., 2000). In living interphase cells a global chromatin condensation is induced by a hyperosmolar environment, which increases intracellular ion concentrations but is completely reversible (Albiez et al., 2006). In accordance with these

findings it is possible that the chromatin condensation that occurs in apoptotic or necrotic cells is connected to the effect described for hyperosmolarity due to the leakage of cellular membranes accompanying cell death.

1.5 Nuclear bodies and nucleoplasmic proteins

The distribution of nuclear proteins is influenced by their interactions with nuclear substructures and the components therein. The regulation of the enzymatic activity in a cell cycle dependent manner as well as the binding to specific target molecules, protein modification, storage and degradation lead to the accumulation in nuclear subcompartments. These sites of action in the different pathways of protein and nucleic acid metabolism can be visualized in fluorescence microscopy using proteins tagged with the **green fluorescent protein** (GFP) or immunofluorescence, often as focal accumulation sites. It has been shown that in the respective foci e.g. active transcription, replication or DNA repair takes place (Fig. 3) (Iborra et al., 1996; Cardoso et al., 1997; Mortusewicz et al., 2005). These represent dynamic structures that exhibit turnover and exchange of molecules with varying dynamics (Sporbert et al., 2002). In addition to being present at sites of focal concentration many proteins and particles are also temporarily or permanent diffusely distributed throughout the nucleoplasm (Fig. 3) (Politz et al., 1999; Shav-Tal et al., 2004). Multiple proteins also accumulate in the interchromatin space and form nuclear bodies such as splicing speckles, cajal and PML bodies. These nuclear bodies are often defined and named by the localization or accumulation of specific proteins e.g. coiled bodies and PML bodies contain the proteins coilin and PML, respectively. In addition, they contain numerous proteins for storage, modification and degradation and serve as processing site for nucleic acids (Lamond and Spector, 2003). The formation of nuclear bodies is the result of the different biochemical processes in the compartment and the interactions of the components, which leads to a concentration of specific proteins and nucleic acids. A fixed underlying structural network with e.g. a filamentous matrix that determines the nuclear structure and body formation is still a matter of debate but has not been shown in the nuclear interior (Hancock, 2000; Pederson, 2000).

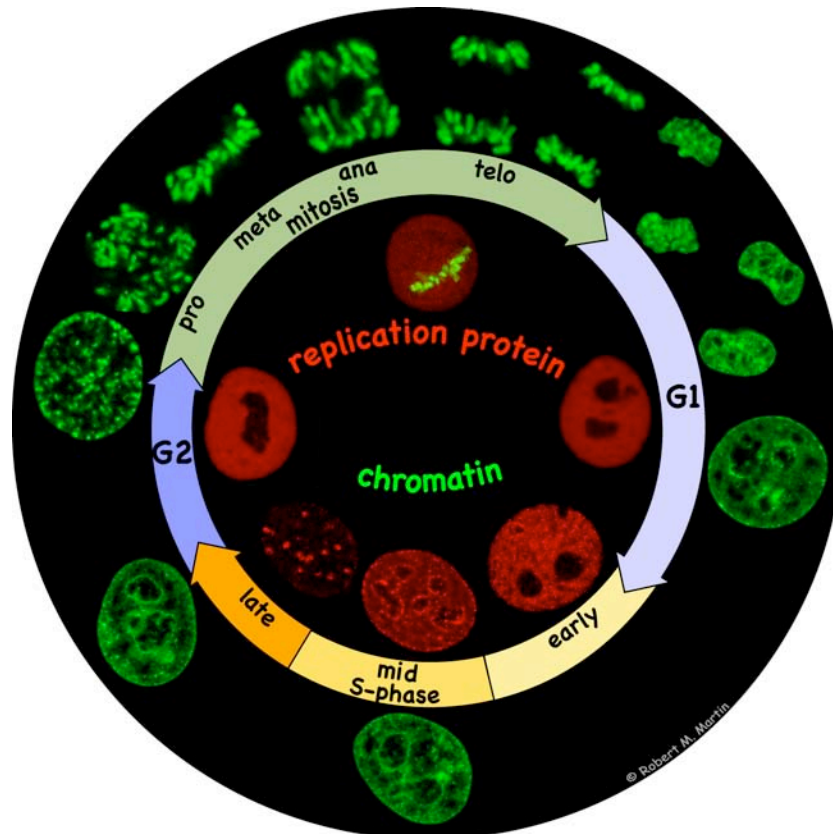


Figure 3: Cell cycle dependent reorganization of chromatin and proteins in the cell nucleus. The figure displays chromatin labeled by H2B-GFP (Kanda et al., 1998) and the fluorescent replication protein fusion mRFP-PCNA (Easwaran et al., 2004). The PCNA distribution changes from diffuse in G1 to a focal accumulation at replication sites with progressing patterns during S-phase in accordance with other replication proteins (Easwaran et al., 2005). The dark nuclear areas correspond to nucleoli, depleted from the replication protein. Chromatin in interphase nuclei is dispersed in the nucleus with dense heterochromatin at the periphery and around nucleoli with less dense euchromatin and interchromatin space in between. At the beginning of mitosis the chromatin forms condensed chromosomes for the mitotic division until the beginning of interphase.

Protein accumulation in the nucleus is dynamic and variable during cell cycle, differentiation and in disease (Fig. 3) (Belmont, 2003; Eskiw et al., 2003). Concurrent, metabolic changes in the cell and the nucleus are reflected in the localization, structure, content and function of these nuclear bodies (Shav-Tal et al., 2005). Furthermore nuclear bodies are not fixed structures and show diffusion like motion in the interchromatin space delineated by the surrounding chromatin. These results indicate an inert and rigid structure of the nuclear bodies and the capability of chromatin to create boundaries in the nuclear interior that influences the compartmentalization (Görisch et al., 2004). Though the dynamic nature of the components of nuclear bodies and the description of

speckles and cajal bodies as sponge like accessible structure suggests compartments open for entry and exit of proteins for a fast diffusive exchange of molecules (Handwerger et al., 2004; Handwerger and Gall, 2006).

1.6 The nucleolus

The nucleolus is often the most prominent nuclear substructure already visible by phase contrast microscopy (Fig. 4). It was first described in 1836 by G.G. Valentin and forms around the rDNA loci (Franke, 1988; Andersen et al., 2002). The nucleolus is the site of both ribosomal RNA transcription as well as assembly and maturation of the ribosomal subunits (Brown and Gurdon, 1964; Perry, 1962; Scheer and Hock, 1999; Raska et al., 2004). Nucleoli in mammals have a tripartite substructure identified in the electron microscope as **fibrillar centers (FC)** (Thiry, 1992), surrounded by a **dense fibrillar component (DFC)** collectively embedded in the **granular component (GC)** (Fig. 4) (Derenzini et al., 2006).

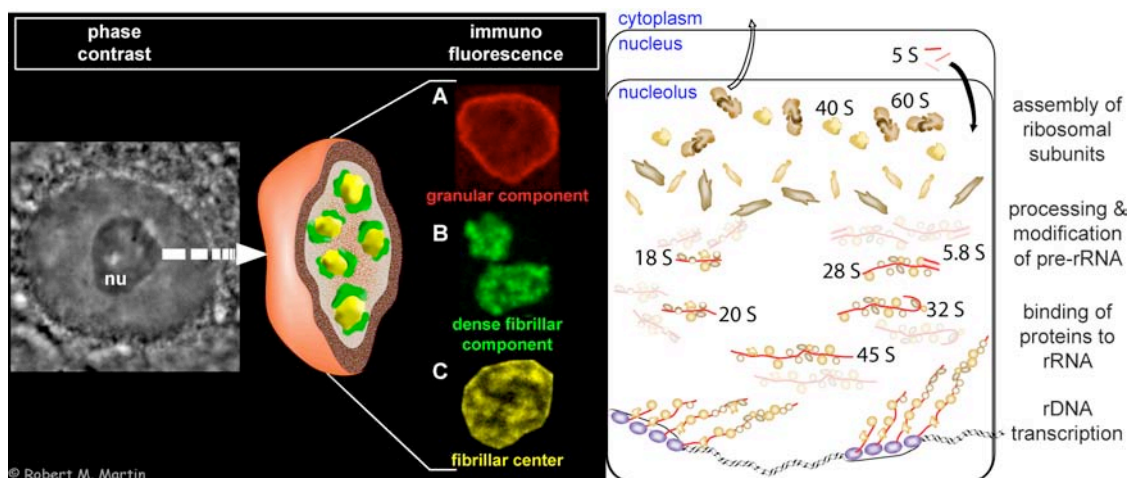


Figure 4: Structure and function of the nucleolus and the biogenesis of ribosomes. The phase contrast image shows the nucleolus (nu) as a large light dense region in the cell nucleus. The illustrated three dimensional nucleolar substructure depicts the spatial distribution of antigens and substructures of the nucleolus: A) immunofluorescence staining against nucleophosmin/B23 in the granular component B), immunofluorescence staining for fibrillarin in the dense fibrillar component and C) nucleolar DNA labeling in the fibrillar centers. A simplified model of the ribosome biogenesis is drawn in accordance to the nucleolar structure and function relationship.

The nucleolar structure is linked to the different steps of ribosome biogenesis starting with the transcription of rDNA genes in the periphery of the FC (Scheer et al., 1997; Mais and Scheer, 2001; Cheutin et al., 2002). The nascent rRNA

transcripts localize to the DFC, where they are modified and associated with nucleolar proteins to form hnRNP particles. Further processing occurs in the GC where pre-ribosomal RNA/protein particles develop into pre-ribosomal subunits ready to be transported into the cytoplasm, illustrated in Fig. 4 (Scheer and Hock, 1999). The metabolic activity of nucleoli is also reflected in their size and number (Hernandez-Verdun, 2006), and considerable progress has been made in the understanding of nucleolar functions and revealed e.g. a role in the regulation of stress response and cellular metabolism (Lyon et al., 1997; Mekhail et al., 2005). Furthermore, the establishment of high resolution imaging techniques like electron spectroscopic imaging (ESI) has helped to resolve the internal molecular structure of nucleoli in more detail (Politz et al., 2005). Also, the localization of proteins in the nucleoli can be explained by the discovery of nucleolar localization sequences often present in viral proteins (Dang and Lee, 1989; Hatanaka, 1990). However, little is known about the assembly of this structure in the cell nucleus or how it establishes its microenvironment (Carmo-Fonseca et al., 2000). Although the nucleolar structure seems to be accessible and nucleolar components are mobile, it remains unknown how numerous nuclear proteins are excluded from nucleoli and remain in the nucleoplasm (Politz et al., 2003; Handwerger et al., 2004).

1.7 The consequences of the dynamic architecture of nuclear structures

The organization of the cell nucleus into functional subcompartments and the genome organization into transcriptionally active and inactive subsets reflects the specific gene expression profiles of cells and tissues as well as their developmental and differentiation status (Regha et al., 2007). Furthermore it allows spatial separation of biochemical reactions of DNA, RNA and protein metabolism in nuclear substructures. The dynamic organization of global and local chromatin preserves the possibility to change epigenetic modifications, condensation level and transcriptional status of a genetic region (Peaston et al., 2007; Stern et al., 2007). This principle of the plasticity of the genome on a dynamic molecular basis seems to be preserved throughout development and differentiation, and gives rise to the idea of inducing specific changes in the gene expression profile of cells, tissues or organs.

The chromatin modifications influence the metabolic and structural status like the transcriptional activity, replication timing and condensation level via direct or indirect effects (Leonhardt et al., 2000; Alexandrova et al., 2003; Klose et al., 2006). Specific proteins recognize and bind epigenetic marks and interact with the modified histones, e.g. heterochromatin protein 1 (HP1) binds to H3K9me3 (Nielsen et al., 2002). The factors binding to histone and DNA modifications interact further with a complex regulatory machinery, which includes other chromatin proteins, chromatin remodeling proteins and transcription activating or repressing factors, involved in the nucleic acid metabolism (Muchardt et al., 2002; Fujita et al., 2003; Fischle et al., 2005; Agarwal et al., 2007; Smallwood et al., 2007). Upon external stimuli epigenetic marks on histones can be removed directly by enzymes like histone deacetylases and demethylases or alternatively by replacing whole nucleosomes (Sun et al., 1990; Gallinari et al., 2007; Wissmann et al., 2007). The integration of these different factors ultimately defines the functionality of chromatin, and determines how the genetic program is expressed in response to external stimuli and internal signaling. As such DNA and histone modifications as well as chromatin composition and structure is subjected to dramatic changes during development, differentiation, disease and cell death (Reik et al., 2001; Quina et al., 2006; Matarazzo et al., 2007). However it is not established how different chromatin condensation levels influence the distribution and access of nucleoplasmic proteins to chromatin and the direct effect on the nuclear compartmentalization and metabolism.

1.8 The dynamic behavior of molecules in the cell nucleus

The structural and functional nuclear compartmentalization also has an effect on the subnuclear distribution and dynamics of proteins. The focus is now laid on the consequences of this organization for the dynamic behavior of proteins moving in and between nuclear structures.

Images of labeled proteins in a cell nucleus with fluorescence microscopy often give the mistaken impression that these proteins exist in static localization patterns. In fact many nuclear proteins are highly mobile and roam throughout the whole nucleus, interrupted by short or long time interaction with

binding partners and substrates (Misteli, 2001; Phair et al., 2004). The high diffusion coefficients measured for diffuse nuclear proteins and inert probe molecules in several experimental studies indicate, that proteins can move at a timescale of milliseconds to seconds through the whole nuclear interior (Seksek et al., 1997; Phair and Misteli, 2000; Verkman, 2002). These data raise the question of how proteins are separated into distinct nuclear compartments and how these structures are established and constructed.

One idea is, that the accumulation of proteins in nuclear compartments is the result of specific interactions and binding to molecules in the respective compartments via specific protein or peptide sequences (Cardoso and Leonhardt, 1998; Isogai and Tjian, 2003). The interaction and thus immobilization times can range from milliseconds for splicing factors up to hours in the case of histones (Kimura and Cook, 2001; Grunwald et al., 2006). The effect of protein immobilization in a specific nuclear structure is an accumulation in comparison to neighboring nuclear compartments where the same protein distributes diffuse without binding. In microscopic images of immunostainings or of ectopically expressed fluorescent fusion constructs, an accumulation is visible as a highlighting of a nuclear structure as shown for H2B-GFP incorporated into chromatin in Fig. 3 (Kanda et al., 1998). Molecules that diffuse freely in the nucleus, with no physical hinderances or interactions, are visible as homogeneous nuclear staining (e.g. replication proteins in non S-phase in Fig. 3). Temporal alterations of available interaction sites and the modulation of protein binding is central to regulatory mechanisms controlling nuclear structure and functions (Cardoso and Leonhardt, 1998).

A concentration of binding sites in one distinct nuclear area combined with a lack of interaction sites in other areas results in a low or high local mobility, that can be detected as protein enrichment or homogeneous distribution respectively (Carrero et al., 2003). The accumulation of proteins in the cell nucleus is illustrated in Fig. 5 as high number of binding particles (red) in the respective substructure with binding sites (yellow, chromatin). The level of accumulation is determined by the density of binding sites. Similarly, a different type of protein (dark grey) accumulates in a structure with the appropriate specific interaction sites (light grey, nucleolus). Particles without binding

properties (green) have a similar concentration in all accessible areas. The reduction of the concentration of diffuse distributed particles (green) in certain structures despite of a high mobility, could be explained by physical exclusion and inaccessible subcompartments (light grey).

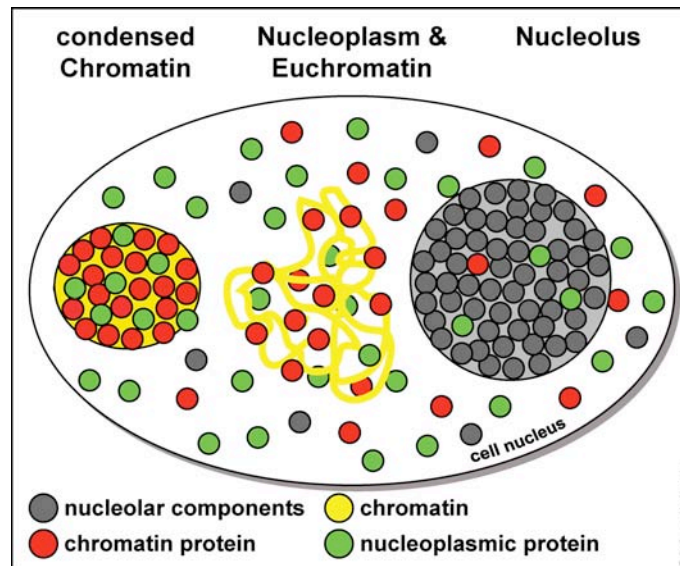


Figure 5: Model for the relationship of mobility and distribution of nuclear proteins.

This was reported for macromolecules that diffusely distribute in e.g. nucleoli and dense chromatin (Gorisch et al., 2003). Nevertheless, in these experiments the detailed dynamic behavior of individual molecules could not be analyzed using fluorescence bleaching and photoactivation due to the spatial and temporal resolution limits of confocal microscopy (Braga et al., 2004; Beaudouin et al., 2006). Short time immobilization as well as the dynamics of individual molecules with respect to nuclear structures could not be analyzed with standard microscopy. However the combination of conventional confocal microscopy techniques with rapid, high resolution single molecule tracking can give a more detailed and integrated view on nuclear molecule movements (Goulian and Simon, 2000). For these experiments it is necessary to develop and test labels for subnuclear structures and improve the delivery of molecules into living cells.

2 Questions and aims of the thesis

The aim of this work was to investigate the molecular mechanisms of nuclear protein movement and distribution as well as the accessibility of nuclear subcompartments e.g. chromatin and nucleolus in living cells. The results should help to elucidate the principles and consequences of functional nuclear organization and effects of compartmentalization on the activity and fidelity of nuclear proteins.

Although past studies have considerably improved our knowledge and view on the cell nucleus, several aspects of the dynamics of nuclear structure and function remain unclear: How are the different nuclear structures established and maintained without separating membranes? Which molecular mechanisms are responsible for spatial separation and coordination of biochemical reactions? How is the protein mobility and distribution influenced by nuclear structures e.g. nucleoplasm, chromatin and nucleolus. And what are the effects of changes in nuclear structures like increased chromatin condensation on protein dynamics? To address these questions it was necessary to:

1. Test and develop markers, which can be used to highlight nuclear substructures, such as chromatin and nucleoli, for further analysis with different techniques of fluorescence microscopy.
2. Characterize and improve methods for the delivery of molecules as neutral or bioactive probe molecules into living cells.
3. Analyze methods to induce changes in the nuclear structure e.g. chromatin condensation.
4. Examine protein mobility and distribution by different live cell microscopy techniques.

This combination of techniques will be used to test the molecule distribution and mobility in subcompartments of live cell nuclei by single molecule and confocal fluorescence microscopy.

3 Results

3.1 DNA labeling in living cells

DNA Labeling in Living Cells

Robert M. Martin,¹ Heinrich Leonhardt,^{1,2} and M. Cristina Cardoso^{1*}

¹Max Delbrück Center for Molecular Medicine, Berlin, Germany

²Ludwig Maximilians University Munich, Department of Biology II, Planegg-Martinsried, Germany

Received 26 January 2005; Revision Received 9 May 2005; Accepted 28 June 2005

Background: Live cell fluorescence microscopy experiments often require visualization of the nucleus and the chromatin to determine the nuclear morphology or the localization of nuclear compartments.

Methods: We compared five different DNA dyes, TOPRO-3, TOTO-3, propidium iodide, Hoechst 33258, and DRAQ5, to test their usefulness in live cell experiments with continuous imaging and photobleaching in widefield epifluorescence and confocal laser scanning microscopy. In addition, we compared the DNA stainings with fluorescent histones as an independent fluorescent label to mark chromatin.

Results: From the dyes tested, only Hoechst and DRAQ5 could be used to stain DNA in living cells. However,

DRAQ5 had several advantages, namely low photobleaching, labeling of the chromatin compartments comparable to that of H2B-GFP fusion proteins, and deep red excitation/emission compatible with available genetically encoded fluorescent proteins such as C/G/YFP or mRFP.

Conclusions: The DNA dye DRAQ5 is well suited for chromatin visualization in living cells and can easily be combined with other fluorophores with blue to orange emission. © 2005 Wiley-Liss, Inc.

Key terms: DNA dyes; DRAQ5; chromatin; nuclear structure; live cell imaging; fluorescence microscopy

In the fields of biological research and medical diagnosis, staining techniques and chemicals to visualize DNA or chromatin with fluorescence microscopy are widely used and have been of high importance for decades (1,2). Many of these dyes are restricted to fixed cell samples and show only roughly the distribution of nuclei in cells and tissues (3). Further, fixation of cells often produces undesired artifacts (4). DNA dyes for live cell fluorescence microscopy should match the criteria of low cytotoxicity and phototoxicity combined with low photobleaching (5). In addition, a suitable live cell DNA dye should specifically label deoxyribonucleic acids stoichiometrically and should be easy to combine with commonly used autofluorescent proteins such as CFP, GFP, YFP, or mRFP (6). Several of the available dyes such as TOPRO, the TOTO dye family, ethidium bromide, and propidium iodide (PI) require permeabilization or similar membrane disruptive methods to label the DNA efficiently (3). Further, several of these dyes bind strongly to RNA requiring a RNase treatment of fixed and permeabilized samples (3,7). The dyes 4',6-diamidino-2-phenylindole (DAPI) and Hoechst are widely used DNA-specific dyes, which emit blue fluorescence under ultraviolet (UV) illumination when bound to DNA. Because UV light damages cellular DNA and other components, the use of Hoechst in live cell microscopy is very restricted in time (1,8). In addition, DAPI and Hoechst have a preference to bind to A/T-rich DNA sequences and highlight a subset of the genome. Thus, the use of these dyes is impossible in long-term live cell

experiments and they also do not necessarily reflect quantitative variations in DNA condensation. Other approaches such as expression of fluorescent histone fusions, albeit an extraordinarily useful tool in cell biology, require prior transfection of cells and a several-hour period until the microscopic visualization can start (9). In addition, several cell types, in particular primary cultures, are very difficult or impossible to transfect (2). In the present study, we compared DNA dyes with chromatin labeling using fluorescent histones to identify a dye that could be used in living cells and could reflect stoichiometrically the spatial distribution of DNA content in living cell nuclei.

MATERIALS AND METHODS

Cell Culture and Viability

Human HeLa cells and HeLa H2B-GFP stable cell line (9) were cultivated in Dulbecco's Modified Eagle's Medium with 10% fetal calf serum plus 5 mM L-glutamine and 5 µg/ml gentamicin. Mouse C2C12 myoblasts and the C2C12 GFP-PCNA stable cell line (10) were grown in Dulbecco's Modi-

Contract grant sponsor: Deutsche Forschungsgemeinschaft.

*Correspondence to: M. Cristina Cardoso, Max Delbrück Center for Molecular Medicine, Franz-Volhard-Klinik, Wiltbergstrasse 50, 13125 Berlin, Germany.

E-mail: cardoso@mdc-berlin.de

Published online 4 August 2005 in Wiley InterScience (www.interscience.wiley.com).

DOI: 10.1002/cyto.a.20172

fied Eagle's Medium with 20% fetal calf serum and the same additives. For live cell microscopy cells were seeded into four-well LabTek glass-bottom chambers (Nalge Nunc International, Naperville, IL, USA) and covered with the desired growth medium the day before.

The effect of DRAQ5 on cell viability was assayed by plating equal numbers of cells and 1 day later adding or not adding the dye to the medium. The next day, cells were trypsinized and counted using a hemacytometer. Experiments were repeated twice and cells were counted in duplicate dishes. To analyze the effect of DRAQ5 on cell cycle progression, the DNA content of HeLa cells treated in the same manner was analyzed after methanol fixation by PI staining in the presence of RNase as described before (10) followed by flow cytometry (FACS-calibur, BD Biosciences, Heidelberg, Germany). Ten runs with 10^4 cells each were analyzed using ModFit 3.0 software and the mean values of cells in each cell cycle stage were calculated for control and DRAQ5 incubated cells.

DNA Stainings

Cells were grown to 50% confluency on 12-mm Ø glass coverslips. The samples were fixed for 10 min with 3.7% formaldehyde (Fluka Chemie GmbH, Buchs, Switzerland) in phosphate buffered saline; for staining with PI, TOPRO-3 and TOTO-3 were permeabilized for 10 min with 0.25% Triton X-100. RNase digestion was performed with 200 µg/ml RNase for 30 min (Sigma, St. Louis, MO, USA). The DNA dyes were applied at the concentrations listed in Table 1 for 5 to 10 min. The coverslips were rinsed with phosphate buffered saline between each incubation step and at the end mounted with Moviol.

For live cell experiments, cells were grown in LabTek chambers and the growth medium was supplied with 1 µM DRAQ5 or 1.6 µM Hoechst 33258 (final concentrations) for 5 min before image acquisition.

DRAQ5 was purchased from Biostatus Limited (Leicestershire, UK), TOPRO-3 and TOTO-3 were obtained from Molecular Probes (Leiden, The Netherlands), Hoechst 33258 was obtained from Hoefer Scientific Instruments (San Francisco, CA, USA), and PI was obtained from Sigma.

Fluorescence Microscopy

Live cell microscopy was performed with an objective heated to 37°C using a confocal laser scanning microscope (LSM510Meta, Carl Zeiss, Jena, Germany) equipped with argon ion and HeNe lasers. Fixed cells were imaged on the same confocal microscope (Fig. 1A) and on a wide-field epifluorescence microscope (Zeiss Axioplan 2) equipped with a 100-W mercury lamp. The latter was used for general bleaching analysis (Table 1). In the live cell photobleaching experiments (Fig. 3A), cells were continuously imaged over time. Excitation, beamsplitters, and emission filters used for imaging of the various fluorophores are listed in Table 2.

Image Analysis

Image analysis (Fig. 3A) was carried out by selecting the nuclei in the images and determining the mean fluorescence intensity of all the pixels selected. Subsequently, the relative fluorescence intensity was calculated by setting the mean fluorescence intensity of the first image in a time series to 100%.

The line scan and colocalization analysis (Pearson's coefficient; Fig. 3B-E) and the above image analysis were performed with Zeiss LSM Image examiner 3.2 and Origin 7.5 software (Origin Lab Corp., North Hampton, MA, USA).

RESULTS

We compared five different DNA binding agents for their ability to fluorescently label nuclear DNA in living cells. In addition, we tested whether they precisely represent the chromatin content in different nuclear compartments imaged by high-resolution confocal fluorescence microscopy. Further experiments were carried out to test the photobleaching behavior of the DNA dyes and the viability of cells in culture in the presence of the dye.

Figure 1A displays representative confocal optical sections of mitotic and interphase HeLa cells stably expressing H2B-GFP (9) and stained with the different dyes with and without RNase treatment. From the five dyes tested, only Hoechst 33258 and DRAQ5 showed membrane-permeable properties and allowed the staining of DNA in living cells (Table 1 and Fig. 1A). The nucleic acid dyes PI, TOTO-3, and TOPRO-3 did not penetrate intact cellular

Table 1
Summary of Nucleic Acid Dyes Characteristics

	TOPRO-3	TOTO-3	Propidium iodide	Hoechst 33258	DRAQ5
Excitation/emission maximum (nm)	642 / 661 ^a	642 / 660 ^a	535 / 617 ^a	352 / 416 ^a	647 / 670 ^b
Cell permeable	—	—	—	+	+
Live/fixed cell application	—/+	—/+	—/+	+/+	+/+
DNA sequence specificity	no ^a	some CTAG preference ^a	no ^a	A/T preference ^a	no ^b
RNA staining	—	+	+	—	—
Bleaching behavior	Very fast (5–10 s)	Fast (20–30 s)	Slow (1–2 min)	Slow (1–2 min)	No bleaching observed
Working concentration	50 µM	1 µM	1.5 µM	1.6 µM	1 µM

^aMolecular Probes.

^bBiostatus Limited.

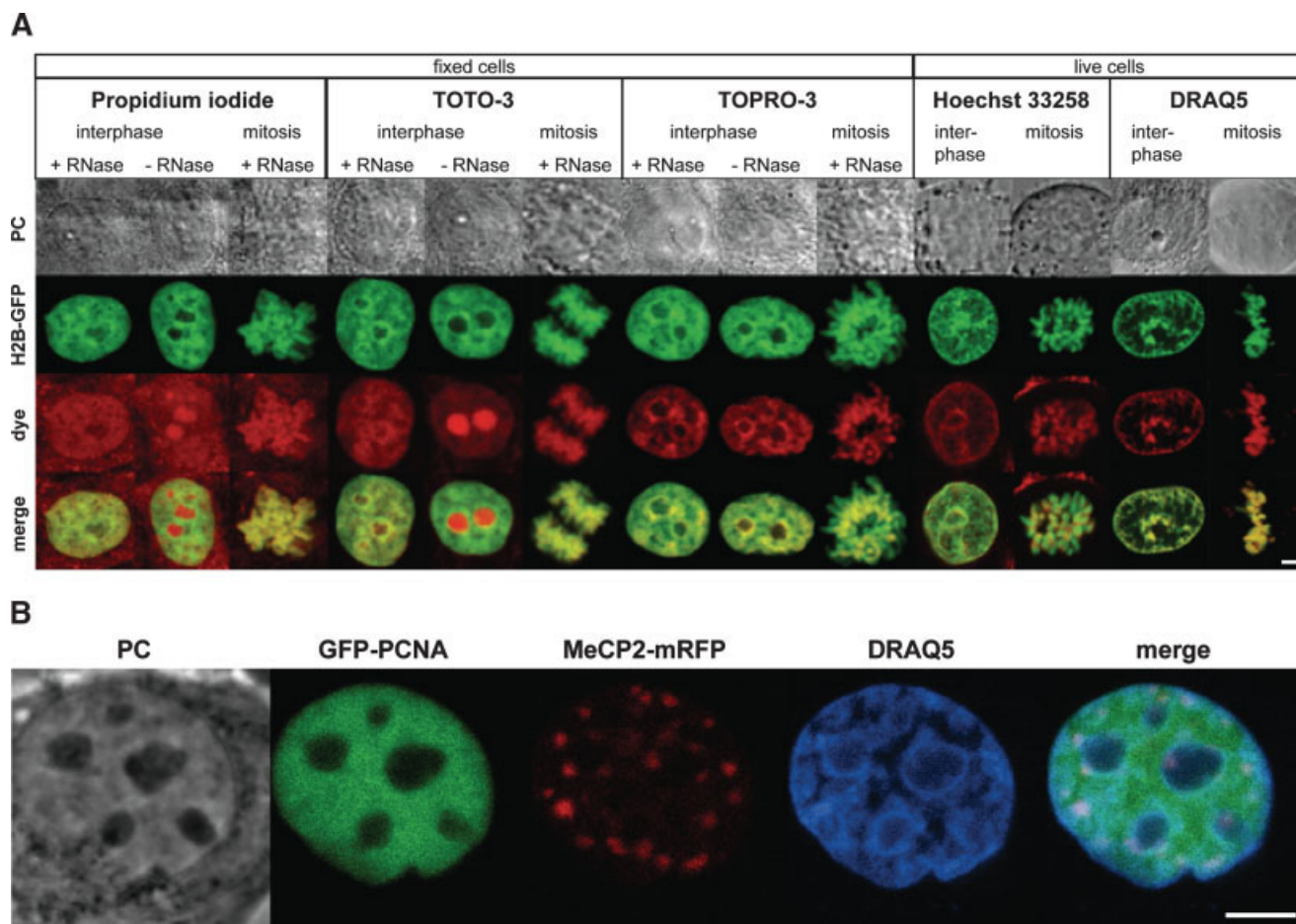


FIG. 1. **A:** Comparison of DNA staining by PI, TOTO-3, TOPRO-3, Hoechst 33258, and DRAQ5 with H2B-GFP chromatin labeling in HeLa cells. For all dyes the H2B-GFP chromatin label and DNA staining were imaged in interphase and mitotic cells. The three fixed-cell dyes TOTO-3, TOPRO-3, and PI were imaged with or without RNase digestion. Dye concentrations are as listed in Table 1. For Hoechst and DRAQ5, only live cell images are shown. In all cases, confocal optical sections are presented with the corresponding phase contrast images. **B:** Combined imaging of DRAQ5 and two different autofluorescent proteins. Living C2C12 mouse myoblast cells expressing the cell cycle marker GFP-PCNA (10) and a protein (MeCP2-mRFP) that binds to pericentric heterochromatin were stained with DRAQ5. The latter also shows that DRAQ5, in contrast to Hoechst/DAPI dyes, does not preferentially stain this type of heterochromatin. The three different fluorophores were excited and detected independently (imaging conditions as listed in Table 2) and no cross-talk was observed. Scale bars = 5 μ m.

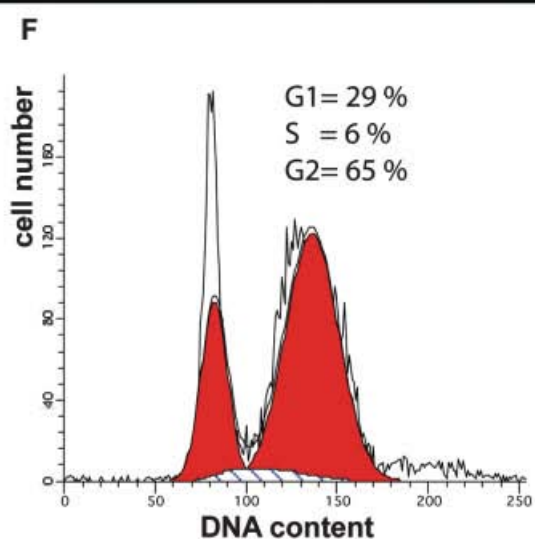
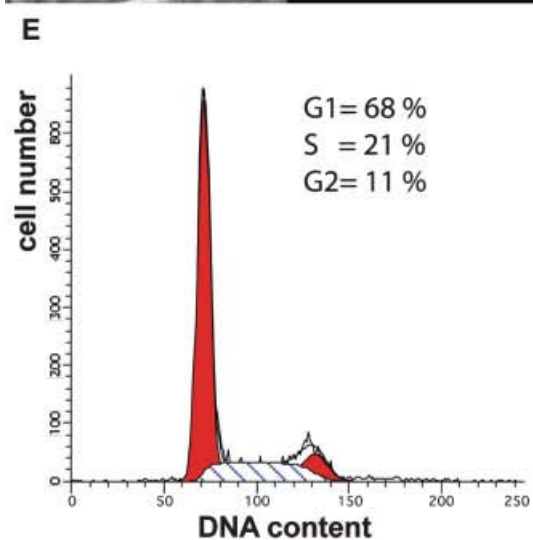
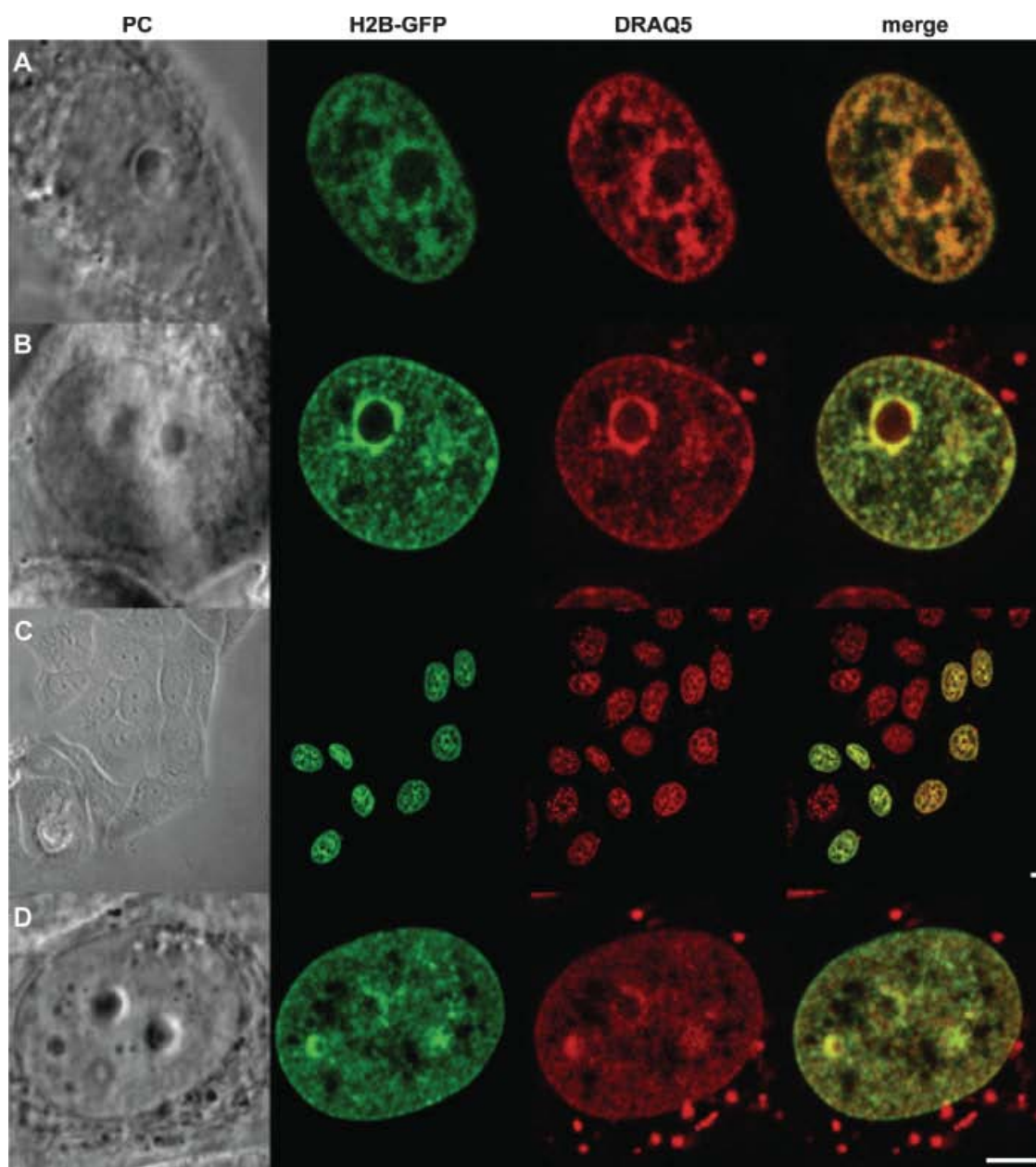
membranes and their application was restricted to permeabilized cells (Fig. 1A). Although TOTO-3 and TOPRO-3 have fluorescence emission in the deep red spectral range, PI emits at wavelengths similar to those of mRFP or rhoda-

mine and strongly compromises the simultaneous use of these fluorophores. Further, PI and TOTO-3 bind to cellular RNA as seen by the strong staining of the nucleolus and required an additional RNase digestion (Fig. 1A).

Table 2
Summary of Imaging Conditions

Fluorophore	Excitation (nm)	Main beamsplitter (nm)	Secondary beamsplitter (nm)	Emission (nm)
LSM510Meta confocal microscope				
Hoechst 33258	2P 762 ^a	KP 680	—	BP 435-485IR
GFP	488	UV/488/543/633	NFT 545	BP500-530IR
PI, mRFP	543	UV/488/543/633	NFT 545	BP585-615
DRAQ5, TOPRO-3, TOTO-3	633	UV/488/543/633	NFT 545	LP 650
Axioplan 2 widefield microscope				
Hoechst 33258	365/12	395	—	397LP
GFP	450-490	510	—	515-565BP
PI	530-585	600	—	615LP
DRAQ5, TOPRO-3, TOTO-3	572-625	645	—	660-710BP

^aTwo-photon excitation.



Only Hoechst 33258 and DRAQ5 could be used to label nuclear DNA in living cells (Fig. 1A). Both dyes were added to the growth medium and stained the nuclear DNA in 5 to 10 min. One major advantage of Hoechst 33258 is the easy combination with many other fluorescent dyes or proteins, from the green to the deep red spectral range of visible light. However, the Hoechst 33258 dye requires excitation with an UV light source or multiphoton laser excitation (Fig. 1A). The former produces additional problems including UV-induced cell damage that decreases cell viability and bleaching due to high-energy excitation light. A continuous imaging of Hoechst-stained living cells with 762-nm two-photon excitation resulted in very fast cell death (data not shown). The fluorescence signals from Hoechst 33258 and H2B-GFP showed a complete overlap but differed in the intensity of the chromatin compartments (Figs. 1A and 3D), which results from the Hoechst 33258 preference to bind to A/T-rich genomic DNA sequences, thereby highlighting some genomic sequences, e.g., pericentric heterochromatin in mouse cells (11).

In view of these caveats of the Hoechst/DAPI DNA dye family, we tested the recently described DNA intercalator DRAQ5 (12,13). The comparison of DRAQ5 nuclear DNA staining with H2B-GFP-labeled chromatin in live cells showed a costaining of the same nuclear regions and the chromosomes in mitotic cells (Fig. 1A). This nucleic acid dye was identified by directed derivatization of fluorescent anthraquinones, which are chemically related to the DNA intercalating anthracycline antibiotic and the anticancer drug mitoxanthrene (12,13). The name DRAQ5 stands for deep red fluorescing anthraquinone Nr. 5 and this compound is a membrane-permeable, DNA intercalating agent with an excitation at 647 nm but is also excitable at a broad range of wavelengths starting from 488 nm (13). These fluorescent properties make DRAQ5 potentially suited for use in combination with the available autofluorescent proteins. We directly tested this by adding DRAQ5 to living mammalian cells coexpressing nuclear mRFP and GFP fusion proteins. As shown in Figure 1B, no bleed-through between the different channels was apparent and the individual nuclear compartments were easy to distinguish and image.

To investigate the dynamics of uptake/labeling of DRAQ5 into living cells, we performed time-lapse fluorescence microscopy. The latter showed a rapid entry of DRAQ5 into the cells and binding to DNA by fluorescence enhancement upon DNA intercalation. The staining was already visible after 3 min and reached the equilibrium at 13 min (data not shown).

To assess the potential toxicity of this intercalating dye at the concentration used, we incubated cells in growth medium with DRAQ5 at a concentration of 1 μ M continuously for 1 day (Fig. 2A-D) or for about 1 h followed by changing to growth medium without the dye and incubated the cells until the next day (data not shown). Both types of incubation with DRAQ5 over a 24-h period did not drastically affect cell viability. In the short DRAQ5 incubation experiment followed by 24-h growth medium incubation, the DRAQ5 signal intensity was decreased in the nuclei and cytoplasmic accumulations became visible (data not shown). In the continuous DRAQ5 incubation experiment, the nuclear DNA staining remained very strong 1 day later (Fig. 2C,D). We further tested the effect on cellular viability by plating equal numbers of cells, subjecting them to the 24-h DRAQ5 incubation scheme as before, and, 1 day later, trypsinizing and counting the number of cells. Compared with untreated cells in the same experiment, there were approximately 50% fewer cells after 24 h of DRAQ5 incubation. This was not due to cell death because the number of cells plated did not decrease and apoptotic cells were not apparent but likely lowered proliferation rate. To directly test this possibility, we performed the same 24-h DRAQ5 incubation scheme and analyzed the cell cycle progression by flow cytometric determination of the DNA content. The results clearly showed no sub-G1 DNA population of cells, which would be indicative of cell death, but a pronounced accumulation of cells in G2 phase (Fig. 2E,F).

Next we compared the photobleaching behavior of the different DNA dyes. Under continuous widefield epifluorescent excitation with a mercury lamp, we observed a fast bleaching of TOPRO-3 (after 5 to 10 s) and to some extent a slower bleaching of TOTO-3 (after 20 to 30 s; Table 1). Accordingly, this allows the acquisition of only one or two images with a laser scanning microscope before the fluorescent signals are bleached. The bleaching rates of PI and Hoechst 33258 were comparable to those of GFP and other more stable fluorophores with the fluorescence signal disappearing after 1 min (Table 1). Under these illumination conditions, DRAQ5 showed no detectable photobleaching. We then directly compared the photobleaching of DRAQ5 with GFP using a confocal laser scanning microscope. In time series, we were able to acquire about 120 images of DRAQ5-labeled nuclei of living HeLa H2B-GFP cells at a high magnification and resolution with minor bleaching, whereas the fluorescent histone label bleached away after about 60 images (Fig. 3A).

We tested whether DRAQ5 accurately reflects the DNA/chromatin distribution within the nucleus by correlating it with the H2B-GFP chromatin label. For this purpose, we

Fig. 2. Viability test for DRAQ5-stained cells. DRAQ5 was added to the growth medium of HeLa H2B-GFP cells and confocal images were acquired at different time points. **A:** A cell nucleus 5 min after application of the dye. The DNA in the cell nucleus is already stained with DRAQ5. **B:** The same can be seen 1 h later, with only a few additional cytoplasmic DRAQ5 signals. After 24 h the overview (**C**) and the magnified image of a nucleus (**D**) show that the cells are viable and appear morphologically unchanged. HeLa cells incubated (**F**) or not (**E**) for 1 day with DRAQ5 were methanol fixed and stained with PI followed by DNA content analysis by flow cytometry. DNA histograms were analyzed with ModFit software to determine the percentage of cells in the different cell cycle stages. Although 11% of the control cells were in G2/M, the cells incubated for 1 day with DRAQ5 at 1 μ M showed a drastic accumulation in G2 phase (65% of all cells). Scale bar = 5 μ m.

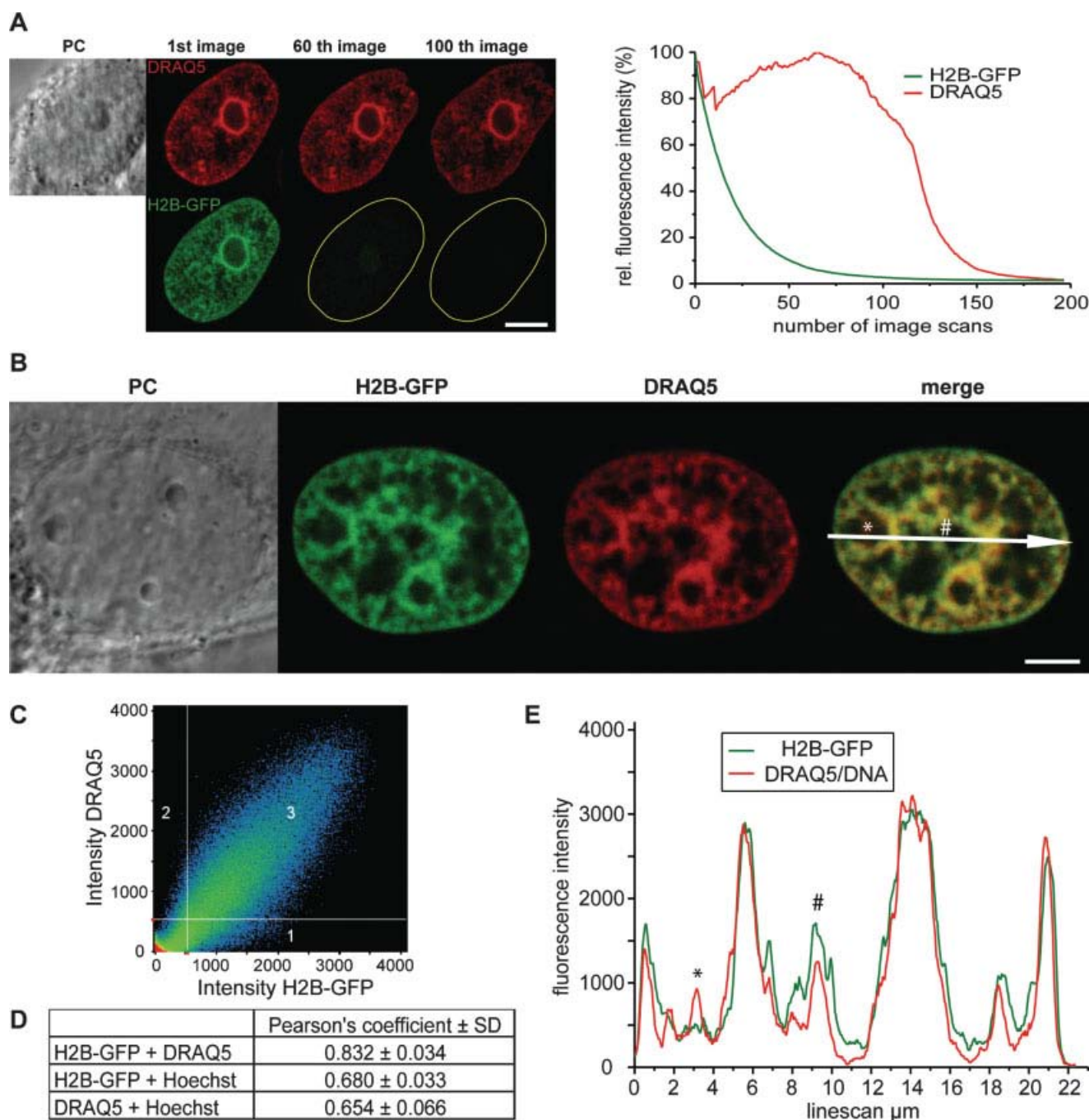


FIG. 3. Quantitative correlation analysis of DNA staining with DRAQ5 versus chromatin labeling with H2B-GFP and comparative photobleaching behavior. **A:** Photobleaching behavior of DRAQ5 versus H2B-GFP. We performed time series with living HeLa H2B-GFP cells and acquired 200 images with a confocal microscope in about 30 min to compare the bleaching of both chromatin labels during imaging. The optical sections and the relative mean fluorescence intensity plotted over the number of images showed that the H2B-GFP label completely disappeared after about 60 images, whereas the DRAQ5 signal did not fade substantially until 120 images. DRAQ5 fluorescence even increased in intensity during the time course. **B:** Quantitative correlation analysis of DNA staining with DRAQ5 versus chromatin labeling with H2B-GFP. The image shows a live HeLa H2B-GFP cell stained with DRAQ5 and the almost complete colocalization in the merged image displayed by the yellow color. **C:** Graphs represent the intensity and localization of the two live cell labels along the line in the merged image. The two graphs follow each other in the displayed structures and label intensity. Minor differences can be seen in one nucleolus (*) or in interchromatin regions (#). **D:** The correlation plot describes the pixel colocalization depending on their intensity on the DRAQ5 and H2B-GFP channels with region 3 displaying colocalizing pixels, whereas regions 1 and 2 contain the noncolocalizing pixels for each label, respectively. All signals with intensity below 500 (region under the cross-line) are background. **E:** The distribution of the pixels in region 3 within a thin cone in a 45° angle reveals a very high degree of pixel colocalization and intensity agreement, which is also reflected in the calculated Pearson's coefficient. The same analysis was performed for Hoechst 33258 versus DRAQ5 or H2B-GFP and the respective Pearson's coefficients are presented in D. Scale bar = $5 \mu\text{m}$.

compared quantitatively the spatial distribution of both labels by (a) line scan analysis, which displays the pixel intensity on a line of both fluorescence labels, and (b) colocalization analysis describing the overlay of pixels and intensities of both labels. The line scan in Figures 3B and 3E shows that the same nuclear regions are labeled with a similar intensity by DRAQ5 and H2B-GFP. Some minor differences in the label intensity appear in the nucleoli (* in Fig. 3B) where DRAQ5 shows slightly higher signals than H2B-GFP. This observation is most probably due to weak RNA binding by this dye. In other nuclear compartments such as euchromatin or the interchromatin compartment (# in Fig. 3B), the slightly more intense H2B-GFP label could represent unbound and diffuse fluorescent histone fusion proteins. In general, no significant differences between DRAQ5- and H2B-GFP-labeled chromatin structures were observed by line scan analysis (Fig. 3B,E). The same set of images (Fig. 3B) was used for a colocalization analysis of DRAQ5 versus H2B-GFP, which displayed a high degree of pixel colocalization with a Pearson's coefficient of 0.832 ± 0.034 (Fig. 3C,D). In contrast, Hoechst 33258-labeled DNA versus H2B-GFP or DRAQ5 showed only 0.680 ± 0.033 and 0.645 ± 0.066 , respectively, reflecting the preferential affinity of Hoechst 33258 to some DNA sequences (Table 1). In summary, at high spatial resolution, DRAQ5 reflects the spatial DNA concentrations in excellent agreement to the chromatin intensity depicted by H2B-GFP.

DISCUSSION

The aim of this work was to find and characterize an easy-to-use live cell DNA stain to label nuclear chromatin compartments for long-term live cell microscopy in combination with the available autofluorescent proteins.

From the five DNA dyes compared, three (PI, TOTO-3, and TOPRO-3) are not suitable for staining living cells, with TOPRO-3 also bleaching very fast (Table 1 and Fig. 1A). Hoechst 33258 can be used to stain DNA in live cells but requires UV excitation, which is toxic to the cells and has a marked preference for A/T-rich sequences, which can bias quantitative studies (1,8). The DNA dye DRAQ5 showed no drastic cytotoxicity effects at $1 \mu\text{M}$ as the cells slowed down proliferation but did not die (Fig. 2). Decrease of nuclear DNA labeling of the dye visible the next day can be mechanistically related to the efflux of dyes, such as Hoechst 33342 and rhodamine 123, mediated by different ABC transporters reported in multi-drug-resistant cells (14,15). These are characterized by high levels of P-glycoprotein, which is responsible for facilitating transport of anticancer drugs out of the cell. DRAQ5 incubation at $1 \mu\text{M}$ for 24 h did hinder cell cycle progression with accumulation of cells in G2 phase of the cell cycle (Fig. 2). Because this dye is an anthracene derivative that intercalates into DNA, it is conceivable that it blocks topoisomerase II, thus causing G2 arrest.

Because DRAQ5 is excited with red light and emits deep red fluorescence, it can be used in combination with

C/G/YFP and mRFP (Fig. 1B). From our live cell experiments, we can conclude that DRAQ5 is not bleached under normal imaging conditions (Fig. 3A). The labeling of DNA and thereby of chromatin with DRAQ5 is nearly identical with an H2B-GFP label (Fig. 3B-E). Some minor differences in the label intensities could result from a mobile fraction of H2B-GFP, which increases the background in the green channel or the incorporation of histone variants (16). In contrast, DRAQ5 seems to bind to a low extent RNA (13) as seen by a low signal in the nucleoli, which contain mostly rRNAs (Fig. 3B,E).

In contrast to fluorescently tagged histones, DRAQ5 DNA staining does not rely on the transfectability of the cells or the evolutionary conservation of histones and is therefore potentially applicable to all organisms.

Altogether DRAQ5 fulfils several of the requirements for a live cell DNA dye, i.e., it (a) is an easy to use cell-permeant DNA dye, (b) is extremely photostable; (c) allows simultaneous imaging of the available genetically encoded fluorescent proteins, and (d) reflects accurately the spatial concentration of DNA in living cells.

ACKNOWLEDGMENTS

This work was funded by grants from the Deutsche Forschungsgemeinschaft to H.L. and M.C.C. We thank Anje Sporbert for getting us started with the DRAQ5 application and fruitful discussions, Hans-Peter Rahn for help with the FACS analysis, and Alessandro Brero for critical reading of the manuscript. The HeLa H2B-GFP cell line was a generous gift of Kevin Sullivan and the mRFP1 cDNA was kindly provided by Roger Y. Tsien.

LITERATURE CITED

1. Durand RE, Olive PL. Cytotoxicity, mutagenicity and DNA damage by Hoechst 33342. *J Histochem Cytochem* 1982;30:111-116.
2. Choi M, Rolle S, Wellner M, Cardoso MC, Scheidereit C, Luft FC, Kietz R. Inhibition of NF-kappaB by a TAT-NEMO-binding domain peptide accelerates constitutive apoptosis and abrogates LPS-delayed neutrophil apoptosis. *Blood* 2003;102:2259-2267.
3. Suzuki T, Fujikura K, Higashiyama T, Takata K. DNA staining for fluorescence and laser confocal microscopy. *J Histochem Cytochem* 1997; 45:49-53.
4. Kozubek S, Lukasova E, Amrichova J, Kozubek M, Liskova A, Slotova J. Influence of cell fixation on chromatin topography. *Anal Biochem* 2000;282:29-38.
5. Haraguchi T, Ding DQ, Yamamoto A, Kaneda T, Koujin T, Hiraoka Y. Multiple-color fluorescence imaging of chromosomes and microtubules in living cells. *Cell Struct Funct* 1999;24:291-298.
6. Zhang J, Campbell RE, Ting AY, Tsien RY. Creating new fluorescent probes for cell biology. *Nat Rev Mol Cell Biol* 2002;3:906-918.
7. van Zandvoort MA, de Grauw CJ, Gerritsen HC, Broers JL, Oude Egbrink MG, Ramaekers FC, Slaaf DW. Discrimination of DNA and RNA in cells by a vital fluorescent probe: lifetime imaging of SYTO13 in healthy and apoptotic cells. *Cytometry* 2002;47:226-235.
8. Davis SK, Bardeen CJ. Cross-linking of histone proteins to DNA by UV illumination of chromatin stained with Hoechst 33342. *Photochem Photobiol* 2003;77:675-679.
9. Kanda T, Sullivan KF, Wahl GM. Histone-GFP fusion protein enables sensitive analysis of chromosome dynamics in living mammalian cells. *Curr Biol* 1998;8:377-385.
10. Leonhardt H, Rahn HP, Weinzierl P, Sporbert A, Cremer T, Zink D, Cardoso MC. Dynamics of DNA replication factories in living cells. *J Cell Biol* 2000;149:271-280.
11. Leonhardt H, Page AW, Weier HU, Bestor TH. A targeting sequence directs DNA methyltransferase to sites of DNA replication in mammalian nuclei. *Cell* 1992;71:865-873.

12. Smith PJ, Blunt N, Wiltshire M, Hoy T, Teesdale-Spittle P, Craven MR, Watson JV, Amos WB, Errington RJ, Patterson LH. Characteristics of a novel deep red/infrared fluorescent cell-permeant DNA probe, DRAQ5, in intact human cells analyzed by flow cytometry, confocal and multiphoton microscopy. *Cytometry* 2000;40:280-291.
13. Smith PJ, Wiltshire M, Davies S, Patterson LH, Hoy T. A novel cell permeant and far red-fluorescing DNA probe, DRAQ5, for blood cell discrimination by flow cytometry. *J Immunol Methods* 1999;229:131-139.
14. Canitrot Y, Lahmy S, Buquen JJ, Canitrot D, Lautier D. Functional study of multidrug resistance with fluorescent dyes. Limits of the assay for low levels of resistance and application in clinical samples. *Cancer Lett* 1996;106:59-68.
15. Uchida N, Dykstra B, Lyons K, Leung F, Kristiansen M, Eaves C. ABC transporter activities of murine hematopoietic stem cells vary according to their developmental and activation status. *Blood* 2004;103:4487-4495.
16. Leach TJ, Mazzeo M, Chotkowski HL, Madigan JP, Wotring MG, Glaser RL. Histone H2A.Z is widely but nonrandomly distributed in chromosomes of *Drosophila melanogaster*. *J Biol Chem* 2000;275:23267-23272.

3.2 Nucleolar marker for living cells

Nucleolar marker for living cells

Robert M. Martin · Gisela Tünnemann ·
 Heinrich Leonhardt · M. Cristina Cardoso

Accepted: 10 November 2006 / Published online: 5 January 2007
 © Springer-Verlag 2006

Abstract In the recent molecular and cell biological research, there is an increasing need for labeling of subcellular structures in living cells. Here, we present the use of a fluorescently labeled cell penetrating peptide for fast labeling of nucleoli in living cells of different species and origin. We show that the short peptide with ten amino acids was able to cross cellular membranes and reach the nucleolar target sites, thereby marking this subnuclear structure in living cells. The treatment of cells with actinomycin D and labeling of B23 protein and fibrillarin provided evidence for a localization to the granular component of the nucleolus. The fluorescently conjugated nucleolar marker could be used in combination with different fluorophores like fluorescent proteins or DNA dyes, and nucleolar labeling was also preserved during fixation and staining of the cells. Furthermore, we observed a high stability of the label in long-term studies over 24 h as well as no effect on the cellular viability and proliferation and on rDNA transcription. The transducible nucleolar marker is therefore a valuable molecular tool for cell biology that allows a fast and easy labeling of this structure in living cells.

Keywords Cell penetrating peptides · Fluorescence microscopy · Living cells · Nucleolus · Transducible nucleolar marker

Abbreviations

AMD	Actinomycin D
DRAQ5	Deep red fluorescing anthraquinone Nr. 5
DMEM	Dulbecco's modified eagle medium
FACS	Fluorescence activated cell sorting
FCS	Fetal calf serum
FITC	Fluorescein isothiocyanate
FU	Fluorouridine
GFP	Green fluorescent protein
HEPES	N-2-hydroxyethylpiperazine-N'-2-ethanesulfonic acid
HIV	Human immunodeficiency virus
mRFP	Monomeric red fluorescent protein
PI	Propidium iodide
PCNA	Proliferating cell nuclear antigen
TAT	Transactivator of transcription

Introduction

The nucleolus is the most prominent substructure in the cell nucleus and it was first described in 1836 by Gabriel Gustav Valentin (Franke 1988). It took more than one century to establish its role in ribosome biogenesis (Brown and Gurdon 1964; Perry 1962). The nucleolus is a very dynamic structure and it forms around the rDNA loci (Andersen et al. 2005). The inner nucleolar structure is organized into fibrillar centers (FC, where rDNA is located and at the periphery of which transcription takes place) surrounded by the dense fibrillar component (DFC, into which nascent

Electronic supplementary material The online version of this article (doi:10.1007/s00418-006-0256-4) contains supplementary material, which is available to authorized users.

R. M. Martin · G. Tünnemann · H. Leonhardt ·
 M. C. Cardoso (✉)
 Max Delbrück Center for Molecular Medicine,
 Robert-Roessle-Str. 10, 13125 Berlin, Germany
 e-mail: cardoso@mdc-berlin.de

H. Leonhardt
 Department of Biology II, Ludwig Maximilians University
 Munich, 82152 Planegg-Martinsried, Germany

transcripts migrate) and all around the granular component (GC), which is filled with ribosomal precursors (Cheutin et al. 2002; Derenzini et al. 2006; Scheer and Hock 1999). Long ago, it has been noted that the nucleolus size reflects the cellular activity, proliferation and differentiation (Hernandez-Verdun 2006). Furthermore, the nucleolus bears the hallmark of other subnuclear compartments, in that it is not delimited by membranes, as is the case for cytoplasmic organelles.

Owing to its higher density and refractivity in comparison to the surrounding nucleoplasm, the nucleolus can be visualized with phase contrast or differential interference contrast microscopy. However, the three-dimensional volume and localization within the nucleus as well as its exact borders are hard to identify by contrast microscopy alone and require a fluorescence label (Lam et al. 2005). In addition, such a marker would facilitate high throughput analysis to sort nuclear proteins according to their intranuclear localization. Finally, the development of new high-resolution optical techniques allows for the first time optical analysis down to the nanometer scale but require fluorescent labels. This gain in information could help to elucidate the functional nuclear and genome organization in relation to the nucleolus in the three-dimensional nuclear structure. Specific antibodies to nucleolar proteins or the transfection of cells with plasmids encoding for fluorescent fusions of nucleolar proteins allow the visualization of the nucleolus by fluorescence microscopy. However, these methods require either fixation of the sample and immunostaining in the case of antibodies or transfection of cells and expression of the fluorescence marker in the case of fluorescent proteins. The latter strategy has the advantage of allowing live-cell microscopy but is first time consuming and second restricted to transfectable cells, which is not the case of most primary cells. Furthermore the analysis of drug effects on the nucleolar organization and function could be simplified by using a fast nucleolar label for living cells. A membrane-permeable fluorescent label for the nucleoli, which is fast and easy to apply on living cells, would therefore be a very useful molecular tool for diagnostics and cell biological research.

The ability of certain peptides and proteins with concentrated basic charges to cross cellular membranes was earlier discovered in 1988 for the HIV TAT protein (Frankel and Pabo 1988; Green and Loewenstein 1988), and the peptide domain responsible for membrane transduction was mapped a decade later (Vives et al. 1997). Further comparison of native and artificial membrane transducing peptides indicated that arginines are superior to lysines in transduction potential (Mitchell et al. 2000; Thoren et al. 2003). Independent studies found that peptide sequences present in several

viral and cellular proteins containing a stretch of 6–10 basic amino acids could serve as a targeting sequence for the nucleus and the nucleolus (Dang and Lee 1989; Hatanaka 1990). In this work we reasoned that if both properties, membrane transduction ability and nucleolar targeting signal, could be combined in the same peptide made of a series of basic amino acids we could exploit these independent biological functions to directly label the nucleolus in living cells.

Materials and methods

Peptides and plasmids

Amino-terminal fluorescein labeled deca-arginine peptide (FITC-R₁₀) was synthesized with D-amino acids by Peptide Specialty Laboratories (Heidelberg, Germany), dissolved in ddH₂O and, for application on living cells, further diluted in growth medium.

The mRFP-PCNA expression construct was described before (Sporbert et al. 2005).

Cell culture and transfection

Human HeLa cells as well as Flp 3T3 mouse fibroblast cells were cultivated in DMEM with 10% FCS + 5 mM L-glutamine and 5 µg/ml Gentamycine. C2C12 mouse myoblasts were grown in DMEM with 20% FCS and the same additives. Transfection of C2C12 cells with mRFP-PCNA was carried out by CaPO₄ precipitation method as described (Cardoso et al. 1997). For live cell microscopy the cells were plated onto 4- or 8-well Lab-Tek coverglass chambers (NalgeNunc) or 8-well Ibidi chambers (Ibidi). Adult ventricular cardiomyocytes were enzymatically isolated by retrograde perfusion from excised adult male Wistar rat hearts at a constant flow of 6 ml per min with a Ca²⁺-free HEPES solution containing collagenase (Worthington type II, 60 IU per ml). The freshly dissociated cells were kept at physiological solution with 0.3 mM Ca²⁺ and 0.5% bovine serum albumin at room temperature (Alvarez et al. 2004). DRAQ5 (Biostatus Ltd) staining of DNA in living cells was as described (Martin et al. 2005).

Transduction assays

All peptide transduction experiments were performed with living cells plated on 4- or 8-well coverglass chambers. Before observation, the medium was removed and growth medium with the different peptide concentrations was directly applied to the cells. To remove the background fluorescence of extracellular peptides a

washing step with PBS was included after 30 min of incubation followed by incubation in growth medium without peptide. For the concentration dependent uptake (Fig. 3a) the cells were incubated with the peptides for 1 h before washing with PBS while for the continuous time series to study the uptake dynamics (Fig. 3b) no washing step was performed. The uptake of the marker peptide was studied under a fluorescence microscope for 1 h starting with the peptide application. After observation and imaging of the nucleolar label the cells were returned to the incubator and further image collection was performed 24 h later. Transduction efficiencies were determined in two independent experiments by counting the number of transduced cells with nucleolar label directly on the fluorescence microscope in ten fields of view ($n = 130$ –180 cells).

Cell viability and proliferation assay

Cell viability and label stability after nucleolar marker application were monitored by the ability of the cells to undergo complete mitotic cell cycles and grow to

confluency as well as monitoring the label intensity in the nucleoli 24 h after application.

The membrane integrity was ascertained by the trypan blue exclusion assay. Into each well of a 4-well LabTek chamber with 400 μ l medium 2 μ l trypan blue solution (Sigma) was added and mixed by pipetting up and down. The number of trypan blue positive cells was counted at 30 min and in separate samples at 24 h.

The impact of the nucleolar marker on cell viability and cell cycle progression was assayed by plating equal number of cells and 1 day later adding or not 10 μ M FITC-R₁₀ to the media for 1 h followed by a washing step in PBS and incubation in growth medium. The next day, cells were trypsinized, fixed with methanol for 20 min and stained with 50 μ M propidium iodide (PI) (Sigma) for 1 h in the presence of 0.1 mg/ml RNase A (Sigma). DNA content was analyzed by flow cytometry (Becton Dickinson FACS Vantage using 488 nm laser excitation and 675/20 nm bandpass filter for detection) as a measure of cell cycle progression (Plander et al. 2003). Five sets of 1×10^4 cells and five sets of 2×10^4 cells were analyzed, and all the data sets were used for the calculation of mean values of cells in

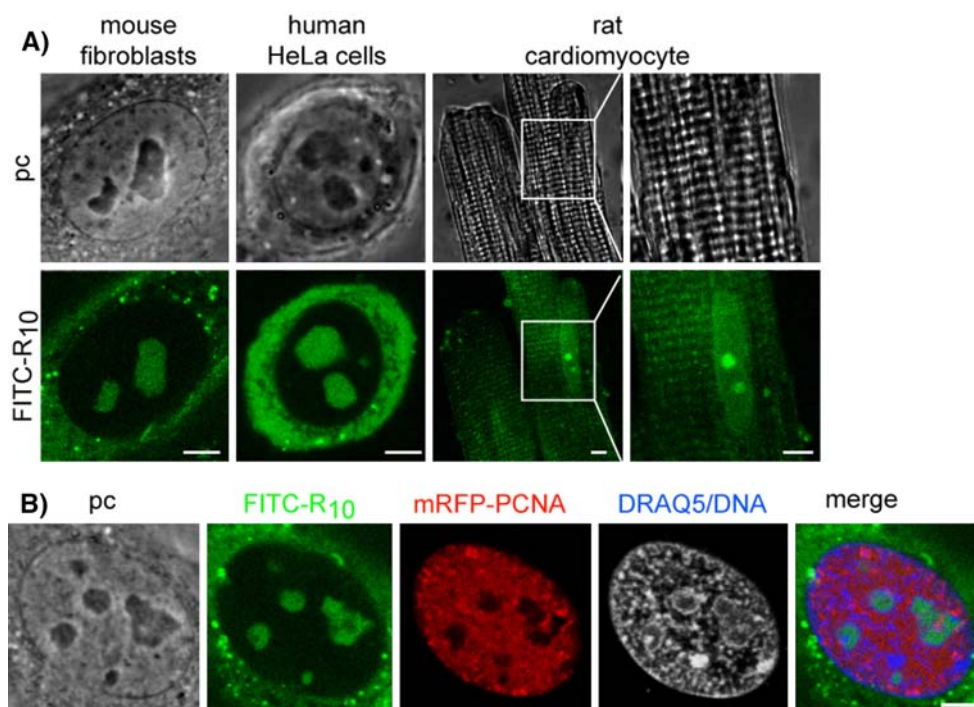


Fig. 1 Transducible nucleolar marker uptake into different cell types and in combination with other fluorophores **a** This figure shows the fluorescently labeled nucleolar marker taken up into cells of different species and origin, which are either from cultured cell lines (fibroblasts, mouse; HeLa, human) or primary cells that are terminally differentiated (adult cardiomyocyte, rat). The cells were incubated with a medium containing the transducible nucleolar marker for 30 min and then washed in PBS and supplied with

the medium. In both cases the marker transduced fast into the cells where it accumulated in the nucleoli and thereby marked this sub-nuclear structure. **b** Displays a C2C12 mouse myoblast transfected with a plasmid coding for mRFP-PCNA (red) and with DNA stained by DRAQ5 (blue). The transducible nucleolar marker labeled with FITC (green) can be used in combination with fluorescent protein labels like mRFP as well as fluorescent dyes such as the live cell DNA stain DRAQ5. Scalebar: 5 μ m

G1, S and G2/M phase for FITC-R₁₀ labeled and control cells using ModFit 3.0 software.

In situ transcription assay and inhibition with actinomycin D

Cells were grown on glass coverslips and 1 day later incubated with FITC-R₁₀ for 1 h or 24 h in a 12-well plate. Actinomycin D (AMD) treatment was performed at 0.04 mg/l for 2 h before adding FITC-R₁₀ at 10 μ M to the same growth medium or for 2 h after the incubation of cells with FITC-R₁₀ for 1 h. For the labeling of nascent RNA cells were incubated with 1.5 mM FU in growth medium for 10 min and washed in PBS.

After the incubation schemes cells were fixed in 3.7% formaldehyde in PBS for 10 min and permeabilized with 0.25% (0.5% for AMD experiments) Triton X100 in PBS for 10–12 min. The samples were immunostained with anti-B23 mouse monoclonal antibody (clone FC82291; Sigma) followed by detection with donkey anti-mouse IgG antibody conjugated with TexasRed (Jackson) and #346 anti-fibrillarin human auto-antibody (kind gift from P. Hemmerich, FLI Jena) followed by donkey anti-human IgG biotin SP (Lot: 47441 Jackson) and streptavidin-Cy5 (Amersham). Fluorouridine incorporated into RNA was detected with anti-BrdU rat monoclonal antibody (clone BU1/75; Harlan Sera Lab) followed by incubation with donkey anti-rat IgG antibody conjugated with Cy5 (Jackson). For the labeling of DNA cells were counterstained with TOPRO-3 at 1.3 μ M final concentration in PBS (Molecular Probes) and mounted with Moviol.

Microscopy, image acquisition and analysis

Live cell microscopy was performed with a Zeiss LSM510Meta confocal setup mounted on an Axiovert 200 M inverted microscope using a 63 \times phase contrast plan-apochromat oil objective NA 1.4 heated to 37°C. For all acquisition settings the main beam splitter was HFT UV/488/543/633 and the parameters specific for each fluorochrome are listed below:

Fluorochrome	Ex (nm)	Em (nm)
FITC	488	BP500–530
mRFP, L-Rhodamine	543	BP565–615
DRAQ5, Cy5	633	LP650

Imaging of AMD treated cells was done at a Leica TCS SP5 confocal setup mounted on a Leica DMI 6000 CS inverted microscope using a 63 \times HCX plan-

apochromat DIC oil objective NA 1.4. The image acquisition was done sequentially to minimize potential crosstalk between the fluorophores. The trypan blue exclusion was determined with brightfield illumination on the Zeiss LSM510 microscope setup. The uptake kinetics analysis (Fig. 3b) was performed by selecting ten nucleoli in ten individual cell nuclei in the image of the last time point and determining their mean fluorescence intensity (FI) at each time point. The fluorescence intensity data for all individual nucleoli were averaged and plotted against the time-scale. Labeling of nascent RNA by FU was analyzed by selecting 60 nuclei from confocal images and determining the mean fluorescence intensity. Background correction was done by applying a threshold according to the mean fluorescence intensity in images from control cells without primary antibody (anti-BrdU). Image analysis was performed with Zeiss LSM Image examiner 3.2 (Zeiss) and Origin 7.5 software (Origin Lab Corp.).

Results and discussion

Our goal was to develop an easy to use live cell fluorescent marker for the nucleolus. Therefore, we tested whether nucleolar targeting ability could be combined with cell penetrating ability in one peptide. The latter would allow non-invasive application to all sorts of cells. We chose a peptide composed of 10 arginines, which had been shown to efficiently transduce into cells (Wender et al. 2000). To prevent proteolytic degradation the peptide was synthesized with D-amino acids. The fluorescent label (FITC) was added to the N-terminal end.

First, we tested the ability of this peptide (FITC-R₁₀) to be taken up by different cells and its intracellular localization. We selected different cell types (fibroblasts, epithelial, muscle) from different species (mouse, rat, human) and not only cell lines (Flp 3T3, HeLa) but also primary cultures (cardiomyocytes). FITC-R₁₀ was diluted in growth medium and applied directly to the cells for 30 min. After the incubation time the cells were washed and analyzed by confocal microscopy. In all cells tested (Fig. 1a) the fluorescence label was found accumulated in the nucleoli identified by the phase contrast images (except in cardiomyocytes where the nucleoli cannot be detected due to the sarcomeric structures) and also diffusely distributed in the cytoplasm. The transfection of the cells with an S-phase marker (mRFP-PCNA; Sporbert et al. 2005 and simultaneous DNA labeling with DRAQ5 Martin et al. 2005) indicated that uptake of the peptide was not cell

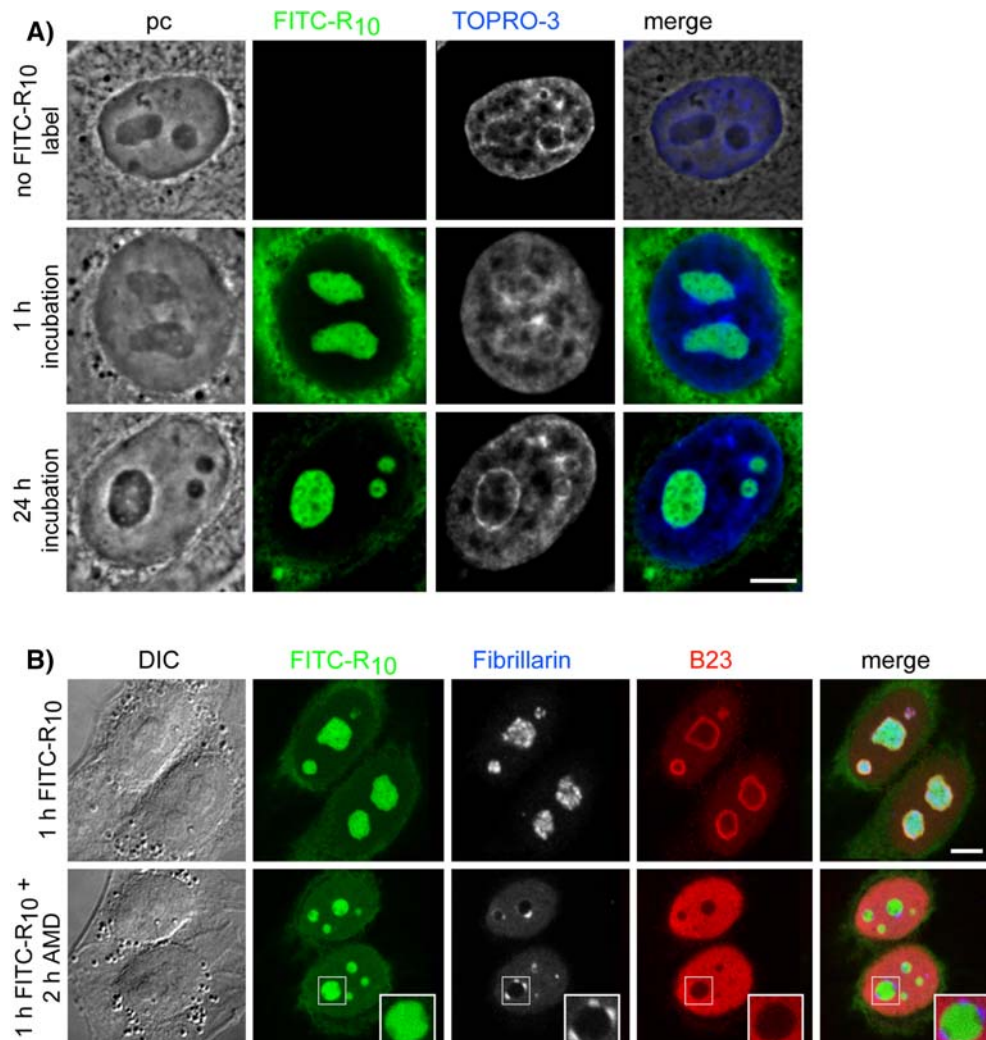
cycle dependent. Indeed, cells in different stages of the S-phase as well as in G1/G2 exhibited nucleolar labeling and also mitotic cells had taken up the marker although the nucleus and the nucleoli are not present (Fig. 1b and data not shown). These data also indicate that combinations with other fluorochromes (e.g., live cell DNA staining with DRAQ5) and fluorescent proteins (e.g., mRFP) are possible. Since any other fluorescent label can be selected for the nucleolar marker peptide, this allows multiple combinations with other fluorochromes.

The FITC-R₁₀ label colocalized with the dark structures in the phase contrast images, which were surrounded by dense chromatin detected by TOPRO-3 staining (Fig. 2a). To confirm the nucleolar localization of FITC-R₁₀ we performed colocalization studies with nucleophosmin/B23 (Fig. 2b), a protein present in the granular component of the nucleolus and fibrillarin localized in the dense fibrillar component (reviewed in Olson and Dundr 2005). The FITC-R₁₀ label

colocalized with the B23 antibody signal at the periphery of the nucleoli and filled the nucleolar interior showing a decreased concentration in the dense fibrillar components labeled by fibrillarin (Fig. 2b). This demonstrated that the FITC-R₁₀ peptide possesses intracellular nucleolar targeting ability and furthermore localizes to the granular component of the nucleolus.

To further test the exclusion of FITC-R₁₀ from fibrillar components we treated cells with AMD. Exposure of cells to this transcription inhibitor leads to a separation of fibrillar and granular components into distinct caps (Reynolds et al. 1964; Chen et al. 1999). The AMD treatment of cells before or after (data not shown) labeling the nucleoli with FITC-R₁₀ showed the persistent localization of FITC-R₁₀ to the granular component remnant separated from the caps formed by the fibrillar components without FITC-R₁₀ (Fig. 2b). In contrast to B23, the nucleolar marker did not redistribute throughout the nucleoplasm after AMD

Fig. 2 Intracellular localization of the FITC-R₁₀. **a** HeLa cells incubated for 1 and 24 h with 10 μ M FITC-R₁₀ as well as unlabeled controls were fixed in 3.7% formaldehyde in PBS and stained with TOPRO-3 to label the DNA. The FITC-R₁₀ label colocalize with the nucleoli identified in the phase contrast during short- and long-term incubation of the cells. **b** The HeLa cells were immunolabeled for B23/nucleophosmin to highlight the granular component of the nucleolus and fibrillarin to label the dense fibrillar components. One sample was treated with actinomycin D (AMD), which leads to a stop in rDNA transcription and the formation of nucleolar caps containing the fibrillar components. The FITC-R₁₀ label was still localized to the nucleolar interior unlike B23, which was redistributed to the nucleoplasm and excluded from the nucleoli. The nucleolar marker does not colocalize with the fibrillarin labeled caps in AMD treated cells. Scalebar: 5 μ m



treatment indicating that it interacts with other molecules of the granular component. Thus, the FITC-R₁₀ can also be used in cells where rDNA transcription was stopped to label the granular components of disassembled nucleoli.

Furthermore, these immunostaining experiments after live cell application of FITC-R₁₀ demonstrated that fixation and further treatments could be performed without losing the label or changing its localization (Fig. 2 and suppl. Fig. 1A). When FITC-R₁₀ was applied to pre-fixed samples though, it did not stain the nucleolus (suppl. Fig. 1A).

The kinetics of uptake of the peptide into cells was then studied by time-lapse confocal microscopy. The time series analysis is shown in Fig. 3b and in the supplementary online movie. The images at the first and last timepoints display the accumulation of the marker over time inside the cells and on the cell membrane. The graph represents the fluorescence increase in the nucleoli of 10 different cells. The peptide was rapidly internalized and labeling of the nucleoli started around 20 min and reached the equilibrium at 40 min. Earlier nucleolar labeling could have been missed due to the strong extracellular fluorescence of non-internalized peptides.

In a separate set of experiments we performed a dose response uptake analysis. Different concentrations of the marker in the growth medium were applied for 1 h

to HeLa cell cultures. A threshold minimal concentration for nucleolar labeling was found at 2.5 μ M. Lower peptide concentration (1 μ M) resulted in no uptake of the marker into the cells (Fig. 3a). A possible explanation for this finding is that a certain concentration of the basic CPP on the cell membrane needs to be reached to enable the membrane transduction process (Dietz and Bdeltahr 2004; Tunnemann et al. 2006). Alternatively, the fluorescence detection method used might not be sensitive enough to detect very low concentrations of fluorescent peptide over the background signal.

Next, we wanted to test the intracellular stability of the marker and its localization. This was examined by applying the transducible fluorescent nucleolar marker to living C2C12 myoblasts for 30 min, which as before resulted in nucleolar accumulation, removing the excess extracellular fluorescent peptide by a washing step with PBS and analyzing the cells by confocal microscopy 24 h later. The fluorescent nucleolar label was surprisingly stable showing very bright nucleolar signal 1 day later without detectable decrease in fluorescence intensity or the number of cells marked (Fig. 3c). No proteolytic degradation or intracellular recycling of the FITC-R₁₀ was observed within this time period. In addition, the morphology of the cells was not changed, and the cultures grew to confluency indicating no overt effect of the nucleolar marker on cell cycle progression and mitotic division. The structure

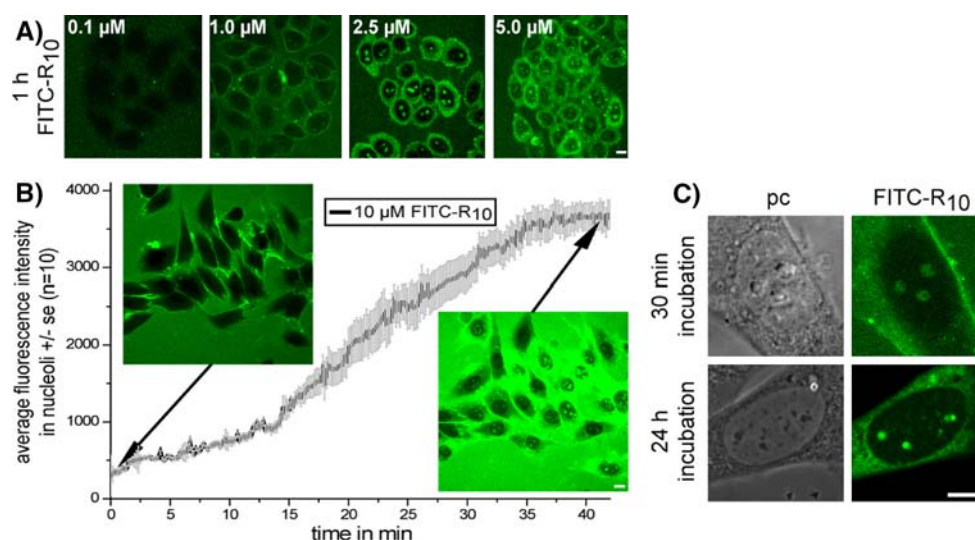


Fig. 3 Kinetics of uptake and intracellular stability of the nucleolar marker. The images in **a** show the concentration dependent labeling of the nucleoli in HeLa cells with a threshold at a concentration of 2.5 μ M FITC-R₁₀. The kinetics of uptake in **b** display the increase of the fluorescent label in the nucleoli directly after application of 10 μ M FITC-R₁₀ in medium to living C2C12 cells without a washing step. The uptake started immediately after the application of the nucleolar marker and was clearly visible after

20 min. A maximum of the nucleolar label was reached 40 min after the start of the experiment (see supplementary movie). **c** C2C12 cells were incubated for 30 min with FITC-R₁₀ in a medium followed by washing in PBS and imaged 24 h later. Representative images are shown and demonstrate the stability of the transducible nucleolar marker over the 1 day period tested (see also Fig. 2a). Scalebar: 5 μ m

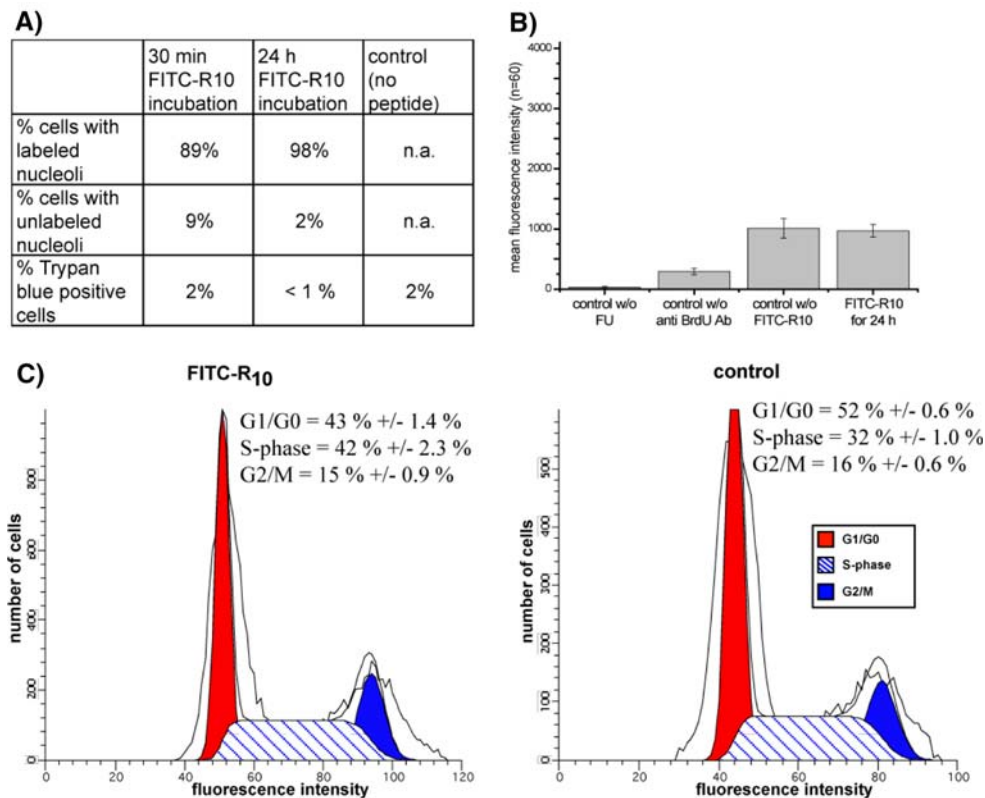


Fig. 4 Effect of the nucleolar marker on the cellular viability, proliferation and rDNA transcription. The table in **a** summarizes the percentage of cells with labeled or unlabeled nucleoli and the trypan blue exclusion test after short- and long-term incubation of living cells with 5 μ M FITC-R₁₀. In both cases a small number of cells remained unlabeled, whereas the majority of cells showed nucleolar labeling after 30 min and also after 24 h incubation with the nucleolar marker. The quantity of trypan blue positive cells during short- and long-time incubation is comparable to the control cells. The diagram in **b** displays in each bar the mean intensity

of fluorescently labeled FU incorporated into rRNA from 60 nuclei measured in confocal images. The signals of labeled rRNA in FITC-R₁₀ labeled or unlabeled control cells differed only a little and within the range of the standard deviation. In **c** the histograms represent fitted curves of flow cytometry measurements. HeLa cells were incubated or not with the transducible nucleolar marker for 1 h following a washing step in PBS and staining with PI in the presence of RNase. The percentage of cells in the respective cell cycle stage, and the standard errors were calculated from ten measurements each

and localization of components of the granular component visualized by antibody labeling of B23 was also not altered between untreated cells and samples labeled for 1 and 24 h with FITC-R₁₀ (Fig. 2a and data not shown).

To measure the efficiency of nucleolar labeling we determined the percentage of labeled cells at different times after application. Nearly 89% of the cells showed nucleolar fluorescence after 30 min and the number even increased to 98% at 24 h (Fig. 4a). Having FITC-R₁₀ in the growth medium for the initial 30 min or during the entire 24 h period yielded no difference in the nucleolar label and the cellular viability (Fig. 4a and data not shown). To further investigate the impact of the peptide transduction on membrane integrity we used the trypan blue exclusion test. No difference was measured between labeled and unlabeled control cells in the number of trypan blue positive cells, which was 1–2% (Fig. 4a).

Next, cells labeled for 24 h with FITC-R₁₀ were incubated for 10 min with fluorouridine (FU), which is preferentially incorporated into rRNA, and the incorporated nucleotide was detected by immunostaining to determine the amount of synthesized RNA in comparison to cells without nucleolar marker (Boisvert et al. 2000). The diagram in Fig. 4b displays the mean fluorescence intensity of 60 nuclei measured from low magnification confocal images. FU labeled cells with and without FITC-R₁₀ exhibited no difference in the level of incorporated nucleotide, i.e., no effect was detected on rDNA transcription.

Finally, to assess potential effects of FITC-R₁₀ on cell proliferation, we subjected HeLa cells with labeled nucleoli and unlabeled control cells to PI staining and flow cytometric analysis of cellular DNA content. The cells were incubated for 1 h with 10 μ M FITC-R₁₀ and then washed in PBS and grown at 37°C for 24 h. After

this incubation scheme the labeled and untreated control cells were methanol fixed and stained with PI including RNase treatment to measure the DNA amount for cell cycle distribution analysis. The control cells showed a cell cycle profile with 52% of cells in G1/G0, 32% in S-phase and 16% in G2/M. In comparison the cells incubated with 10 μ M of the nucleolar marker for 1 h showed some deviations from the control cell cycle profile 24 h post-labeling. The quantity of cells in G1/G0 was decreased to 43%, whereas the cells in S-phase increased to 42% concomitantly. The fraction of G2/M cells remained similar to the control cells (15%; Fig. 4c). These data suggest some delay in cells proceeding through S-phase indicated by an increase and a corresponding decrease of cells in G1/G0. The quantity of cells that exit the S-phase and continued to G2 and the mitotic division was stable also under the influence of the nucleolar marker, which fits the observation of increased confluency in cultures after 24 h.

Altogether, no major effect of the nucleolar marker on either membrane integrity, cell viability and proliferation, RNA synthesis or distribution of nucleolar components was observed at short- or long-incubation times.

Such a label is totally non-invasive and importantly works well in combination with other fluorochromes such as autofluorescent proteins or various dyes. Moreover, most cells not only established cell lines but also non-transfectable primary cultures were transduced with 90% or higher efficiency, and the nucleolar labeling needed only about 20 min to be readily visualized. Curiously, always a few cells remained unlabeled, which could be due to genetic or epigenetic differences in gene expression among the cells in the culture (Tyagi et al. 2001).

We conclude that the FITC labeled deca-arginine peptide does not interfere with major cellular processes at the concentrations tested. The combination of membrane permeability and nucleolar targeting in one peptide makes this transducible fluorescent marker for the nucleoli applicable to most mammalian cells and a novel and non-invasive tool for live cell microscopy.

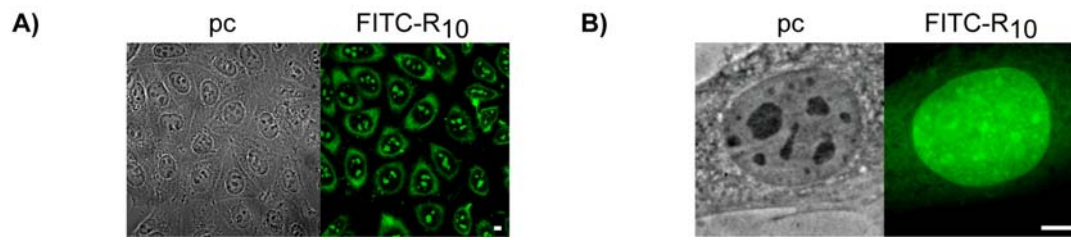
Acknowledgments We thank H.-P. Rahn and P. Pierschalek for technical help. GT was supported by the European Union (ESF Program). This work was funded by grants from the Deutsche Forschungsgemeinschaft to HL and MCC.

References

- Alvarez J, Hamplova J, Hohaus A, Morano I, Haase H, Vassort G (2004) Calcium current in rat cardiomyocytes is modulated by the carboxyl-terminal ahnak domain. *J Biol Chem* 279:12456–12461
- Andersen JS, Lam YW, Leung AK, Ong SE, Lyon CE, Lamond AI, Mann M (2005) Nucleolar proteome dynamics. *Nature* 433:77–83
- Boisvert FM, Hendzel MJ, Bazett-Jones DP (2000) Promyelocytic leukemia (PML) nuclear bodies are protein structures that do not accumulate RNA. *J Cell Biol* 148:283–292
- Brown DD, Gurdon JB (1964) Absence of ribosomal RNA synthesis in the nucleolate mutant of *Xenopus laevis*. *Proc Natl Acad Sci USA* 51:139–146
- Cardoso MC, Joseph C, Rahn HP, Reusch R, Nadal-Ginard B, Leonhardt H (1997) Mapping and use of a sequence that targets DNA ligase I to sites of DNA replication in vivo. *J Cell Biol* 139:579–587
- Chen HK, Pai CY, Huang JY, Yeh NH (1999) Human Nopp140, which interacts with RNA polymerase I: implications for rRNA gene transcription and nucleolar structural organization. *Mol Cell Biol* 19:8536–8546
- Cheutin T, O'Donohue MF, Beorchia A, Vandelaer M, Kaplan H, Defever B, Ploton D, Thiry M (2002) Three-dimensional organization of active rRNA genes within the nucleolus. *J Cell Sci* 115:3297–3307
- Dang CV, Lee WM (1989) Nuclear and nucleolar targeting sequences of c-erb-A, c-myc, N-myc, p53, HSP70, and HIV tat proteins. *J Biol Chem* 264:18019–18023
- Derenzini M, Pasquinelli G, O'Donohue MF, Ploton D, Thiry M (2006) Structural and functional organization of ribosomal genes within the mammalian cell nucleolus. *J Histochem Cytochem* 54:131–145
- Dietz GP, Bdeh M (2004) Delivery of bioactive molecules into the cell: the Trojan horse approach. *Mol Cell Neurosci* 27:85–131
- Franke WW (1988) Matthias Jacob Schleiden and the definition of the cell nucleus. *Eur J Cell Biol* 47:145–156
- Frankel AD, Pabo CO (1988) Cellular uptake of the tat protein from human immunodeficiency virus. *Cell* 55:1189–1193
- Green M, Loewenstein PM (1988) Autonomous functional domains of chemically synthesized human immunodeficiency virus tat trans-activator protein. *Cell* 55:1179–1188
- Hatanaka M (1990) Discovery of the nucleolar targeting signal. *Bioessays* 12:143–148
- Hernandez-Verdun D (2006) Nucleolus: from structure to dynamics. *Histochem Cell Biol* 125:127–137
- Lam YW, Trinkle-Mulcahy L, Lamond AI (2005) The nucleolus. *J Cell Sci* 118:1335–1337
- Martin RM, Leonhardt H, Cardoso MC (2005) DNA labeling in living cells. *Cytometry A* 67:45–52
- Mitchell DJ, Kim DT, Steinman L, Fathman CG, Rothbard JB (2000) Polyarginine enters cells more efficiently than other polycationic homopolymers. *J Pept Res* 56:318–325
- Olson M.O, Dunder M (2005) The moving parts of the nucleolus. *Histochem Cell Biol* 123:203–216
- Perry RP (1962) The cellular sites of synthesis of ribosomal and 4s RNA. *Proc Natl Acad Sci USA* 48:2179–2186
- Plander M, Brockhoff G, Barlage S, Schwarz S, Rothe G, Knuechel R (2003) Optimization of three- and four-color multiparameter DNA analysis in lymphoma specimens. *Cytometry A* 54:66–74
- Reynolds RC, Montgomery PO, Hughes B (1964) Nucleolar “Caps” produced by actinomycin D. *Cancer Res* 24:1269–1277
- Scheer U, Hock R (1999) Structure and function of the nucleolus. *Curr Opin Cell Biol* 11:385–390
- Sporbert A, Domaing P, Leonhardt H, Cardoso MC (2005) PCNA acts as a stationary loading platform for transiently interacting Okazaki fragment maturation proteins. *Nucleic Acids Res* 33:3521–3528

- Thoren PE, Persson D, Isakson P, Goksor M, Onfelt A, Norden B (2003) Uptake of analogs of penetratin, Tat(48–60) and oligoarginine in live cells. *Biochem Biophys Res Commun* 307:100–107
- Tunnemann G, Martin RM, Haupt S, Patsch C, Edenhofer F, Cardoso MC (2006) Cargo-dependent mode of uptake and bioavailability of TAT-containing proteins and peptides in living cells. *Faseb J* 20:1775–1784
- Tyagi M, Rusnati M, Presta M, Giacca M (2001) Internalization of HIV-1 tat requires cell surface heparan sulfate proteoglycans. *J Biol Chem* 276:3254–3261
- Vives E, Brodin P, Lebleu B (1997) A truncated HIV-1 Tat protein basic domain rapidly translocates through the plasma membrane and accumulates in the cell nucleus. *J Biol Chem* 272:16010–16017
- Wender PA, Mitchell DJ, Pattabiraman K, Pelkey ET, Steinman L, Rothbard JB (2000) The design, synthesis, and evaluation of molecules that enable or enhance cellular uptake: peptoid molecular transporters. *Proc Natl Acad Sci USA* 97:13003–13008

supplementary Fig. 1



3.3 Cargo-dependent mode of uptake and bioavailability of TAT-containing proteins and peptides in living cells

Cargo-dependent mode of uptake and bioavailability of TAT-containing proteins and peptides in living cells

Gisela Tünnemann,* Robert M. Martin,* Simone Haupt,[†] Christoph Patsch,[†] Frank Edenhofer,[†] and M. Cristina Cardoso*¹

*Max Delbrück Center for Molecular Medicine, Berlin, Germany; and [†]Institute of Reconstructive Neurobiology, Stem Cell Engineering Group, University of Bonn-Life and Brain Center and Hertie Foundation, Bonn, Germany

ABSTRACT Cell-penetrating peptides (CPPs) are capable of introducing a wide range of cargoes into living cells. Descriptions of the internalization process vary from energy-independent cell penetration of membranes to endocytic uptake. To elucidate whether the mechanism of entry of CPP constructs might be influenced by the properties of the cargo, we used time lapse confocal microscopy analysis of living mammalian cells to directly compare the uptake of the well-studied CPP TAT fused to a protein (>50 amino acids) or peptide (<50 amino acids) cargo. We also analyzed various constructs for their subcellular distribution and mobility after the internalization event. TAT fusion proteins were taken up largely into cytoplasmic vesicles whereas peptides fused to TAT entered the cell in a rapid manner that was dependent on membrane potential. Despite their accumulation in the nucleolus, photobleaching of TAT fusion peptides revealed their mobility. The bioavailability of internalized TAT peptides was tested and confirmed by the strong inhibitory effect on cell cycle progression of two TAT fusion peptides derived from the tumor suppressor p21^{WAF/Cip} and DNA Ligase I measured in living cells.—Tünnemann, G., Martin, R. M., Haupt, S., Patsch, C., Edenhofer, F., Cardoso, M. C. Cargo-dependent mode of uptake and bioavailability of TAT-containing proteins and peptides in living cells. *FASEB J.* 20, 1775–1784 (2006)

Key Words: cell-penetrating peptide • protein transduction • PCNA • PBD • Cre recombinase

THE PHENOMENON OF transduction denotes the size-independent *in vivo* delivery of a wide variety of cargoes into cells and is mediated by cell-penetrating peptides (CPPs). Although the internalization of fluorophores, nucleotides, peptides, globular proteins, nanoparticles, lipids, and drugs interconnected to CPPs into living cells has been described in the literature and resulted in measurable biological effects (1), the reported transduction experiments need to be critically evaluated in terms of the invasiveness of the detection methods utilized (2). Most known CPPs are parts of viral proteins or artificial derivatives thereof, and include several

arginines and/or lysines (reviewed in ref. 3). One of the best-studied CPP is a basic amino acid peptide from the transactivator of transcription (TAT) protein of the HIV-1 with the minimal transduction domain comprising amino acids 48–57 (4). The initializing step in the mechanism of cellular entry of CPPs is thought to be the strong ionic interaction between the positively charged amino acid residues and negatively charged plasma membrane constituents (5–7). Among the cationic groups mediating cellular uptake, the guanidinium group of arginine has been shown to be the most effective (8–10). Subsequent events needed for the internalization, however, differ between reports and are often conflicting. The first mechanistic studies led to the proposal that CPP internalization occurs rapidly in a receptor- and energy-independent manner (6, 9, 11–13) perhaps by destabilizing the lipid bilayer or by the formation of inverted micelles with subsequent release of their contents within the intracellular space (reviewed in ref. 14). More recently, an active mechanism based on vesicular uptake has been proposed as the general mode of internalization of CPP constructs into cells (15–19).

To understand whether the mechanism of entry is dependent on the cargo connected to the CPP, we directly compared TAT fused to globular proteins and TAT-containing peptides with respect to their uptake kinetics and their intracellular distribution after internalization in living cells. Transduced constructs were also analyzed for their ability to reach their targets inside the cell and to exert their biological activity.

MATERIALS AND METHODS

Peptides and proteins

Peptides (complete description in **Table 1**) were synthesized by Biosyntan GmbH (Berlin, Germany), Peptide Specialty Laboratories (Heidelberg, Germany), and Bachem (Weil am

¹Correspondence: Max Delbrück Center for Molecular Medicine, Robert-Rössle-Str. 10, Berlin 13125, Germany. E-mail: cardoso@mdc-berlin.de
doi: 10.1096/fj.05-5523com

TABLE 1. List of peptides and their uptake efficiencies^a

Peptide and label	aa sequence	kDa	pI	Peptide concentration	Transduction efficiency	Transduction threshold
R-PTD ₄	YARAARQARA	1.13	11.71	10 μ M	0%	400 μ M
F(Ahx)-TAT	YGRKKRRQRRR	1.93	12.31	1 μ M	90%	1 μ M
R-TAT (ri)	rrrqrkkrg	1.81	13.3	1 μ M	90%	1 μ M
bt-NLS	SGYGPKKKRKVG	1.93	10.68	10 μ M	0%	n.a.
Lig1-PBD-F	MQRDIMSFFQPTKEFKAKK	2.80	10.00	10 μ M	0%	n.a.
R-TAT-HA2(ri)	rrrqrkkrg-gdimgewneifgaigflg	3.24	11.71	10 μ M	80%	0.1 μ M
F(Ahx)-TAT-Control	YGRKKRRQRRR-TALDASALQTE	3.05	11.72	20 μ M	70%	n.d.
R-TAT(ri)-p21-PBD	rrrqrkkrg-aaA-GRKKRRQTSMTDFYHSKRRLIFSa	4.96	12.43	20 μ M	90%	7.5 μ M
TAT-Lig1-PBD-R	YGRKKRRQRRR-GGG-MQRSIMSFFQPTKEGKAKK	4.38	12.14	10 μ M	80%	5 μ M

^aR, TAMRA/rhodamine; F, FITC; Ahx, aminohexanoic acid; capital letters, L-amino acids; small letters, D-amino acids; ri, retro inverso; n.a., not applicable; n.d., not determined.

Rhein, Germany). The PCNA binding domain (PBD) peptide TAT-p21-PBD is derived from human p21^{WAF/Cip} (20) and the Lig1-PBD as well as TAT-Lig1-PBD from mouse DNA Ligase I (21, 22). The peptides were analyzed by HPLC a second time at the end of the experiments to assure their stability under the storage conditions. The pI of the peptides was calculated using the program ProtParam (<http://au.expasy.org/cgi-bin/protparam>). His-NLS-TAT-Cre-recombinase (TAT-Cre) protein was produced, purified (23), and labeled with Alexa Fluor 633 or rhodamine as described (24). BL21(DE3) cells (Novagen, Madison, WI, USA) were used for production of His-PTD₄-PCNA. Bacterial cultures were grown at 37°C until early-mid log phase and expression was induced by addition of 1 mM IPTG. Cells were harvested 3 h after induction, lysed by lysozyme treatment and ultrasonification, and His-tagged protein purified to >95% purity from cell lysates by affinity chromatography using Talon resin material (BD Bioscience, Franklin Lakes, NJ, USA) according to the manufacturer's instructions. The purified protein was labeled with Atto 633 NHS ester (Fluka, St. Louis, MO, USA) in 0.1 M bicarbonate buffer pH 8.5, then further purified and rebuffered into PBS pH 7.4 over a G25-Sephadex column (Pharmacia, Cambridge, MA, USA). BL21(DE3) CodonPlus-RIL cells (Novagen) were used to produce His-TAT-MK2 (MAPKAP kinase 2). Bacterial cultures were grown and induced as above, and harvested cells were disrupted by 2-fold homogenization at a 1000 bar with a SLM AMINCO FrenchPress (Spectronic Instruments, Leeds, UK). More than 98% pure protein was obtained from the lysates upon Talon affinity chromatography, as before (BD Bioscience). The purified protein was labeled with Cy5 NHS ester (Amersham Bioscience, Arlington Heights, IL, USA) in 0.1 M bicarbonate buffer pH 8.5, then further purified and rebuffered into PBS pH 7.4 over a G25-Sephadex column (Pharmacia). The Cy5-labeled streptavidin (Amersham) was incubated for 30 min prior to the experiments with NLS-biotin peptides at molar ratios of 1:1 for biotin and biotin binding sites at homotetrameric streptavidin. The streptavidin-coated Quantum dots 525 were obtained from Quantum dot Corp. (Hayward, CA, USA).

Cell culture

The C2C12 mouse myoblast cells and C2C12 mouse myoblasts stably transfected with GFP-PCNA as a fluorescent cell cycle marker were cultured as described (25, 26). Flp 3T3 mouse fibroblasts were from Invitrogen (Carlsbad, CA, USA). 3T3-FDR1.2 Cre reporter cells (27) were cultured in Dulbecco's modified Eagle medium (DMEM) containing 10% fetal calf serum (Life Technologies, Inc., Grand Island, NY, USA). For

live cell microscopy, cells were plated onto 4- or 8-well LabTek coverglass chambers (NalgeNunc, Rochester, NY, USA).

Transduction assays and inhibitor treatments

All peptide and protein transduction experiments, except for the Cre recombinase assay (see below), were performed exclusively with living cells plated on 4- or 8-well LabTek coverglass chambers using an objective heated to 37°C. For transduction experiments, the medium was removed and PBS with the different peptides or proteins was applied directly to the cells. After 10 min incubation, PBS was replaced with the growth medium. Usually uptake was studied continuously starting with the peptide application over a period of at least 2 h, followed by incubation of the cells at 37°C under humidified atmosphere until additional image collection. Transduction efficiencies of peptides were determined by counting the numbers of cells with or without nucleolar signals and internalization efficiencies of proteins by counting cells with or without intracellular vesicles directly on the fluorescence microscope in three fields of view, each containing ~50 cells, or by a similar analysis performed on low magnification overview images. Cell viability after peptide or protein application was monitored by their ability to undergo complete mitotic cell cycles and grow to confluency over a period of 24 to 48 h. Membrane integrity was ascertained by the Trypan blue exclusion assay. Cytochalasin D (Sigma, St. Louis, MO, USA) was dissolved to 10 mg/ml in DMSO and sodium azide (Sigma) to 10% (w/v) in ddH₂O. Both stock solutions were adjusted to 1×PBS at the indicated final concentrations (Fig. 2) before being applied to living cells. The potassium buffer (Fig. 2) corresponds to PBS with all sodium-containing compounds substituted for the equivalent potassium-containing analogues. C2C12 mouse myoblasts were preincubated for the indicated times (t in Fig. 2) with different inhibitors in PBS or the potassium buffer. The TAT-containing peptide and protein were applied directly to the cells and mixed gently. For the potassium phosphate buffer experiment, the protein was dialyzed against the potassium buffer prior to application. After 10 min the cells were washed twice and incubated for another 20–60 min (as annotated in the phase contrast images for each treatment) in DMEM medium, except for the potassium buffer treatment where the medium was replaced by potassium buffer. Transduction thresholds were determined by incubating C2C12 mouse myoblasts with CPP-containing peptides in medium at different concentrations ranging from 0.1 to 500 μ M for 1 h. The lowest peptide concentration leading to accumulation

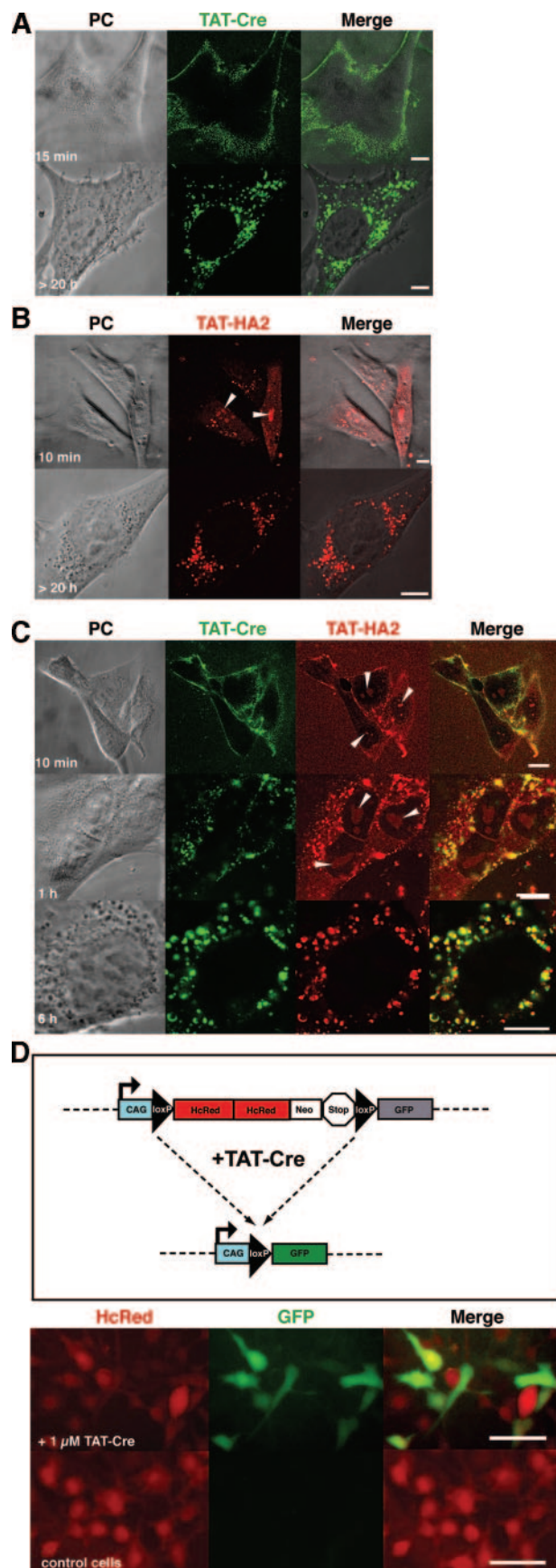


Figure 1. Differences in subcellular distribution of proteins and peptides fused to TAT after internalization in living cells. TAT-Cre and TAT-HA2 were applied to the cells for 10 min,

inside nucleoli was considered to be the transduction threshold from which transduction occurs.

Microinjection and bead loading

Intracellular delivery of the Lig1-PBD-F peptide was accomplished by bead loading using 100 μ m silica beads. The beads were washed first in ethanol, then in growth medium, and finally pipetted onto the medium of cells grown in a self-made culture dish with a coverglass bottom. The Lig1-PBD-F solution was added subsequently and the chamber was shaken a few times. The beads were removed for microscopic observation of the labeled cells. Microinjection of the NLS-biotin peptide complexed with streptavidin-Cy5 was performed using an Eppendorf microinjection and micromanipulation system mounted on a Zeiss LSM510Meta inverted microscope setup. The parameters for cytoplasmic microinjection were set to 0.7 s injection time with 15 fPa injection pressure.

Cre recombinase double reporter assay

3T3-FDR1.2 cells (27) were cultured to 50% confluency in 6-well plates. The pFDR reporter gene construct allows detection of bioactive Cre recombinase by switching from constitutive HcRed to GFP expression (Fig. 1 D). For transduction, the cells were incubated with 2 μ M TAT-Cre protein diluted into a 50:50 mixture of PBS and DMEM for 3 h, washed once with PBS, then cultivated in normal medium. Fluorescence microscopy was performed 24 h after transduction.

Live cell assay for cell cycle inhibition

C2C12 mouse myoblasts stably expressing GFP-PCNA (26) were synchronized by mitotic shake-off and plated onto 8-well LabTek coverglass chambers. After becoming adherent, the number of cells that entered S-phase was counted and cells

followed by a washing step and change to growth medium without the protein/peptide. Confocal microscopy of live cells was started immediately and cells were returned to the incubator between time points, which are indicated. Representative images and time points are shown. A) Uptake of 2.5 μ M TAT fusion protein TAT-Cre (rhodamine-labeled) in living mouse myoblasts. After application of TAT-Cre, internalization started throughout the plasma membrane in the form of vesicles. The next day vesicles containing fluorescent TAT-Cre accumulated in the cytoplasm. B) Diffused and vesicular distribution of the TAT-HA2 peptide (rhodamine-labeled, 5 μ M final concentration) soon and a long time after application. C) Simultaneous application of 2.5 μ M TAT-Cre protein (Alexa Fluor 633-labeled; 1.7 label to protein ratio) and 5 μ M TAT-HA2 peptide (rhodamine-labeled) on living cells resulted in prominent vesicular uptake of the protein into the cytoplasm, whereas the TAT-HA2 peptide also displays a diffuse distribution in cytoplasm and nucleoplasm, and accumulation in nucleoli. The fluorescent fusions colocalize in the majority of vesicles. Nucleoli are indicated by arrowheads. Scale bar = 10 μ m. D) Analysis of Cre recombinase activity in TAT-Cre-treated reporter cells. 3T3-FDR1.2 reporter cells contain a loxP-flanked HcRed gene, followed by a nonexpressed GFP gene. TAT-Cre treatment induces recombination of the reporter gene, resulting in a shift from red to green fluorescence (scheme). Untreated control cells do not exhibit green fluorescence. Cells were incubated with 2 μ M TAT-Cre for 3 h and analyzed by fluorescence microscopy 24 h later. Scale bar = 50 μ m.

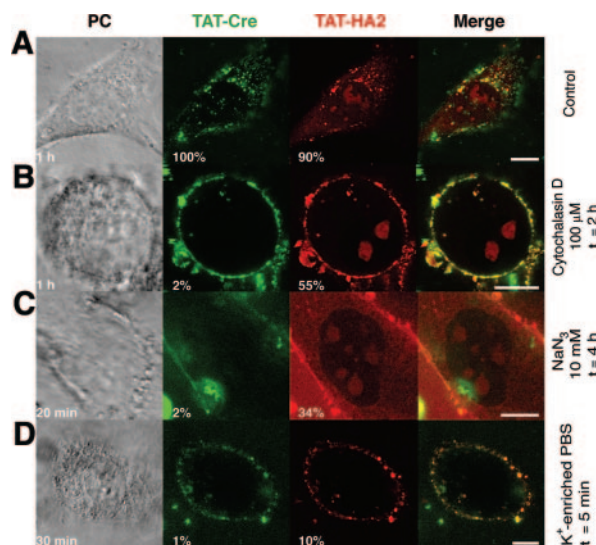


Figure 2. Different mode of uptake of proteins and peptides fused to TAT in living cells. Simultaneous incubation of living mouse myoblasts with 2.5 μ M TAT-Cre and 5 μ M TAT-HA2 was as shown in Fig. 2C. Confocal images show representative snapshots at the indicated time points in the phase contrast image. The numbers in the images reflect the overall percentage of cells showing intracellular vesicles for the TAT fusion protein and the nucleolar signal for the TAT-HA2 peptide. Substances at the concentrations indicated were preincubated with the cells before addition of the TAT fusions for the indicated time (t) and kept in the culture medium or buffer throughout the experiment. A) Control C2C12 mouse myoblasts treated with the TAT-containing protein and peptide mixture showed internalization in 100% and 90% of the cells, respectively. B) Preincubation of the cells with 100 μ M of the F-actin elongation inhibitor cytochalasin D blocked protein uptake completely, but the peptide still transduced into the cells. C) ATP depletion with 10 mM sodium azide reduced entry of both species, albeit a third of the cells still took up the peptide. D) 5 min incubation of the cells in sodium-deficient, iso-osmolar PBS strongly reduced peptide transduction and blocked protein uptake. t = preincubation time, scale bar = 10 μ m.

were transduced with fluorescently labeled TAT-p21-PBD, TAT-Lig1-PBD, and the unspecific TAT control peptide at 20 μ M concentration in PBS. 10 min later the solutions were aspirated, and the cells were washed twice with medium and kept in growth medium thereafter. The percentage of cells in S-phase was determined directly from the subnuclear focal pattern of GFP-PCNA by counting 10 fields of view at the indicated time points for each peptide. Data of three independent experiments were evaluated.

Microscopy, image acquisition, and analysis

Live cell microscopy was performed with a Zeiss LSM 510 Meta confocal setup mounted on an Axiovert 200 M inverted microscope using a 63 \times phase contrast plan apochromat oil objective NA1.4. For all acquisition settings, the main beam splitter was HFT UV/488/543/633. The parameters specific for each fluorochrome were: FITC, excited at 488 nm light, detected with a 500–530 nm bandpass (BP) filter; TAMRA or rhodamine excited with 543 nm, detected with 565–615 BP and Cy5 or Alexa633 excited at 633 nm and detected with a 650 nm longpass filter.

Image acquisition was done sequentially to minimize cross-talk between the fluorophores. Phase contrast images were

recorded simultaneously with FITC/GFP fluorescence in the transmission channel. Fluorescence recovery after bleaching (FRAP) experiments (Fig. 3) was performed on a Zeiss LSM 5 Live confocal microscope with 100% power of a 75 mW DPSS 532 nm laser. The bleaching was performed in a stripe for 0.44 s, followed by a time series with 400 images recorded at 20 frames per second. Using the Zeiss LSM 510 software version 3.2, the mean fluorescence intensity in the bleached nucleoli and cytoplasm was determined over the time course and averaged for 10 cells. Fluorescence intensity was normalized to zero at the start of recovery and to one at equilibrium to directly compare the curves for both subcellular regions. The FRAP curves were generated with Origin 7 software.

RESULTS

Direct comparison of TAT-mediated peptide and protein uptake in living cells

To study the characteristics of TAT-mediated introduction of globular proteins into living cells, the rhodamine-labeled fusion protein R-TAT-Cre consisting of the CPP TAT moiety and the site-specific Cre recombinase of bacteriophage P1 (23) was applied onto C2C12 mouse myoblasts. As soon as the fluorescent solution was washed off (after 10 min of incubation), fluorescent vesicles emerging from the intracellular side of the plasma membrane were detectable by confocal microscopy (Fig. 2A, upper panel). After additional overnight cultivation, all cells showed a substantial amount of internalized protein stored in vesicles, but release of the protein from the vesicles could not be detected by this method (Fig. 2A, lower panel). Other recombinant proteins showed identical trapping in cytoplasmic vesicles (data not shown) independent of 1) which short basic CPP they were fused to, 2) the fluorophore they were conjugated to, and 3) their known subcellular localization. For instance the nuclear protein His-PTD₄-PCNA (Atto 633-labeled) as well as the nuclear and cytoplasmic protein His-TAT-MK2 (Cy5-labeled) could only be detected inside cytoplasmic vesicles after internalization, and refused to localize at their targets during an observation period of up to 48 h. Proteins lacking a transduction domain could also be internalized in the same manner but the efficiency of internalization was shown to be much lower (23). TAT-Cre was also tested at concentrations between 0.1 and 10 μ M with no difference in the uptake behavior (data not shown).

A recent report proposed that the uptake of proteins fused to TAT belongs to the class of rapid lipid raft-mediated macropinocytosis and that the protein could be released from macropinosomes by cotransduction of the fusogenic peptide TAT-HA2 (17). We therefore used TAT-HA2 (Table 1) to 1) work out the characteristics of TAT-mediated peptide (<50 amino acids; ref. 28) transduction and 2) try and liberate the TAT fusion protein trapped into vesicles. Compared to the internalization of proteins, uptake of the TAT-HA2 peptide occurred on a quite different time scale and also showed dissimilarities in its subcellular localization. During the first 3–5 min of incubation with the peptide

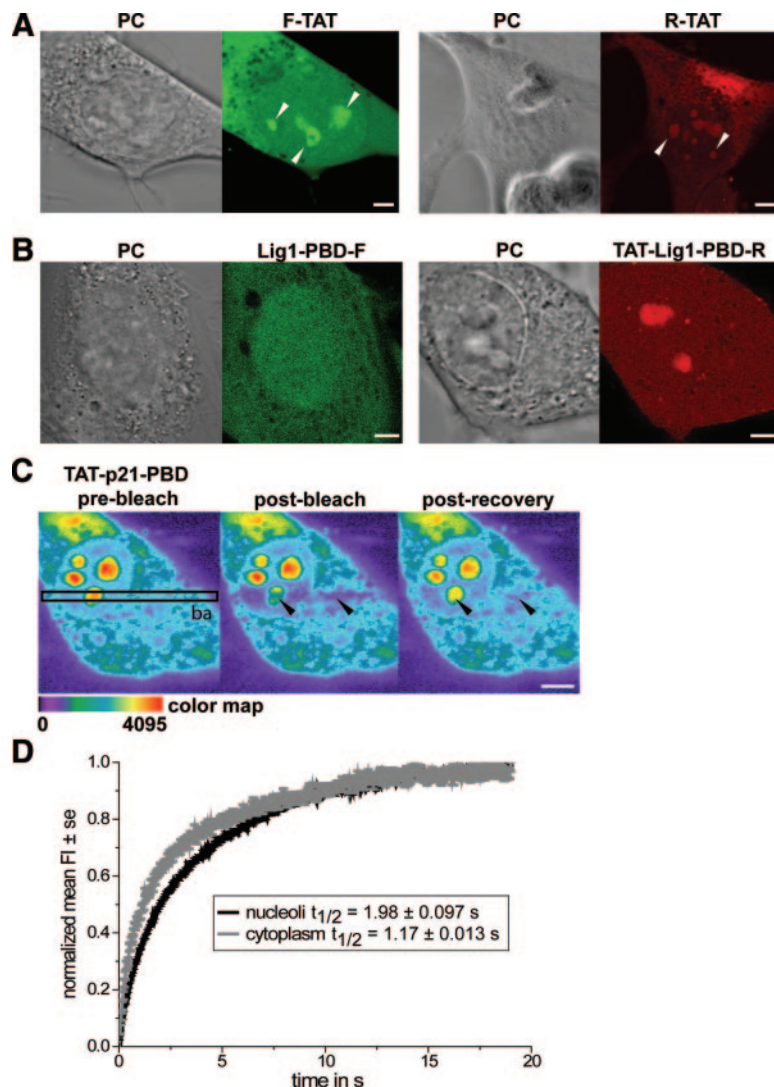


Figure 3. Subcellular localization and intracellular mobility of TAT peptides. *A*) FITC- and rhodamine-labeled TAT peptides (F-TAT 1 μ M, R-TAT 1 μ M) applied to mouse myoblasts were rapidly internalized and accumulated in the nucleoli (white arrowheads). The fluorescent label has no influence on peptide distribution. *B*) In contrast, the non-TAT-containing peptide Lig1-PBD (FITC-labeled) delivered by bead loading showed a homogeneous distribution in nucleus and cytoplasm whereas the addition of the TAT sequence in TAT-Lig1-PBD (rhodamine-labeled) again led to nucleolar accumulation. *C*) Mouse myoblasts were transduced with 20 μ M of TAMRA-labeled TAT-p21-PBD for 10 min, washed, then incubated in growth medium. The FRAP experiment was performed by bleaching a stripe (ba) encompassing one nucleolus and a part of the cytoplasm as seen in the prebleach image. After bleaching, a time series was recorded at a time resolution of 20 frames/second over 20 s. False color images depicting the fluorescence intensity distribution as color map (red denotes highest intensity) of one photobleached cell are shown. The black arrowheads point to the bleached nucleolus and cytoplasmic regions in the first image after the bleaching process (postbleach) and after full fluorescence recovery (postrecovery). *D*) Curves represent the normalized mean fluorescence intensity of the fluorescence recovery in the nucleoli and cytoplasm averaged for 10 measurements. Albeit accumulated in the nucleoli, the TAT-p21-PBD peptide was highly mobile with a half-time of recovery of 1.98 ± 0.097 s. In the cytoplasm, the half-time of recovery is faster (1.17 ± 0.013 s). Scale bar = 5 μ m.

solution, fluorescence signals had already become visible in the nucleoli; after exchange of the fluorescent solution against medium, a diffuse distribution throughout the cell, with accumulation in the nucleoli, could be detected (Fig. 2*B*, upper panel, arrowheads; see also supplemental movie) in addition to a few developing vesicles adjacent to the membranes. Over longer periods of observation, the diffuse population of the peptide in the cytoplasm, nucleoplasm, and nucleoli became markedly weaker, and in most of the cells vanished overnight. In stark contrast, the peptide-containing cytoplasmic vesicles seemed to be unaffected and their number increased overnight, resulting in a vesicular ring concentrated around the nucleus (Fig. 2*B*, lower panel). The diffusely distributed fraction of the transduced peptide was detected in $\sim 90\%$ of the cells (Table 1) whereas after overnight incubation all cells showed peptide uptake into vesicles. The loss of diffusely distributed fluorescent peptide in the cytoplasm and nuclei overnight cannot be just a consequence of instability of the fluorophore/peptide in the cell since 1) a rhodamine-labeled antibody (Ab) persisted inside cells for > 24 h (data not shown) and 2)

the fluorescently labeled peptide TAT-HA2 is composed of protease-resistant D-amino acids.

To directly compare the mode and kinetics of uptake of TAT peptides and globular proteins fused to TAT into cells and determine whether TAT-HA2 could drive release of the protein stored in macropinosomes, the Alexa Fluor 633-labeled TAT-Cre protein and the rhodamine-labeled TAT-HA2 peptide were applied simultaneously to living cells. The short- and long-term uptake characteristics for both species remained mostly unchanged (Fig. 2*C*). Detectable TAT fusion protein was restricted to cytoplasmic vesicles whereas the TAT-HA2 peptide, besides being trapped into vesicles, was rapidly distributed throughout the entire cell. TAT-HA2 and TAT-Cre colocalized in the majority of cytoplasmic vesicles (Fig. 2*C*, yellow color in merged images). Although both species intermingled substantially, a release of the TAT fusion protein from macropinosomes and entry into the nucleus could not be detected by this method. To test the presence of a low level of TAT-Cre within the nucleus, we used a far more sensitive reporter assay based on Cre-mediated recombination. Since site-specific recombination provides a stable and unambigu-

ous read-out for protein transduction (23, 29–31), we used a NIH-3T3 Cre reporter cell line containing a stably integrated gene cassette consisting of a constitutively expressed HcRed gene, followed by a nonexpressed GFP gene. Upon Cre recombinase-mediated site-specific recombination, excision of the HcRed gene takes place with concomitant expression of the GFP gene (Fig. 2D; L. Nolden and F. Edenhofer, personal communication). Using this more sensitive assay, several cells within the culture exhibited GFP expression upon incubation with TAT-Cre overnight (Fig. 2D). These data indicate that a low level of TAT-Cre below the detection range of confocal microscopy was biologically available and could exert its enzymatic activity.

Different mode of entry of proteins and peptides fused to TAT in living cells

To test whether TAT fusion proteins and TAT-containing peptides use different routes of entry and can, as a result, be affected differently in their uptake by treatment with inhibitors, mouse myoblasts were preincubated with inhibitors or buffers, followed by simultaneous application of TAT-Cre and TAT-HA2 (as in Fig. 2C). Subsequently, cells were washed twice and kept in the indicated buffer or medium with constant inhibitor concentration throughout the entire experiment.

Endocytosis requires the formation and migration of vesicles along the cytoskeleton. Therefore, constant concentrations of the F-actin depolymerizing drug cytochalasin D should delay or block internalization of the endocytosed TAT constructs at the membrane level (32, 33). After cytochalasin D treatment, the TAT fusion protein and TAT-HA2 showed strong membrane association, but the diffused fraction of the TAT-HA2 peptide was still detectable inside the cells in nucleoli, albeit the transduction efficiency (as scored by the percentage of cells showing intracellular fluorescence) was reduced to half. All vesicular uptake was abolished (Fig. 1B). Despite the round appearance of the cells indicative of the disruptive effect of the drug on the actin cytoskeleton, the membrane integrity was not decreased as assayed by Trypan blue exclusion (data not shown).

Endocytosis is an energy-consuming process and is therefore blocked by the metabolic inhibitor sodium azide. Accordingly, treatment with 10 mM sodium azide resulted in almost complete inhibition of the internalization of the TAT fusion protein (scored by the absence of intracellular vesicles), whereas the diffused population of the TAT-HA2 was still detected in about one-third of the cells (Fig. 1C).

A recent report proposed that synthetic guanidinium-rich molecules traverse biological membranes by formation of lipophilic ion pairs between the guanidinium groups and abundant phosphate, sulfate, and carboxylate functions on the membrane surface, allowing cell entry by diffusion along the membrane potential and subsequent release of the positively charged CPP into the cytoplasm (5, 10). The directionality of

this process is achieved by the membrane potential and the latter can be efficiently reduced by addition of an isotonic buffer with potassium concentrations equivalent to those found intracellularly (34, 35). We tested this hypothesis by preincubating the cells for 5 min with potassium-enriched, isotonic PBS and adding the peptide/protein solution in the same buffer. This treatment abolished the vesicular internalization of both TAT species. Furthermore, it resulted in strong inhibition of the uptake mode responsible for the intracellularly diffused fraction of TAT-HA2 (Fig. 1D). In summary, in contrast to TAT fused to globular proteins, TAT fusion peptides transduce into cells by a different and very rapid mode that is dependent on the plasma membrane potential. We therefore further investigated the transduction potential and biological applicability of TAT fusion peptides.

Uptake and intracellular availability of TAT-containing peptides

In the first minutes of incubation, the TAT-HA2 peptide flooded into living cells and accumulated in nucleoli; later it was also localized in cytoplasmic vesicles (Fig. 2B, C). To test whether these uptake characteristics were influenced by the HA2 moiety or instead were a general feature of TAT-mediated peptide internalization, several TAT peptide complexes were analyzed for their transduction behavior and intracellular distribution after internalization. Table 1 summarizes the peptides and their respective transduction efficiencies determined, as earlier, by counting the percentage of cells showing intracellular diffused fluorescence upon 10 min incubation with the indicated peptide concentrations and analyzed by confocal microscopy of living cells. The most efficient peptide was the 11 amino acid TAT peptide covalently linked to either a FITC (F) or a rhodamine (R) fluorophore, which was transduced into 90% of all cells at 1 μ M concentration within the first 3 min of observation. The fluorescent signal appeared diffused in the cytoplasm and nucleoplasm and showed strong accumulation of the labeled peptide in nucleoli (Fig. 3A). To test whether the nucleoli accumulation was due to the TAT moiety, we used non-TAT-containing peptides (Lig1-PBD in Fig. 3B and NLS-biotin peptide complexed with streptavidin-Cy5 [data not shown]) and delivered them into the cytoplasm using either bead loading or microinjection. Both peptides were stable intracellularly and able to enter the nucleus, but were not accumulated in the nucleoli (Fig. 3B and data not shown). The same Lig1-PBD peptide fused to TAT (TAT-Lig1-PBD) transduced into cells and again showed nucleolar localization (Fig. 3B), indicating that the nucleolar localization is dependent on the TAT characteristics. We investigated other reported CPPs—namely, PTD4 (36)—which showed only detectable uptake (Table 1) at very high concentrations (400 μ M). This suggests that nucleolar association is mediated by the high concentration of positive charges due to arginine and lysine residues.

Since TAT fusion peptides exhibited accumulation in the nucleolar compartment whereas the cargo peptide or protein may perform its function in a different subcellular compartment, we tested the overall bioavailability of cargoes connected to TAT by directly measuring the mobility in living cells using fluorescence photobleaching analysis. Cells transduced with a TAT-containing peptide (TAT-p21-PBD, Table 1) were imaged, and a rectangular region was selected to include one nucleolus and a stripe of cytoplasm. The peptide fluorescence in this stripe was subsequently photobleached with a high intensity laser beam, and redistribution of fluorescence was measured over time until full equilibrium was regained. The peptide intensity distribution before (prebleach), immediately after (postbleach), and at full recovery (postrecovery) is shown in representative false color images in Fig. 3C. The recovery of fluorescence in the bleached region indicates the mobility of peptides from unbleached cellular regions into the bleached area, and therefore is a direct measure of peptide mobility in the living cells. The kinetics of recovery (Fig. 3D) indicated that the peptides, although concentrated in the nucleoli, were mobile with a half-time of recovery of 1.98 and 1.17 s in the nucleoli and cytoplasm respectively. This kinetic difference between nucleoli and cytoplasm suggests binding of the TAT-PBD-p21 within the nucleoli. The high intracellular mobility of the TAT peptides raises the possibility of achieving successful biological effects despite the unfavorable subcellular accumulation.

Cell cycle inhibition by transduced PCNA binding peptides

To directly test whether the transduced TAT peptides in view of their high mobility could be effective in reaching their intracellular targets and exerting a biological effect, we used fusions of TAT with two different peptides comprising the proliferating cell nuclear antigen (PCNA) binding domain (PBD) of p21^{WAF/CIP} and DNA Ligase 1 (Table 1). These two peptides have been shown to bind to PCNA (20, 22). We reasoned that since several PCNA interacting proteins required for S-phase progression utilize the same binding interface on the surface of PCNA, competition for binding should ensue and inhibition of cell cycle progression would be expected. Mouse myoblasts stably expressing the cell cycle progression marker GFP-PCNA (26) were synchronized in the G₁ phase of the cell cycle by mitotic shake off. After becoming adherent, the G₁ synchronized cells were incubated for 10 min with either of these two TAT-PBD peptides as well as a control TAT fusion peptide (37). After washing, peptide uptake efficiency was controlled for by counting the percentage of cells showing intracellular peptide fluorescent signal as before. At different times thereafter, the ability of cells to progress into S-phase was determined by counting the number of S-phase cells scored by the characteristic focal GFP-PCNA subnuclear distribution pattern (see green subnuclear signal in the examples

shown in images in Fig. 4 and ref. 26) directly under the fluorescent microscope. The results of this live cell cycle assay are summarized in Fig. 4. While 70% control cells and cells incubated with TAT control peptide were in S-phase 6 h after peptide incubation, only ~40% TAT-PBD-treated cells entered S-phase within the same time. This inhibition is even more noteworthy if one considers that the peptides were incubated with the cells for only 10 min, after which they were washed away. Toxic effects were not detected by either the Trypan blue exclusion test or by changes in cell morphology. These data demonstrate that both TAT-PBD peptides were bioactive and capable of decelerating cell cycle progression despite the short incubation time and their accumulation in the nucleolus (see also red fluorescence peptide signal in the images in Fig. 4).

DISCUSSION

Although it is generally agreed that the first step in the internalization process of CPP-mediated transduction is the strong ionic interaction between the cationic CPP and negatively charged plasma membrane constituents (6, 15, 38), subsequent steps for CPP-induced cell entry differ in the recent literature and range from endocytic (15, 19) to a rapid and energy-independent process (6, 12). Most studies so far have used fixed cell analysis, which has been shown to result in artificial internaliza-

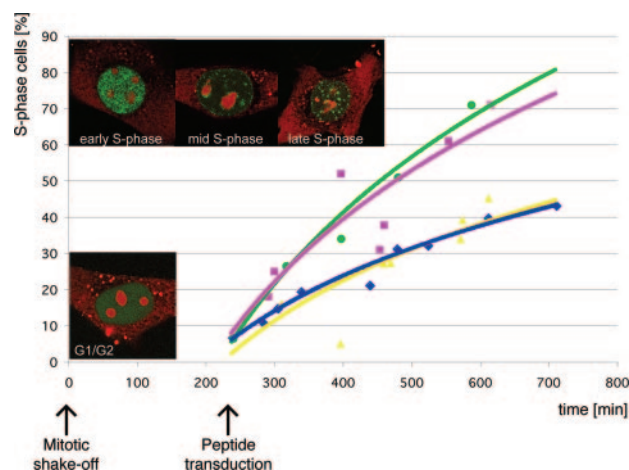


Figure 4. Effect of transduced PBD-containing TAT peptides on cell cycle progression. After mitotic shake-off, GFP-PCNA-expressing mouse myoblasts were allowed to attach and were incubated with different peptides (20 μ M) for 10 min, followed by washing and a change to growth medium. The percentage of S-phase cells was determined at various time points by the subnuclear replication foci pattern of GFP-PCNA. Representative confocal microscopy images of mouse myoblasts transduced with the TAMRA-labeled TAT-p21-PBD peptide (red) show either a diffused distribution of GFP-PCNA (green) in the nucleus, indicating G₁- or G₂-phase or focal GFP-PCNA labeling of replication foci during early, mid and late S-phase. Data points of three independent experiments were fitted logarithmically. Control cells, pink squares; TAT control peptide, green spheres; TAT-Lig1-PBD peptide, yellow triangles; and TAT-p21-PBD peptide, blue diamonds.

tion of CPP-containing constructs. In this work we used exclusively live cell analysis and tested whether the mode of entry is dependent on the cargo connected to the CPP and what the fate and bioavailability of the transduced peptides is.

By directly comparing the uptake of TAT connected to peptides and globular proteins into living cells, we found that the mechanism of entry depends on the size of the cargo fused to TAT. The major fraction of TAT-containing proteins or peptides was taken up into living cells by distinct modes, with the proteins mostly ending up in cytoplasmic vesicles and the peptides distributing throughout the cell and accumulating in the nucleoli (Fig. 2).

The vesicular storage inside the cytoplasm was a general feature of different recombinant proteins fused to a CPP and was independent of protein function, CPP (data not shown), and fluorescent label (Fig. 2A, C). A small population of TAT fusion protein reached the cytosol and nucleus via a different pathway or leaked out from the vesicles, as we detected Cre recombination activity in the nuclei using an extremely sensitive and unambiguous reporter assay for TAT-Cre. This fraction of bioavailable TAT-Cre was not high enough, however, to be detected by direct confocal microscopy of the labeled TAT-Cre protein whereas the population trapped in vesicles was easily detectable. Furthermore, cotransduction of the fusogenic peptide TAT-HA2 (17) did not substantially increase the release of the different TAT fusion proteins from cytoplasmic vesicles as assayed by live cell confocal microscopy (Fig. 2C).

Unlike CPP fusion proteins, TAT fusion peptides could be seen diffusely distributed throughout the cell and concentrated in nucleoli (Fig. 2 and Table 1). Uptake occurred rapidly within 3–5 min after application of the TAT construct on living cells. Upon longer observation times, the diffusely distributed fraction of the TAT peptides disappeared and cytoplasmic vesicles containing the peptides became apparent, suggesting that the peptides were either redistributed or underwent an additional vesicular uptake.

In addition to different uptake kinetics and localization after internalization of proteins and peptides fused to CPPs, inhibitors of endocytosis efficiently blocked the vesicular uptake of both species while having a minor effect on the TAT peptide transduction (Fig. 1), indicating that the latter does not depend on vesicle formation and/or traffic along the cytoskeleton. In fact, the only treatment capable of blocking not only the vesicular uptake of CPP-containing proteins and peptides, but also the rapid translocation of TAT peptides leading to a diffuse intracellular distribution, was incubation of the cells with a sodium-deficient iso-osmolar buffer (Fig. 1), indicating an alternative distinct cellular entry pathway based on membrane potential.

To understand which properties of cargoes fused to TAT allow the rapid membrane transduction, we compared the cellular entry of various TAT-containing constructs (Table 1). Fluorescently labeled TAT had already appeared inside the nucleoli of 90% of living

cells at a concentration of 1 μ M. The uptake efficiencies were decreased for TAT fusion peptides. By comparison, differences in the overall pI of TAT due to the addition of a cargo resulted only in minor effects on transduction efficiencies, whereas the amino acid composition of the CPP itself seemed to be more important. For instance, PTD₄ containing three arginines transduced into living cells only at concentrations of >400 μ M whereas TAT peptides with eight positive charges (six of them arginines) transduced quite efficiently in a range of 0.1–10 μ M (Table 1). Most transduction efficiencies were tested for the CPP TAT at concentrations of 10 μ M and resulted in comparable high percentages of transduced cells. However, differences for individual peptides were found to be dependent on the concentration used; for instance, the TAT-HA2 peptide was already diffusely distributed inside cells at a concentration of 0.1 μ M, whereas for TAT-p21-PBD uptake was restricted to endocytosis below a concentration of 7.5 μ M, and only above 7.5 μ M did the peptide enter rapidly and appear in the nucleoli (Table 1). The existence of such a concentration threshold can also explain conflicting reports assigning CPP-mediated membrane translocation to endocytosis (19, 39) or to an unknown mechanism, resulting in a homogeneous distribution in the whole cell (7). Another parameter that should be taken into account is the stability of the transducible peptides themselves since it was shown that CPP peptides could be degraded by extra- and intracellular proteases (40). However, we have not observed dramatic differences in the transduction efficiencies between TAT-HA2 consisting of D-amino acids and other potentially degradable peptides consisting of L-amino acids at comparable concentrations (Table 1).

The TAT-containing peptides exhibited a strong affinity to the nucleolar compartment, with a lower steady-state concentration in the rest of the cell. Alternatively, their enrichment in the nucleoli could be due to a higher viscosity in this subnuclear compartment. However, our fluorescence photobleaching results (Fig. 3) revealed that despite their accumulation in the nucleolus, TAT peptides were mobile and able to reach their targets in the nucleus and cytoplasm. Measurements of protein dynamics in the cell nucleus showed half recovery times of <3 s, and so the peptide dynamics measured for TAT-p21-PBD in nucleoli and cytoplasm (<2 s) can be considered to be similar (41). As a direct test of their bioavailability, we investigated the cell cycle effects of TAT fusion to PBD peptides. PCNA forms a sliding clamp around DNA and plays a central role in DNA replication (reviewed in ref. 42). Multiple factors required for DNA synthesis and cell cycle progression bind PCNA (20) via a consensus PBD Qxx(M/L/I)xxF(Y/F) (43). We fused two different PBD peptides to TAT and tested their effect on cell cycle progression using a novel live cell cycle progression assay. In fact, incubation of the cells with both peptides for as little as 10 min substantially inhibited cell cycle progression (Fig. 4). These data clearly showed that, albeit accumulated in nucleoli, the peptides are fully

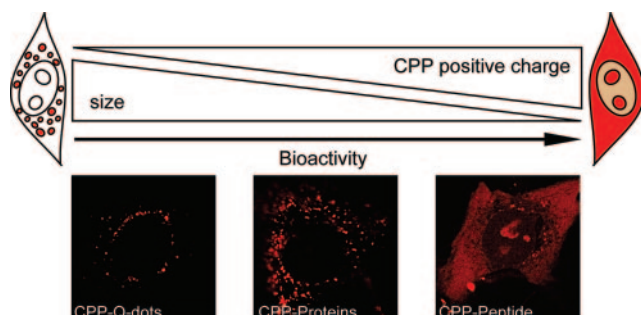


Figure 5. Influence of molecule size and charge on cellular uptake through endocytosis vs. transduction. Cargoes fused to CPPs follow different routes of entry into living mammalian cells. The complexes or fusions of CPPs with large 20 nm diameter Quantum Dots down to globular proteins are mainly endocytosed and remain trapped in cytoplasmic vesicles. Small, nonglobular peptides fused to CPPs are to a certain extent also endocytosed, but in addition are taken up into living cells by membrane transduction; inside the cells they are highly mobile and capable of reaching any subcellular compartment. Thus, transduction of peptides leads to rapid internalization in a bioactive manner whereas globular particles are largely trapped inside vesicles. The mode of uptake is influenced by the charge of the CPP and the size of the cargo connected to it.

able to reach their biological targets elsewhere in the cell and exert a biological effect.

In summary, our data indicate that the translocation of TAT-containing constructs through biomembranes takes place with high efficiency, but at least two functionally distinct mechanisms are involved. Complexes with a globular structure like TAT fused to Q-dots (Fig. 5) or TAT fusion proteins seem to be mostly restricted in their uptake to an endocytic mechanism that is associated with trapping in cytoplasmic vesicles. A minor fraction of internalized TAT fusion proteins, undetectable by confocal microscopy but sufficient to induce enzymatic activity, seems to escape vesicles in the cells. Besides being endocytosed, TAT-containing peptides have the ability to enter living cells by a different pathway. The exact underlying mechanism for this rapid translocation is unknown and could be explained by transient membrane perturbations (14) or lipophilic ion pair diffusion along the membrane potential (5, 10). In general, increasing positive charge of the CPP itself and decreasing size of the cargo fused to the CPP allows rapid internalization to occur in addition to the slow process of adsorptive endocytosis (Fig. 5). The latter implies that CPP-mediated uptake of globular proteins is restricted to cell types capable of endocytosis. CPP-containing peptides can rapidly transduce all cell types tested and, despite their high affinity to the nucleolus, transduced peptides have access to all intracellular compartments, thus making them an ideal tool for therapeutic applications. FJ

We thank A. Krella, P. Domaing, and M. Peitz for their participation at earlier stages of this project. We are indebted to R. Ketritz (Franz Volhard Clinic, Berlin) and U. Kubitschek (University of Bonn) for providing some of the pep-

tides used, M. Gaestel (University of Hannover) for the gift of expression plasmids for MK2, and H. Leonhardt (Ludwig Maximilians University, Munich) for advice throughout this work. We thank members of the Stem Cell Engineering Group (University of Bonn) for support and valuable discussions. This work was supported in part by the Max Delbrueck Center and by grants from the Deutsche Forschungsgemeinschaft and the Volkswagen Foundation (M.C.C.) as well as by grants from the Stem Cell Network North Rhine Westphalia, the European Union and the Volkswagen Foundation (F.E.).

REFERENCES

1. Dietz, G. P., and Bdeltahr, M. (2004) Delivery of bioactive molecules into the cell: the Trojan horse approach. *Mol. Cell Neurosci.* **27**, 85–131
2. Richard, J. P., Melikov, K., Vives, E., Ramos, C., Verbeure, B., Gait, M. J., Chernomordik, L. V., and Lebleu, B. (2003) Cell-penetrating peptides. A reevaluation of the mechanism of cellular uptake. *J. Biol. Chem.* **278**, 585–590
3. Cardoso, M. C., and Leonhardt, H. (2002) Protein transduction: a novel tool for tissue regeneration. *J. Biol. Chem.* **383**, 1593–1599
4. Vives, E., Brodin, P., and Lebleu, B. (1997) A truncated HIV-1 Tat protein basic domain rapidly translocates through the plasma membrane and accumulates in the cell nucleus. *J. Biol. Chem.* **272**, 16010–16017
5. Dom, G., Shaw-Jackson, C., Matis, C., Bouffieux, O., Picard, J. J., Prochiantz, A., Mingeot-Leclercq, M. P., Brasseur, R., and Rezsos, R. (2003) Cellular uptake of Antennapedia Penetration peptides is a two-step process in which phase transfer precedes a tryptophan-dependent translocation. *Nucleic Acids Res.* **31**, 556–561
6. Mai, J. C., Shen, H., Watkins, S. C., Cheng, T., and Robbins, P. D. (2002) Efficiency of protein transduction is cell type-dependent and is enhanced by dextran sulfate. *J. Biol. Chem.* **277**, 30208–30218
7. Ziegler, A., Blatter, X. L., Seelig, A., and Seelig, J. (2003) Protein transduction domains of HIV-1 and SIV TAT interact with charged lipid vesicles. Binding mechanism and thermodynamic analysis. *Biochemistry* **42**, 9185–9194
8. Mitchell, D. J., Kim, D. T., Steinman, L., Fathman, C. G., and Rothbard, J. B. (2000) Polyarginine enters cells more efficiently than other polycationic homopolymers. *J. Pept. Res.* **56**, 318–325
9. Thoren, P. E., Persson, D., Isakson, P., Goksor, M., Onfelt, A., and Norden, B. (2003) Uptake of analogs of penetratin, Tat(48–60) and oligoarginine in live cells. *Biochem. Biophys. Res. Commun.* **307**, 100–107
10. Rothbard, J. B., Jessop, T. C., and Wender, P. A. (2005) Adaptive translocation: the role of hydrogen bonding and membrane potential in the uptake of guanidinium-rich transporters into cells. *Adv. Drug Deliv. Rev.* **57**, 495–504
11. Scheller, A., Wiesner, B., Melzig, M., Bienert, M., and Oehlke, J. (2000) Evidence for an amphipathic independent cellular uptake of amphipathic cell-penetrating peptides. *Eur. J. Biochem.* **267**, 6043–6050
12. Ziegler, A., Nervi, P., Durrenberger, M., and Seelig, J. (2005) The cationic cell-penetrating peptide CPP(TAT) derived from the HIV-1 protein TAT is rapidly transported into living fibroblasts: optical, biophysical, and metabolic evidence. *Biochemistry* **44**, 138–148
13. Futaki, S., Suzuki, T., Ohashi, W., Yagami, T., Tanaka, S., Ueda, K., and Sugiura, Y. (2001) Arginine-rich peptides. An abundant source of membrane-permeable peptides having potential as carriers for intracellular protein delivery. *J. Biol. Chem.* **276**, 5836–5840
14. Prochiantz, A. (2000) Messenger proteins: homeoproteins, TAT and others. *Curr. Opin. Cell Biol.* **12**, 400–406
15. Vives, E. (2003) Cellular uptake [correction of utake] of the Tat peptide: an endocytosis mechanism following ionic interactions. *J. Mol. Recognit.* **16**, 265–271
16. Fittipaldi, A., Ferrari, A., Zoppe, M., Arcangeli, C., Pellegrini, V., Beltram, F., and Giacca, M. (2003) Cell membrane lipid rafts

- mediate caveolar endocytosis of HIV-1 Tat fusion proteins. *J. Biol. Chem.* **278**, 34141–34149
17. Wadia, J. S., Stan, R. V., and Dowdy, S. F. (2004) Transducible TAT-HA fusogenic peptide enhances escape of TAT-fusion proteins after lipid raft macropinocytosis. *Nat. Med.* **10**, 310–315
 18. Caron, N. J., Quenneville, S. P., and Tremblay, J. P. (2004) Endosome disruption enhances the functional nuclear delivery of Tat-fusion proteins. *Biochem. Biophys. Res. Commun.* **319**, 12–20
 19. Kaplan, I. M., Wadia, J. S., and Dowdy, S. F. (2005) Cationic TAT peptide transduction domain enters cells by macropinocytosis. *J. Control Release* **102**, 247–253
 20. Gulbis, J. M., Kelman, Z., Hurwitz, J., O'Donnell, M., and Kuriyan, J. (1996) Structure of the C-terminal region of p21(WAF1/CIP1) complexed with human PCNA. *Cell* **87**, 297–306
 21. Cardoso, M. C., Joseph, C., Rahn, H. P., Reusch, R., Nadal-Ginard, B., and Leonhardt, H. (1997) Mapping and use of a sequence that targets DNA ligase I to sites of DNA replication in vivo. *J. Cell Biol.* **139**, 579–587
 22. Montecucco, A., Rossi, R., Levin, D. S., Gary, R., Park, M. S., Kutycha, T. A., Ciarrochi, G., Villa, A., Biamonti, G., and Tomkinson, A. E. (1998) DNA ligase I is recruited to sites of DNA replication by an interaction with proliferating cell nuclear antigen: identification of a common targeting mechanism for the assembly of replication factories. *EMBO J.* **17**, 3786–3795
 23. Peitz, M., Pfannkuche, K., Rajewsky, K., and Edenhofer, F. (2002) Ability of the hydrophobic FGF and basic TAT peptides to promote cellular uptake of recombinant Cre recombinase: a tool for efficient genetic engineering of mammalian genomes. *Proc. Natl. Acad. Sci. U. S. A.* **99**, 4489–4494
 24. Caron, N. J., Torrente, Y., Camirand, G., Bujold, M., Chapdelaine, P., Leriche, K., Bresolin, N., and Tremblay, J. P. (2001) Intracellular delivery of a Tat-eGFP fusion protein into muscle cells. *Mol. Ther.* **3**, 310–318
 25. Cardoso, M. C., Leonhardt, H., and Nadal-Ginard, B. (1993) Reversal of terminal differentiation and control of DNA replication: cyclin A and Cdk2 specifically localize at subnuclear sites of DNA replication. *Cell* **74**, 979–992
 26. Leonhardt, H., Rahn, H. P., Weinzierl, P., Sporbert, A., Cremer, T., Zink, D., and Cardoso, M. C. (2000) Dynamics of DNA replication factories in living cells. *J. Cell Biol.* **149**, 271–280
 27. Nolden, L., Edenhofer, F., Haupt, S., Koch, P., Wunderlich, F. T., Siemen, H., and Brustle, O. (2006) Site specific recombination in human ES cells induced by cell permeable Cre recombinase. *Nat. Methods* In press
 28. Seewald, N., and Jakubke, H.-D. (2002) *Peptides: Chemistry and Biology*, Wiley-VCH, Weinheim, Germany
 29. Jo, D., Nashabi, A., Doxsee, C., Lin, Q., Unutmaz, D., Chen, J., and Ruley, H. E. (2001) Epigenetic regulation of gene structure and function with a cell-permeable Cre recombinase. *Nat. Biotechnol.* **19**, 929–933
 30. Joshi, S. K., Hashimoto, K., and Koni, P. A. (2002) Induced DNA recombination by Cre recombinase protein transduction. *Genesis* **33**, 48–54
 31. Will, E., Klump, H., Heffner, N., Schwieger, M., Schiedlmeier, B., Ostertag, W., Baum, C., and Stocking, C. (2002) Unmodified Cre recombinase crosses the membrane. *Nucleic Acids Res.* **30**, e59
 32. Goddette, D. W., and Frieden, C. (1986) The kinetics of cytochalasin D binding to monomeric actin. *J. Biol. Chem.* **261**, 15970–15973
 33. Flanagan, M. D., and Lin, S. (1980) Cytochalasins block actin filament elongation by binding to high affinity sites associated with F-actin. *J. Biol. Chem.* **255**, 835–838
 34. Aidley, D., and Stanfield, P. (1996) *Ion Channels: Molecules in Action*, Cambridge University Press, Cambridge, England
 35. Watanabe, Y., Kameoka, S., Gopalakrishnan, V., Aldape, K. D., Pan, Z. Z., Lang, F. F., and Majumder, S. (2004) Conversion of myoblasts to physiologically active neuronal phenotype. *Genes Dev.* **18**, 889–900
 36. Ho, A. (2001) Synthetic protein transduction domains: enhanced transduction potential in vitro and in vivo. *Cancer Res.* **61**, 474–475
 37. Choi, M., Rolle, S., Wellner, M., Cardoso, M. C., Scheidereit, C., Luft, F. C., and Kettritz, R. (2003) Inhibition of NF-kappaB by a TAT-NEMO binding domain peptide accelerates constitutive apoptosis and abrogates LPS-delayed neutrophil apoptosis. *Blood* **102**, 2259–2267
 38. Tyagi, M., Rusnati, M., Presta, M., and Giacca, M. (2001) Internalization of HIV-1 tat requires cell surface heparan sulfate proteoglycans. *J. Biol. Chem.* **276**, 3254–3261
 39. Vives, E., Richard, J. P., Rispal, C., and Lebleu, B. (2003) TAT peptide internalization: seeking the mechanism of entry. *Curr. Protein Pept. Sci.* **4**, 125–132
 40. Fischer, R., Kohler, K., Fotin-Mlecsek, M., and Brock, R. (2004) A stepwise dissection of the intracellular fate of cationic cell-penetrating peptides. *J. Biol. Chem.* **279**, 12625–12635
 41. Phair, R. D., and Misteli, T. (2000) High mobility of proteins in the mammalian cell nucleus. *Nature* **404**, 604–609
 42. Maga, G., and Hubscher, U. (2003) Proliferating cell nuclear antigen (PCNA): a dancer with many partners. *J. Cell Sci.* **116**, 3051–3060
 43. Warbrick, E. (1998) PCNA binding through a conserved motif. *Bioessays* **20**, 195–199

Received for publication December 3, 2005.

Accepted for publication April 10, 2006.

3.4 Live-cell analysis of cell penetration ability and toxicity of oligo-arginines



Live-cell analysis of cell penetration ability and toxicity of oligo-arginines[‡]

GISELA TÜNNEMANN,^a GOHAR TER-AVETISYAN,^a ROBERT M. MARTIN,^a MARTIN STÖCKL,^b ANDREAS HERRMANN^b and M. CRISTINA CARDOSO^{a*}

^a Max Delbrueck Center for Molecular Medicine, D-13125 Berlin, Germany

^b Institute of Biology/Biophysics, Humboldt University of Berlin, D-10115 Berlin, Germany

Received 9 July 2007; Revised 21 September 2007; Accepted 1 October 2007

Abstract: Cell penetrating peptides (CPPs) are useful tools to deliver low-molecular-weight cargoes into cells; however, their mode of uptake is still controversial. The most efficient CPPs belong to the group of arginine-rich peptides, but a systematic assessment of their potential toxicity is lacking. In this study we combined data on the membrane translocation abilities of oligo-arginines in living cells as a function of their chain length, concentration, stability and toxicity. Using confocal microscopy analysis of living cells we evaluated the transduction frequency of the L-isomers of oligo-arginines and lysines and then monitored their associated toxicity by concomitant addition of propidium iodide. Whereas lysines showed virtually no transduction, the transduction ability of arginines increased with the number of consecutive residues and the peptide concentration, with L-R9 and L-R10 performing overall best. We further compared the L- and D-R9 isomers and found that the D-isomer always showed a higher transduction as compared to the L-counterpart in all cell types. Notably, the transduction difference between D- and L-forms was highly variable between cell types, emphasizing the need for protease-resistant peptides as vectors for drug delivery. Real-time kinetic analysis of the D- and L-isomers applied simultaneously to the cells revealed a much faster transduction for the D-variant. The latter underlies the fact that the isomers do not mix, and penetration of one peptide does not perturb the membrane in a way that gives access to the other peptide. Finally, we performed short- and long-term cell viability and cell cycle progression analyses with the protease-resistant D-R9. Altogether, our results identified concentration windows with low toxicity and high transduction efficiency, resulting in fully bioavailable intracellular peptides. Copyright © 2007 European Peptide Society and John Wiley & Sons, Ltd.

Supplementary electronic material for this paper is available in Wiley InterScience at <http://www.interscience.wiley.com/jpages/1075-2617/suppmat/>

Keywords: arginine-rich peptides; cell cycle; cell penetrating peptides; cell viability; membrane integrity; membrane translocation; oligo-lysines; oligo-arginines

INTRODUCTION

Cell penetrating peptides (CPPs) possess the unique ability to shuttle linked cargoes such as drugs [1], peptides [2–6], proteins [7–9], peptide nucleic acids (PNAs) [10–12] and nanoparticles [13,14] across the plasma membrane which is otherwise virtually impermeable for hydrophilic compounds. CPPs can be subdivided into two major groups: model amphiphilic peptides (MAPs) [15,16] developed on the basis of spatial separation of positively charged and hydrophobic amino acid residues; and arginine-rich peptides (R-RPs) delineated from natively occurring minimal transduction domains of proteins, e.g. TAT from HIV-1 TAT protein [7,17–19] and penetratin from the homeobox of antennapedia protein [20–22]. However, plasma membrane translocation of MAPs structurally requires at

least four helical turns but does not depend on the positively charged amino acid residues [15], whereas the transduction ability of R-RPs depends on a minimum number of arginines [23,24], suggesting that the entry mechanisms of both types of CPPs are unrelated. The translocation ability of R-RPs does not seem to be solely a matter of charge, but has been proposed to reside in the guanidinium group of the arginine itself [25]. The formation of lipophilic ion pairs with abundant sulfate, phosphate or carboxylate groups of membrane constituents via the two amino functions of arginine provides a mechanistic framework for the translocation of a highly charged compound through the plasma membrane [26]. CPP-mediated delivery of cargoes into the cytoplasm can be achieved by at least two independent mechanisms: (i) adsorptive endocytosis and subsequent release of the enclosed compounds from endosomes or lysosomes [7,27–29]; and (ii) rapid crossing of the membrane by a seemingly energy-independent, not-well-understood mechanism referred to as transduction [5,30–32]. Whereas R-RPs coupled

*Correspondence to: M. Cristina Cardoso, Max Delbrueck Center for Molecular Medicine, Robert-Roessle-Str. 10, D-13125 Berlin, Germany; e-mail: cardoso@mdc-berlin.de

[‡] This article is part of the Special Issue of the Journal of Peptide Science entitled “2nd workshop on biophysics of membrane-active peptides”.

to high-molecular-weight cargoes are restricted to the endocytic mode of uptake [5,33,34], R-RPs themselves or interconnected to low-molecular-weight cargoes have both options. Above a certain concentration (transduction threshold), which varies between 1 and 10 μM depending on the cell type and the size of the cargo [5], R-RPs directly translocate across the plasma membrane into the cell. Several live-cell studies have shown that functional peptides attached to R-RPs exert biological effects after the transduction event [2–6]. Importantly, R-RP-mediated transduction circumvents the inefficient step of release from cytoplasmic vesicles after the endocytic uptake. However, a systematic evaluation of the cell penetration ability, in combination with an assessment of potential short- and long-term toxic effects of R-RPs, is lacking. In this study, we combined data on the membrane translocation abilities of oligo-arginines in living cells as a function of their chain length, concentration, stability and toxicity.

MATERIAL AND METHODS

Peptides

Consecutive arginines (5–12) and lysines (5–12) as L-isomers and TAMRA-R9 and Fluos-R10 also as D-isomers were synthesized and coupled directly to fluorescein (Fluos) or 5,6-TAMRA at the N-terminus by Peptide Specialty Laboratories GmbH (Heidelberg, Germany). The peptides were purified by HPLC and their appropriate masses confirmed by mass spectrometry. The isoelectric points (pI) were estimated using the freeware tool ProtParam.

Cells

All cell types were cultured in Dulbecco's modified Eagle medium (DMEM) with fetal calf serum (FCS) (Life Technologies, Inc., USA) at the following concentrations: C2C12 mouse myoblasts 20%, human HeLa cells 10%, MDCKII dog epithelial kidney cells 10% and BJ-hTERT human fibroblasts 10%. Primary cultures from male WKY rats aged 3 months were performed as described previously [35].

Transduction Experiments

As peptide transduction is influenced by the peptide-to-cell ratio [36], for all transduction experiments μ -Slide VI observation chambers were used (Ibidi, Martinsried, Germany), which guarantee a defined and equal liquid volume above the cells throughout the entire observation channel. The respective cell types were seeded at 70% confluency into the observation chambers and incubated overnight at 37 °C at 5% CO₂. Special care was taken that cell densities were equal throughout sets of experiments. The oligo-arginines and oligo-lysines were diluted in DMEM medium without FCS to avoid precipitation of the peptides. For the chain-length-dependent transduction assay, 2 $\mu\text{g}/\text{ml}$ propidium iodide (PI) was added directly to the diluted peptide solution prior to the transduction experiment. The culture medium was gently

aspirated from the cells and exchanged against the respective peptide dilutions in a volume of 60 μl . The cells were kept for 1 h in the incubator until imaging at the microscope under the same conditions. For each peptide concentration, between 140 and 250 cells were analyzed and the experiments were performed in duplicate. The images were collected with two different laser settings, one set resulting in images without overexposed signals and one set with higher laser intensities, so that weaker signals could not be missed. The microscope settings per concentration and within these two sets were identical. Acquired images were analyzed visually, and cells unambiguously showing fluorescent signal inside the nucleus were scored as transduced. The graphics were generated using the Origin version 7.5 software (OriginLab Corp., Northampton, USA).

Cell Cycle and Viability Assays

For the modified (3-(4,5-dimethylthiazol-2-yl)-2,5 diphenyl-tetrazolium-bromide (MTT) assay, C2C12 cells were incubated for 2 h with different concentrations of the peptides D-R9 and L-R9. MTT was dissolved at 0.4 mg/ml in DMEM. Subsequently, the cells were washed once, followed by addition of 100 μl of the MTT solution and were returned to the incubator for 5 h. Cells were then analyzed by confocal laser scanning microscopy (CLSM). The transduction frequency was monitored by the fluorescence of the Fluos- or TAMRA-labeled peptides, respectively, and the formation of the blue-violet formazan complex was monitored by excitation with 488 nm and detection in the transmission channel. For each peptide concentration, five fields of view with a 40 \times objective corresponding to a total number of \sim 150 cells were collected. Cells with less formazan signal intensity than the control cells were counted as nonviable.

For the analysis of the plasma membrane integrity during and after transduction, we used 2 $\mu\text{g}/\text{ml}$ PI mixed together with the transducing peptides in DMEM to detect transient pore formation or membrane perturbations, and 0.5% (V/V) trypan blue to distinguish, after the transduction period of 2 h, the cells with permanently compromised membranes. Data were displayed by using Microsoft Excel.

To analyze relatively short-term effects on DNA condensation by the peptides, C2C12 cells were preincubated for 10 min with the DNA dye DRAQ5 (Biostatus Limited, UK) as described [37] and then incubated with different concentrations of the D-R9 peptide. Cells were imaged by CLSM before and after the treatment. Long-term effects on the cell cycle progression were determined by fluorescence activated cell sorting (FACS) analysis of PI-stained C2C12 cells. For this purpose, C2C12 cells were plated onto 150 mm diameter dishes and incubated with different concentrations of the respective peptides at a density of 40% in DMEM for 2 h. Then the medium was replaced by DMEM with 20% FCS and the cells were cultivated for further 16 h until they reached a density of 60%. For FACS analysis the cells were trypsinized, washed with PBS, fixed with ice-cold 90% EtOH, washed with PBS, treated with 0.1 mg/ml RNase and stained with 33 $\mu\text{g}/\text{ml}$ PI, and DNA content was measured with a FACSCalibur (Becton Dickinson). Data were analyzed and plotted with the flow cytometry software FLOWJO (Tree Star, Inc., USA).

Microscopy, Image Acquisition and Analysis

Confocal images were acquired with a Zeiss confocal laser scanning microscope, LSM510 Meta, mounted on an Axiovert 200M inverted microscope equipped with a live-cell microscope incubation cage (Okolab, Italy) using either a 40 \times plan-neofluar NA1.3 or a 63 \times plan-apochromat NA1.4 oil-immersion, phase-contrast objectives. For all settings the main beam splitter was HFT UV/488/543/633, and the specific parameters for the single fluorophores were as follows: Fluos, excited at 488 nm, detected with a 500–530 nm band-pass filter; TAMRA, excited at 543 nm, detected with 565–615 nm band-pass filter; and trypan blue, PI and DRAQ5, excited with 633 nm, detected with 650 nm long-pass filter. Phase contrast images were recorded with excitation at 488 nm and detection in the transmission channel. Laser power for observation was typically 1–5% (488 nm, 25 mW), 50–60% (543 nm, 1 mW) and 3–5% (633 nm, 5 mW) unless otherwise indicated. Settings were adjusted in a way that image pixels were not over- or underexposed with the range indicator function in the Zeiss LSM software version 3.2. To ensure that weak intracellular fluorescence signals of the peptides were not missed, a set of overexposed images were collected in addition.

RESULTS AND DISCUSSION

The decisive role of arginine clusters for translocation over the plasma membrane has been known for some time. Therefore, several studies were aimed at determining the optimal number of arginines or minimal structural requirements that permit efficient transduction. Surprisingly, most of them analyzed either fixed cells [23,24,38] and/or used FACS analysis without a protocol to efficiently remove the cationic peptides sticking to the extracellular side of the plasma membrane [39]. To exclude the above artifacts, we analyzed the transduction frequency of oligo-arginines and -lysines with chain length from 5 to 12 directly by CLSM of living cells. In addition, we compared only data from experiments using the same incubation times for all peptides and at the same cell density and varied only the concentrations for each peptide. Figure 1(A) displays the possible uptake phenotypes of C2C12 mouse myoblasts after addition of the fluorescent peptide for 1 h. The images on the left side, upper panel, show cells that endocytosed the L-R9 peptide incubated at a concentration of 10 μ M, where the fluorescence of the peptide solely resided in cytoplasmic vesicles, and no free cytoplasmic peptide was detectable by means of fluorescence microscopy. The images on the right side, upper panel, depict cells that incorporated L-R6 peptide added at a concentration of 50 μ M with fluorescence detected throughout the cytoplasm and nucleus, which we hereafter refer to as transduction. Cells with mixed phenotypes (Figure 1(A), lower panel) that show in addition to transduction vesicular uptake were also scored as transduced cells. Only the uptake mode of transduction yields peptide available in all intracellular

compartments and, therefore, is able to reach all potential targets. In order to detect any possible membrane perturbations or transient pore formation, the vital dye PI was added to mouse myoblast cultures simultaneously with the oligo-arginines (see scheme in Figure 1(A)). The plots in Figure 1(B) summarize the transduction results for all oligo-arginine peptides. None of the oligo-arginines tested (R5–R12) was able to transduce at a concentration of 0.5, 1 or 5 μ M in a total volume of 60 μ L. Transduction could be observed at 10 μ M for the peptides R8–R12, with frequencies over 50% for the peptides R10–R12. Whereas R5 did not transduce over the whole concentration range tested (between 0.5 to 100 μ M), R6 appeared intracellularly only in 4% of the cells at 50 μ M and 28% at 100 μ M. R7–R9 transduced between 18 and 42% of the cells at 50 μ M and reached frequencies between 75 and 90% at 100 μ M. The peptides R10–R12 transduced already to a level of 70–90% at 10 μ M concentration and the percentage of transduction increased only slightly at 5- or 10-fold higher concentration. In stark contrast, either no or very low frequency of cell penetration could be detected with all the oligo-lysines tested (K5–K12) at an even wider concentration range (data not shown). The uptake of PI by the oligo-arginine transduced cells (Figure 1(B)) indicated severe toxicity only with R8, R10, R11 and R12 at the highest peptide concentration tested (100 μ M) and for R11 and R12 already at 50 μ M. For the transducing peptides with lower chain length, the percentage of PI-stained cells in all cases was below 10%. At 10 μ M, except for R12 all transducing peptides caused no membrane damage that could be detected by simultaneous PI staining. Notably, PI was not observed inside transduced cells by peptides with a low number of arginines or at low concentrations. This fact argues against the formation of transient pores or strong membrane perturbations. Whereas previous studies found an optimum number of consecutive arginines for transduction [24,38], our results support a linear dependence of the transduction frequencies on the number of consecutive arginines. Considering also the PI uptake data, R9 or R10 peptides combine a medium to high transduction level associated with a tolerable toxicity. To verify and extend our live-cell analysis, we selected three oligo-arginine peptides (namely, R5, R7 and R9) and tested their uptake potential into artificial membranes. The R5 peptide was chosen, as it did not transduce into cells, whereas the R7 was able to transduce, albeit at a low level, and R9 was the most efficient while still retaining low toxicity. The 7-nitro-2-1,3-benzoxadiazol-4-yl (NBD) labeled peptides were applied to large unilamellar vesicles (LUVs) and the percentage of transduced peptide over time was measured with a spectrofluorometer after quenching the outer fluorescence with the NBD quencher, dithionite. The percentage of transduction rose with the number of consecutive arginines in a manner

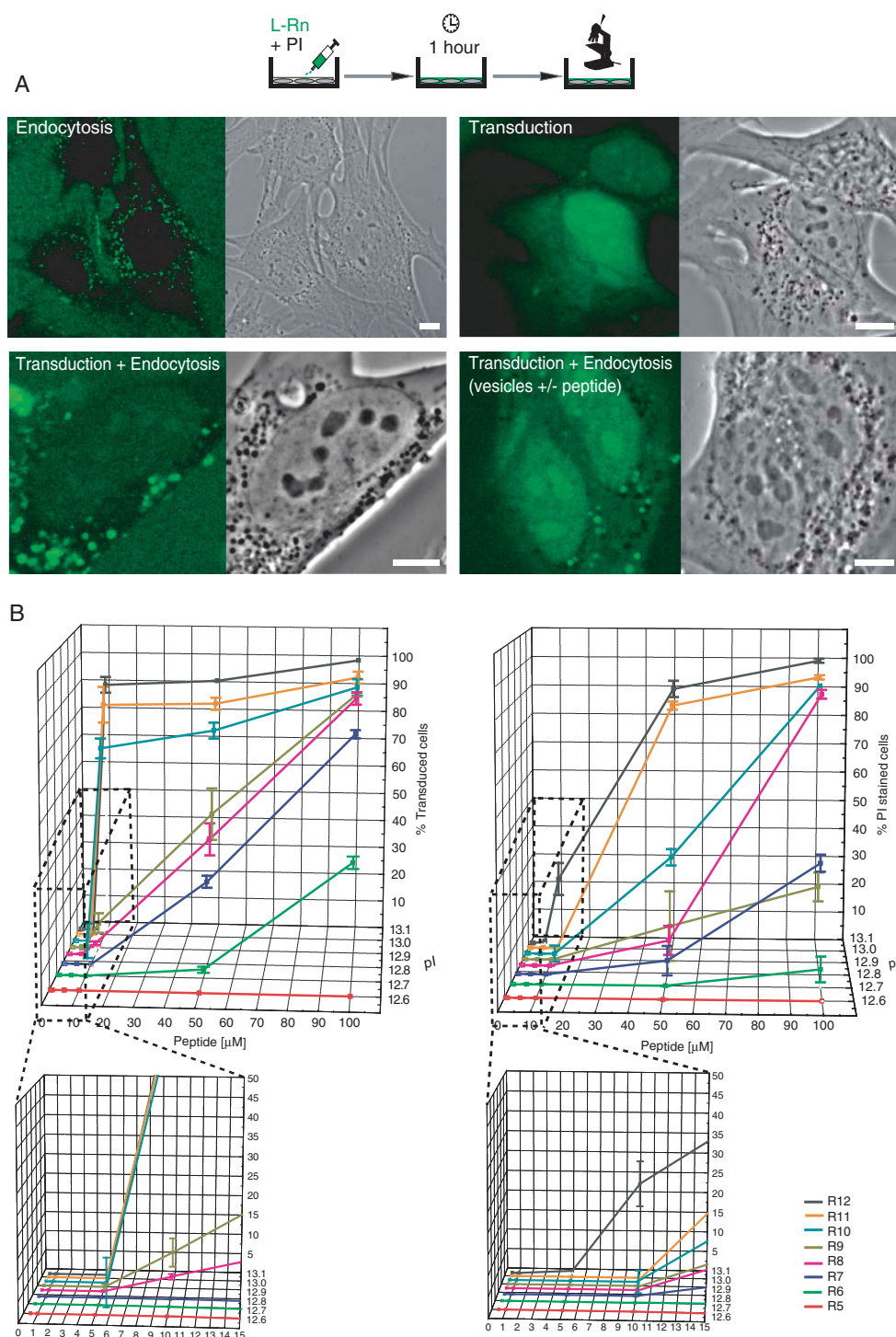


Figure 1 Assessment of dose-dependent transduction frequency of oligo-arginine peptides. (A) Confocal microscopy images displaying examples of endocytic uptake (upper, left panel, L-R9 at 10 μM) versus transduction (upper, right panel, L-R6 at 50 μM) of oligo-arginines (L-Rn; $n = 5-12$) into mouse C2C12 myoblasts. Two mixed forms of transduction + endocytosis are shown below: transduction and endocytic peptide vesicles (left panel L-R9 at 10 μM) versus transduction and peptide enclosed in endocytic vesicles (+) as well as excluded from endocytic vesicles (-) (right panel L-R6 at 50 μM). Scale bars 10 μm . The experimental procedure is shown above. Only cells showing the transduction mode of uptake (including the mixed phenotypes shown in the lower panels) were counted for the quantification in B. (B) The peptide transduction frequency shown as a fraction of C2C12 cells (in %) was scored as explained in A. Peptide transduction frequencies are shown plotted against peptide concentration (0.5, 1, 5, 10, 50, 100 μM) and corresponding estimated isoelectric point (pI). The fraction of PI-stained C2C12 cells (in %) within the transduced cell population is plotted similarly. The lower peptide concentration plots are also shown magnified for better visualization. Error bars display the standard deviation of two independent experiments. The total number of cells counted was between 140 and 250 for each experiment.

analogous to that in the living-cell uptake analyses (Supplementary Figure S1).

Octa-, nona- and deca-arginines have been shown to transduce successfully into living cells under noninvasive conditions and at lower concentrations [31,32,40], but different cell types as well as D- and L-isomers were used in those studies. Therefore, we next assessed the influence of D- and L-isomeric forms on the transduction efficiencies in different cell types. For that purpose, we incubated different cell types of various mammalian species and also primary cells with 10^{-6} M of the TAMRA-labeled D-isomer and the Fluos-labeled L-isomer of R9 and determined the percentage of transduced cells after 1 h incubation (Figure 2(A)). In general, the transduction frequencies for the L-form in all cell types were lower than that of the D-form, illustrating that peptide stability is an important issue for transduction. By calculating the index for the percentage of cells transduced by the L-isomer divided by the percentage of cells transduced by the D-isomer, we found characteristic values for individual cell types, which most

probably reflect their extracellular proteolytic activity [41]. Whereas diploid human fibroblasts were very inefficiently transduced, rat cardiomyocytes and mouse myoblasts showed higher levels of transduction for the L-form, approaching the level of the D-form. As the D-isomer of R9 reached transduction efficiencies of over 95% in all cell types, the isomer-specific differences cannot be due to cell-type-specific membrane composition. The loss of only one arginine from L-R9 would already reduce the transduction efficiency to half at a concentration of 10^{-6} M and lead to the disappearance of the transduction potential with further proteolysis (see plot in Figure 1(B)). To ensure that the different indices were not a result of the distinct fluorescent labels attached to the peptides, the same set of experiments was performed with Fluos-labeled D- and L-isomers of R10 with the same outcome (data not shown). The overview images of the different cell types after transduction also revealed that the fluorescence intensity varied between individual cells. This variation was not correlated to

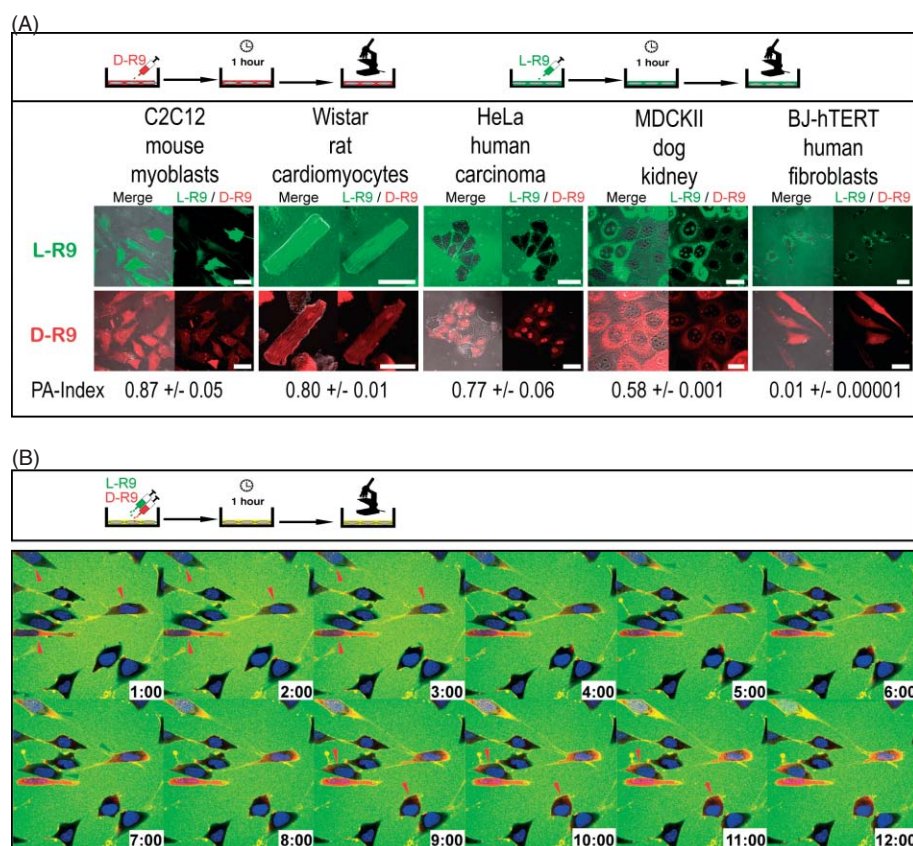


Figure 2 Cell-type-specific differences in transduction frequencies and kinetics of L- and D-isomers of R9. (A) Confocal microscopy sections of different cell types from various mammalian species 1 h after application of 10^{-6} M of the Fluos-labeled L-isomer (upper panel, green fluorescence) and the TAMRA-labeled D-isomer (lower panel, red fluorescence) of R9. For each cell type, merge images of phase contrast and fluorescence and fluorescence images alone are displayed. The index corresponds to the ratio (% transduced cells by L-isomer/% transduced cells by D-isomer) \pm standard deviation. (B) Confocal microscopy time lapse (minutes:seconds) of the transduction of the L- and D-isomers of R9 simultaneously applied to C2C12 mouse myoblasts at a concentration of 10^{-6} M each. Red and green arrowheads indicate the initial detection of the transduced corresponding peptides in intracellular compartments. The cells are counterstained with the live-cell DNA dye DRAQ5 (blue). Scale bar 50 μ m.

the size and, therefore, to the total accessible membrane surface of the transduced cells. Next, we tested whether kinetic differences between the transduction of D- and L-isomers occurred. For this, we applied 20 μM of a 1:1 mixture onto mouse myoblasts and monitored the uptake in real time by CLSM. Surprisingly, several cells selectively took up the TAMRA-labeled D-isomer but not the Fluos-labeled L-form, although some cells also showed yellow color seen in the overlay of the two fluorescence images (Figure 2(B) and Movie 1). Nevertheless, the kinetics of transduction was quite different for both isomers, even though after a certain time both species had been internalized. This result argues against the formation of mixed D- and L-isomers into multimeric assemblies. We can, however, not rule out the existence of single-species multimers. In addition, no change in the transduction efficiency of the individual D- or the L- chiral forms was observed, which would be expected from the higher total peptide concentration. Finally, these data clearly show the absence of membrane damage by the penetration of one peptide species since the other species in the same cell at the same time was not taken up concomitantly.

In view of the therapeutic potential of peptide vectors for the delivery of low-molecular-weight compounds and considering the relatively high transduction rate and low percentage of PI-stained cells (Figure 1(B) and 2), we selected the nondegradable D-isomer of R9 for further detailed analysis of toxicity on mouse myoblasts. Transduction was observed starting from a concentration threshold of 5 μM with a transduction frequency of about 10% (Figure 3(A)). Ten micromolar D-R9 was transduced into more than 50%, and 25 μM into 70% of the cells. For concentrations of 50 and 100 μM , transduction was nearly complete. Next, we examined the viability of mouse myoblasts after 2 h of incubation with different concentrations with D-R9. The ability of the cells to exclude the vital dye trypan blue was used to judge membrane integrity. Furthermore, we assessed by an MTT assay whether the transduction of D-R9 influences enzymatic activities inside the cells detected here by their ability to produce formazan [42]. Starting from the transduction threshold of 5 μM , a constant decrease in viability by both assays was observed, which was mild between 5 and 25 μM peptide concentration. At a concentration of 50 μM , about 17% of the cells stained positive for trypan blue, and 15% of the cells produced formazan to a lesser extent than the controls. Cell death in 60% of cells resulted from 100 μM of D-R9, and also the formazan levels of those cells were greatly reduced in comparison to the control cells. The slope of the trypan blue exclusion curve is steeper than that of the viability assayed by the MTT test, indicating that the membranes are the first location where massive damage occurs. Arginine-rich clusters can be found in RNA-binding proteins and are targeted to the nuclear compartment. To test long-term

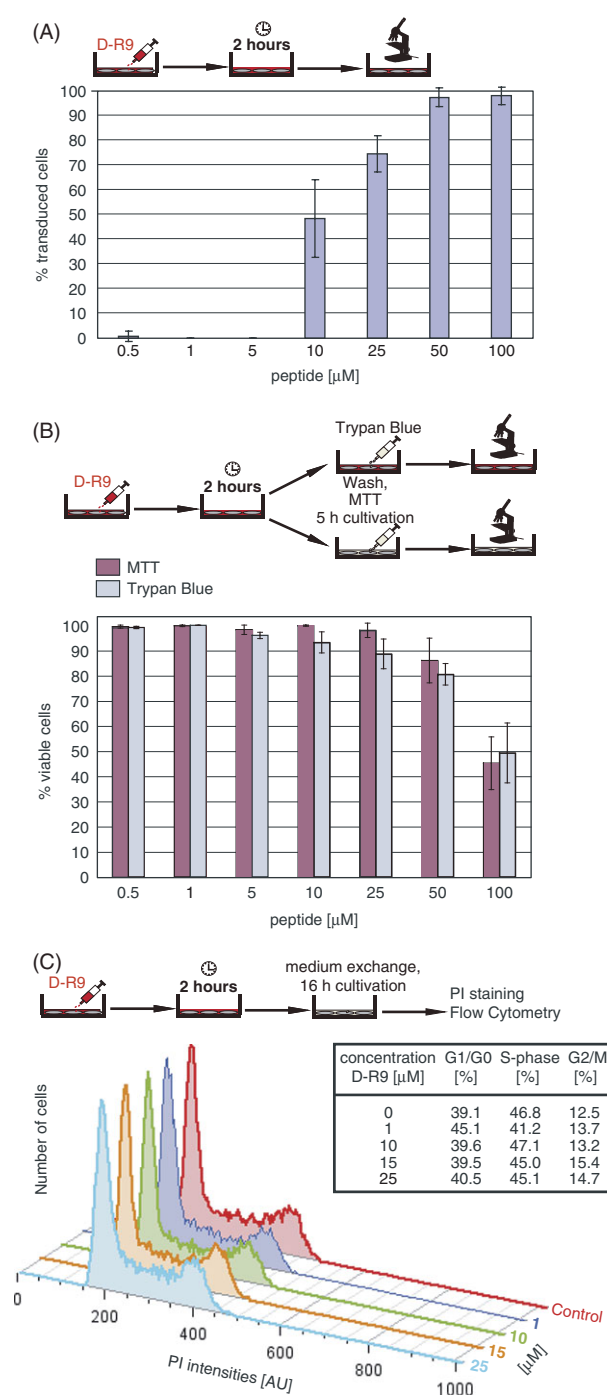


Figure 3 Short- and long-term dose-dependent effects of D-R9 transduction on cell viability and proliferation. (A) Transduction frequencies of D-R9 in C2C12 mouse myoblasts determined as in Figure 1. (B) Cell viability determined by trypan blue exclusion and enzymatic activity MTT assay after 2 h of incubation with different concentrations of D-R9. (C) Long-term effects on the cell cycle distribution assayed by flow cytometry analysis of DNA content stained with PI. The respective experiments are explained in the schemes. For (A) and (B) the error bars display the standard deviation of two independent experiments. The total number of cells counted was between 140 and 250 for each experiment. In (C), one example of three independent experiments is depicted.

effects on DNA replication and cell cycle progression, mouse myoblasts were incubated for 2 h with the D-R9 peptide, the medium was exchanged and they were kept in culture until the next day. Cultures were then fixed, DNA was stained with PI and the cell cycle distribution was analyzed by flow cytometry. The cell cycle profiles and the statistics are displayed in Figure 3(C) and show no concentration-dependent effect of the D-R9 peptide on the cell cycle. Altogether, the toxicological effects of the D-R9 peptide in a range of 5–25 μ M can be classified as mild and cell proliferation was also not affected.

CONCLUSIONS

In summary, we evaluated the transduction frequency of the L-isoforms of oligo-arginines and monitored their associated toxicity. This risk-benefit analysis of transduction led us to the selection of R9 for further analysis. With its nondegradable counterpart D-R9, we established an assay that allows the quantification of the proteolytic activity of different cell types, and emphasize the need for protease-resistant peptides as vectors for drug delivery. Importantly, the D-isoform always showed a higher transduction as compared to the L-counterpart in all cell types. The transduction difference between D- and L-forms was highly variable between cell types. Finally, our toxicity results indicate concentration windows with low toxicity and high transduction efficiency, not requiring further treatments to force endocytic vesicle rupture.

Supplementary Material

Supplementary electronic material for this paper is available in Wiley InterScience at: <http://www.interscience.wiley.com/jpages/1075-2617/suppmat/>

Acknowledgements

We thank I. Kocman for help with the flow cytometry, P. Domaing for excellent technical assistance and F. Witzel for her participation at the earlier stages of this project. G.T. was supported in part by the European Union (ESF Program). This work was funded by grants of the Deutsche Forschungsgemeinschaft and the Volkswagen Foundation to M.C.C.

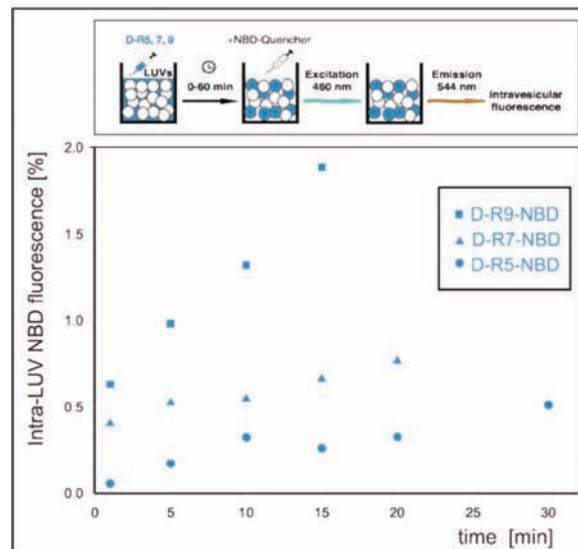
REFERENCES

- Nori A, Jensen KD, Tijerina M, Kopeckova P, Kopecek J. Tat-conjugated synthetic macromolecules facilitate cytoplasmic drug delivery to human ovarian carcinoma cells. *Bioconjugate Chem.* 2003; **14**: 44–50.
- Chen CH, Gray MO, Mochly-Rosen D. Cardioprotection from ischemia by a brief exposure to physiological levels of ethanol: role of epsilon protein kinase C. *Proc. Natl. Acad. Sci. U.S.A.* 1999; **96**: 12784–12789.
- Choi M, Rolle S, Wellner M, Cardoso MC, Scheidereit C, Luft FC, Kettritz R. Inhibition of NF-kappaB by a TAT-NEMO-binding domain peptide accelerates constitutive apoptosis and abrogates LPS-delayed neutrophil apoptosis. *Blood* 2003; **102**: 2259–2267.
- Rohrbach S, Muller-Werdan U, Werdan K, Koch S, Gellerich NF, Holtz J. Apoptosis-modulating interaction of the neuregulin/erbB pathway with anthracyclines in regulating Bcl-xS and Bcl-xL in cardiomyocytes. *J. Mol. Cell. Cardiol.* 2005; **38**: 485–493.
- Tünnemann G, Martin RM, Haupt S, Patsch C, Edenhofer F, Cardoso MC. Cargo-dependent mode of uptake and bioavailability of TAT-containing proteins and peptides in living cells. *FASEB J.* 2006; **20**: 1775–1784.
- Tünnemann G, Karczewski P, Haase H, Cardoso MC, Morano I. Modulation of muscle contraction by a cell permeable peptide. *J. Mol. Med.* (in press). DOI: 10.1007/s00109-007-0238-6.
- Fawell S, Seery J, Daikh Y, Moore C, Chen LL, Pepinsky B, Barsom J. Tat-mediated delivery of heterologous proteins into cells. *Proc. Natl. Acad. Sci. U.S.A.* 1994; **91**: 664–668.
- Nagahara H, Vocero-Akbani AM, Snyder EL, Ho A, Latham DG, Lissy NA, Becker-Hapak M, Ezhevsky SA, Dowdy SF. Transduction of full-length TAT fusion proteins into mammalian cells: TAT-p27Kip1 induces cell migration. *Nat. Med.* 1998; **4**: 1449–1452.
- Schwarze SR, Ho A, Vocero-Akbani A, Dowdy SF. *In vivo* protein transduction: delivery of a biologically active protein into the mouse. *Science* 1999; **285**: 1569–1572.
- Oehlke J, Wallukat G, Wolf Y, Ehrlich A, Wiesner B, Berger H, Bienert M. Enhancement of intracellular concentration and biological activity of PNA after conjugation with a cell-penetrating synthetic model peptide. *Eur. J. Biochem.* 2004; **271**: 3043–3049.
- Turner JJ, Ivanova GD, Verbeure B, Williams D, Arzumanov AA, Abes S, Lebleu B, Gait MJ. Cell-penetrating peptide conjugates of peptide nucleic acids (PNA) as inhibitors of HIV-1 Tat-dependent trans-activation in cells. *Nucleic Acids Res.* 2005; **33**: 6837–6849.
- Wolf Y, Pritz S, Abes S, Bienert M, Lebleu B, Oehlke J. Structural requirements for cellular uptake and antisense activity of peptide nucleic acids conjugated with various peptides. *Biochemistry* 2006; **45**: 14944–14954.
- Santra S, Yang H, Stanley JT, Holloway PH, Moudgil BM, Walter G, Mericle RA. Rapid and effective labeling of brain tissue using TAT-conjugated CdS:Mn/ZnS quantum dots. *Chem. Commun.* 2005; **25**: 3144–3146.
- Lewin M, Carlesso N, Tung CH, Tang XW, Cory D, Scadden DT, Weissleder R. Tat peptide-derivatized magnetic nanoparticles allow in vivo tracking and recovery of progenitor cells. *Nat. Biotechnol.* 2000; **18**: 410–414.
- Scheller A, Oehlke J, Wiesner B, Dathe M, Krause E, Beyermann M, Melzig M, Bienert M. Structural requirements for cellular uptake of alpha-helical amphipathic peptides. *J. Pept. Sci.* 1999; **5**: 185–194.
- Oehlke J, Scheller A, Wiesner B, Krause E, Beyermann M, Klauschenz E, Melzig M, Bienert M. Cellular uptake of an alpha-helical amphipathic model peptide with the potential to deliver polar compounds into the cell interior non-endocytically. *Biochim. Biophys. Acta* 1998; **1414**: 127–139.
- Frankel AD, Pabo CO. Cellular uptake of the tat protein from human immunodeficiency virus. *Cell* 1988; **55**: 1189–1193.
- Green M, Loewenstein PM. Autonomous functional domains of chemically synthesized human immunodeficiency virus tat trans-activator protein. *Cell* 1988; **55**: 1179–1188.
- Vives E, Brodin P, Lebleu B. A truncated HIV-1 Tat protein basic domain rapidly translocates through the plasma membrane and accumulates in the cell nucleus. *J. Biol. Chem.* 1997; **272**: 16010–16017.
- Perez F, Joliot A, Bloch-Gallego E, Zahraoui A, Triller A, Prochiantz A. Antennapedia homeobox as a signal for the cellular internalization and nuclear addressing of a small exogenous peptide. *J. Cell Sci.* 1992; **102**: 717–722.

21. Joliot A, Le Roux I, Volovitch M, Bloch-Gallego E, Prochiantz A. Neurotrophic activity of a homeobox peptide. *Prog. Neurobiol.* 1994; **42**: 309–311.
22. Derossi D, Joliot AH, Chassaing G, Prochiantz A. The third helix of the Antennapedia homeodomain translocates through biological membranes. *J. Biol. Chem.* 1994; **269**: 10444–10450.
23. Suzuki T, Futaki S, Niwa M, Tanaka S, Ueda K, Sugiura Y. Possible existence of common internalization mechanisms among arginine-rich peptides. *J. Biol. Chem.* 2002; **277**: 2437–2443.
24. Futaki S, Goto S, Sugiura Y. Membrane permeability commonly shared among arginine-rich peptides. *J. Mol. Recognit.* 2003; **16**: 260–264.
25. Rothbard JB, Kreider E, VanDeusen CL, Wright L, Wylie BL, Wender PA. Arginine-rich molecular transporters for drug delivery: role of backbone spacing in cellular uptake. *J. Med. Chem.* 2002; **45**: 3612–3618.
26. Rothbard JB, Jessop TC, Wender PA. Adaptive translocation: the role of hydrogen bonding and membrane potential in the uptake of guanidinium-rich transporters into cells. *Adv. Drug Delivery Rev.* 2005; **57**: 495–504.
27. Ferrari A, Pellegrini V, Arcangeli C, Fittipaldi A, Giacca M, Beltram F. Caveolae-mediated internalization of extracellular HIV-1 tat fusion proteins visualized in real time. *Mol. Ther.* 2003; **8**: 284–294.
28. Wadia JS, Stan RV, Dowdy SF. Transducible TAT-HA fusogenic peptide enhances escape of TAT-fusion proteins after lipid raft macropinocytosis. *Nat. Med.* 2004; **10**: 310–315.
29. Richard JP, Melikov K, Brooks H, Prevot P, Lebleu B, Chernomordik LV. Cellular uptake of unconjugated TAT peptide involves clathrin-dependent endocytosis and heparan sulfate receptors. *J. Biol. Chem.* 2005; **280**: 15300–15306.
30. Ziegler A, Nervi P, Durrenberger M, Seelig J. The cationic cell-penetrating peptide CPP(TAT) derived from the HIV-1 protein TAT is rapidly transported into living fibroblasts: optical, biophysical, and metabolic evidence. *Biochemistry* 2005; **44**: 138–148.
31. Fretz MM, Penning NA, Al-Taei S, Futaki S, Takeuchi T, Nakase I, Storm G, Jones AT. Temperature-, concentration- and cholesterol-dependent translocation of L- and D-octa-arginine across the plasma and nuclear membrane of CD34+ leukaemia cells. *Biochem. J.* 2007; **403**: 335–342.
32. Duchardt F, Fotin-Mieczek M, Schwarz H, Fischer R, Brock R. A comprehensive model for the cellular uptake of cationic cell-penetrating peptides. *Traffic* 2007; **8**: 848–866.
33. Silhol M, Tyagi M, Giacca M, Lebleu B, Vives E. Different mechanisms for cellular internalization of the HIV-1 Tat-derived cell penetrating peptide and recombinant proteins fused to Tat. *Eur. J. Biochem.* 2002; **269**: 494–501.
34. Maiolo JR, Ferrer M, Ottinger EA. Effects of cargo molecules on the cellular uptake of arginine-rich cell-penetrating peptides. *Biochim. Biophys. Acta* 2005; **1712**: 161–172.
35. Alvarez J, Hamplova J, Hohaus A, Morano I, Haase H, Vassort G. Calcium current in rat cardiomyocytes is modulated by the carboxyl-terminal ahnak domain. *J. Biol. Chem.* 2004; **279**: 12456–12461.
36. Hallbrink M, Oehlke J, Papsdorf G, Bienert M. Uptake of cell-penetrating peptides is dependent on peptide-to-cell ratio rather than on peptide concentration. *Biochim. Biophys. Acta* 2004; **1667**: 222–228.
37. Martin RM, Leonhardt H, Cardoso MC. DNA labeling in living cells. *Cytometry A* 2005; **67**: 45–52.
38. Futaki S, Suzuki T, Ohashi W, Yagami T, Tanaka S, Ueda K, Sugiura Y. Arginine-rich peptides. An abundant source of membrane-permeable peptides having potential as carriers for intracellular protein delivery. *J. Biol. Chem.* 2001; **276**: 5836–5840.
39. Goun EA, Pillow TH, Jones LR, Rothbard JB, Wender PA. Molecular transporters: synthesis of oligoguanidinium transporters and their application to drug delivery and real-time imaging. *ChemBiochem* 2006; **7**: 1497–1515.
40. Martin RM, Tünnemann G, Leonhardt H, Cardoso MC. Nucleolar marker for living cells. *Histochem. Cell Biol.* 2007; **127**: 243–251.
41. Trehin R, Nielsen HM, Jahnke HG, Krauss U, Beck-Sickingen AG, Merkle HP. Metabolic cleavage of cell-penetrating peptides in contact with epithelial models: human calcitonin (hCT)-derived peptides, Tat(47–57) and penetratin(43–58). *Biochem. J.* 2004; **382**: 945–956.
42. Mosmann T. Rapid colorimetric assay for cellular growth and survival: application to proliferation and cytotoxicity assays. *J. Immunol. Methods* 1983; **65**: 55–63.

Tünnemann et al.

Supplementary figure 1

**Supplemental figure legend:****Supplementary Figure 1 Penetration of artificial membranes by oligo-arginines.**

LUVs (Large Unilamellar Vesicles) were prepared from a mixture from 70 mol% of DOPC (dioleoylphosphatidylcholine) and 30 mol% of DOPS (dioleoylphosphatidylserine). In total 1 μ mol of lipids were mixed in chloroform. A dry lipid film was formed by solvent evaporation under a nitrogen stream. The dried lipids were resolubilized in 2 ml of PBS (pH 7.4) by 5 min of vortexing. To yield LUVs the lipid suspension was processed by freeze/thaw-cycles (5x) and extrusion through a 0.1 μ m filter (10x). Consecutive arginines (R5, R7, R9) as D-isomers were synthesized and coupled directly to the NBD (7-nitro-2-1,3-benzoxadiazol-4-yl)-group at the N-terminus by Peptide Specialty Laboratories GmbH (Heidelberg, Germany). For the quenching assay 740 μ l of PBS were mixed with 60 μ l of LUV suspension and incubated with the NBD-labeled peptides at 5 μ M for different time spans. NBD fluorescence from peptides remaining in the exterior of the LUVs was then quenched by adding 25 mM of the non membrane permeable sodium dithionite. Fluorescence was detected with a FluoroMax-4-spectrofluorometer (Horiba Jobin Yvon, Edison, USA). NBD was excited at 460 nm and the fluorescence was recorded at 544 nm. For measuring the maximal quenchable fluorescence of the peptides present in the exterior and also in the interior of the LUVs, 0.5 % Triton X-100 was added afterwards to dissolve the vesicles. Counts for total fluorescence and fluorescence after quenching were corrected by subtracting this non-quenchable fraction. The intravesicular peptide in LUVs was displayed as percentage of total fluorescence after dithionate quenching for the different NBD-peptides (●) R5-NBD, (▲) R7-NBD and (■) R9-NBD. At a first glance the percentage of transduction as measured by the non-quenched intra-LUV peptide fluorescence seemed to be low in comparison to the experiments in living cells. However, under our experimental conditions the total volume of LUVs corresponded to about 0.2 % of the suspension volume assuming a LUV diameter of 100 nm and a surface area of lipids of 0.6 nm². In the light of this estimate the results indicate an enrichment of peptides in the lumen of LUVs at least for R9.

3.5 An unexpected link between energy metabolism, calcium, chromatin condensation and cell cycle

Letter to the Editor

An Unexpected Link Between Energy Metabolism, Calcium, Chromatin Condensation and Cell Cycle

Robert M. Martin¹Sabine M. Görisch¹Heinrich Leonhardt²M. Cristina Cardoso^{1,*}¹Max Delbrück Center for Molecular Medicine; Berlin, Germany²Department of Biology; Ludwig Maximilians University Munich; Planegg-Martinsried, Germany

*Correspondence to: M. Cristina Cardoso; Max Delbrück Center for Molecular Medicine; Robert Rössle Str. 10; Berlin 13125 Germany; Email: cardoso@mdc-berlin.de

Original manuscript submitted: 07/10/07

Manuscript accepted: 07/13/07

Previously published online as a *Cell Cycle* E-publication:
<http://www.landesbioscience.com/journals/cc/article/4738>

KEY WORDS

ATP, calcium, chromatin condensation, fluorescence microscopy, histones, mitochondria, mitosis, sodium azide

ACKNOWLEDGEMENTS

We are indebted to Tony J. Collins (McMaster University, Hamilton, Canada) for extensive comments on the manuscript. We thank Christiane Alexander (MDC, Berlin, Germany) and Christian Freund (FMP, Berlin, Germany) for reagents. This work was supported by grants from the Volkswagen Foundation and the Deutsche Forschungsgemeinschaft to M. Cristina Cardoso and Heinrich Leonhardt.

NOTE

Supplemental material can be found at:
<http://www.landesbioscience.com/supplement/MartinCC6-19-Suppl.pdf>

Energy metabolism and calcium homeostasis play a central role in cell cycle progression and other cellular functions making them important targets for high throughput drug screenings. In the course of our studies on molecule dynamics and chromatin throughout the cell cycle we uncovered an unexpected link between energy metabolism, calcium release and chromatin condensation. To differentiate cellular processes driven by molecule diffusion versus active transport, cellular energy depletion experiments are commonly performed.¹⁻⁴ One of the chemicals often used is sodium azide (NaN₃), which inhibits the cytochrome oxidase and thus the mitochondrial respiratory chain resulting in ATP depletion.⁵

During our experiments on the live-cell dynamics of chromatin labeled with fluorescent histones throughout the cell cycle we made the observation that 10 min NaN₃ incubation causes a concentration dependent condensation of nuclear chromatin and a correspondingly enlarged interchromatin space (Fig. 1A).² In NaN₃ treated Hela cells the chromatin volume decreased down to 64 % of its size in untreated cells (Fig. 1A). In images of untreated cells, the diffuse borders of the chromatin result from decondensed chromatin fibers too small to be resolved by conventional microscopy. After NaN₃ incubation, this type of chromatin structure disappears in the images and only condensed chromatin is visible (Fig. 1). A similar effect was recently reported when living cells were subjected to hyperosmolar media. We, therefore, tested whether the NaN₃ induced chromatin condensation could be the result of intracellular changes of ion levels.⁶

First we tested the direct effect of different cations (Na⁺, K⁺, Ca²⁺ and Mg²⁺) on chromatin in cells. We permeabilized the plasma membrane briefly with digitonin⁷ and incubated the cells with hypertonic salt solutions (Fig. 1B). Fluorescently labeled dextrans were added to the media to monitor the permeabilization since the plasma membrane of untreated cells excludes dextrans (Fig. S1). In agreement with previous results⁶ we could observe chromatin condensation in intact cells incubated with any of the four cations tested (Fig. S1). However, in permeabilized cells only Ca²⁺ ions caused chromatin condensation, while even at high concentrations the other ions had no effect (Fig. 1B and Fig. S1). Calcium as a bivalent cation binds to DNA and was shown to be associated with chromatin during mitosis.⁸ We measured the change in chromatin volume by following cells progressing from mitosis into interphase and treating them with NaN₃. In this manner we overcome the problem of high variability within the cell population (Fig. 1C). While NaN₃ treatment caused a decrease of the chromatin volume to 74%, in mitosis this was further reduced to 41 % compared to untreated interphase cells. These data indicate that the NaN₃ causes chromatin condensation within a physiological range, which is lower than mitotic chromosomal condensation.

Next we tested whether intracellular calcium level changes in living cells during NaN₃ incubation using a fluorescent sensor molecule Fluo 3.⁹ The cell permeable Fluo 3 AM was loaded for 30 min into living cells and the Fluo 3 fluorescence emission measured before and during NaN₃ incubation. The data indeed revealed a 1.5 fold increase of the calcium levels following the NaN₃ incubation (Fig. 2A). The drop of the Fluo 3 fluorescence over time is likely due to the depletion of free calcium from the cytosol and nucleoplasm by binding to chromatin. The dynamic range of Fluo 3 fluorescence was tested by adding 5 µM ionomycin to the medium and reached a maximum of five-fold increase leading concomitantly to chromatin condensation (Fig. S2). The fact that NaN₃ induced chromatin condensation also in calcium free PBS with 10 mM EGTA (Fig. S3) indicates that the calcium increase is caused by release from intracellular stores and not by uptake from the extracellular milieu. Beside the endoplasmic reticulum, mitochondria are potent buffering sites for calcium and NaN₃ impairs mitochondrial functions.⁵ The effect of

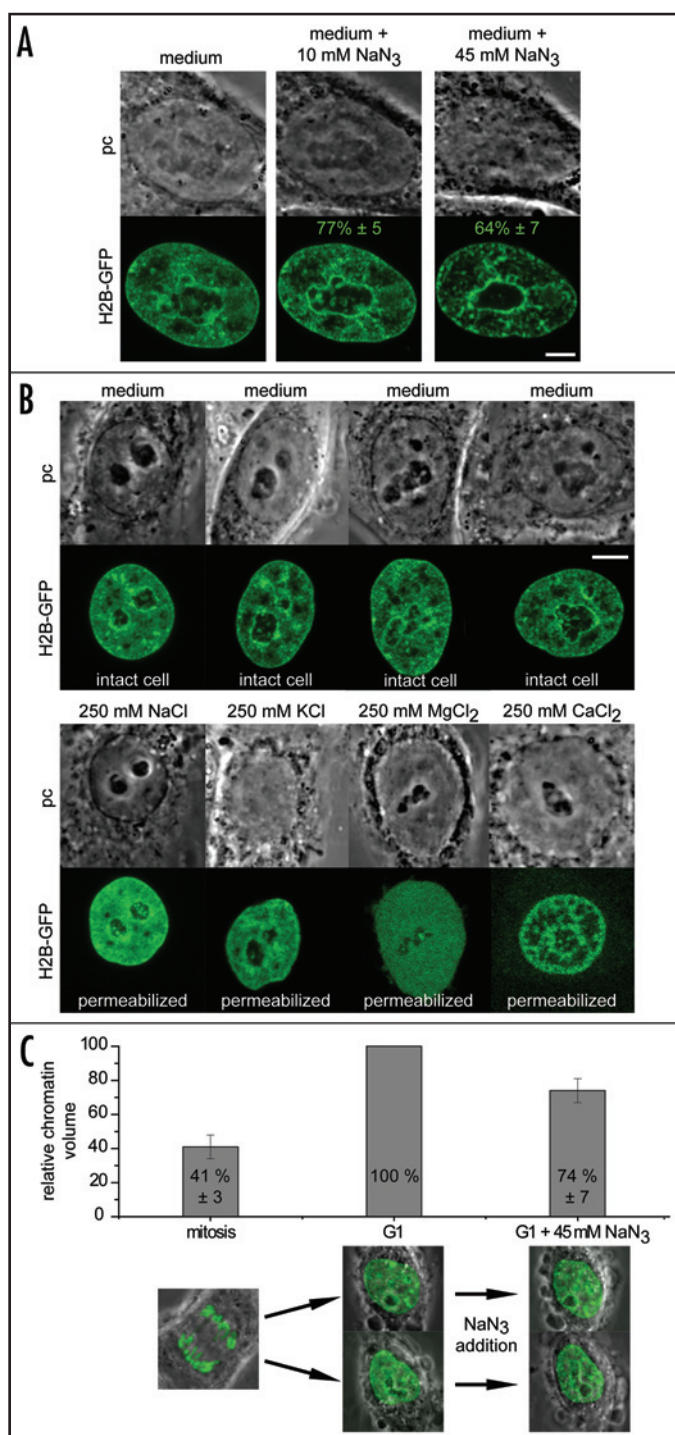


Figure 1. Chromatin condensation in living cells induced by NaN₃. (A) NaN₃ (Calbiochem) induces within 10 min a condensation of the nuclear chromatin in living HeLa cells expressing a histone H2B-GFP chromatin label. The chromatin volume is reduced progressively with increasing amounts of NaN₃ and the interchromatin space extends. The quantitative evaluation of the chromatin volume relative to the untreated cells was performed using ImageJ software and is given in the lower panels \pm standard deviation ($n = 10$ cells). The analysis was performed by determining and subtracting the background, followed by Gauss filtering and applying a fluorescence intensity threshold that included all chromatin. Finally, the thresholded chromatin volume for whole 3D image series was calculated using the voxel counter tool. (B) The effect of different salt ions on the chromatin condensation level. The plasma membranes of the living cells were mildly permeabilized by digitonin to test for direct effects of ions on chromatin. The top images show the intact cells in medium and the bottom images the same cells after digitonin treatment in the different 250 mM salt solutions. A condensation of the nuclear chromatin occurs only as a result of incubation in Ca²⁺ solution. The other ions Na⁺, K⁺ and Mg²⁺ do not induce condensation. The addition of Mg²⁺ caused a rather homogeneous distribution of chromatin, which probably is the result of nuclease activation by this cation. (C) The bar diagram displays the percentage of the chromatin volume of mitotic and NaN₃ treated G₁ cells compared to the chromatin volume in the same G₁ cell before treatment (see scheme below). For the comparison, the combined chromatin volume of the two G₁ daughter cells was taken to keep the total amount of chromatin constant relative to the mitotic cell. The chromatin is most condensed in mitosis with only about 41% of the interphase chromatin volume, while in cells treated with 45 mM NaN₃ the chromatin volume decreases to 74 % of the interphase volume. Scale bars, 5 μ m. pc, phase contrast.

an increase in the calcium level in the nucleus. Since extracellular calcium was not required for chromatin condensation, the intracellular calcium rise could be due to release from mitochondria or from the endoplasmic reticulum. The lowering of the ATP production by NaN₃ should concomitantly prevent calcium buffering by inhibiting the transport of free calcium by ATP dependent ion pumps into the mitochondria, endoplasmic reticulum as well as to the outside of the cell.¹⁰

These findings have important consequences for the interpretation of experiments using NaN₃ for ATP depletion and the analysis of molecule dynamics within the nucleus. Although the diffusive mobility of nuclear proteins is not ATP dependent,¹¹ the enlarged interchromatin space on the one hand and the higher condensation of chromatin on the other hand likely affects local protein concentration, mobility and access. Most importantly, our results show that external stimuli, manipulations and drugs directly or indirectly changing cellular calcium levels, by either energy depletion or direct interference with calcium homeostasis, have an effect on chromatin condensation and arrest cell cycle progression. These unexpected links between energy metabolism, calcium homeostasis, chromatin condensation and cell cycle should be taken in account for the design of drug screenings and the interpretation of cellular responses. Even small changes of free intracellular calcium levels may affect chromatin condensation and gene expression with still unknown consequences.

NaN₃ on mitochondria in living cells can be directly tested with dyes (e.g., MitoTrackerRed) that are taken up into the organelle and accumulated via the membrane potential. We incubated living cells with MitoTracker for 30 min followed by change to media without dye for 45 min. Cells were imaged before and after adding NaN₃ to monitor possible changes in the mitochondria. Within a few minutes of NaN₃ incubation the filamentous mitochondrial population were fragmented into small sphere like remains (Fig. 2B). Furthermore the decrease of the dye signal from the mitochondria indicates a lowering or loss of the membrane potential. Altogether, these results show that NaN₃ disrupts the mitochondrial membrane potential inducing

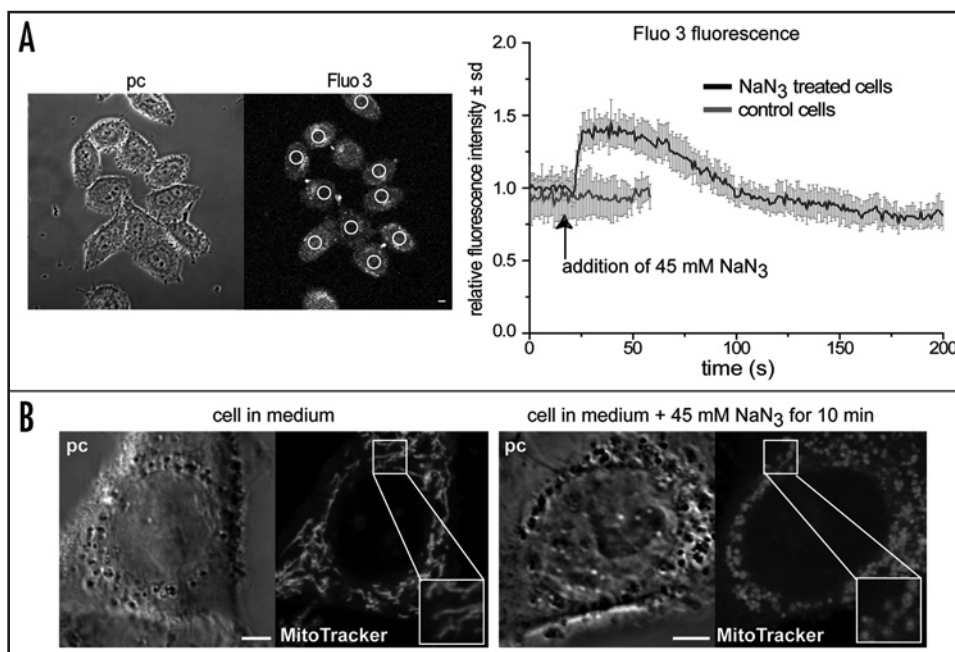


Figure 2. NaN_3 triggers cellular calcium rise and fragmentation of mitochondria. (A) Microscopic fluorescence imaging of the calcium sensor Fluo 3 (Molecular Probes) in living cells. The fluorescence image shows Fluo 3 loaded into HeLa cells in normal growth medium (corresponding to 10 s in the curve). The areas of measurement (white circles) were chosen according to the position of the nuclei identified in the phase contrast image. The curve describes the mean nuclear Fluo 3 fluorescence over time ($n = 10$ cells \pm standard deviation), showing a rise of fluorescence shortly after addition of NaN_3 to the culture medium, indicated by the arrow. The Fluo 3 fluorescence increases up to 1.5 fold over the normal level before NaN_3 addition and in control cells (gray curve) which corresponds to a calcium rise of about two-fold according to the fluorescence calibration curve given by the manufacturer. (B) The mitochondria of living HeLa cells expressing histone H2B-GFP were imaged using MitoTrackerRed (Molecular Probes). The images display confocal optical sections of control cells (left) and 10 min after NaN_3 incubation (right). The tubular and filamentous mitochondrial structure in the left image and inset collapse into small dot-like remains and indicate a loss of mitochondrial fission and fusion events. Scale bar, 5 μm . pc, phase contrast.

References

- Calapez A, Pereira HM, Calado A, Braga J, Rino J, Carvalho C, Tavanetz JP, Wahle E, Rosa AC, Carmo-Fonseca M. *J Cell Biol* 2002; 159:795-805.
- Görsch SM, Wachsmuth M, Itrich C, Bacher CP, Rippe K, Lichter P. *Proc Natl Acad Sci USA* 2004; 101:13221-6.
- Heun P, Laroche T, Shimada K, Furrer P, Gasser SM. *Science* 2001; 294:2181-6.
- Phair RD, Misteli T. *Nature* 2000; 404:604-9.
- Leary SC, Hill BC, Lyons CN, Carlson CG, Michaud D, Kraft CS, Ko K, Glerum DM, Moyes CD. *J Biol Chem* 2002; 277:11321-8.
- Albiez H, Cremer M, Tiberi C, Vecchio L, Schermelleh L, Dittrich S, Kupper K, Joffe B, Thormeyer T, von Hase J, Yang S, Rohr K, Leonhardt H, Solovei I, Cremer C, Fakan S, Cremer T. *Chromosome Res* 2006; 14:707-33.
- Adam SA, Sterne-Marr R, Gerace L. *Methods Enzymol* 1992; 219:97-110.
- Strick R, Strissel PL, Gavrillov K, Levi-Setti R. *J Cell Biol* 2001; 155:899-910.
- Hanley PJ, Musset B, Renigunta V, Limberg SH, Dalpke AH, Sus R, Heeg KM, Preisig-Muller R, Daut J. *Proc Natl Acad Sci USA* 2004; 101:9479-84.
- Duszynski J, Kozziel R, Bratkowski W, Szczepanowska J, Zablocki K. *Biochim Biophys Acta* 2006; 1757:380-7.
- Phair RD, Gorski SA, Misteli T. *Methods Enzymol* 2004; 375:393-414.

Letter to the Editor

An Unexpected Link Between Energy Metabolism, Calcium, Chromatin Condensation and Cell Cycle

Robert M. Martin¹Sabine M. Görisch¹Heinrich Leonhardt²M. Cristina Cardoso^{1,*}¹Max Delbrück Center for Molecular Medicine; Berlin, Germany²Department of Biology; Ludwig Maximilians University Munich; Planegg-Martinsried, Germany*Correspondence to: M. Cristina Cardoso; Max Delbrück Center for Molecular Medicine; Robert Rössle Str. 10; Berlin 13125 Germany; Email: cardoso@mdc-berlin.de

Original manuscript submitted: 07/10/07

Manuscript accepted: 07/13/07

This manuscript has been published online, prior to printing for Cell Cycle, Volume 6, Issue 18. Definitive page numbers have not been assigned. The current citation is: Cell Cycle 2007; 6(18):

<http://www.landesbioscience.com/journals/cc/article/4738>

Once the issue is complete and page numbers have been assigned, the citation will change accordingly.

KEY WORDS

ATP, calcium, chromatin condensation, fluorescence microscopy, histones, mitochondria, mitosis, sodium azide

ACKNOWLEDGEMENTS

We are indebted to Tony J. Collins (McMaster University, Hamilton, Canada) for extensive comments on the manuscript. We thank Christiane Alexander (MDC, Berlin, Germany) and Christian Freund (FMP, Berlin, Germany) for reagents. This work was supported by grants from the Volkswagen Foundation and the Deutsche Forschungsgemeinschaft to M. Cristina Cardoso and Heinrich Leonhardt.

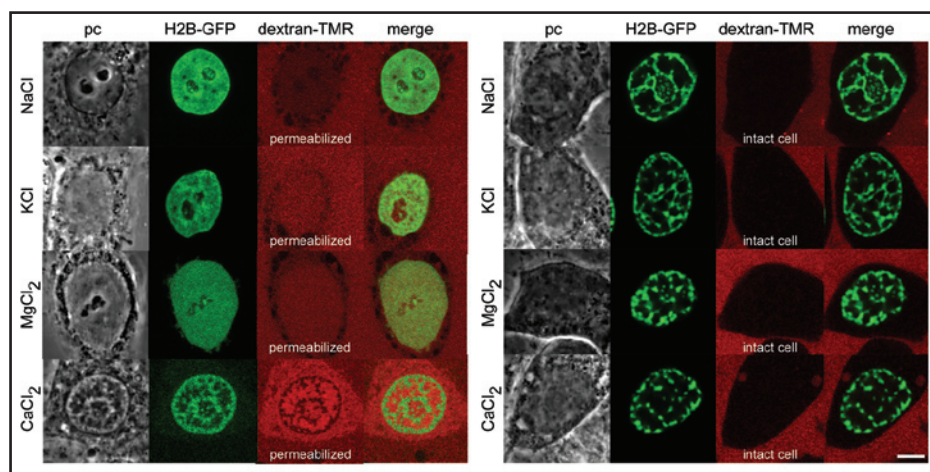


Figure S1. Effect of different cations combined with digitonin permeabilization on chromatin condensation. The effect of digitonin visualized in living HeLa cells was controlled by the exclusion or not of fluorescently labeled 10 kDa dextrans added to the cell medium. In permeabilized cells the dextrans reach also the nucleus (left panel) and the effect of the different ions is displayed as in Figure 1. In intact cells all of the hyperosmolar ion solutions (250 mM) induce chromatin condensation (right panel). Scalebar 5 μ m. pc = phase contrast.

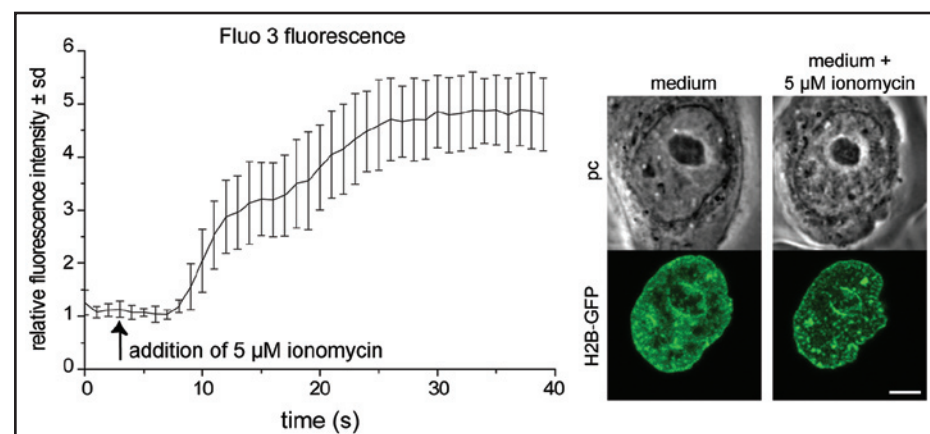


Figure S2. Extracellular calcium influx triggered by ionomycin causes chromatin condensation. Adding ionomycin (5 μ M; Calbiochem) to the medium of living cells results in a transport of extracellular calcium to the cellular interior. The fluorescence intensity increase of Fluo 3 displays the maximal intensity of the calcium sensor with the highest intracellular calcium concentration. Our measurements (mean nuclear fluorescence intensity, $n=10$ cells \pm standard deviation) show a five-fold increase of the Fluo 3 fluorescence over the basic fluorescence intensity in untreated cells. The influx of extracellular calcium causes also chromatin condensation, which is shown in the images. Scalebar 5 μ m. pc = phase contrast.

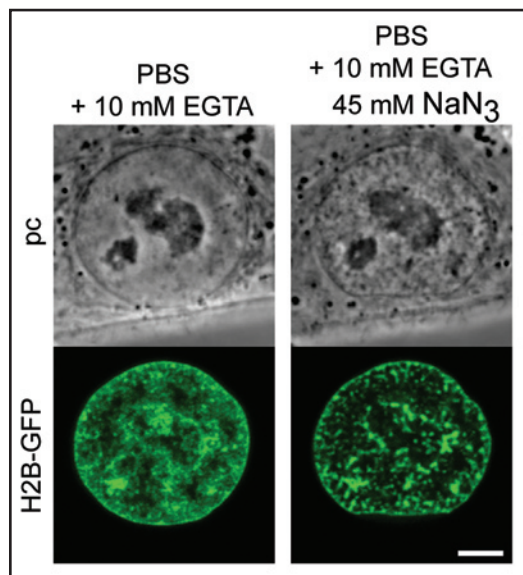


Figure S3. NaN₃ induces chromatin condensation independent of extracellular calcium. The condensation of chromatin using NaN₃ is also achieved in a calcium free buffer, which excludes extracellular calcium as a possible source for the intracellular calcium rise. The cells were incubated in PBS supplemented with 10 mM EGTA for 15 min to deplete extracellular calcium and subsequently 45 mM NaN₃ was added. Scalebar 5 μ m. pc = phase contrast.

3.6 Chromatin condensation modulates access and binding of nuclear proteins

Martin et al.

Chromatin condensation modulates access and binding of nuclear proteins

Robert M. Martin¹ and M.Cristina Cardoso^{1,2*}

¹ Max Delbrück Center for Molecular Medicine, 13125 Berlin, Germany

² Darmstadt University of Technology, Department of Biology, 64287 Darmstadt, Germany

* Correspondence to: M. Cristina Cardoso, e-mail: cardoso@mdc-berlin.de, Tel. +49-30-94062109, Fax +49-30-94063343

Running title

Dynamics of chromatin accessibility

Abstract

The condensation level of chromatin is controlled by epigenetic modifications and associated regulatory factors that change throughout differentiation and cell cycle progression. To test whether changes of chromatin condensation levels *per se* affect access and binding of proteins we used a hypertonic cell treatment. This shift to hyperosmolar media caused increased nuclear calcium concentrations and induced a reversible chromatin condensation comparable to levels in mitosis but independent of mitotic histone H3 serine 10 phosphorylation. Photobleaching experiments with H2B-GFP and GFP-HP1 α before and after induced chromatin condensation showed that the exchange of integral as well as associated chromatin proteins is affected. Photoactivation of PAGFP-HP1 α demonstrated that hypercondensation reduces the dissociation rate and stabilized HP1 chromatin binding. Finally, measuring the distribution of nucleoplasmic proteins in the range from 30 to 230 kDa we found that even relatively small proteins like GFP are at least partially excluded from hypercondensed chromatin in living cells. These results suggest that structural changes in condensed chromatin by themselves affect chromatin access and binding of chromatin proteins independent of regulatory histone modifications.

Key words

Chromatin accessibility, chromatin condensation, fluorescence microscopy, photoactivation, photobleaching

Martin et al.

The cell nucleus is a highly organized organelle storing and translating genetic information. Although there are no substructures separated by membranes, the nucleus is compartmentalized for different functions in nucleic acid metabolism.¹ The nuclear DNA is organized together with structural proteins into dynamic higher order chromatin structures, which reflect and control gene expression during the cell cycle and cellular differentiation.^{2,3} As a consequence of a complex and not yet understood interplay between chromatin condensation state, transcriptional activity and modifications of chromatin organizing proteins, chromatin subsets are termed eu- and heterochromatin.^{4,5} Euchromatin in interphase cells is actively transcribed and less condensed while heterochromatin is transcriptionally inactive with a condensation level similar to mitotic chromosomes.⁶ During mitotic chromatin condensation, DNA metabolism (e.g., transcription and replication) stops and only resumes after chromatin decondensation in early G1 phase. The condensation of chromatin is characterized by a reduction of volume due to a spatial organization into densely packed higher order structures.⁷ Specific histone modifications, e.g. histone H1 and H3 phosphorylation, occur at mitosis and contribute to the individualization and condensation of chromosomes. The consequences of this compaction into condensed chromosomes at mitosis are reduced free volumes and less exposed surface of the chromatin substructures on which molecules could interact.^{8,9} However, it is unclear whether and how changes in the chromatin condensation state and/or histone modifications affect the distribution and access of nucleoplasmic proteins and the mobility of chromatin organizing proteins.

Interphase chromatin has been shown to be accessible to macromolecules^{10,11}, chromatin proteins¹² and neutral inert proteins even at the single molecule level¹³. Furthermore, certain transcription and chromatin factors have been shown to still have access to chromosomes in mitosis when the DNA metabolism stops.¹⁴ Therefore, the relationship between nuclear protein distribution, chromatin accessibility and how changes in chromatin condensation over the cell cycle impact on DNA metabolism remains unclear. In this study, we have manipulated chromatin condensation in interphase cells to test whether the level of chromatin condensation independently of mitotic histone modifications can impact on mobility and accessibility of nuclear proteins.

Manipulation and quantitative evaluation of chromatin condensation mechanisms

The maximal chromatin condensation takes place at every mitosis in cycling cells and results in a cessation of DNA metabolism. The latter could be the result of M-phase specific modifications of chromatin proteins (e.g., histone modifications) directly preventing the access of factors to the genome and/or structural changes of chromatin hindering access by increased compaction. To distinguish between these possibilities, we made use of an approach to induce hypercondensation of chromatin during interphase.¹⁵

We first compared the chromatin volumes of individual living HeLa cells labeled with histone H2B-GFP fusion proteins in different cell cycle stages and after chromatin condensing treatment. The same cells were imaged beginning in mitosis and through reentry into G1 followed by induced chromatin condensation by incubation in hyperosmolar medium for 5 minutes. We then measured the chromatin volumes in the three conditions to test whether the treatment reduced interphase chromatin volumes to the level of mitotic chromosome volumes (Fig 1). The chromatin volume measurements for mitosis and hyperosmolar condensation in G1 showed similar levels of 39% \pm sd 9% and 40% \pm sd 11% respectively, relative to G1 chromatin in the same cells before treatment (Fig 1). This hypercondensation of chromatin was reversible within 10 minutes of returning to normal osmolar medium and resulting in cessation of DNA metabolic processes such as transcription and replication (data not show and ¹⁵). We, therefore, conclude that this approach generated condensation of chromatin in interphase nuclei to the same extent as mitotic chromatin. Next, we assessed the occurrence of typical chromatin modifications in mitotic chromosomes and hypercondensed interphase chromatin. At mitosis, phosphorylated histone H3 at serine 10 is associated with the individualization and condensation of chromosomes.¹⁶ Although we found similar levels of chromatin condensation (Fig 1), no mitosis specific histone H3 phosphorylation was detected (Fig 2A). Hence, the process of hyperosmolar chromatin condensation relies on a different pathway, which does not involve cell cycle specific histone modifications but rather profound structural changes.

Since we had previously reported that cellular energy depletion using Na-azide leads to interphase chromatin condensation with increased calcium level in the nucleus¹⁷, we measured the levels of

Martin et al.

this cation using the fluorescent calcium sensor Fluo 3 before and after hypertonic treatment. Our data demonstrates that the condensation of chromatin by hyperosmolarity is accompanied by a seven-fold rise in the intranuclear calcium level (Fig 2B). Subsequent addition of the calcium ionophore ionomycin to the cells led to an even higher increase establishing that our measurements were not performed under saturating conditions.

Taken together these results indicate that reversible hypercondensation of interphase chromatin occurs in the absence of mitotic histone modifications, likely as a result of increased intranuclear calcium levels, and leads to a stop in DNA metabolism.

Accessibility of proteins to different chromatin condensation states

Next, we assayed the impact of chromatin condensation levels on the accessibility of nuclear proteins.

Large number of nuclear proteins bind to or are incorporated into chromatin structures throughout the cell cycle. We therefore tested whether chromatin condensation level affects their access to and their dynamics at chromatin. We selected a nucleosome core histone (H2B) and a heterochromatin binding protein (HP1) as representative chromatin proteins and analyzed their chromatin access and mobility by photobleaching and photoactivation experiments.

The nucleosome protein H2B-GFP was not redistributed upon hyperosmotic chromatin hypercondensation (Fig 3A). Fluorescence recovery after photobleaching (FRAP) analysis showed, in accordance to previous reports¹², that the half-time of recovery ($t_{1/2}$) in interphase chromatin for this core histone was about 180 min. Upon hyperosmolar treatment, only about 5% fluorescence recovery could be measured within the same time, indicating that the access to and/or release of the core histone H2B from fully condensed interphase chromatin was affected.

Chromatin proteins that are not core components of the nucleosome often associate less tightly to chromatin and DNA than histones. The heterochromatin protein HP1 α binds to methylated histone H3 and accumulates in heterochromatin. We measured the half recovery time of GFP-HP1 α in interphase heterochromatin of HeLa cells and compared it with hypercondensed chromatin in interphase and mitotic cells. In interphase heterochromatin the $t_{1/2}$ was 2 s (Fig 3B), which fits well with previously reported half recovery times of 1 to 10 s.^{18,19} In hypercondensed interphase

Martin et al.

chromatin though HP1 α recovery in the FRAP analysis was slower with a $t_{1/2}$ increased to 20 s. To clarify whether HP1 α was transiently trapped in the hypercondensed interphase chromatin, we performed photoactivation experiments and measured the dissociation of fluorescent PAGFP-HP1 α molecules from the heterochromatin spots in the photoactivated area. Analysis of the fluorescence decay curves (Fig 3C) revealed that HP1 α $t_{1/2}$ of dissociation from interphase heterochromatin was 8 s, compared to a 6.5 fold slower $t_{1/2}$ of 52 s in hypercondensed interphase chromatin. These results indicate a reduced mobility and a transient trapping of HP1 α .

Taken together we could demonstrate that the hypercondensed interphase chromatin was less accessible and reduced the exchange of chromatin proteins like core histones and heterochromatin binding proteins.

We then measured the access of non-chromatin proteins to the differently condensed chromatin. We chose GFP as a neutral probe protein and imaged the same cells before and after hyperosmolar treatment to directly compare the distribution of proteins relative to chromatin within the same cell. Furthermore, we compared the results to mitotic chromatin.

Fig 4 shows confocal optical sections of living cells displaying the distribution of the inert tracer protein GFP relative to H2B-mRFP labeled chromatin. The relative distribution was then analyzed quantitatively first by plotting the GFP signal intensity versus the histone-labeled chromatin along a line across the nucleus (linescan analysis, Fig 4B) and second by a correlation analysis (Fig 4C). The latter included both the display of all red and green pixels within the nucleus, excluding the nucleoli, in intensity scatter plots, and the calculation of the Pearson's coefficient R as a measure for correlation (+1), anti-correlation (-1) or no correlation (0) of two color channels in images.²⁰

In mitosis the GFP was mostly excluded from chromatin, visible as dark areas where the chromosomes are located (Fig 4A, left column). The exclusion is displayed in the linescan by a drop of the GFP intensity and inverse progression of the chromatin intensity. The scatter plot showed a distribution in a sharp cone of moderate negative slope, with the lowest GFP intensities in the region of occupied by the chromosomes. Finally, the Pearson's correlation coefficient of $R = -0.8 \pm \text{sd } 0.2$ clearly demonstrated an anti-correlation of GFP and mitotic chromosomes. In the interphase cell (Fig 4A, middle column) GFP showed an overall much more homogeneous

Martin et al.

distribution throughout the nucleus with exception of the nucleoli, corroborated further by the linescan analysis depicting a reduction of GFP in the nucleoli (Fig 4B, arrowhead). In some larger heterochromatin spots we could observe some reduction of the GFP concentration (Fig 4B, arrow). The scatter plot displayed the GFP and chromatin pixel intensities as a cloud in the center of the plot and the R-value of $-0.1 \pm \text{sd } 0.1$ close to zero indicated no correlation (Fig 4C). After induced condensation of interphase chromatin to mitotic chromosome volume, a chromatin network like structure became apparent. The GFP redistributed mostly to the regions not occupied by chromatin, which corresponded to an enlarged interchromatin space (Fig 4A, right column). The GFP exclusion from condensed interphase chromatin was clearly shown by the inverse correlation of the linescan data (Fig 4B) and the shift towards a negative slope on the scatter plot and the negative R-value of $-0.6 \pm \text{sd } 0.1$ (Fig 4C).

To test whether this exclusion of proteins from the compacted chromatin was a general phenomenon for non chromatin bound nuclear proteins we extended this analysis to several nucleoplasmic proteins of increasing size up to 230 kDa (Fig S1). As for GFP, all proteins tested independent of their size showed a similar level negative correlation with mitotic as well as interphase hypercondensed chromatin.

In summary, making use of a hypertonic treatment we could achieve in interphase cells a chromatin condensation level similar to mitotic chromosomes in the absence of the typical mitotic histone modifications and likely due to increased intranuclear calcium level. Increasing the chromatin condensation lead to a slowed exchange of chromatin proteins. Furthermore, although in general interphase chromatin was accessible to non-chromatin proteins within a size range of 30-230 kDa, upon hypercondensation they redistributed away and exhibited an anti-correlated distribution to the same level than to mitotic chromatin. This concentration reduction of non chromatin proteins could therefore, concomitantly with other chromatin modifications, be involved in the shutdown of DNA metabolism in mitosis. These data are also consistent with the results from our recent analysis of the mobility and access of single streptavidin proteins to heterochromatin where these interphase chromatin domains exhibited quite some permeability to this neutral average sized protein.¹³

Martin et al.

It has been debated over the past years whether and how chromatin can exclude nuclear factors and the contribution of this effect for DNA metabolism and heterochromatin function. Different studies indicated that macromolecules have access to interphase chromatin. However, these studies have used carbohydrates like dextrans, which may behave differently from nuclear proteins.^{21,10} In addition, access to chromatin was not analyzed at different condensation levels. Photodynamic studies showed that chromatin in interphase and mitosis is accessible to chromatin factors like histones and heterochromatin proteins.^{14,22,19} Our data also showed that condensed chromatin was accessible to nucleosomal proteins and other chromatin associated factors that are involved in heterochromatin maintenance. On the other hand, our results indicate that the concentration of nucleoplasmic proteins that are not associated with nucleosomes is low in chromatin with higher condensation level. We suggest that the partial exclusion of nucleoplasmic proteins is due to increased structural restrictions and dense environments occupied by condensed chromatin and concentrated chromatin binding factors. In the condensed chromatin structures the competition for available volume favors high affinity chromatin binding factors and decreases the number of nucleoplasmic proteins with less or no affinity to those structures. In mitosis the reduced access of proteins could, in addition to specific chromatin modifications, reduce genome wide accessibility and, thereby, contribute to the mitotic shutdown of transcription, replication and other DNA dependent processes. The modulation of protein access and consequently local protein concentration could constitute a general mechanism for the regulation of binding dynamics, enzymatic activities and DNA metabolism.

Acknowledgements

We thank Sabine Görsch for many discussions, Jeffrey H. Stear for comments on the manuscript and Ulrike Ziebold for the kind gift of anti-phospho H3 antibody. We are indebted to Heinrich Leonhardt for numerous discussions and helpful suggestions throughout the course of this project. This work was funded by grants of the German Research Council (DFG) to MCC.

References

1. Cremer, T., Kreth, G., Koester, H., Fink, R. H., Heintzmann, R., Cremer, M., Solovei, I., Zink, D. & Cremer, C. (2000). Chromosome territories, interchromatin domain compartment, and nuclear matrix: an integrated view of the functional nuclear architecture. *Crit Rev Eukaryot Gene Expr* **10**, 179-212.
2. Belmont, A. S., Dietzel, S., Nye, A. C., Strukov, Y. G. & Tumber, T. (1999). Large-scale chromatin structure and function. *Curr Opin Cell Biol* **11**, 307-11.
3. Cremer, T., Kupper, K., Dietzel, S. & Fakan, S. (2004). Higher order chromatin architecture in the cell nucleus: on the way from structure to function. *Biol Cell* **96**, 555-67.
4. Richards, E. J. & Elgin, S. C. (2002). Epigenetic codes for heterochromatin formation and silencing: rounding up the usual suspects. *Cell* **108**, 489-500.
5. Kouzarides, T. (2007). Chromatin modifications and their function. *Cell* **128**, 693-705.
6. Francastel, C., Schubeler, D., Martin, D. I. & Groudine, M. (2000). Nuclear compartmentalization and gene activity. *Nat Rev Mol Cell Biol* **1**, 137-43.
7. Mora-Bermudez, F. & Ellenberg, J. (2007). Measuring structural dynamics of chromosomes in living cells by fluorescence microscopy. *Methods* **41**, 158-67.
8. Belmont, A. S. (2006). Mitotic chromosome structure and condensation. *Curr Opin Cell Biol* **18**, 632-8.
9. Daban, J. R. (2003). High concentration of DNA in condensed chromatin. *Biochem Cell Biol* **81**, 91-9.
10. Verschure, P. J., Van Der Kraan, I., Manders, E. M., Hoogstraten, D., Houtsmuller, A. B. & Van Driel, R. (2003). Condensed chromatin domains in the mammalian nucleus are accessible to large macromolecules. *EMBO Rep* **4**, 861-866.
11. Görisch, S. M., Wachsmuth, M., Toth, K. F., Lichter, P. & Rippe, K. (2005). Histone acetylation increases chromatin accessibility. *J Cell Sci* **118**, 5825-34.
12. Kimura, H. & Cook, P. R. (2001). Kinetics of core histones in living human cells: little exchange of H3 and H4 and some rapid exchange of H2B. *J Cell Biol* **153**, 1341-53.

Martin et al.

13. Grünwald, D., Martin, R. M., Buschmann, V., Bazett-Jones, D. P., Leonhardt, H., Kubitscheck, U. & Cardoso, M. C. (2008). Probing intranuclear environments at the single-molecule level. *Biophys J* **94**, 2847-58.
14. Chen, D., Dundr, M., Wang, C., Leung, A., Lamond, A., Misteli, T. & Huang, S. (2005). Condensed mitotic chromatin is accessible to transcription factors and chromatin structural proteins. *J Cell Biol* **168**, 41-54.
15. Albiez, H., Cremer, M., Tiberi, C., Vecchio, L., Schermelleh, L., Dittrich, S., Kupper, K., Joffe, B., Thormeyer, T., von Hase, J., Yang, S., Rohr, K., Leonhardt, H., Solovei, I., Cremer, C., Fakan, S. & Cremer, T. (2006). Chromatin domains and the interchromatin compartment form structurally defined and functionally interacting nuclear networks. *Chromosome Res* **14**, 707-33.
16. Hendzel, M. J., Wei, Y., Mancini, M. A., Van Hooser, A., Ranalli, T., Brinkley, B. R., Bazett-Jones, D. P. & Allis, C. D. (1997). Mitosis-specific phosphorylation of histone H3 initiates primarily within pericentromeric heterochromatin during G2 and spreads in an ordered fashion coincident with mitotic chromosome condensation. *Chromosoma* **106**, 348-60.
17. Martin, R. M., Gorisch, S. M., Leonhardt, H. & Cardoso, M. C. (2007). An Unexpected Link Between Energy Metabolism, Calcium, Chromatin Condensation and Cell Cycle. *Cell Cycle* **6**.
18. Cheutin, T., McNairn, A. J., Jenuwein, T., Gilbert, D. M., Singh, P. B. & Misteli, T. (2003). Maintenance of stable heterochromatin domains by dynamic HP1 binding. *Science* **299**, 721-5.
19. Schmiedeberg, L., Weissbart, K., Diekmann, S., Meyer Zu Hoerste, G. & Hemmerich, P. (2004). High- and low-mobility populations of HP1 in heterochromatin of mammalian cells. *Mol Biol Cell* **15**, 2819-33.
20. Manders, E. M., Verbeek, E. J. & Aren, J. A. (1993). Measurement of colocalization of objects in dual-colour confocal images. *J Microsc* **169**, 175-182.
21. Görisch, S. M., Richter, K., Scheuermann, M. O., Herrmann, H. & Lichter, P. (2003). Diffusion-limited compartmentalization of mammalian cell nuclei assessed by microinjected macromolecules. *Exp Cell Res* **289**, 282-94.

Martin et al.

22. Dialynas, G. K., Terjung, S., Brown, J. P., Aucott, R. L., Baron-Luhr, B., Singh, P. B. & Georgatos, S. D. (2007). Plasticity of HP1 proteins in mammalian cells. *J Cell Sci* **120**, 3415-24.
23. Kanda, T., Sullivan, K. F. & Wahl, G. M. (1998). Histone-GFP fusion protein enables sensitive analysis of chromosome dynamics in living mammalian cells. *Curr Biol* **8**, 377-385.
24. Ellenberg, J., Lippincott-Schwartz, J. & Presley, J. F. (1999). Dual-colour imaging with GFP variants. *Trends Cell Biol* **9**, 52-6.
25. Campbell, R. E., Tour, O., Palmer, A. E., Steinbach, P. A., Baird, G. S., Zacharias, D. A. & Tsien, R. Y. (2002). A monomeric red fluorescent protein. *Proc Natl Acad Sci U S A* **99**, 7877-82.
26. Patterson, G. H. & Lippincott-Schwartz, J. (2002). A Photoactivatable GFP for Selective Photolabeling of Proteins and Cells. *Science* **297**, 1873-1877.
27. Cardoso, M. C., Joseph, C., Rahn, H. P., Reusch, R., Nadal-Ginard, B. & Leonhardt, H. (1997). Mapping and use of a sequence that targets DNA ligase I to sites of DNA replication in vivo. *J Cell Biol* **139**, 579-87.
28. Easwaran, H. P., Schermelleh, L., Leonhardt, H. & Cardoso, M. C. (2004). Replication-independent chromatin loading of Dnmt1 during G2 and M phases. *EMBO Rep* **5**, 1181-6.
29. Leonhardt, H., Rahn, H. P., Weinzierl, P., Sporbert, A., Cremer, T., Zink, D. & Cardoso, M. C. (2000). Dynamics of DNA replication factories in living cells. *J Cell Biol* **149**, 271-80.
30. Easwaran, H. P., Leonhardt, H. & Cardoso, M. C. (2007). Distribution of DNA replication proteins in Drosophila cells. *BMC Cell Biol* **8**, 42.

Figure legends**Fig 1 Manipulation and quantification of chromatin condensation states**

Individual HeLa cells expressing H2B-GFP as a marker for chromatin²³ were visualized starting in mitosis (left panel) into G1 (mid panel) and following incubation in hyperosmolar medium (right panel). The cells were grown in DMEM with 10% fetal calf serum, 5 mM L-glutamine, 5 g/ml Gentamycine and the hypercondensation medium was composed of a dilution of 10x PBS in growth medium to yield 4x PBS equivalent to a 500 mM saline solution. Cells were in plated in 8-well Ibidi chambers (Ibidi, Munich, Germany). Live cell microscopy was performed with a Zeiss LSM510Meta confocal setup on a Zeiss Axiovert 200M inverted microscope with a 63x phase contrast plan-apochromat oil objective NA 1.4 (Carl Zeiss, Germany). The microscope is housed in a humidified chamber heated to 37°C (Okolab, Ottaviano, Italy). For acquisition the main beam splitter was HFT UV/488/543/633, GFP was excited by 488 nm Argon laser and detected with a 500-530 nm bandpass filter. Acquisition settings were identical for individual cells in repeated imaging experiments. At each time-point complete high resolution confocal z-stacks were acquired and projections are shown. Scale bar 5 μ m. Chromatin volume calculations were derived from complete z-stacks and processed in Image J. Images were gauss filtered and background subtracted, then thresholded and the volumes calculated with the voxel counter plugin. The bar diagram summarizes the chromatin volume data as mean \pm standard deviation (N = ten cells) relative to the value for G1 interphase chromatin in the same cell.

Fig 2 Different pathways of chromatin condensation in mitosis and hyperosmolar condensation

A) Histone H3 is modified by phosphorylation at serine 10 during mitosis and was detected in formaldehyde fixed HeLa H2B-GFP cells using anti-phospho H3S10 specific antibodies. For immunofluorescence staining, cells were washed in PBS and, in case of hyperosmolar treatment incubated for 15 min in 4x PBS, fixed in 3.7% formaldehyde diluted in PBS or 4x PBS respectively and permeabilized with 0.25% Triton X100 in PBS. The primary anti-phospho H3 rabbit polyclonal antibody (catalog number 06-570, Millipore, Schwalbach, Germany) was diluted in PBS containing

Martin et al.

0.2 % fish skin gelatin and detected using goat anti-rabbit IgG (Jackson, Newmarket, UK). In the top panel the phosphorylated histone H3 signal (red) co-localizes with the histone H2B-GFP labeled chromosomes in the mitotic cell but it is not detected in the interphase cell. In the lower panel the chromatin was condensed by hyperosmolar treatment to induce a interphase chromatin volume comparable to mitotic chromosomes (see Fig 1). As in the untreated cells, the mitosis specific histone H3 phosphorylation is not detectable in the interphase nucleus and only in the mitotic chromosomes suggesting a different pathway of mitotic and hyperosmolar chromatin condensation.

The graph in B) displays intranuclear calcium levels in HeLa cells (N = 10) measured by timelapse microscopy using the fluorescent calcium sensor Fluo 3. The Fluo 3 (Invitrogen, Paisley, UK) labeling and measurements were performed as described before.¹⁷ For untreated cells the initial Fluo 3 fluorescence intensity was normalized to 1 and, following the incubation in hyperosmolar 4x PBS solution, increased seven fold. To test for saturation effects and dynamic range of the Fluo 3 measurement conditions, the calcium ionophore ionomycin was added subsequently to the cells to induce maximum calcium uptake. This displays the whole range of fluorescence intensities measurable by the calcium sensor under the same imaging conditions and further suggests that the change in chromatin condensation after 4xPBS incubation involves a significant change in the calcium level. Scale bar 5 μ m.

Fig 3 Distribution and mobility of chromatin proteins in different chromatin condensation states

HeLa cells stably expressing H2B-GFP as well as HeLa cells transiently transfected with plasmids coding for H2B-mRFP and either GFP-HP1 α or PAGFP-HP1 α were used in photobleaching or photoactivation experiments of the respective chromatin proteins as indicated.

The histone H2B-mRFP plasmid was constructed by cutting out CFP from pH2B-CFP²⁴ with BamHI + MfeI and ligating in the mRFP cDNA cut with EcoRI + BamHI from pRSET-mRFP1.²⁵

The photoactivatable HP1 α construct was created by inserting the human HP1 α cDNA derived from pBCHGN-HP1-alpha¹⁸ cut with Hind III and BamH I into the Hind III and Bgl II of pPAGFP-

Martin et al.

C1.²⁶ Double transfection of cells was carried out by CaPO₄ precipitation method²⁷ or using Transfectin reagent (BioRad, Munich, Germany). Live cell microscopy was performed as described in Fig 1 and mRFP was excited by a 543 nm HeNe laser and detected using a 585-615 bandpass filter. Photobleaching and photoactivation were performed with a short intense pulse of 488 nm Argon laser beam. For all experiments, the areas photobleached (ba) and photoactivated (pa) are indicated by squares and the times after photobleaching/activation are given in the images. FRAP data were corrected for cell translational and rotational movements with the Image J 'stack_reg' plugin. The datasets were analyzed, evaluated and displayed in Origin 7. The photobleaching and photoactivation redistribution data were normalized, averaged and corrected for photobleaching or photoactivation by the image acquisition process. The half equilibrium times $t_{1/2}$ were derived in Origin 7 from bi-exponential decay fit curves.

The photobleaching experiment in A) shows histone H2B-GFP dynamics in interphase HeLa cells. Untreated interphase chromatin (top) and hyperosmolar condensed chromatin (bottom) are shown. In B) photobleaching experiments with HP1 α -GFP are displayed for cells in interphase (top) and with hyperosmolar condensed interphase chromatin (bottom). Corresponding fluorescence recovery curves are shown on the right as the mean of ten cells with standard deviation. C) depicts the photoactivation experiments with HP1 α fused to PAGFP. In the images before fluorescence activation the nucleus and chromosomes visualized independently with H2B-mRFP fusion are encircled by a dotted line. The dissociation of HP1 α from chromatin measured by the loss of photoactivated fusion protein from the interphase chromatin is shown in the graphs on the right (mean of 10 cells with standard deviation). The insets in B) and C) are magnifications of the accumulations of HP1 α at heterochromatin marked by the arrows.

Scale bars 5 μ m.

Fig 4 Effect of chromatin condensation state on protein accessibility

The distribution of the inert tracer protein GFP, from the plasmid construct EGFP (Clontech, Heidelberg, Germany), and histone H2B-mRFP labeled chromatin is shown in representative optical sections of cells in mitosis (left column), in interphase (middle column) and in the same interphase cells again after induced chromatin condensation (right column). The double

Martin et al.

transfections and live cell microscopy were carried out as described in Fig 3 with identical acquisition settings for individual cells in repeated imaging experiments. Image analysis was performed with the Zeiss LSM Image Examiner software for fluorescence intensity and colocalization measurements. The latter included the Pearson correlation coefficient (R), measured by selecting the nuclear areas excluding the nucleoli or for mitotic cells an oval area including the chromosomes and cytoplasm. The linescan analysis in B) displays the pixel intensity distribution of GFP (green) and chromatin (red) along the yellow arrow in the respective merged image in A). Regions with reduced protein concentration correspond to heterochromatin (arrow) and nucleoli (arrowhead). In C) the scatter plots display the pixel of the merged image according to the intensity values of the red and green channel and the frequency of the red-green pixel combination is coded by the color (hot colors represent higher frequencies). The red line demarcates the pixels corresponding to the mitotic chromosomes as well as to the interphase nucleus excluding the nucleoli (referred to as nucleoplasm). The Pearson correlation coefficient (R) is the mean \pm standard deviation of 10 midsections in individual cells. Scale bar 5 μ m.

Martin et al.

Figure 1

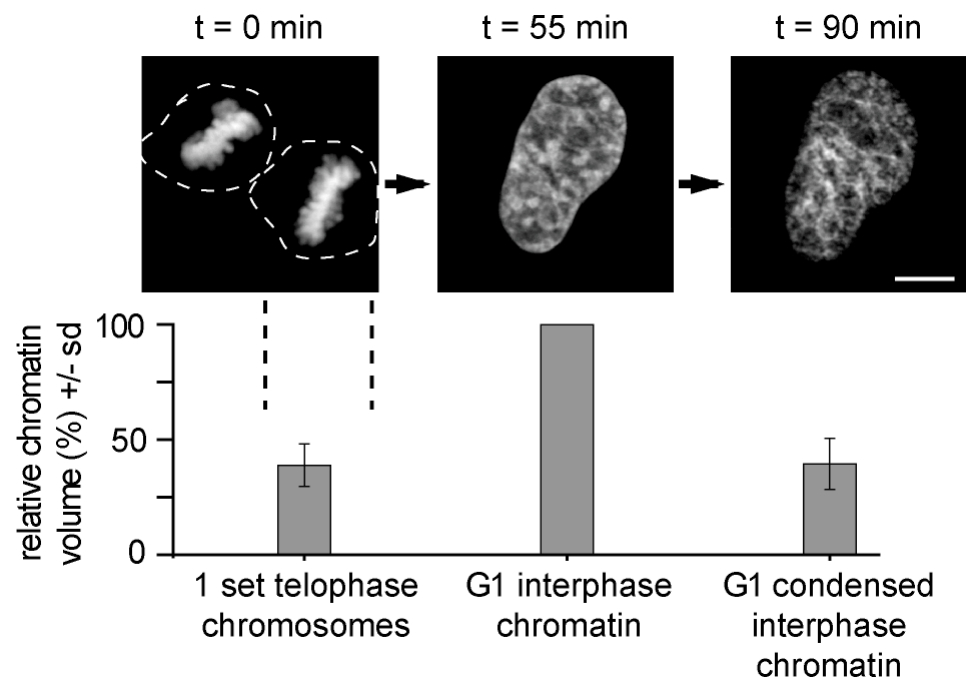
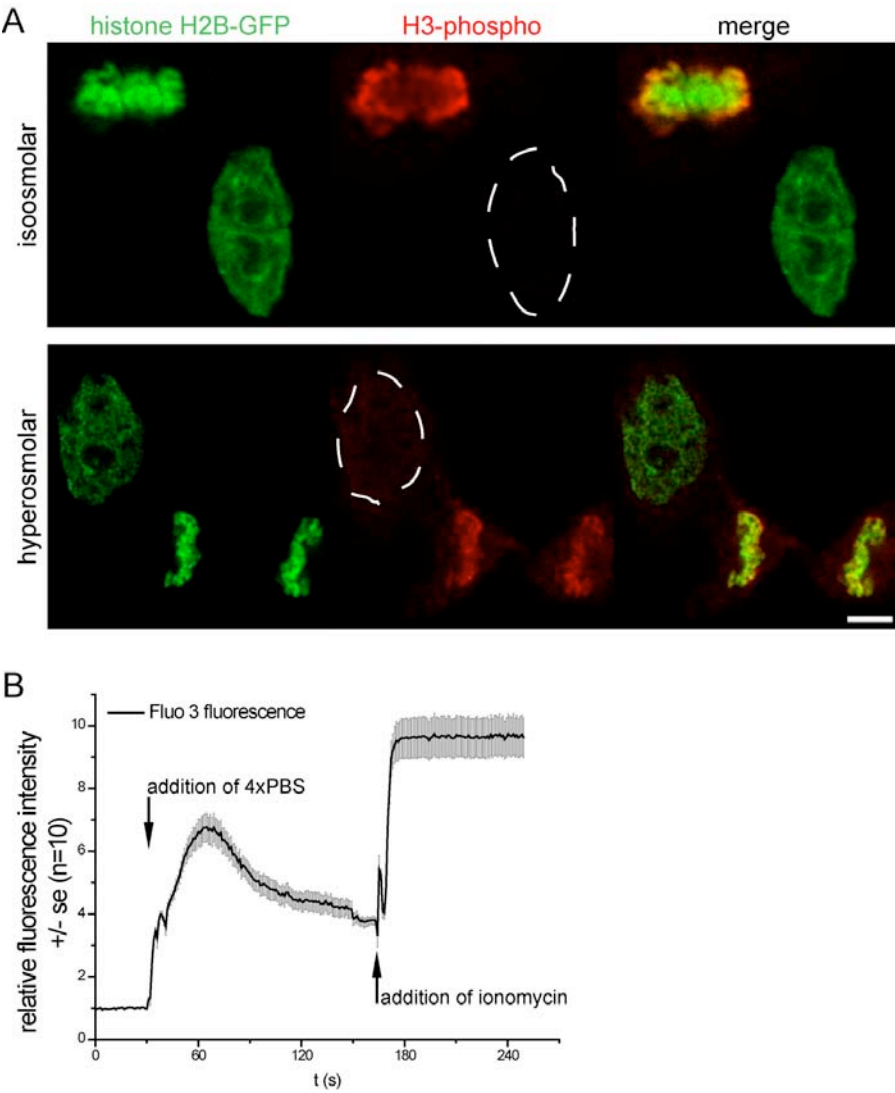


Figure 2



Martin et al.

Figure 3

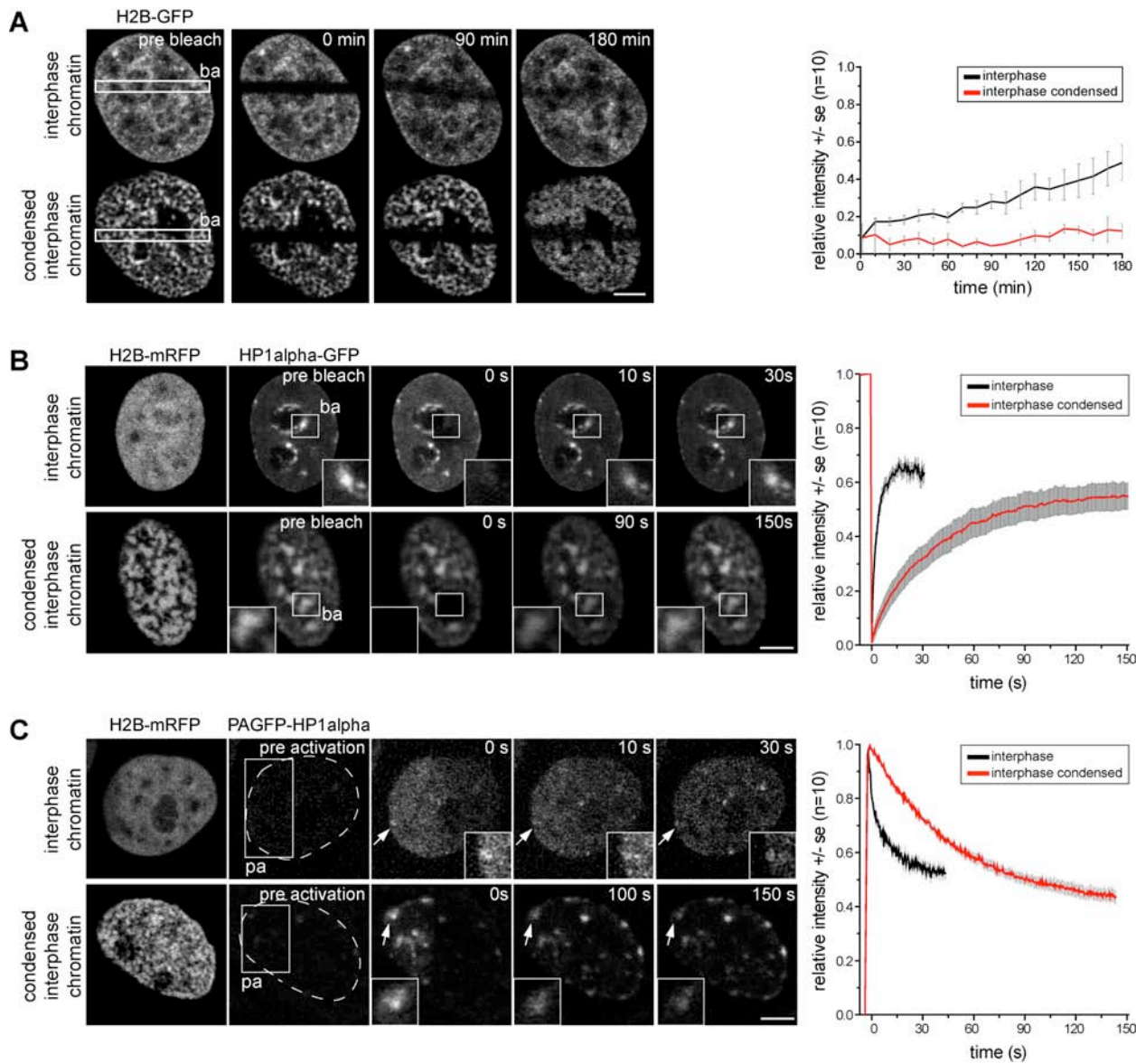


Figure 4

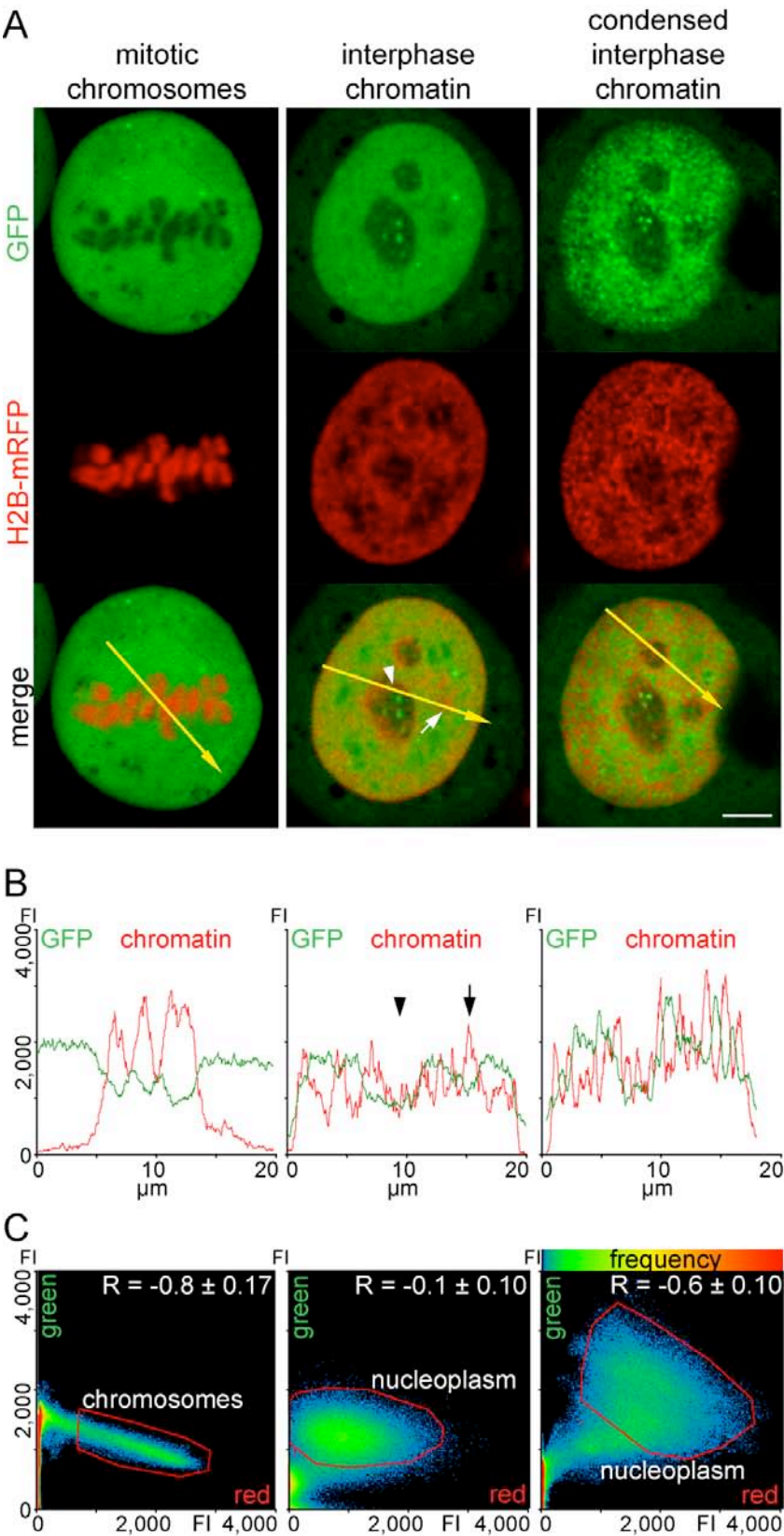


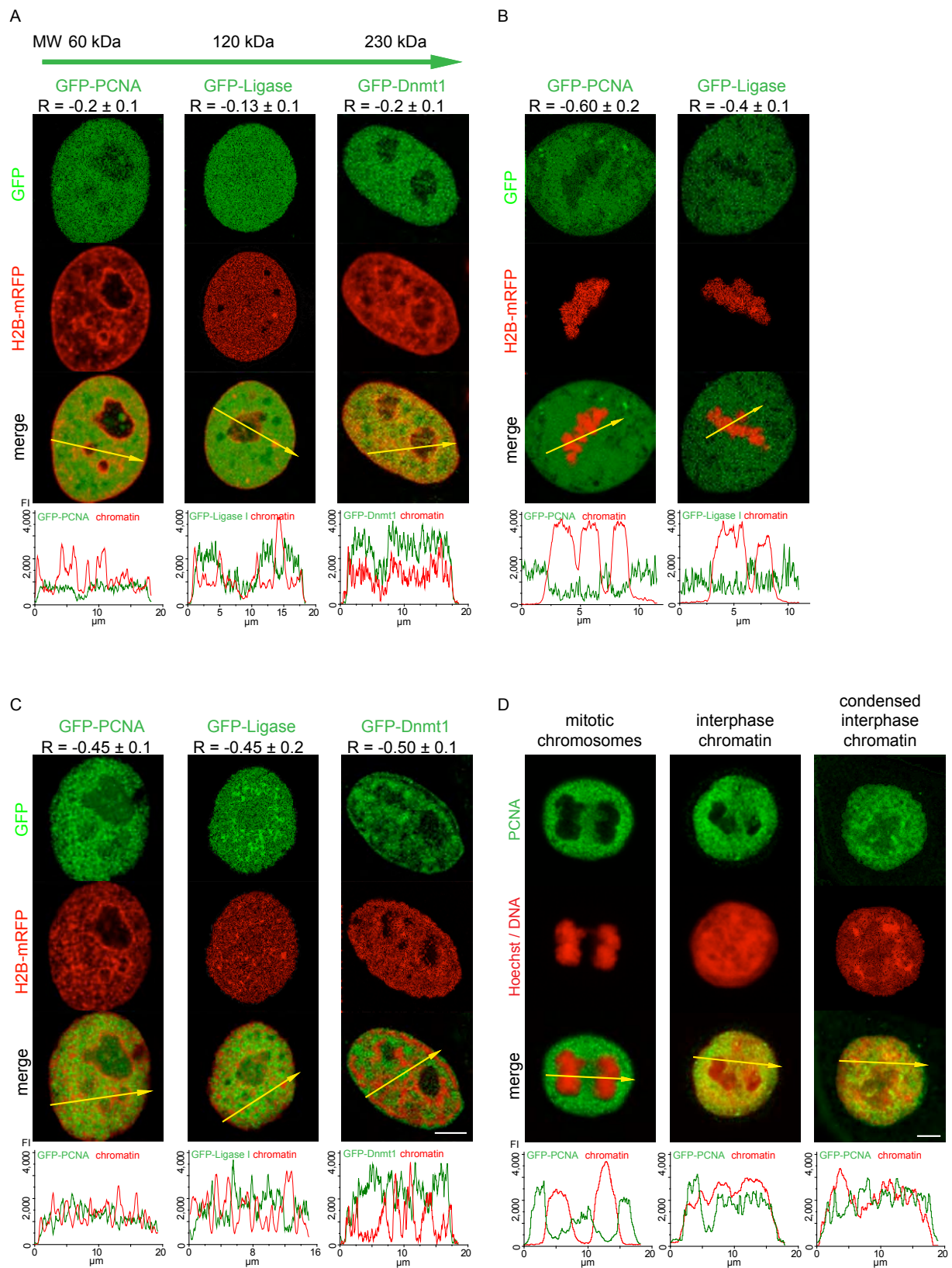
Figure S1

Fig S1 Effect of chromatin condensation state on accessibility of nucleoplasmic proteins of different size

Distribution of fusion proteins of different size GFP-DNA Ligase I,²⁷ GFP-Dnmt1²⁸ and GFP-PCNA²⁹ in representative optical sections of live HeLa cells relative to chromatin labeled with H2B-mRFP in interphase A), mitosis B) and in C) the same cells as in A) upon hyperosmolar treatment yielding hypercondensation of chromatin to the level of mitotic chromosomes. The Pearson's correlation coefficients (R) given above the images were calculated excluding the nucleoli (mean of ten cells). The linescans below the images show the pixel intensity distribution along the direction of the arrow in the merged images.

In A) as with GFP alone the proteins were homogeneously distributed in the nucleoplasm as described before.^{27,28,29} The lowest level of the fusion proteins was found in nucleoli and a slight reduction could be measured in large heterochromatin regions as displayed in the images and linescans. The increasing size of the proteins had no influence on their chromatin access in interphase nuclei as demonstrated by the correlation analysis (nucleoli excluded) with R-values between -0.13 and -0.2 indicating almost no correlation.

In B) cells in mitosis are shown with the chromosomes mostly excluding the proteins, supported by the drop of the protein fluorescence intensity in the area locating the condensed chromosomes in the linescans. The strong negative correlation coefficient with R-values of -0.6 and -0.4, respectively, further confirms the exclusion of non chromatin nuclear proteins from chromosomes. The GFP-Dnmt1 was not included in the mitosis analysis since it associates with constitutive heterochromatin from late S-phase to early G1.²⁸

The hypercondensation of interphase chromatin in C) again leads to an exclusion of the fusion proteins from the condensed chromatin structures and an accumulation in the enlarged interchromatin space, This is also visible in the linescans by the inverse correlation of the protein and chromatin labeling intensity curves. Importantly, for interphase nuclei with induced hypercondensation of chromatin the Pearson coefficient for GFP fusion proteins drops to a level similar to mitotic cells R= -0.45 and -0.5 respectively.

In D) optical sections of fixed HeLa cells stained with an antibody to PCNA in mitosis, interphase and with interphase chromatin condensed to the mitotic chromosome volume are shown. Immunofluorescence staining was performed as described earlier.³⁰ As with the GFP fusions, in mitosis no protein labeling was visible in the chromosome area labeled with the DNA dye Hoechst 33258 whereas in interphase PCNA was distributed in the whole nucleus with some reduction in the nucleoli. Upon hyperosmolar condensation of interphase chromatin redistribution of the proteins could be observed with a concentration of protein in the enlarged interchromatin regions.

Scale bars 5 μ m.

3.7 Probing intranuclear environments at the single-molecule level

Probing Intranuclear Environments at the Single-Molecule Level

David Grünwald,* Robert M. Martin,[†] Volker Buschmann,^{†‡} David P. Bazett-Jones,[§] Heinrich Leonhardt,[‡] Ulrich Kubitscheck,* and M. Cristina Cardoso[†]

*Institute of Physical and Theoretical Chemistry, Rheinische Friedrich-Wilhelms-University, 53115 Bonn, Germany; [†]Max Delbrück Center for Molecular Medicine, 13125 Berlin, Germany; [‡]Munich Center for Integrated Protein Science, Nanosystems Initiative Munich, Department of Biology, Ludwig Maximilians University Munich, 82152 Planegg-Martinsried, Germany; and [§]The Hospital for Sick Children, Toronto, Ontario M5G 1L7, Canada

ABSTRACT Genome activity and nuclear metabolism clearly depend on accessibility, but it is not known whether and to what extent nuclear structures limit the mobility and access of individual molecules. We used fluorescently labeled streptavidin with a nuclear localization signal as an average-sized, inert protein to probe the nuclear environment. The protein was injected into the cytoplasm of mouse cells, and single molecules were tracked in the nucleus with high-speed fluorescence microscopy. We analyzed and compared the mobility of single streptavidin molecules in structurally and functionally distinct nuclear compartments of living cells. Our results indicated that all nuclear subcompartments were easily and similarly accessible for such an average-sized protein, and even condensed heterochromatin neither excluded single molecules nor impeded their passage. The only significant difference was a higher frequency of transient trappings in heterochromatin, which lasted only tens of milliseconds. The streptavidin molecules, however, did not accumulate in heterochromatin, suggesting comparatively less free volume. Interestingly, the nucleolus seemed to exclude streptavidin, as it did many other nuclear proteins, when visualized by conventional fluorescence microscopy. The tracking of single molecules, nonetheless, showed no evidence for repulsion at the border but relatively unimpeded passage through the nucleolus. These results clearly show that single-molecule tracking can provide novel insights into mobility of proteins in the nucleus that cannot be obtained by conventional fluorescence microscopy. Our results suggest that nuclear processes may not be regulated at the level of physical accessibility but rather by local concentration of reactants and availability of binding sites.

INTRODUCTION

Although the nucleus is the hallmark of all eukaryotic cells, remarkably little is known of its internal structure and function. The development of antibodies and, more recently, the ability to tag proteins fluorescently have revealed a complex structure with multiple discrete subcompartments involved in RNA and DNA metabolism (1,2). Unlike cytoplasmic or-

ganelles, however, subnuclear compartments are not surrounded by membranes. This raises the question of how they arise and whether they impose constraints on the accessibility and mobility of other molecules. Such constraints would impact and thereby control nuclear functions; e.g., restricted access to chromatin or subsets thereof would have as a consequence their transcriptional silencing. Furthermore, such general restricted access to a particular subnuclear compartment in combination with sequestration of subsets of factors to the same compartment mediated by protein or protein–nucleic acid interactions would increase not only the speed of individual nuclear reactions but also their specificity (3). It is therefore necessary to elucidate whether and how the physical structure of the nucleus affects the dynamics and access of proteins.

Earlier studies with fluorescent dextrans showed that diffusion in the cell is four to eight times slower than in aqueous solutions (4,5). Moreover, diffusion measurements of macromolecules in cells using fluorescence photobleaching, correlation microscopy, and time-resolved anisotropy revealed unexpectedly high mobilities (6). From such studies, a view of the cell's interior as a watery but crowded environment rather than a homogeneous viscous gel has emerged.

Recent studies have now combined fluorescent macromolecules with subnuclear compartment labels. Labeling whole chromatin with either fluorescent histones or with DNA dyes and measuring the intranuclear steady-state distribution of injected dextrans relative to chromatin density provided evidence for a high degree of penetration of the probes into

Submitted June 14, 2007, and accepted for publication November 16, 2007.

Ulrich Kubitscheck and M. Cristina Cardoso contributed equally to this work.

Address reprint requests to Ulrich Kubitscheck, Institute of Physical and Theoretical Chemistry, Rheinische Friedrich-Wilhelms-University, Wegelerstr. 12, 53115 Bonn, Germany. E-mail: u.kubitscheck@uni-bonn.de; or to M. C. Cardoso, Max Delbrück Center for Molecular Medicine, Robert Rössle Str. 10, 13125 Berlin, Germany. E-mail: cardoso@mdc-berlin.de.

David Grünwald's present address is Dept. of Anatomy and Structural Biology, Albert Einstein College of Medicine, Bronx, NY 10461.

Volker Buschmann's present address is PicoQuant GmbH, 12489 Berlin, Germany.

Abbreviations used: GFP, green fluorescent protein; ASF/SF2, alternative splicing factor/splicing factor 2; ESI, electron spectroscopic imaging; FLIP, fluorescence loss in photobleaching; MeCP2, methyl cytosine binding protein 2; NLS, nuclear localization sequence; SAV-Cy5, streptavidin-Cy5; SMT, single-molecule tracking; SNR, signal/noise ratio.

This is an Open Access article distributed under the terms of the Creative Commons-Attribution Noncommercial License (<http://creativecommons.org/licenses/by-nc/2.0/>), which permits unrestricted noncommercial use, distribution, and reproduction in any medium, provided the original work is properly cited.

Editor: Thomas Schmidt.

© 2008 by the Biophysical Society
0006-3495/08/04/2847/12 \$2.00

doi: 10.1529/biophysj.107.115014

chromatin (7–9). The facts that dextrans do not have a rigid shape and that the polymer preparations are not always homogeneous in size introduce some variability in the results from different reports. Nevertheless, gradual exclusion from chromatin was observed for dextrans of 77 kDa or larger (10).

Kinetic studies have also been performed investigating RNA movement through nuclear subcompartments using fluorescence photobleaching or uncaging as well as single-molecule video microscopy (11–15). The outcome of these studies indicated that most regions of the nucleus are accessible to RNA particles, although some results pointed to a preferential movement through the interchromatin space (12), and the reports differed on its energy dependence (11,13).

A profusion of kinetics studies in recent years (16) have measured the mobility of fluorescently tagged nuclear proteins, mostly employing fluorescence photobleaching/activation and in some cases also fluorescence correlation microscopy. Such analyses provided a highly dynamic view of the nuclear interior with proteins diffusing rapidly within the nucleus and most often showing a fast exchange at their binding sites. The experimental limitations of such photobleaching/activation measurements and corresponding data analysis have recently been discussed (17,18) and include a relatively low temporal and spatial resolution as well as the difficulty in extracting accurate physicochemical parameters (e.g., residence times). Because most of the factors measured have endogenous binding partners, probing the structural accessibility of the nuclear interior independent of their specific interactions was not feasible. Although in other reports GFP^{ss} was used as an inert tracer protein to probe the nuclear interior, no correlation with the different subnuclear compartments was made.

In this study, we set out to measure how a single protein travels through the nucleus and to determine whether its movement is controlled by subnuclear compartmentalization, in particular whether dense chromatin regions or the nucleolus restricts its access and/or mobility.

MATERIALS AND METHODS

Cell culture and transfection

Mouse C2C12 myoblasts were cultured as described previously (19). For live cell analysis, cells were seeded onto either one-well LabTek chambers (Nalge Nunc International, Rochester, NY) or glass-bottom dishes (MatTek, Ashland, MA). Transfection using the CaPO₄-DNA coprecipitation method (20) and microinjection were performed 1 and 2 days later, respectively. Mouse RAW264.7 macrophage cells were grown in RPMI-1640 medium. The human Sk-N-SH neuroblastoma cell line was grown in Minimum Essential Medium supplemented with fetal bovine serum.

Plasmids

As reference label for the interchromatin space (“speckled compartment”) and for pericentric heterochromatin, we transfected cells with plasmids coding for fusion proteins of ASF/SF2-GFP (21) or MeCP2-GFP (22), respectively. To monitor the cell cycle stage, cells were additionally transfected with RFP-PCNA (23). Only non-S-phase cells were selected for measurements.

Probe preparation and microinjection

SAV-Cy5 (20 μ M; Amersham Life Sciences, Arlington Heights, IL; labeling ratio four to five molecules per protein) and biotin-NLS (1 μ M) were mixed 1:5 ~30 min before the injection and, after 15 min of incubation at room temperature, centrifuged at 13,000 rpm for 15 min. For the SMT experiments, the solution was further diluted 1:10 with PBS before centrifugation. Microinjection was carried out with an Eppendorf injection and micromanipulation setup. The parameters for cytoplasmic microinjection were set to 0.7-s injection time with 20-fPa injection pressure and 15-fPa holding pressure. Imaging and measurements were started 60 min after microinjection to allow cells to recover, which was ascertained by examining the cellular morphology.

Confocal microscopy and fluorescence photobleaching

Steady-state distributions for NLS-SAV-Cy5 complexes were analyzed by live cell microscopy using a confocal laser scanning microscope LSM510Meta (Carl Zeiss, Jena, Germany) equipped with a 63 \times planapochromat phase-contrast oil-immersion objective, NA 1.4, heated to 37°C. GFP was excited with the 488-nm line of an argon ion laser, whereas Cy5 was excited at 633-nm light from a HeNe laser. The main beam splitter for both settings was a UV/488/543/633 filter, and the secondary beam splitter was NFT545. For the detection of GFP fluorescence, we used a band-pass filter BP500-530, and for Cy5 detection, a long-pass filter LP650. The constitutive heterochromatin domains were marked by the MeCP2-GFP label, and the nucleoli were identified according to the phase-contrast image. In these domains, the respective mean fluorescence intensities were calculated in the red channel and normalized to the maximum values. The time series and FLIP experiments were done on the same equipment using 100% power of the 633-nm HeNe laser for photobleaching. The FLIP was performed by bleaching a spot of 3.6- μ m diameter for 554-ms duration followed by one imaging scan of 0.8-s duration and repeated 200 times.

Single-molecule microscopy

Single-molecule experiments were performed at room temperature using an inverted wide-field microscope equipped with a 63 \times NA 1.4 objective lens employing three fluorescence channels (24,25). For identification of the pericentric heterochromatin, cells were transfected with MeCP2-GFP. In these cells, the pericentric heterochromatin and nucleoplasmic trajectories were recorded. The nucleoplasm was defined as the nuclear space excluding the MeCP2 domains. Therefore, the nucleoplasmic trajectories also contained a small fraction of traces occurring in the nucleoli. Because the nucleoli displayed a low concentration of SAV-Cy5 molecules (42%, see Table S1) and occupied on average only 35% of the non-MeCP2-GFP regions within the nuclei, this gives an approximate contribution of 15%. Single-molecule experiments aimed at analyzing the trajectories within the nucleoli were performed using C2C12 cells transfected with ASF/SF2-GFP. In these experiments, nucleoli were identified according to their exclusion of ASF/SF2-GFP. For all measurements, non-S-phase cells were selected according to their RFP-PCNA subnuclear distribution (26), and the RFP fluorescence was bleached completely before microinjection of NLS-SAV-Cy5 into the cytoplasm. After imaging of the green channel with an Axiocam (Zeiss), movies were recorded in the red channel and illustrated the intranuclear motion of SAV-Cy5 molecules after their nuclear import. Movies comprising 2000 frames were acquired at a frame rate of 191 Hz using an image integration time of 5 ms. A total of 22 cells were examined yielding more than 40 single molecule movies. The green and red fluorescence channels were scaled and aligned to each other as described (27).

Image processing of video images

Before data analysis, all images were filtered using a FFT band-pass filter (high frequency threshold, 2 pixels; low frequency threshold, 20 pixels)

A Single-Molecule View of the Nucleus

using ImageJ (W. S. Rasband, ImageJ, U.S. National Institutes of Health, Bethesda, MD, <http://rsb.info.nih.gov/ij/>, 1997–2005) to facilitate the automatic detection of single-molecule signals. The effect of the filter can be noted in Fig. 1 *C* (lower panels). Identification and tracking of the single-molecule signals were performed using Diatrack 3.0 (Semasopht, Chavannes, Switzerland), a commercial software package developed specifically to identify and localize single-particle signals and also to detect single-particle tracks. A maximal displacement of 15 pixels from frame to frame was allowed, and a point spread function of 1.7 pixels corresponding to 325 nm was assumed. The application of an automated scheme to our data was not straightforward because the single-molecule data often featured low SNR ratios. For this reason, we visually verified each detected single-molecule track identified by Diatrack in the original, unprocessed data. The analysis of trajectories was performed by means of user-written macros in Origin 7.5 (Microcal, Northampton, MA). The tracks were assigned to the following compartments: pericentric heterochromatin, nucleoplasm, nucleoli, and cytoplasm. Each compartment was marked in a specific color using IPLab, and this false color reference image was used for compartment assignment of the individual tracks. All tracks in the cytoplasm and a 10-pixel border region at the nuclear envelope were discarded to avoid evaluation of molecules being imported into the nucleus. Furthermore, all tracks within a distance of eight pixels from the image border were discarded.

Trajectory analysis

Identification and tracking of the single-molecule signals and analysis of the trajectories were performed as described elsewhere (27). The probe molecules moved in all three spatial directions; therefore, most molecules were observed for only a few frames because our focal depth was limited to less than ± 400 nm (28). Such tracks were too short for an analysis based on an approach to analyze stochastic motion, namely the plot of the mean-square displacement of single molecules against time (29). A jump distance analysis of the trajectories was performed. In this type of analysis, the probability that a particle starting at a specific position will be encountered within a shell of radius r and width dr at time t from that position is considered. For a single species diffusing in two dimensions (30),

$$p(r, t)dr = \frac{1}{4\pi Dt} e^{-r^2/4Dt} 2\pi r dr \quad (1)$$

if we identify the starting position with the origin. Experimentally, this probability distribution can be approximated by a frequency distribution, which is obtained by counting the jump distances within respective intervals $[r, r + dr]$ traveled by single particles after a given time. For each compartment, the displacements within 2 to 20 frames were calculated and drawn in a histogram to visualize the global displacement distribution as a function of time. In cases of particles with multiple diffusive species, the jump distance distributions cannot satisfactorily be fitted by Eq. 1, assuming a single diffusion coefficient. Such different mobility populations can be detected and quantified by curve fitting taking several diffusion terms into account (27).

Three-dimensional movement and tracking

If single molecules are tracked, all three degrees of freedom have to be considered. In case of free and isotropic diffusion in the three-dimensional space, all degrees of freedom are equivalent, and the observation of the movement in respect to a single axis is sufficient to characterize the movement of the probe in the three-dimensional space. Therefore, a time sequence of images is a valid two-dimensional representation of the three-dimensional movement of the molecule. For the limited focal depth of the SMT setup, it was considered that the assumption above holds.

For tracking of particles within the nucleolus or the heterochromatin region, there was the possibility that the molecule traveled below or above the

compartment but within the focal depth of the microscope. To reduce false-positive observations, we restricted the analysis for the nucleolus and the chromatin region to signals presenting a higher SNR than accepted in the nucleoplasm. A high SNR is most likely a result of the molecule being central in the focal plane rather than at the border of the depth of field. Effectively such a SNR-based filter reduces the depth of field below the ± 400 nm we estimate for the nucleoplasm. The z extension of a nucleus in a living fibroblast cell is in the range of several micrometers. The focal plane was adjusted to the center of the labeled compartment. Although the nucleolus can span the entire nucleus, the pericentric heterochromatin compartments are more likely restricted to less than $2 \mu\text{m}$.

Electron spectroscopic imaging

Electron spectroscopic imaging (ESI) was performed as previously described (31,32). Nitrogen and phosphorus maps were collected using a transmission electron microscope (Tecnai 20 (FEI)) fitted with an electron imaging spectrometer (Gatan). Cryopreservation of the macrophage cells was performed by freeze-slaming and cryosectioning (Leica). Frozen sections were transferred under liquid nitrogen (Gatan) to the column of the electron microscope (Tecnai20 (FEI)), where they were freeze-dried before imaging.

RESULTS AND DISCUSSION

Distribution of SAV within the cell nucleus

In a first series of experiments, the overall distribution and potential interactions of SAV-Cy5 within the cell nucleus were examined by live-cell confocal laser scanning microscopy and fluorescence photobleaching experiments. SAV-Cy5 was chosen as a mobility probe because it represents an average-size protein (60 kDa) and has no known binding sites within the nuclear interior. SAV-Cy5 was preincubated with a biotinylated nuclear localization sequence peptide (NLS-biotin), and this complex was microinjected into the cytoplasm of living mouse myoblast C2C12 cells (Fig. 1 *A*), which expressed GFP-tagged MeCP2 (22). The latter recognizes 5-methylcytosines, which are very abundant in mouse constitutive heterochromatin around centromeres, and thus, pericentric heterochromatin was very selectively marked by green fluorescence (Fig. 1 *B*, central panel). The complex was imported into cell nuclei within a few minutes (Fig. 1 *B*, right panel). In the absence of NLS-biotin, no detectable import of SAV-Cy5 into the nucleus was detected over 30 min. Careful examination of the confocal images did not show signs of aggregation or accumulation processes of SAV-Cy5 within specific nuclear domains (Fig. 1 and Fig. S1). Rather, the probe fluorescence was homogeneously distributed with a slight reduction within the pericentric heterochromatin and unambiguous reduction within nucleolar domains, which was already apparent when the first nuclear SAV-Cy5 fluorescence was detected (Fig. 1 *B*, right panel, 60 s). A quantitative analysis revealed that the concentration of the probe molecules was reduced by only 4% within the pericentric heterochromatin domains, whereas it was significantly reduced within the nucleoli to 42% of the nucleoplasmic level (Table S1). Clearly, the pericentric het-

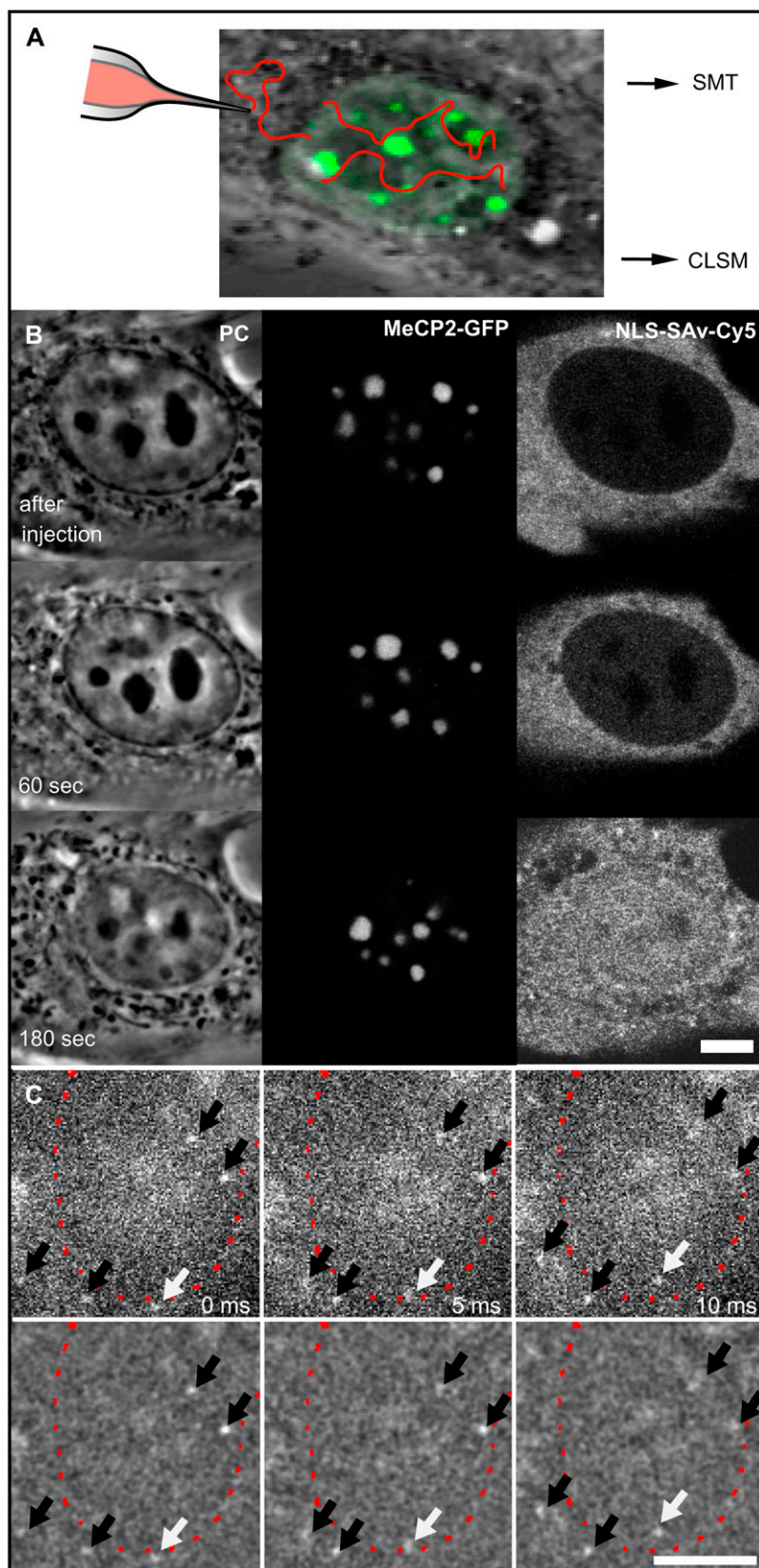


FIGURE 1 NLS-SAv-Cy5 complexes in living cells and their nuclear import. (A) Scheme of the experimental approach for confocal imaging and photobleaching experiments and for single-molecule detection. Mouse myoblast C2C12 cells transfected with plasmids coding for MeCP2-GFP (green) were microinjected into the cytoplasm with preformed NLS-SAv-Cy5 complexes as tracer molecules. Nuclear import was followed by confocal microscopy (CLSM), and after its completion, photobleaching experiments were performed. In a separate experimental setup, single molecules were tracked using a widefield fluorescence microscope (SMT). (B, left panel) Phase contrast (PC) images of a nucleus, time points of the image sequence as indicated. (B, middle panel) Green channel showing the distinct MeCP2-GFP labeling of the pericentric heterochromatin. (B, right panel) confocal time lapse images acquired in the red channel after the cytoplasmic microinjection of NLS-SAv-Cy5 complexes, demonstrating efficient nuclear import. (C) In the single-molecule setup, single SAv-Cy5 molecules could be observed while entering into the nucleus (white arrows) across the nuclear envelope (red dotted line). Further molecules could be identified and tracked within cytoplasm or nucleus (black arrows). In the upper panel unprocessed data are shown; in the lower panel, the effect of bandpass filtering used for further processing is demonstrated. Scale bars, 5 μ m.

erchromatin was not packed densely enough to produce a significant exclusion of proteins of the size of SAv, which is similar to measurements of the distributions of fluorescently labeled sugars (7,9).

To more rigorously control for possible interactions of our probe molecules with intranuclear structures, we performed FLIP experiments. On repeated bleaching of selected spots within nuclei, the fluorescence intensity inside the remaining nuclear space decreased homogeneously (Fig. S2). Altogether, the confocal and photobleaching data clearly indicated that SAv-Cy5 did not bind noticeably within any nuclear domain and suggested that compartment borders presented no major hindrances for the molecules to enter and leave distinct nuclear compartments.

Single-molecule tracking allows real-time imaging of intracellular molecular motions

We recently demonstrated that single SAv-Cy5 molecules in aqueous buffer solution may be visualized by high-speed single-molecule microscopy at a frame rate of 340 Hz (20). Because it is generally assumed that the intracellular viscosity is at least four times higher than in aqueous solution (6), we were confident that movies recorded at frame rates of 200 Hz would produce realistic real-time movies of the intracellular motion of SAv-Cy5 molecules. SAv-Cy5 coupled to NLS-biotin was microinjected at a low concentration so that the diffraction-limited signals originating from single probe molecules within the cell nuclei could be singled out. One hour after the microinjection, single cell nuclei were imaged in the green fluorescence channel to identify the nucleoplasmic, pericentric heterochromatin and nucleolar compartments. Then, SAv-Cy5 fluorescence was excited with 633-nm laser light, and single-molecule signals were recorded with high temporal and spatial resolution for ~ 10 s with a frame rate close to 200 Hz (see Movie S1). In Fig. 1, three sample frames from one of the movies are shown, where, e.g., the entry of a single probe molecule into a cell nucleus can be observed (*white arrows*). Further mobile single molecules within the nucleus or the cytoplasm (*black arrows*) can be recognized as diffraction-limited bright spots.

Such movies showing the intracellular motion of single molecules contain a wealth of information. To extract this information we identified and localized the single-particle signals and the corresponding single-molecule trajectories. Because we had taken the GFP reference images for all nuclei, we could exactly locate each track within the context of the different intranuclear domains (Fig. S1).

Individual trajectories reveal predominantly highly mobile probe molecules

A plot of all probe molecule trajectories observed within a 10-s time window within the corresponding green reference image provided a direct first impression of the intranuclear

probe molecule mobility (Fig. 2). It was immediately obvious that the great majority of the molecules were mobile. At first glance, the trajectories within the pericentric heterochromatin showed no obvious difference from those in the nucleoplasm. Most importantly, it appeared as if the probe molecules could jump into and roam through the pericentric heterochromatin with apparently no hindrance (Movie S1). Most trajectories were relatively short with a mean length of 6.2 frames (median four frames) for this cell, which supported the existence of a high mobility because highly mobile molecules tend to leave the focal plane very rapidly (28).

In the next step, we distinguished two main classes of traces: whereas most molecules traversed larger distances, others stayed in confined regions (Fig. 2). The individual positions of tracks belonging to the second class were typically scattered in small regions with diameters of ~ 100 nm (Fig. 2). This size corresponded to the localization precision of the instrument, which is mainly limited by the SNR of the single-molecule signals (33). Therefore, either these molecules were completely

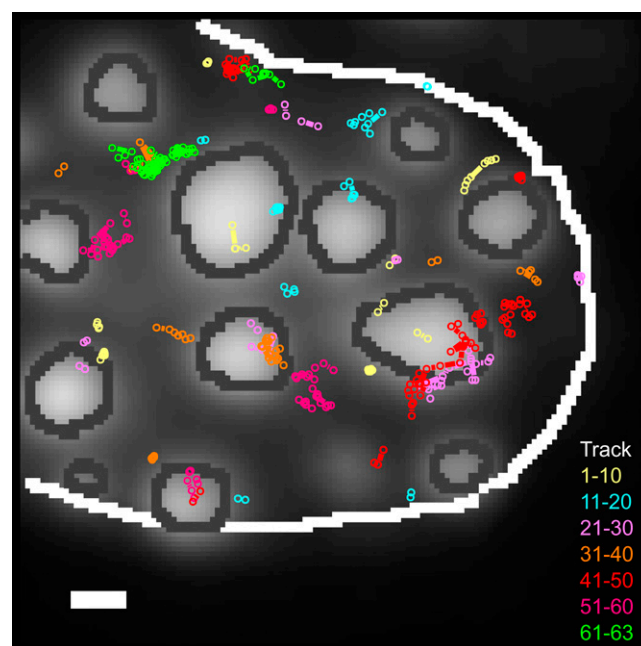


FIGURE 2 Individual SAv trajectories within a MeCP2-GFP-labeled cell nucleus. Trajectories of single NLS-SAv-Cy5 (Fig. 1 C and Movie S1) showing different mobilities and located in different nuclear subcompartments were located and identified with Diatrack 3.0. The MeCP2-GFP reference image was recorded before the acquisition of the single-molecule movie and inserted as a background for the trajectory plot. The figure shows all trajectories identified in the data of Movie S1. The dark gray lines show the borders of the MeCP2 domains (*light gray*), and the white line indicates the nuclear region considered for the evaluation. The overlaid single-molecule tracks are shown in different colors to better distinguish tracks that appear in the same nuclear region. In total, 63 tracks were identified at this measurement, and each 10 consecutive tracks are drawn in the same color. The radius of the spots (100 nm) corresponds to 2σ with σ designating the experimental localization precision of ± 50 nm. Hence, movements beyond that radius represent true diffusional steps with a probability of 95%. Scale bar, 1 μ m.

immobile, or their restricted motion within the 100-nm-sized region could not be further resolved. Binding processes can lead to the occurrence of this behavior, as was observed in the case of intranuclear splicing factor mobility (34,27). For example, for single uridine-rich small nuclear ribonucleoprotein particle (U1snRNP) we observed immobilization in $\sim 75\%$ of all trajectories analyzed, and measured local dwell times often longer than 150 ms in live cells. However, such a behavior was neither expected nor observed for a nonfunctional, ectopic protein such as SAV, and our photobleaching results (Fig. S2) directly argued against binding of SAV to intracellular structures. Thus, we concluded that the virtually motionless molecules were actually trapped in local structures with dimensions smaller than the ± 50 -nm localization precision of our instrument. The intranuclear space is filled with an extremely complex and intricate network of chromatin fibers, which presumably form all types of structures including caves and mazes. Mobile protein molecules encountering such structures may be caught and transiently trapped there until their own stochastic motion—or chromatin movements—lead to liberation.

The analysis of individual molecule trajectories provided further insights into the intranuclear probe dynamics. An example is given in Fig. 3, where the last frame represents a maximum-intensity projection of the frames shown. The trajectory revealed a molecule that was obviously moving from one trap to another. Although trapping of the molecule leads to an accumulation of signal, the mobile part of the trajectory presents a fading signal in the time projection because of the short time the molecule is observed at any one position. Hence, trapping was a reversible process and sometimes persisted long enough that such traces could be identified.

The existence of structural traps would be further supported if trapping would occur repeatedly in the same spatial intranuclear regions. SAV distributed homogeneously within the nucleus and showed no specific binding sites. Therefore, the observation of two different molecules at exactly the same site by pure chance would be exceptionally improbable considering the extremely low concentration used in our experiments, which argues for the existence of stable structural traps in the nucleus. But indeed, such events were observed (Fig. S3).

Different modes of mobility were present within the cell nucleus, but probe molecules were extremely mobile within all three compartments

To obtain a general picture of the SAV-Cy5 mobility, we analyzed the distances covered by the probe molecules between subsequent frames, the so-called jump distances. Because the probe molecules moved in all three spatial directions and our focal depth was limited to less than ± 400 nm (28), most molecules were observed for only a few frames. Fig. 4, *A*, *C*, and *E* shows the jump distance distributions for SAV-Cy5 molecules that were observed within

nucleoplasm, pericentric heterochromatin, and nucleoli, respectively, with the largest number observed within the nucleoplasm. All three distributions could not satisfactorily be fitted assuming a single diffusion coefficient (Eq. 1), in contrast to jump distance distributions of molecules moving in free solution (35,33). An advantage of the jump distance analysis is, nonetheless, that different mobility populations can be detected and quantified by curve fitting (27). For the SAV-Cy5 data, a sum of three diffusion terms was required, and the fitting results were indicated by the red lines in Fig. 4, *A*, *C*, and *E*. Two fractions, f_2 and f_3 , corresponded to fast motion with diffusion coefficients of $D_2 = 0.8 \mu\text{m}^2/\text{s}$ and $D_3 = 5 \mu\text{m}^2/\text{s}$, whereas the first fraction f_1 corresponded to molecules that appeared motionless on the time scale of the measurements (Table 1). This latter fraction corresponded to those molecules that were interpreted above as trapped.

The data in Table 1 suggested differences between compartments in the ratios of shorter to longer jumps, which were only apparent and partly caused by differences in the sub-compartment size and geometry. Therefore, we conclude that the general mobility pattern in all three nuclear compartments was comparable.

Single-molecule tracking revealed short-lived trapping of the probe molecules

SAV-Cy5 molecules of fraction f_1 (Table 1) did not move beyond the average localization precision of our system, namely $\sigma_p = 50$ nm ($\sigma_p^2 = 4\mathbf{D}_1 t$, with $t = 5$ ms). This fraction corresponding to trapped molecules occurred predominantly within the pericentric heterochromatin (49% in f_1), less within the nucleoplasm (25% in f_1), and least within the nucleoli (10% in f_1). The latter value was especially striking because there was still a 2.5-fold reduction between nucleoplasm and nucleoli. The fact that a noticeably smaller fraction of trapped molecules was observed here than in the pericentric heterochromatin suggested that the nucleolar environment contained fewer traps for SAV-size molecules than pericentric heterochromatin.

To highlight the distinct properties of the three compartments, we divided the jumps into two fractions and examined their time dependence. The first fraction contained jumps of trapped molecules, with jump distances smaller than $2\sigma_p$. The second fraction contained the mobile molecules performing jumps between 100 and 700 nm. Fig. 4, *B*, *D*, and *F*, shows the time dependence of these fractions. It was obvious that the number of observations for both fractions decreased very rapidly with time. Although this was expected for mobile molecules because they frequently and rapidly jumped out of the focal plane, it was not so for trapped molecules. For these, the decay time, rather, reflected the time span for which they were motionless. The number of the total trapped events detected decayed rapidly with a kinetics that could be described by a biexponential decay with an averaged time constant of 22–25 ms for the pericentric chromatin domains

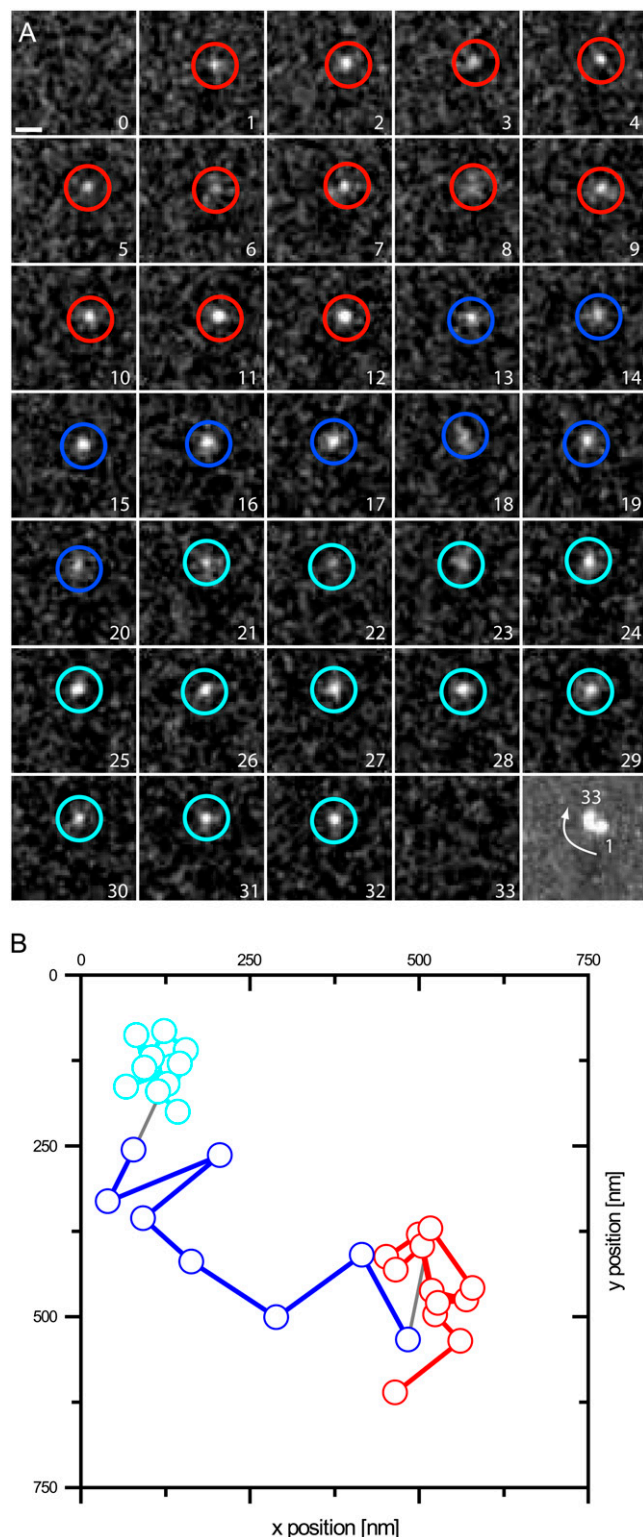


FIGURE 3 Repeated trapping of a single SAV molecule. An example of a molecule switching between different modes of motion is shown in a magnified view. (A) The raw data sequence, filtered with an FFT band pass (see Material and Methods), is shown. The last image shows a maximum projection of the trace. Scale bar, 1 μm . Individual frames are marked in a color corresponding to the fitted positions shown in B. Although the molecule was seen in a fixed state at the beginning (*red positions*, state

and nucleoplasm and even faster (7 ms) for the nucleoli. Clearly, the immobilization or trapping incidents were short-lived in comparison to functionally relevant binding events, as in the case of splicing factors, which displayed a threefold larger immobile fraction with average binding times of >60 ms (34). The short trapping times of the SAV-Cy5 explain why they could not be measured in the bulk photobleaching experiments, which were performed at much longer time scales (Fig. S2).

Altogether, we conclude that on a time scale >100 ms, SAV was freely mobile in all nuclear compartments. However, on the millisecond timescale, many more molecules were trapped within the pericentric heterochromatin than within the nucleoplasm and especially the nucleoli. The different trapping abilities could in part be related to SAV complexation with the NLS peptide.

Compartment borders did not form barriers

In contrast to cytoplasmic organelles, functional compartments in cell nuclei are not separated from each other by membranes. The question of how nuclear subcompartments are maintained is therefore a matter of debate. In principle, even molecules that, at equilibrium, are equally concentrated in two distinct domains may encounter hindrance in crossing the domain borders. Thus, we analyzed in detail the jumps performed by molecules that crossed between nucleoplasm and pericentric heterochromatin and between nucleoplasm and nucleoli, respectively. The distance distributions of these jumps are shown in Fig. S4. For both types of compartment crossings, broad distributions of jump distances were found. Very short jumps were underrepresented compared with the distribution within the compartments (compare to Fig. 4) because of the selection criterion that a border had to be crossed. Still, it was remarkable that all jump distances up to 800 nm occurred, indicating that the border region of neither compartment represented a significant hindrance for the SAV-Cy5 probe. This view was supported by the visual impressions from the movies, where one could see in several cases that the probe molecules changed from the nucleoplasm into the perichromatin domains with no apparent hindrance or delay. Finally, it could be clearly seen that, for jumps crossing the pericentric heterochromatin, the ratio of short jumps to longer jumps was significantly higher than for the nucleolus, strengthening the result of a higher mobility in the nucleolus (Fig. 4 and Fig. S4).

Different environments in the nucleus

On the basis of the almost 60% lower accumulation of SAV-Cy5 in the nucleolus (Table S1), we postulated that there is

1), it was released after 12 frames (*blue*, state 2) but was trapped again for eight more frames (*cyan*, state 3). (B) The positions of the molecule observed in A were fitted and plotted on a nanometer scale.

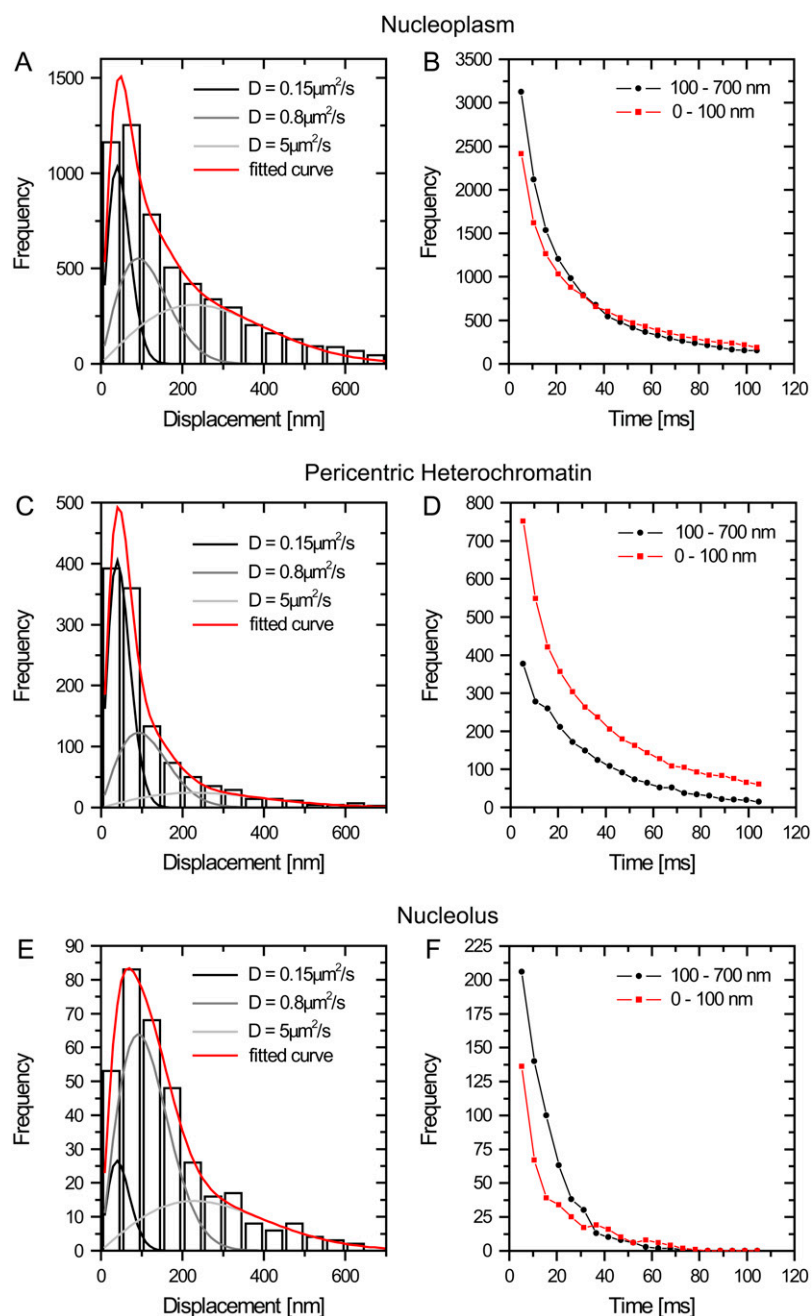


FIGURE 4 Global distributions of jump distances in the nuclear subcompartments. The distributions of jump distances occurring between subsequent frames (within 5.22 ms) are shown in panels A, C, and E for the three compartments. The distributions were fitted with a three-component model using the diffusion coefficients $D_1 = 0.15 \mu\text{m}^2/\text{s}$ (for the fixed fraction), $D_2 = 0.8 \mu\text{m}^2/\text{s}$, and $D_3 = 5 \mu\text{m}^2/\text{s}$. The data could not be fitted satisfactorily assuming only one or two diffusing components. The fraction of molecules in each mobility class varies strongly between compartments (see Table 1). In panels B, D, and F, the loss of observations over time was monitored for the different compartments. The jumps were binned into two classes: displacements <100 nm (corresponding to the twofold localization precision) and >100 nm. The limited compartment size of pericentric heterochromatin and the nucleolus makes the observation of large jumps less probable, and hence, very long jumps >700 nm were not considered.

less free volume available than in the surrounding nucleoplasm. This would be in accord with measurements of protein concentrations in different nuclear bodies performed in *Xenopus* egg nuclei (36). The lower percentage of immobilized molecules (Fig. 4) and the fact that the nucleolar border did not impede the access of SAV-Cy5 molecules (Fig. S4) nevertheless reflect a highly permeable compartment. This is surprising because this nuclear subcompartment is thought to be a mass-dense structure comprised of rDNA, RNA polymerase I transcription/splicing apparatus, rRNA transcripts, preribosomes, and many proteins that are not involved in ri-

bosome biogenesis. To address this question, it is important to consider whether the viscosity of the nucleolus is high because of a high concentration of nucleic acid and protein or whether molecules experience a reduced free volume but have unimpeded access. Therefore, we measured the relative mass density of the nucleolus and nucleoplasm from sections of conventionally fixed cells by ESI and from freeze-dried cryosections of cryofixed cells.

With ESI, the biological structure is visible without heavy atom contrast agents (e.g., uranium salts) because of energy loss events detected by an imaging electron spectrometer.

TABLE 1 Fraction of molecules in each mobility class derived from the analysis of jump distances occurring within 5.22 ms

Nuclear domain	$f_1^{*†} D = 0.15 \mu\text{m}^2/\text{s}$	$f_2^\dagger D = 0.8 \mu\text{m}^2/\text{s}$	$f_3^\dagger D = 5 \mu\text{m}^2/\text{s}$	$f_2 + f_3$
Nucleoplasm	25 ± 1	32 ± 1.5	43 ± 2.5	75
Pericentric heterochromatin	49 ± 1	34 ± 2	17 ± 2	51
Nucleoli	10 ± 1	57 ± 1	33 ± 2.5	90

*The first fraction with $D = 0.15 \mu\text{m}^2/\text{s}$ corresponded to the immobile fraction (because $\sigma_p = 50 \text{ nm} \approx \sqrt{4 \times 0.15 \mu\text{m}^2/\text{s} \times 0.005 \text{ s}}$ and $f_2 + f_3$ to the total mobile fraction).

†These fits were performed with the diffusion coefficients held constant to obtain results for the amplitudes that were directly comparable. Free fits yielded similar results with only slight deviations from the given parameters.

Background mass contributions from the embedding resin can be removed in the analysis. Intensity values in an image recorded at 120 eV, before the carbon K edge, provide a direct measure of the mass density. Relative mass densities of various regions of interest can also be obtained. A region corresponding to a nucleolus and a region corresponding to the nucleoplasm are shown (Fig. 5 A). The ratio of the mean intensity of these two regions was $112/58 = 1.93$. The mean ratio of nucleolus mass density to nucleoplasm mass density, measured for eight nucleoli in six cells, was 1.64 ± 0.34 and varied from 1.20 to 2.17. The variation between measurements may be related to the degree of extraction of soluble protein from the nucleoplasm during the fixation, dehydration, and embedding procedure. It is possible that the degree of extraction is greater from the nucleoplasm than from the nucleolus. To avoid this complication, and to obtain a ratio of mass density between the nucleolus and nucleoplasm that accurately reflects that of an intact cell, we cryofixed a pellet of RAW cells (macrophages) by freeze-slamming. The cell morphology indicated good cryopreservation with a minimal degree of ice crystal damage. The mass density of the nucleolus relative to that of the nucleoplasm in the regions indicated (Fig. 5 B) was $62/47 = 1.32$. The average ratio measured from 12 nucleoli in 12 cells was 1.55 ± 0.32 . These measurements clearly indicate substantially less free space within the nucleolus in relation to the surrounding nucleoplasm, which likely is a major reason for the lower concentration of proteins such as the SAV-Cy5 with no binding sites in this compartment.

Although the nucleolus showed a higher mass density, the probe molecules had no hindrance in penetrating the nucleolus and were highly mobile within it. Therefore, we further analyzed the ultrastructure of this compartment by acquiring high-resolution electron spectroscopic images of the nucleolus. Nitrogen and phosphorus mapping by ESI can be used to delineate protein- from nucleic acid-based structures and provide structural detail without the use of heavy atom contrast agents. The phosphorus map provides contrast predominantly of nucleic acid. Chromatin fibers, for example, were readily apparent (Fig. 5, C–G, *yellow fibers* in the region

labeled “Nucleoplasm/Chromatin”). If the phosphorus signal is subtracted from the nitrogen signal, protein structures that do not overlap with chromatin can be visualized (*blue signal* in Fig. 5, E–G). Features of nucleolar structure could be identified with this approach, such as the chromatin on the periphery (Ch), chromatin within the nucleolus (NuChromatin), the granular compartment (GC), and the dense fibrillar component (DFC). It is apparent that the nucleolus could be permeable to proteins, such as SAV-Cy5 (5.3-nm \times 4.5-nm barrel-shaped structure). The structural features that support this are:

1. Channels through the interior of the nucleolus (Fig. 5 G, *arrowhead*).
2. Gaps of 10–30 nm between granules (preribosome subunits) in the granular component.
3. Spaces between RNA fibers in the dense fibrillar component (DFC). Although there is also a high concentration of protein in this subcompartment, it may reflect protein that became fixed in place during fixation and dehydration steps. It should be possible for small molecules to diffuse through this provided they do not bind to the RNA or the RNA-associated proteins. Molecules from the nucleoplasm could easily penetrate the nucleolus through regions where the peripheral chromatin density was not extreme, such as that seen in Fig. 5 D, or through the granular component, which is typically observed on the periphery of the nucleolus.

Our main conclusions are summarized in Fig. 6. Nucleoplasm and pericentric heterochromatin are dominated by the presence of chromatin fibers, albeit to different densities, whereas the nucleolus is composed largely of ribonucleoprotein particles, i.e., ribosomes. It should be noted that the nucleoplasm is a very heterogeneous compartment, and, for simplicity, splicing speckles, Cajal bodies, and other nuclear bodies were not considered. Because pericentric heterochromatin in the mouse constitutes 10% of the total genome and occupies a volume of $\sim 5\%$ of the nucleus (data not shown), this results in a twofold higher chromatin concentration on average in the pericentric heterochromatin subcompartment and consequently less free space. This agrees with measurements of the relative concentration of GFP-tagged histone distribution (37). In the case of the nucleolus, based on the almost 60% lower accumulation of SAV and the 1.5 times higher mass density, we conclude that there is less free volume available than in the surrounding nucleoplasm. In general, the nuclear subcompartments were easily accessible to a small protein such as SAV, and their borders did not form barriers because molecules could move unimpeded in and out of each compartment. Obviously, the pericentric heterochromatin was not packed densely enough to produce significant exclusion of proteins of the size of SAV, and, hence, reduced heterochromatin physical accessibility per se should not be a major determinant of genome silencing. Different mobility distributions were detected on a millisecond

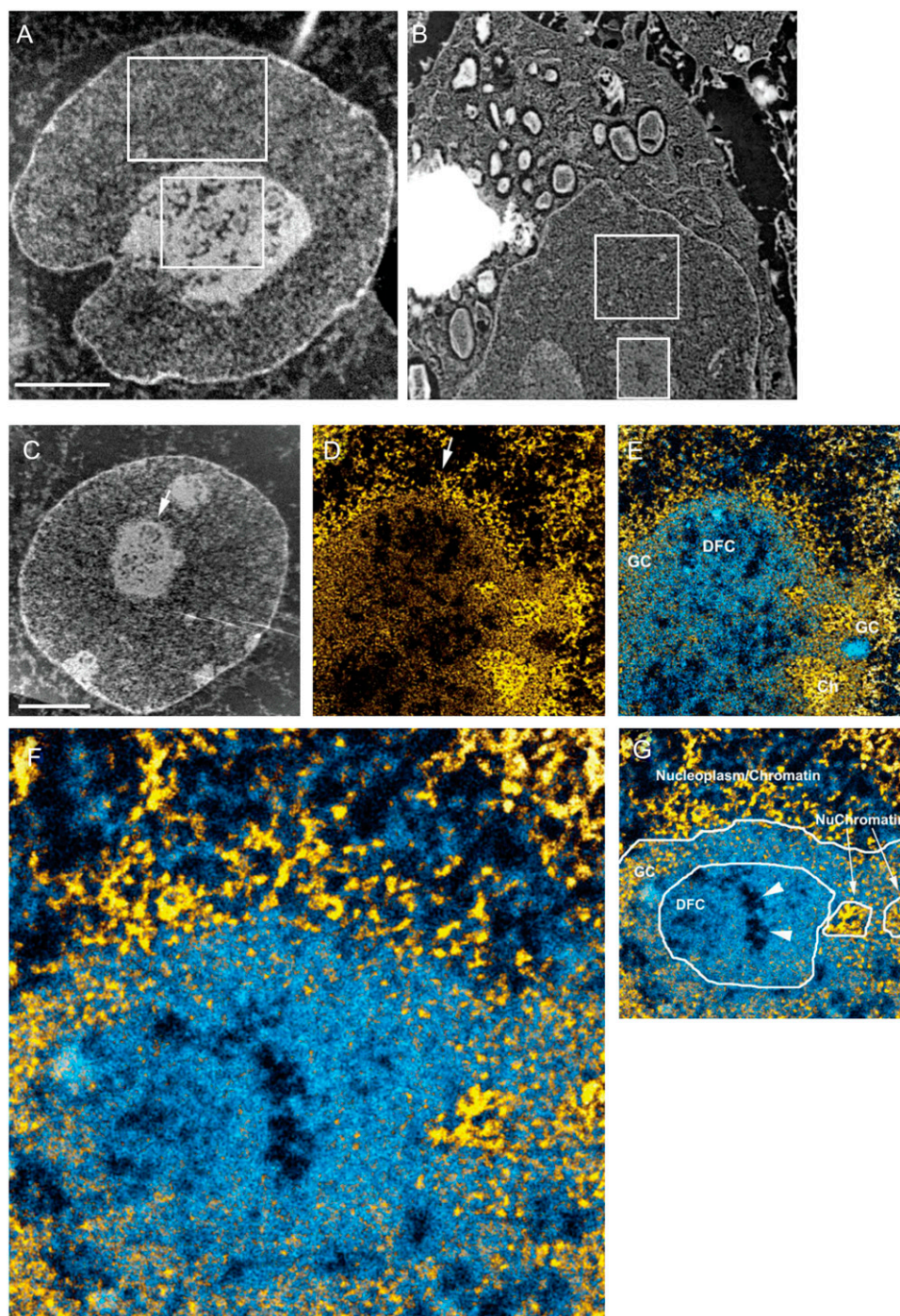


FIGURE 5 ESI mass-density measurements of the subnuclear compartments. (A) ESI of an Sk-N-SH neuroblastoma cell nucleus. The image was recorded at 120 eV energy loss. Sample preparation involved fixation in 2% paraformaldehyde for 30 min, followed by fixation in 0.5% glutaraldehyde overnight. Cells were dehydrated in ethanol and embedded in Qetol resin. Then 70-nm sections were picked up on 400-mesh electron microscopy grids, which were subsequently covered with a 3-nm carbon film picked up from the surface of water. The ratio (nucleolus divided by nucleoplasm) of the average intensity values of the two regions indicated is 1.93. (B) Bright-field image of a macrophage cell (RAW) cryopreserved by slam-freezing. The frozen hydrated sections were picked up onto a copper grid coated with a 3-nm carbon film. The grid was transferred to the electron microscope at liquid nitrogen temperature. The section was freeze-dried in the microscope column before imaging. The removal of water and the absence of a resin embedding material allow for very high contrast without the need for heavy atom contrast agents. The images, therefore, provide mass-density information. The ratio (nucleolus divided by nucleoplasm) of the average intensity values of the two regions indicated is 1.32. (C) Low-magnification mass-sensitive image of an Sk-N-SH cell recorded at 120 eV. (D) Net phosphorus image of a field from the nucleus presented in C. The arrows in C and D provide a fiduciary for each image and indicate the slight rotation between the images recorded at different magnifications. (E) The net phosphorus image was subtracted from the net nitrogen image (the resulting signal was represented in shades of blue). The net phosphorus signal (yellow) was superimposed on the nitrogen-phosphorus signal. GC, DFC and Ch represent granular component, dense fibrillar component, and chromatin, respectively. (F) High magnification of a field in E. Chromatin fibers can be visualized in the nucleoplasm, bordering the nucleolus, and within the nucleolus (referred to as NuChromatin in G). (G) Identification of different regions and structures associated with nucleolus. Scale bar represents 4 μm in A–C, 1 μm in D and E, and 280 nm in F.

ond time scale by SMT with short-term trapped molecules in all compartments. In detail, the percentage of trapped SAV molecules was higher in the pericentric heterochromatin and lowest in the nucleolus; i.e., it correlated inversely with

the amount of chromatin. Also, the retention or decay times of immobile molecules in heterochromatin and nucleoplasm were longer (>20 ms) than in the nucleolus (~ 7 ms). These observations suggested that molecular trapping is

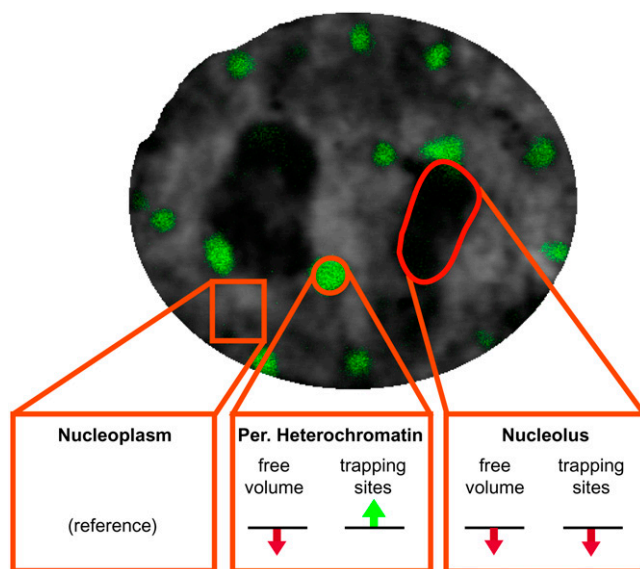


FIGURE 6 A view of different environments in the nucleus. Nucleoplasm and pericentric heterochromatin are dominated by the presence of chromatin fibers, whereas the nucleolus is composed largely of ribonucleoprotein particles. The green and red arrows summarize the increase and decrease, respectively, of trapping sites and available space by comparison to the nucleoplasm. See text for details.

possibly a result of short-term nonspecific chromatin interactions.

An alternative explanation for the very large differences detected in local mobility (Fig. 3) would be strongly differing local viscosities. However, this possibility could clearly be ruled out by our data. Small local domains of higher viscosity would not be stable over time but would rapidly be smeared out and vanish. However, we observed that the structural properties leading to the immobilization or trapping were stable over time (Fig. S3). We, therefore, conclude that short-term trapping of proteins is responsible for their slower diffusion within the cell nucleus.

In summary, our results indicate that nuclear structure affects the mobility and local concentration of proteins and may thus contribute to the regulation of nuclear processes. The transient, short-time trapping of proteins at chromatin may be a feature of the functional architecture of the nucleus and a general strategy to scan the genome for potential binding sites. An additional function of the cationic NLS could also be to enhance such binding. The observation that single molecules move freely in and out of the nucleolus sheds new light on the accessibility of this most prominent structure of the nucleus. Although wide-field epifluorescence images suggest a blocked access, the single-molecule tracings and ESI presented here rather argue for a reduced free volume in combination with a lower ability to trap molecules, i.e., lower retention. This free accessibility of the nucleolus has obvious consequences for possible modes of regulation and underscores the importance of SMT in studying the access and interaction of proteins with subcellular compartments.

SUPPLEMENTARY MATERIAL

To view all of the supplemental files associated with this article, visit www.biophysj.org.

We thank J. Sleeman (University of Dundee, UK) and M. Elbaum (The Weizmann Institute of Science, Israel) for the generous gift of ASF/SF2-GFP plasmid and NLS-biotin, respectively. U.K. is indebted to R. Peters for using numerous experimental facilities in his laboratory. We thank R. Temkin and R. Li for the electron microscopy.

ESI was funded by an operating grant to D.P.B.-J. from the Natural Sciences and Engineering Research Council of Canada. D.P.B.-J. holds a Canada Research Chair in Molecular and Cellular Imaging. M.C.C., H.L., and U.K. gratefully acknowledge financial support by the Volkswagen Foundation and the German Research Council.

REFERENCES

- Handwerger, K. E., and J. G. Gall. 2006. Subnuclear organelles: new insights into form and function. *Trends Cell Biol.* 16:19–26.
- Spector, D. L. 2001. Nuclear domains. *J. Cell Sci.* 114:2891–2893.
- Leonhardt, H., H. P. Rahn, and M. C. Cardoso. 1999. Functional links between nuclear structure, gene expression, DNA replication, and methylation. *Crit. Rev. Eukaryot. Gene Expr.* 9:345–351.
- Lang, I., M. Scholz, and R. Peters. 1986. Molecular mobility and nucleocytoplasmic flux in hepatoma cells. *J. Cell Biol.* 102:1183–1190.
- Seksek, O., J. Biwersi, and A. S. Verkman. 1997. Translational diffusion of macromolecule-sized solutes in cytoplasm and nucleus. *J. Cell Biol.* 138:131–142.
- Verkman, A. S. 2002. Solute and macromolecule diffusion in cellular aqueous compartments. *Trends Biochem. Sci.* 27:27–33.
- Görisch, S. M., K. Richter, M. O. Scheuermann, H. Herrmann, and P. Lichter. 2003. Diffusion-limited compartmentalization of mammalian cell nuclei assessed by microinjected macromolecules. *Exp. Cell Res.* 289:282–294.
- Görisch, S. M., M. Wachsmuth, K. F. Toth, P. Lichter, and K. Rippe. 2005. Histone acetylation increases chromatin accessibility. *J. Cell Sci.* 118:5825–5834.
- Verschure, P. J., I. van der Kraan, E. M. Manders, D. Hoogstraten, A. B. Houtsmuller, and R. van Driel. 2003. Condensed chromatin domains in the mammalian nucleus are accessible to large macromolecules. *EMBO Rep.* 4:861–866.
- Görisch, S. M., P. Lichter, and K. Rippe. 2005. Mobility of multi-subunit complexes in the nucleus: accessibility and dynamics of chromatin subcompartments. *Histochem. Cell Biol.* 123:217–228.
- Molenaar, C., A. Abdulle, A. Gena, H. J. Tanke, and R. W. Dirks. 2004. Poly(A)⁺ RNAs roam the cell nucleus and pass through speckle domains in transcriptionally active and inactive cells. *J. Cell Biol.* 165:191–202.
- Politz, J. C., R. A. Tuft, T. Pederson, and R. H. Singer. 1999. Movement of nuclear poly(A) RNA throughout the interchromatin space in living cells. *Curr. Biol.* 9:285–291.
- Politz, J. C., R. A. Tuft, K. V. Prasanth, N. Baudendistel, K. E. Fogarty, L. M. Lifshitz, J. Langowski, D. L. Spector, and T. Pederson. 2006. Rapid, diffusional shuttling of poly(A) RNA between nuclear speckles and the nucleoplasm. *Mol. Biol. Cell.* 17:1239–1249.
- Shav-Tal, Y., X. Darzacq, S. M. Shenoy, D. Fusco, S. M. Janicki, D. L. Spector, and R. H. Singer. 2004. Dynamics of single mRNPs in nuclei of living cells. *Science.* 304:1797–1800.
- Vargas, D. Y., A. Raj, S. A. Marras, F. R. Kramer, and S. Tyagi. 2005. Mechanism of mRNA transport in the nucleus. *Proc. Natl. Acad. Sci. USA.* 102:17008–17013.
- Gorski, S. A., M. Dundr, and T. Misteli. 2006. The road much traveled: trafficking in the cell nucleus. *Curr. Opin. Cell Biol.* 18:284–290.

17. Beaudouin, J., F. Mora-Bermudez, T. Klee, N. Daigle, and J. Ellenberg. 2006. Dissecting the contribution of diffusion and interactions to the mobility of nuclear proteins. *Biophys. J.* 90:1878–1894.
18. Braga, J., J. M. Desterro, and M. Carmo-Fonseca. 2004. Intracellular macromolecular mobility measured by fluorescence recovery after photobleaching with confocal laser scanning microscopes. *Mol. Biol. Cell.* 15:4749–4760.
19. Cardoso, M. C., H. Leonhardt, and B. Nadal-Ginard. 1993. Reversal of terminal differentiation and control of DNA replication: cyclin A and Cdk2 specifically localize at subnuclear sites of DNA replication. *Cell.* 74:979–992.
20. Cardoso, M. C., C. Joseph, H. P. Rahn, R. Reusch, B. Nadal-Ginard, and H. Leonhardt. 1997. Mapping and use of a sequence that targets DNA ligase I to sites of DNA replication in vivo. *J. Cell Biol.* 139:579–587.
21. Sleeman, J., C. E. Lyon, M. Platani, J. P. Kreivi, and A. I. Lamond. 1998. Dynamic interactions between splicing snRNPs, coiled bodies and nucleoli revealed using snRNP protein fusions to the green fluorescent protein. *Exp. Cell Res.* 243:290–304.
22. Brero, A., H. P. Easwaran, D. Nowak, I. Grunewald, T. Cremer, H. Leonhardt, and M. C. Cardoso. 2005. Methyl CpG-binding proteins induce large-scale chromatin reorganization during terminal differentiation. *J. Cell Biol.* 169:733–743.
23. Sporbert, A., P. Domaing, H. Leonhardt, and M. C. Cardoso. 2005. PCNA acts as a stationary loading platform for transiently interacting Okazaki fragment maturation proteins. *Nucleic Acids Res.* 33:3521–3528.
24. Kubitscheck, U., D. Grünwald, A. Hoekstra, D. Rohleder, T. Kues, J. P. Siebrasse, and R. Peters. 2005. Nuclear transport of single molecules: dwell times at the nuclear pore complex. *J. Cell Biol.* 168:233–243.
25. Siebrasse, J. P., D. Grünwald, and U. Kubitscheck. 2007. Single-molecule tracking in eukaryotic cell nuclei. *Anal. Bioanal. Chem.* 387:41–44.
26. Leonhardt, H., H. P. Rahn, P. Weinzierl, A. Sporbert, T. Cremer, D. Zink, and M. C. Cardoso. 2000. Dynamics of DNA replication factories in living cells. *J. Cell Biol.* 149:271–280.
27. Kues, T., A. Dickmanns, R. Lührmann, R. Peters, and U. Kubitscheck. 2001. High intranuclear mobility and dynamic clustering of the splicing factor U1 snRNP observed by single particle tracking. *Proc. Natl. Acad. Sci. USA.* 98:12021–12026.
28. Kues, T., and U. Kubitscheck. 2002. Single molecule motion perpendicular to the focal plane of a microscope: application to splicing factor dynamics within the cell nucleus. *Single Mol.* 3:218–224.
29. Saxton, M. J., and K. Jacobson. 1997. Single-particle tracking: applications to membrane dynamics. *Annu. Rev. Biophys. Biomol. Struct.* 26:373–399.
30. Crank, J. 1975. *The Mathematics of Diffusion*. Clarendon Press, Oxford.
31. Eskiw, C. H., G. Dellaire, J. S. Mymryk, and D. P. Bazett-Jones. 2003. Size, position and dynamic behavior of PML nuclear bodies following cell stress as a paradigm for supramolecular trafficking and assembly. *J. Cell Sci.* 116:4455–4466.
32. Dellaire, G., R. Nisman, and D. P. Bazett-Jones. 2004. Correlative light and electron spectroscopic imaging of chromatin in situ. *Methods Enzymol.* 375:456–478.
33. Kubitscheck, U., O. Kückmann, T. Kues, and R. Peters. 2000. Imaging and tracking of single GFP molecules in solution. *Biophys. J.* 78:2170–2179.
34. Grünwald, D., B. Spottke, V. Buschmann, and U. Kubitscheck. 2006. Intranuclear binding kinetics and mobility of single U1 snRNP particles in living cells. *Mol. Biol. Cell.* 17:5017–5027.
35. Grünwald, D., A. Hoekstra, T. Dange, V. Buschmann, and U. Kubitscheck. 2006. Direct observation of single protein molecules in aqueous solution. *ChemPhysChem.* 7:812–815.
36. Handwerger, K. E., J. A. Cordero, and J. G. Gall. 2005. Cajal bodies, nucleoli, and speckles in the *Xenopus* oocyte nucleus have a low-density, sponge-like structure. *Mol. Biol. Cell.* 16:202–211.
37. Weidemann, T., M. Wachsmuth, T. A. Knoch, G. Muller, W. Waldeck, and J. Langowski. 2003. Counting nucleosomes in living cells with a combination of fluorescence correlation spectroscopy and confocal imaging. *J. Mol. Biol.* 334:229–240.

Online Supporting Information

Online Supporting Table

Table SI. Quantitative analysis of the nuclear distribution of NLS-SAv-Cy5.

Nuclear compartment	Mean Fluorescence (CLSM) [§]	Relative Particle Density (SMT) [§]
Nucleoplasm	1	1
Pericentric Heterochromatin	0.96 ± 0.09	0.83 ± 0.16
Nucleolus	0.42 ± 0.05	0.58 ± 0.12

[§] Mean intensity of the Cy5 fluorescence was determined in MeCP2-GFP labeled pericentric heterochromatin, the nucleoli and remaining nucleoplasm from confocal microscopy (CLSM) images (see Fig. S1).

[§] In the single molecule tracking data (SMT) the number of particles per total compartment area was calculated. The particle number was extrapolated from the number of jumps.

Online Supporting Figures

Figure S1. Steady state distribution of NLS-SAv-Cy5 complexes in nuclear subcompartments.

(A) A C2C12 cell expressing MeCP2-GFP was microinjected into the cytoplasm with NLS-SAv-Cy5 complexes, and imaged 90 min later by confocal laser scanning microscopy. (B) The complexes distributed homogeneously in the cytoplasm and nucleus but showed a much lower concentration in the nucleoli, (C) which were identified according to the phase contrast (PC) image. (D) For the quantitative analysis of steady state distributions (see Table SI) the boundaries of the nuclei were determined in the green fluorescence (MeCP2-GFP) or phase contrast image. A border region near the nuclear envelope (width 0.95 μm , orange) was excluded from the analysis. The pericentric heterochromatin was identified by the bright MeCP2-GFP signal (yellow). Nucleoli (blue) were marked according to the phase contrast image. Scale bar, 5 μm .

Figure S2. NLS-SAv-Cy5 complexes do not form aggregates and are completely mobile within the nucleus and cytoplasm.

Fluorescence photobleaching experiments were performed in C2C12 mouse cells expressing MeCP2-GFP (green, pericentric heterochromatin), which had been microinjected into the cytoplasm with NLS-SAv-Cy5 (red) 90 min before. (A) For FLIP, the Cy5 fluorescence was bleached within a small spot (BA) in the nucleus (N) with 100% laser power at 633 nm followed by acquisition of an image. This cycle was repeated 200 times and numbers above the NLS-SAv-Cy5 fluorescence image indicate the imaging/bleaching cycle. At the end of the FLIP experiment the nuclear and cytoplasmic Cy5 fluorescence was completely lost. The FLIP curve in (B) shows the loss of Cy5 fluorescence (as mean fluorescence intensity, FI) in the nucleus (red curve) averaged for 10 cells. A fast loss of the nuclear fluorescence indicated a very high mobility and no binding or aggregation of the NLS-SAv-Cy5 complexes.

Figure S3. Temporal stability of trapping sites in the nucleoplasm.

The existence of structural traps would be supported, if trapping could occur repeatedly in the same spatial intranuclear regions. The observation of two different molecules at exactly the same site by pure chance is, however, exceptionally improbable considering the extremely low concentration used in our experiments. However, we did observe such an event. The first molecule entered into the confined region at frame 421 and remained there for 41 frames. The same region was revisited at frame 522 and finally at frame 883. Revisiting events were rare, but still they show the temporal stability of nuclear structures. Scale bar, 5 μm .

Figure S4. Streptavidin can cross compartment borders without hindrance.

Examples for tracks of molecules diffusing rapidly between the nucleoplasm and the heterochromatin (dark green, A and B) and to the nucleolus (bright green, C). (D) Jump distance distributions of particles crossing compartment borders. The relative frequency of short jumps is significantly decreased compared to the individual compartments (see Fig. 4), since crossing of the border is more probable when a particle performs a large jump than for an almost immobile particle. Scale bar, 1 μm .

Movie 1. Probing mammalian nuclear compartments with single streptavidin molecules.

The movie shows NLS-SAv-Cy5 molecules after microinjection into the cytoplasm. An overlay of the heterochromatin compartment staining (green) and the NLS-SAv-Cy5 moving through the cell (red) is shown. The data was recorded at 191 Hz, and the display rate is 20 Hz, which corresponds to about 10-fold slower motion. On the right hand side raw single molecule data are displayed; on left hand side the SMT raw data were processed using a 2-20 pixel band pass filter. One pixel corresponds to 96 nm and the whole object field shown is 12.2 μm x 12.2 μm . NLS-SAv-Cy5 is concentrated around the nuclear border, while single molecules can be distinguished inside the nucleus.

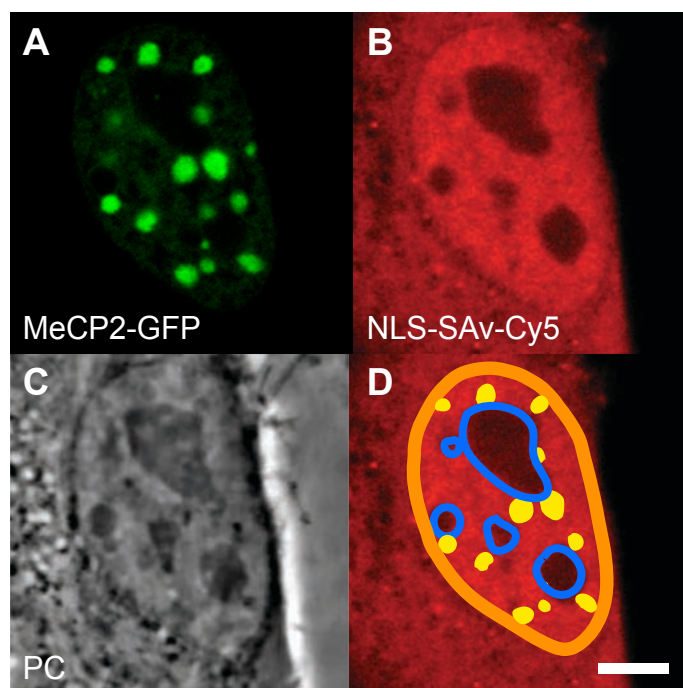


Fig. S1 - Grünwald et al.

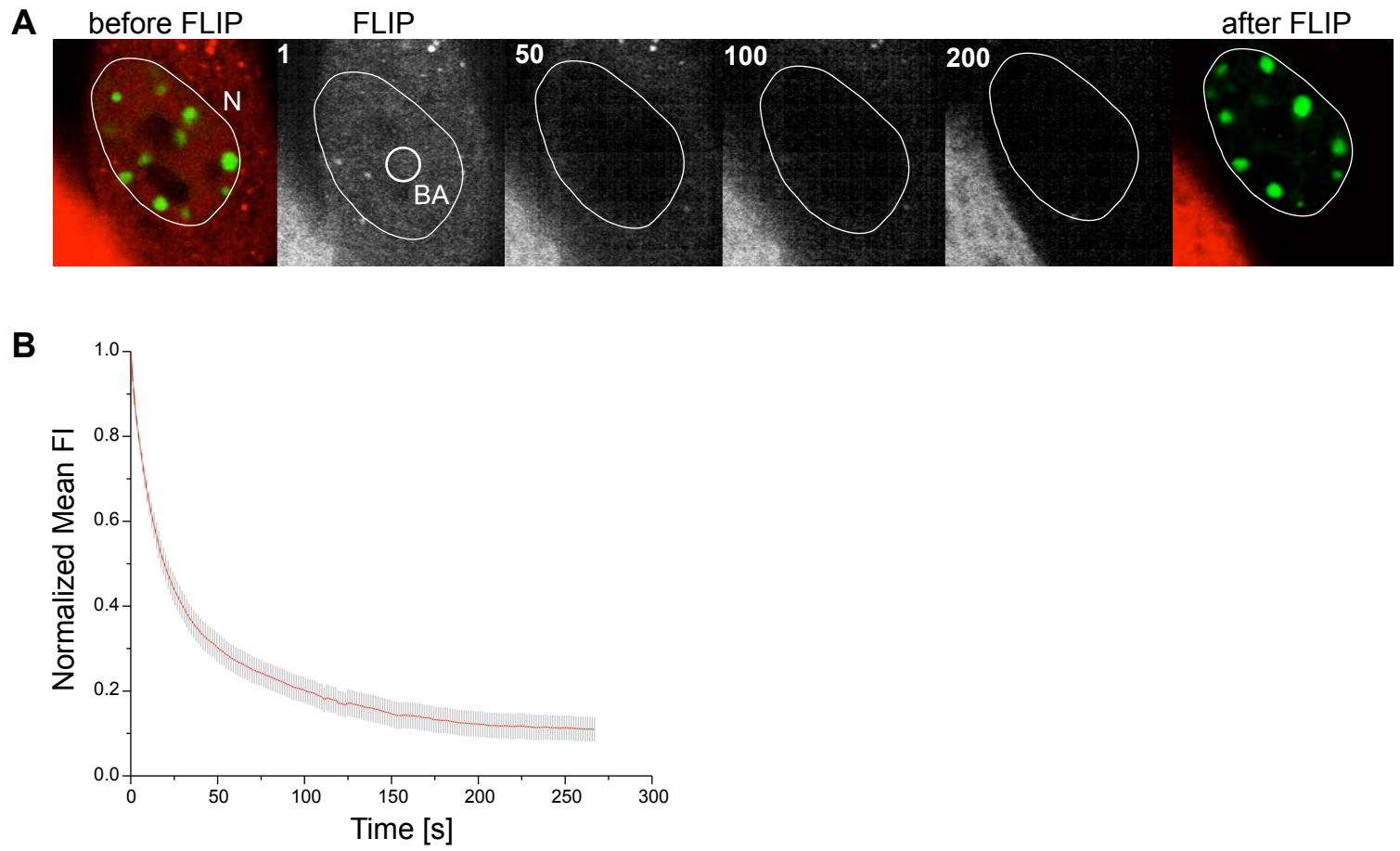


Fig. S2 - Grünwald et al.

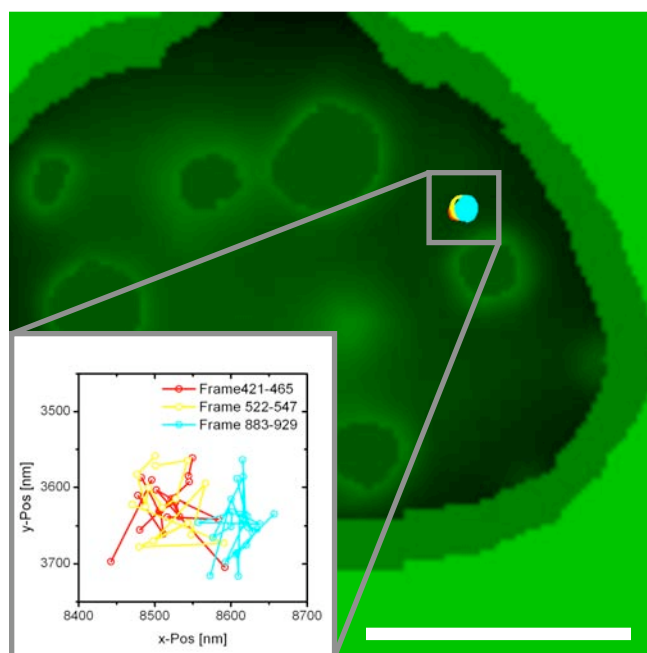


Figure S3 - Grünwald et al.

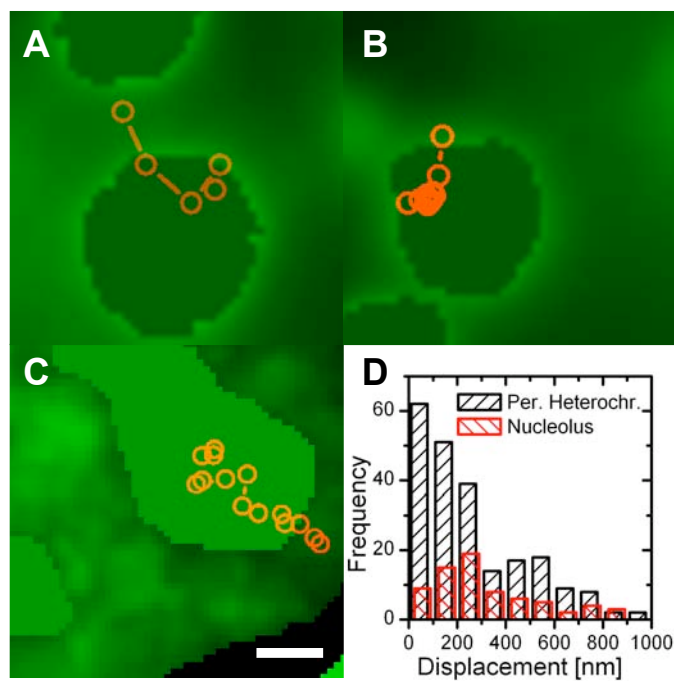


Fig. S4 - Grünwald et al.

4 Discussion and outlook

The relationship between nuclear structure and function and its impact on the regulation and performance of cellular functions are studied today more and more in living cells. With the development of new microscope techniques we gain higher resolution in space and time for the observation of molecule distribution and mobility. We have analyzed the influence of nuclear structures on the localization and movement of proteins and its implications for the regulation of the nuclear metabolism in living cells. During these investigations we developed techniques to label nuclear structures, improved and characterized the delivery of molecules and studied the distribution and mobility of molecules by confocal and single molecule fluorescence microscopy in living cells.

4.1 The labeling of nuclear substructures in living cells

In this work different DNA dyes were compared and tested for their usefulness in labeling chromatin in living cells. The purpose was to use fluorescent dyes as costainings in confocal fluorescence microscopy studies to test molecule distribution and dynamics with respect to chromatin in living cells. General requirements for a live cell DNA dye are membrane permeability, stoichiometric labeling without sequence specificity, low cytotoxicity, complementation with many other fluorophores, a high fluorescence yield and low photobleaching as well as non-harmful excitation.

We have tested five nucleic acid dyes (propidium iodide [PI], TOTO-3, TOPRO-3, Hoechst 33258 and DRAQ 5), from which only Hoechst and DRAQ5 show membrane permeability and could be used in living cells. The DNA dye DRAQ5 fulfills several of the requirements listed above. It exhibits a good correlation with the labeling of chromatin like histone GFP fusion proteins and its fluorescence excitation and emission is in the deep red spectrum of visible light ($\lambda_{\text{ex}} = 647 \text{ nm}$ \ $\lambda_{\text{em}} = 670 \text{ nm}$). Furthermore, it displays almost no photobleaching, low cytotoxicity and can be easily applied to living cells. The disadvantages of DRAQ5 are that it inhibits cell cycle progression in late S/G2 phase, which make its long time use over several cycles impossible. A minor point is the decrease of labeling over many hours in certain cell types with

efficient detoxifying metabolism (Martin et al., 2005). Altogether DRAQ5 fulfills several of the requirements for a live cell DNA dye. The Hoechst family of DNA dyes is one of the few alternatives for DNA specific, cell permeable dyes, but is highly toxic to live cells and requires harmful UV excitation, which leads to a very restricted observation time (Durand and Olive, 1982). Furthermore one has to take into account interference effects of dye molecules that bind to DNA with the dynamics on chromatin proteins (Davis and Bardeen, 2003).

The general advantage of fluorescent dyes over fluorescent fusion proteins is that they are easily introduced into cells. Upon addition to the growth medium labeling occurs within minutes. Transfections are more complex procedures and it takes several hours until expression. Finally, in live cell experiments it could be useful to identify the DNA and chromatin only from a defined time point on in an experimental series e.g. timeseries imaging, photobleaching of fluorescent dyes or proteins with similar spectral properties. On the other hand fluorescent fusion proteins are not toxic at moderate expression level and enable long term observations without disturbing cellular functions (Kanda et al., 1998).

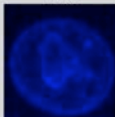
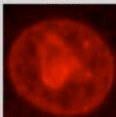
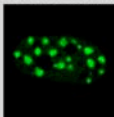
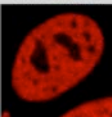
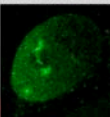

Dyes	Fluorescent proteins and fusion constructs			Fluorescence labeled cell penetrating peptides	
Application: <ul style="list-style-type: none">- staining of DNA- covalent labeled probe molecules Pro: <ul style="list-style-type: none">- fast and easy to use Con: <ul style="list-style-type: none">- cytotoxicity- different labeling properties	Application: <ul style="list-style-type: none">- labeling of chromatin and chromatin subsets- label for proteins- use as probe molecules Pro: <ul style="list-style-type: none">- available in many colors- specific labeling of nuclear structures- dynamic studies with photo bleaching and photoactivation Con: <ul style="list-style-type: none">- time until expression- transfection rate unpredictable- protein overexpression			Application: <ul style="list-style-type: none">- labeling of nucleoli Pro: <ul style="list-style-type: none">- labeling with many dyes- easy to use- no cytotoxic effects at low concentrations Con: <ul style="list-style-type: none">- variable labeling time- no control over ammount of delivered peptide	
Hoechst33258/ DNA	DRAQ5/ DNA	MeCP2-GFP/ chromocenter	H2B-mRFP/ chromatin	GFP photoactivation	FITC-D-R10/ nucleolus
					

Figure 6: Summary of methods used to label nuclear structures in live cells.

A relatively novel method to non-invasively introduce molecules into living cells for labeling purposes is the use of membrane penetrating peptides also termed

cell penetrating peptides (CPP) (Wadia and Dowdy, 2002). We exploited this mechanism and developed a peptide combining membrane penetration with the ability to accumulate and thereby label the nucleoli of living cells. The peptide consists of 10 arginines in the D-conformation to prevent proteolytic degradation and is coupled to a fluorescent dye molecule for visualization in fluorescence microscopy. The nucleolar marker can simply be added to the culture medium of living cells and then quickly labels the nucleoli of different cell types with high efficiency and no harmful side effects (Martin et al., 2007a). The combination of DNA and chromatin labeling by dyes and protein fusions with permanent, photoactivatable or photoconvertible GFP versions in diverse colors as well as transducible fluorescent peptide markers are powerful tools to study the structure and function of the nuclear components in living cells. A summary of the advantages and disadvantages of the different methods is given in Fig. 6.

4.2 Delivery of macromolecules by cell penetrating peptides in live cells

Beside the introduction of labeling components the membrane penetrating peptides can also shuttle bioactive cargoes like drugs, signal molecules or connected peptides into living cells. Several groups have shown intracellular effects transmitted by the introduction of molecules by CPP into live cells (Nagahara et al., 1998; Nolden et al., 2006; McCusker et al., 2007). We have analyzed the mechanism of membrane transduction, intracellular fate and effects of delivered bioactive peptides and proteins directly in live cells by fluorescence microscopy (Tunnemann et al., 2006; Tunnemann et al., 2008). With this approach we have prevented artifacts in the cell permeation and localization due to fixation treatments (Richard et al., 2003; Vives et al., 2003). In accordance with other studies we found that peptides cross plasma membranes of cells via a unique endocytosis independent mechanism that does not require energy, but is linked to the membrane potential and of differing efficiency between cell types (Duchardt et al., 2007; Fretz et al., 2007). In contrast to peptide constructs, the proteins and nanoparticles coupled to CPP are taken up exclusively in endocytic vesicles of live cells. The lack of detectable transduced CPP proteins and nanoparticles is probably due

to the large MW and a globular conformation added to the CPP. On the other hand we could demonstrate intracellular effects of internalized TAT-Cre-recombinase protein constructs in a very sensitive recombination assay. The Cre recombinase was fused to the transduction peptide domain of the HIV transactivator of transcription (TAT). It remains unclear whether and how the TAT-Cre escapes from vesicles or whether they enter by transduction.

A major advantage of the application of CPP is that the transduction functions with virtually all cell types including primary cells, that are usually very difficult to transfect (Mi et al., 2000). On the other hand the labeling of specific cells in a tissue is difficult because of the non selective membrane transduction affecting many cells or tissues (Fawell et al., 1994). Curiously, in all our experiments a few cells always resisted membrane transduction, which could represent genetic or epigenetic differences in gene expression among the cells in the culture (Tyagi et al., 2001) or in their metabolic state. Other groups have shown that the unspecific uptake of CPP can be reduced in some cell types by designing peptide constructs with a protease sensitive linker. This peptide is exclusively cleaved on the surface of certain tumor cells and taken up preferentially by this cell type (Jiang et al., 2004).

Our results show that membrane penetration is a concentration dependent process with a requirement for an amino acid composition consisting of poly-arginines in contrast to non transducing poly-lysines. Very high concentrations of CPP added to live cells exert toxic effects most probably due to membrane disruptions, but concentration windows with high transduction and low cytotoxicity could be determined. Further the transduction potential increases with the length of the arginine peptide chain with an optimum at 9-10 Arg and is further improved by the use of protease resistant D-isomers of the amino acids (Tunnemann et al., 2008). These results are in contrast to other findings that reported a transduction threshold concentration (Fretz et al., 2007) and are in more agreement with a report suggesting a dependency on the peptide to cell ratio (Hallbrink et al., 2004). Accordingly, in our study very low concentrations of the optimal performing poly-arginines also did not show transduction, most probably due to a low charge to membrane area ratio. These different results on the transduction dependency could be explained by

the high variability of transduction between different cell types and the use of peptides with different length, varying concentrations and amino acid isomers. Although we found a linear dependency of peptide concentration and transduction, the control of the amounts of CPP entering the cells remains difficult since the transduction process can not be stopped.

The intracellular fate of CPPs is determined to a large extent by their similarity with nuclear and nucleolar targeting sequences that contain a high number of basic charged amino acids. This leads to the accumulation of CPP like TAT and poly-arginines in the nucleolus (Martin et al., 2007a). Despite this fact, we could show a high mobility, fast exchange rates and overall intracellular availability of a TAT-p21^{WAF/Cip}-PBD construct. Additionally, the functional interaction of the PCNA binding domain (PBD) peptide with PCNA exhibited a biological effect and affected cell cycle progression.

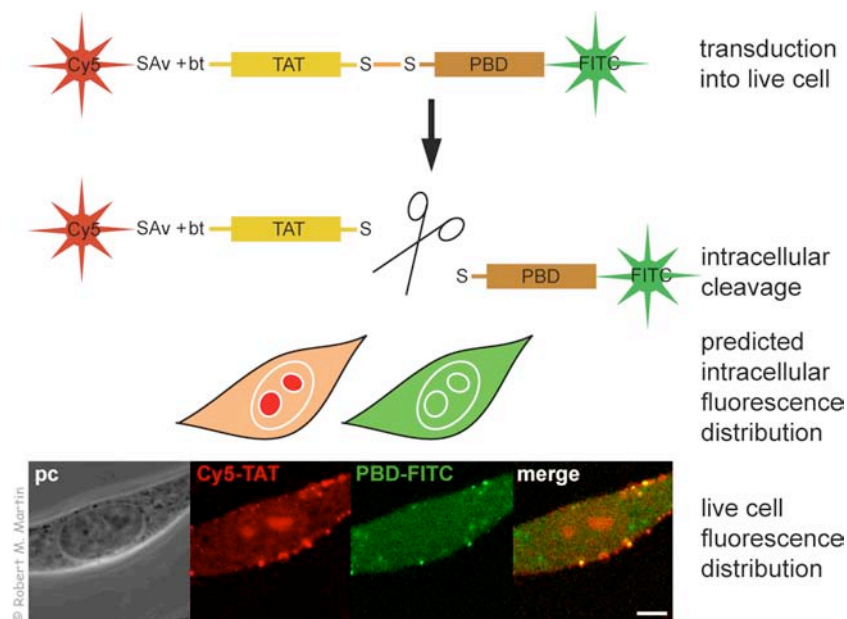


Figure 7: Application of cleavable peptide constructs for efficient intracellular release of cargo peptides. The TAT-PBD construct with a double cysteine linker was coupled with streptavidin Cy5 and transduced into C2C12 mouse myoblasts. The two different labels, FITC and Cy5, are located in the cytoplasm and nucleus of the cell. Only the TAT coupled Cy5 label accumulates in the nucleoli indicating a cleavage of the disulfide bond and release of the PBD-FITC. The predicted differential distribution and accumulation of the labeled peptides visualized in live cells demonstrate the possibilities of this method. Scalebar = 5 μm

The association of the TAT with nucleolar components probably interferes with the binding of the cargo PBD peptide and thus reduces its effect. Our preliminary results show, that the use of peptide constructs containing a cleavable linker that separates TAT and the cargo in the cytoplasm, results in distinct localization patterns depicted in Fig. 7.

The development of improved approaches using cell penetrating peptide constructs that can be specifically targeted may progress into key technologies in the delivery of bioactive peptides, drugs, signal molecules and label in future research and molecular medicine (Bullok et al., 2006).

4.3 Mechanisms and effects of chromatin condensation

After exploring the possibilities in labeling of nuclear structures and the delivery of molecules to test the dynamics of nuclear organization we characterized different methods of inducing chromatin condensation by different pathways and the subsequent effects in living cells.

We have analyzed the effects of hyperosmolarity and ATP depletion on chromatin condensation in interphase nuclei and compared these changes with the condensed chromosomes in mitosis (Martin et al., 2007b; Martin and Cardoso, 2008 submitted at JMB). Although the induced changes in the chromatin condensation state occur via different pathways compared to mitotic condensation we did observe several common characteristics (Albiez et al., 2006; Maddox et al., 2006). The chromatin labeled by fluorescent histones shows an increase in the labeling intensity in the condensed form compared to interphase chromatin. This applies for the condensation in mitosis, by hyperosmolarity and during ATP depletion, indicating a reduction of volume by closer packing of nucleosomes. Furthermore, the hyperosmolar chromatin condensation level is similar to mitosis and an example for a reversible global chromatin compaction observable in interphase nuclei (Martin and Cardoso, 2008, submitted at JMB). Condensed chromatin in terminally differentiated cells, in disease or in dying cells could adapt similar levels of condensation by endogenous pathways.

Our findings have important consequences for the interpretation of experiments using NaN_3 for ATP depletion or solutions with high salt

concentrations in the analysis of molecule dynamics within the nucleus. Although the diffusive mobility of nuclear proteins is independent of salts and energy in form of ATP (Phair et al., 2004), the enlarged interchromatin space on the one hand and the higher condensation of chromatin on the other hand is likely to affect local protein concentration, mobility and access. The direct effect of chromatin condensation on protein distribution and mobility was also investigated and is discussed in the following chapters.

Most importantly, our results show that external stimuli, manipulations and drugs directly or indirectly changing cellular calcium levels, by either energy depletion or direct interference with calcium homeostasis, have an effect on chromatin condensation and arrest cell cycle progression. These unexpected links between energy metabolism, calcium homeostasis, chromatin condensation and cell cycle should be taken in account for the design of drug screenings and the interpretation of cellular responses. Even small changes of free intracellular calcium levels may affect chromatin condensation and gene expression with still unknown consequences.

4.4 Accessibility of chromatin in living cell nuclei

In these sets of experiments we analyzed also the distribution of proteins and chromatin in live cell nuclei following changes in the chromatin condensation state. We used confocal microscopy to study bulk localizations of fluorescently tagged nucleoplasmic proteins and chromatin proteins. In addition, we assessed the accessibility of chromatin by measuring the mobility of fluorescent chromatin proteins histone H2B and HP1 α using photobleaching and photoactivation in chromatin with different condensation levels. The data reveals ascending exclusion of nucleoplasmic proteins from chromatin with increasing condensation level. The mitotic condensed chromosomes and interphase chromatin condensed to the mitotic level by hyperosmolarity show reduced concentrations of nucleoplasmic proteins. But in the same time chromatin proteins localize and accumulate in these condensed chromatin structures (Martin and Cardoso, 2008, submitted at JMB).

This observation could be explained by the formation of higher order chromatin structures below the resolution limit including 30 nm fibers or condensed

heterochromatin substructures involving e.g. MBD proteins and polycomb group proteins (Georgel et al., 2003; Francis et al., 2004). The reduction of nucleoplasmic protein concentrations in condensed chromatin could be the result of exclusion and inaccessibility below the resolution limit. Small inaccessible chromatin structures in close proximity to accessible space, both in the scale of 10 – 250 nm, would result in reduced protein concentrations in large heterochromatin domains compared to the fully accessible nucleoplasm.

4.5 The effect of chromatin condensation on DNA metabolism

The chromatin compaction in condensed heterochromatin and mitotic chromosomes in comparison to loose euchromatin fibers reduces the available space between the nucleosomal subunits (Bednar et al., 1998; Dorigo et al., 2004). The resulting fiber structures might be accessible to proteins on the surface but only few proteins could move inside. Heterochromatin proteins, e.g. HP1 and other transcriptional repressors, show a fast exchange in interphase heterochromatin and mitotic chromosomes, demonstrating the accessibility of large condensed chromatin structures (Ng et al., 1999; Schmiedeberg et al., 2004) (Martin and Cardoso, 2008, submitted at JMB). The accumulation of heterochromatin specific proteins could therefore result in a competition with nucleoplasmic proteins for space on the nucleosomal fiber. The differences in the association and binding affinities to chromatin lead to different immobilization times with short trapping or fast transit of non binding proteins and long term stable binding of chromatin factors. This results in the increase of the concentration of chromatin proteins, that could compete with or displace proteins and thus reduce the number of proteins with lower affinity to chromatin components such as modified or unmodified DNA and histones or other recruiting factors.

The transcription and replication of the genetic material is a fundamental aspect of the nuclear metabolism and is regulated at multiple levels. Interactions between genetic elements and proteins in cis and trans are part of these regulatory mechanisms (Huang and Prystowsky, 1996). The start and elongation of transcription and replication depends on the opening of chromatin to give initiation factors, polymerases and elongation factors direct

access to the DNA strand. This includes the release of chromatin condensation factors as well as nucleosome remodeling (Alexandrow and Hamlin, 2005).

The regulation of protein concentrations by occupied and inaccessible chromatin could influence these processes in different ways: 1. The interaction between genetic sequences in cis and trans may be weakened or inhibited.

2. The molecule number and thus activity of initiation factors is reduced and decreases the frequency of transcription initiation. 3. The insufficient opening of chromatin could result in interference of the RNA polymerases with chromatin proteins. This would cause a reduction of the enzymatic activity and processivity by pausing or falling of the template DNA (Levine et al., 1993; Dellino et al., 2004).

It was shown that in interphase the transcription of active genes is a stochastic process that also contributes to the heterogeneity of clonal cell populations (Blake et al., 2003). Premature terminated RNA fragments, termed transcriptional noise, are generated frequently due to premature transcript termination, paused transcription and falling off of RNA polymerases from the template DNA. Accordingly, a low number of transcripts can still be generated from silenced genetic regions (Struhl, 2007; Voliotis et al., 2008). In housekeeping genes the ratio between transcriptional noise and full length mRNAs is shifted to the finished transcripts due to the unhindered progress of the transcription machinery in open chromatin. The formation of condensed chromatin could reduce the number of finished mRNAs by reducing the access and action of the transcription machinery in less dense chromatin structures. Thus, in condensed chromatin that contains downregulated or silenced genetic regions, the level of interrupted transcription processes and unfinished RNAs increases. Accordingly the assembly of histone variants that mark active chromatin and destabilize the nucleosomal fiber for transcription requires accessible chromatin structures (Henikoff, 2008).

Besides transcription also DNA replication is affected by chromatin condensation and errors can cause mutations with severe consequences. In contrast to transcription, after the licensing of replication during the cell cycle, improper DNA synthesis can result in cell death due to a loss of genetic information or inheritance of mutations that lead to genetic diseases. Thus the

condensed chromatin has to be completely remodeled and opened for high fidelity of DNA synthesis. The affinity of nucleoplasmic proteins to chromatin and DNA changes throughout the cell cycle. For example, during S-phase following the transduction of signals from the cell cycle regulation network the replication machinery assembles on chromatin (Chevalier and Blow, 1996; Fujita et al., 2002). The temporal modulation of chromatin structures during DNA or RNA metabolism is thus necessary and the dissociation of proteins forming condensed chromatin is achieved by specific modifications like phosphorylation or incorporation of histone variants (Contreras et al., 2003; Henikoff and Ahmad, 2005; Hirota et al., 2005). Similarly, topoisomerases and transcription factors that interact with chromatin proteins can induce the remodeling of chromatin (Varga-Weisz et al., 1997; Muller et al., 2001; Poot et al., 2004). In accordance with these findings, mutations in the histone sequence can prevent chromatin remodeling and reduce gene expression (Xu et al., 2005).

4.6 Dynamics of protein movement in the nucleus of living cells

It has been debated over the past years whether and how chromatin excludes molecules in the cell nucleus and how this situation could affect DNA metabolism and heterochromatin function (Verschure et al., 2003; Görisch et al., 2004; Chen et al., 2005). Significant effort has also focused on the analysis of the mobility of nuclear proteins and the contribution of molecule dynamics to the structure and function of the cell nucleus (Pederson, 2001; Verkman, 2002). Numerous studies have revealed a high mobility of fluorescently tagged nuclear proteins mostly by fluorescence bleaching, photoactivation, fluorescence uncaging or fluorescence correlation microscopy (Politz et al., 1999; Wachsmuth et al., 2003; Catez et al., 2004). Fluorescence photobleaching or activation studies and the corresponding data analysis have a relatively low temporal and spatial resolution and do not provide biophysical parameters like modes of movement and individual residence times (Braga et al., 2004; Beaudouin et al., 2006). Recent developments of detecting and analyzing the movement of single molecules and particles in living cells can overcome these limitations. The **single molecule tracking (SMT)** microscopy

enables the determination of single molecule localizations to ≈ 50 nm in 5 ms time frames allowing the identification of short term movements and immobilization (Kubitscheck et al., 2000; Grunwald et al., 2006). Because it is not yet possible to gain the same spatial resolution for the molecular structures in nuclear compartments by live cell fluorescence microscopy (Shao et al., 2008), we combined the SMT approach with ESI (Bazett-Jones and Hendzel, 1999). With this technique it is possible to determine mass densities and the distribution mapping of elements characteristic for nuclear components at electron microscopy (EM) resolution (phosphorus – DNA, RNA; nitrogen – proteins) (Dellaire et al., 2004; Politz et al., 2005).

4.7 The dynamics of single molecules in the nuclear interior

Our findings using single molecule microscopy are consistent with previous studies and show that the nuclear interior is widely accessible for proteins. Even condensed chromatin structures and nucleoli allow molecules to enter without hindrance and are thus not closed compartments as suggested before (Phair and Misteli, 2000; Handwerger et al., 2004; Politz et al., 2006). The neutral Cy5 labeled probe molecule streptavidin coupled to a nuclear localization sequence (NLS) was found to diffuse with high mobility in the nucleoplasm, heterochromatin and nucleoli.

Slow and fast movements as well as immobilization were observed in all nuclear subcompartments. With respect to the different molecular environments we show increased trapping and less fast diffusing molecules in condensed heterochromatin compared to less dense nucleoplasm. Surprisingly the streptavidin molecules show less trapping and a high mobility in the nucleoli, but a much lower concentration compared to the nucleoplasm (Grunwald et al., 2008). This is in contrast to the high mass density inside nucleoli compared to the nucleoplasm. In the condensed pericentromeric heterochromatin the trapping was still increased compared to the nucleoplasm, which is in agreement with the mass density and concentration of DNA and chromatin proteins (Nielsen et al., 2001; Daban, 2003; Dillon, 2004).

It was shown in previous studies that chromatin undergoes constrained diffusional movements and chromatin proteins constantly exchange in these

structures (Abney et al., 1997; Marshall et al., 1997; Kimura and Cook, 2001; Cheutin et al., 2003). On the other hand, nuclear compartments like pericentromeric heterochromatin domains are persistent higher order structures that are maintained over many cell cycles and form stable clusters during differentiation (Brero et al., 2005). The movement of NLS-streptavidin molecules between nucleoplasm and heterochromatin without obstruction when crossing the compartment borders, supports the view of condensed chromatin as accessible structures (Verschure et al., 2003). A decrease of mobility, measured by the diffusion coefficients in pericentromeric heterochromatin, is consistent with the higher molecular density compared to less dense nucleoplasm. Accordingly, the frequency of trapping events increases in heterochromatin. These molecular dynamics might be substantially different for proteins with different sequence and charge composition in comparison to the neutral probe molecule streptavidin. Interestingly, we identified the trapping of different molecules at the same nuclear position, which could result from stable molecular structures within the localization precision. The structures responsible for repeated trapping, e.g. molecular cavities, could be formed by higher order folding of chromatin. These trapping sites would be more frequent in stable and highly organized structures like condensed heterochromatin in contrast to loose euchromatin fibers in the nucleoplasm.

The data suggest that short trapping events on the one hand result from unspecific associations by weak ionic or electrostatic forces between amino acids, DNA and RNA. This could account for the observed reduction of mobility of macromolecule solutes in the cytoplasm compared to aqueous solutions (Lang et al., 1986; Seksek et al., 1997). Otherwise structural features in chromatin could account for repeated immobilization events. This may represent a substantial basic feature of molecule interaction, which could serve to scan molecular complexes for substrates and binding sites as a first contact that precedes specific binding. The existence of specific binding motives and substrates would therefore increase the immobilization times and number of immobilized molecules as shown for enzymatically active splicing factors (Grunwald et al., 2006).

The nucleolus as a paradigm of nuclear bodies has a completely different structure and composition than heterochromatin (Dehghani et al., 2005; Politz et al., 2005). However, similar mechanisms could apply for the localization, accumulation or reduction of proteins in the nucleoli. The molecular structure of nucleoli in electron spectroscopic images is visible as dense areas with scarce available space but also channel like structures and gaps between ribosomal particles. We conclude that nucleoplasmic proteins can freely diffuse into nucleoli but due to space limitations, no specific interactions, and low number of trapping sites quickly transit out of the nucleolus. The channel like structures might facilitate the fast transit of nucleolus non interacting proteins. Thus the amount of unspecific proteins in this compartment is kept low. Still it remains unclear whether the nucleolar structures identified by ESI are stably persistent or highly dynamic due to the mobility of the components (Leung and Lamond, 2003; Olson and Dundr, 2005; Grunwald et al., 2008). The reduction of trapping events and times in the nucleolus was surprising when the mass density and possibilities for unspecific interactions are taken into consideration. A possible explanation for this phenomenon could be the low number of the persistent structures as trapping sites in nucleoli caused by the dynamics of the nucleolar components. This would be in agreement with our data on the high mobility of TAT peptides in the nucleolus (Tunnenmann et al., 2006). Alternatively, the nucleolar components could create a microenvironment with a general electrostatic repulsion of the NLS-streptavidin probe molecules. This model would predict, that the visible exclusion of proteins from the nucleolus is a result of the high mass density and fast transit of non nucleolar components. The nucleolar localization and accumulation of TAT peptides seems to be a consequence of exclusive interactions via specific sequences with a basic charge (Hatanaka, 1990; Martin et al., 2007a). The immobilization events of proteins and peptides accumulating in the nucleolus are very likely increased in number and time compared to neutral probes like streptavidin.

4.8 Compartmentalized micro environments provide an additional regulation level for the nuclear metabolism

In conclusion, a general hypothesis from the results presented here is, that the formation and maintenance of nuclear substructures are the result of a dynamic competition. The nuclear subcompartments are accessible to different proteins largely independent of size as well as sequence (Fig. 8). Substructures such as heterochromatin or the nucleolus are enriched in specific binding sites for chromatin proteins and nucleolar components respectively, where the charge of the protein or peptide is also of importance. All proteins move rapidly inside and along the substructures and the trapping events we observed might be a mechanism to scan a macromolecular structure like chromatin for exposed targets and binding sites.

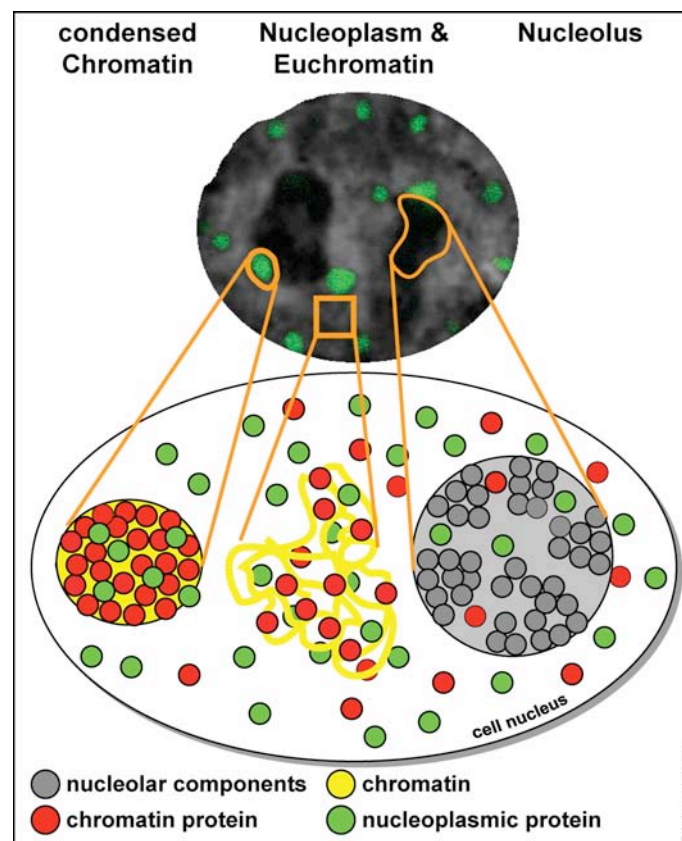


Figure 8: Model for the distribution and mobility of nuclear proteins
(modified from Grunwald et al., 2008)

Proteins with specific interaction motives, in addition to the short time trapping, bind more frequently and for increased duration. Thus, they localize

preferentially and accumulate at the respective structure e.g. heterochromatin proteins and nucleolar proteins. This is illustrated in Fig. 8 as red particles in the yellow structure. The number of proteins with less affinity or binding partners becomes moderately reduced by a competition for the space in structures like condensed chromatin and in addition by a fast transit through the nucleolar compartment. This is shown in Fig. 8 as the green particles in the yellow and grey structure, respectively. The separation of different chromatin domains may be achieved by boundary elements and insulators on the DNA sequence level or specific chromatin modifications. These create environments with spatial distance of biochemically different interaction sites and prevent the transformation of epigenetic states in adjacent chromatin domains (Pikaart et al., 1998; Felsenfeld and Groudine, 2003).

4.9 Outlook

In future studies, SMT analysis of proteins involved in DNA, RNA and protein metabolism will increase the understanding of functional nuclear protein dynamics. In contrast to neutral probe molecules like streptavidin, the transcription and replication factors contain specific binding motives or have enzymatic activity with influence on this dynamic behavior (Cardoso et al., 1997). In addition, the protein exchange between nuclear compartments in coordination with specific metabolic pathways would give a more complete picture of molecular trafficking and processing dynamics in live cells. Going further, one could imagine that the next level of single molecule microscopy will enable the analysis of the interaction of two or more proteins with different labels at the same time in living cells. Furthermore, it will be of high importance to obtain a high resolution view on the nuclear structures like chromatin, nucleoli, nuclear bodies and structural elements in live cells. Resolving the structure of chromatin, nucleoli and nuclear bodies to a scale of 50 nm or further in live cells, similar to the SMT localization precision, would provide direct insight into structure, function and interaction dynamics. Future aims include the analysis of the influence of protein and peptide charge on the distribution, mobility and accumulation in nuclear subcompartments. The charge of a given polypeptide has a profound influence on protein targeting

and localization. This will be combined with the analysis of the dynamics of protein and peptide accumulation in the nucleolus.

The present results help to explain the molecular mechanisms of protein and peptide accumulation and exclusion as well as interactions in and with nuclear substructures. The nuclear protein dynamics regulates the nuclear metabolism and thus cellular function. Understanding the dynamics of the compartmentalized nuclear structures and how this relates to nuclear function will allow the prediction of effects that go along with alterations of protein localization or nuclear structures. These nuclear processes are fundamental basic aspects of life and determine the differential use of the genetic information on a local and global level. The regulation of gene expression is directly linked to the function and fate of any cell starting with the oocyte and going through the development, differentiation and disease of tissues, organs and organisms. Understanding the genetic program, its function and regulation is a fundamental part of understanding life.

5 Literature

- Abney, J.R., B. Cutler, M.L. Fillbach, D. Axelrod, and B.A. Scalettar. 1997. Chromatin dynamics in interphase nuclei and its implications for nuclear structure. *J Cell Biol.* 137:1459-68.
- Agarwal, N., T. Hardt, A. Brero, D. Nowak, U. Rothbauer, A. Becker, H. Leonhardt, and M.C. Cardoso. 2007. MeCP2 interacts with HP1 and modulates its heterochromatin association during myogenic differentiation. *Nucleic Acids Res.* 35:5402-8.
- Albiez, H., M. Cremer, C. Tiberi, L. Vecchio, L. Schermelleh, S. Dittrich, K. Kupper, B. Joffe, T. Thormeyer, J. von Hase, S. Yang, K. Rohr, H. Leonhardt, I. Solovei, C. Cremer, S. Fakan, and T. Cremer. 2006. Chromatin domains and the interchromatin compartment form structurally defined and functionally interacting nuclear networks. *Chromosome Res.* 14:707-33.
- Alexandrova, O., I. Solovei, T. Cremer, and C.N. David. 2003. Replication labeling patterns and chromosome territories typical of mammalian nuclei are conserved in the early metazoan Hydra. *Chromosoma.* 112:190-200.
- Alexandrow, M.G., and J.L. Hamlin. 2005. Chromatin decondensation in S-phase involves recruitment of Cdk2 by Cdc45 and histone H1 phosphorylation. *J Cell Biol.* 168:875-86.
- Andersen, J.S., C.E. Lyon, A.H. Fox, A.K. Leung, Y.W. Lam, H. Steen, M. Mann, and A.I. Lamond. 2002. Directed proteomic analysis of the human nucleolus. *Curr Biol.* 12:1-11.
- Anderson, D.J., and M.W. Hetzer. 2007. Nuclear envelope formation by chromatin-mediated reorganization of the endoplasmic reticulum. *Nat Cell Biol.* 9:1160-6.
- Ascoli, C.A., M.R. Link, N. Ventura, R.J. Kuchler, and S. Mandeles. 1988. Identification of a rosette-enriched chromatin fraction from mouse fibroblast nuclei. *Arch Biochem Biophys.* 263:334-48.
- Bazett-Jones, D.P., and M.J. Hendzel. 1999. Electron spectroscopic imaging of chromatin. *Methods.* 17:188-200.
- Beaudouin, J., F. Mora-Bermudez, T. Klee, N. Daigle, and J. Ellenberg. 2006. Dissecting the contribution of diffusion and interactions to the mobility of nuclear proteins. *Biophys J.* 90:1878-94.
- Bednar, J., R.A. Horowitz, S.A. Grigoryev, L.M. Carruthers, J.C. Hansen, A.J. Koster, and C.L. Woodcock. 1998. Nucleosomes, linker DNA, and linker histone form a unique structural motif that directs the higher-order folding and compaction of chromatin. *Proc Natl Acad Sci U S A.* 95:14173-8.
- Belmont, A. 2003. Dynamics of chromatin, proteins, and bodies within the cell nucleus. *Curr Opin Cell Biol.* 15:304-10.
- Belmont, A.S. 2006. Mitotic chromosome structure and condensation. *Curr Opin Cell Biol.* 18:632-8.
- Bird, A. 2007. Perceptions of epigenetics. *Nature.* 447:396-8.
- Bird, A.P. 1986. CpG-rich islands and the function of DNA methylation. *Nature.* 321:209-213.
- Blake, W.J., K.A. M, C.R. Cantor, and J.J. Collins. 2003. Noise in eukaryotic gene expression. *Nature.* 422:633-7.
- Boyes, J., and A. Bird. 1991. DNA methylation inhibits transcription indirectly via a methyl-CpG binding protein. *Cell.* 64:1123-34.
- Boyes, J., and A. Bird. 1992. Repression of genes by DNA methylation depends on CpG density and promoter strength: evidence for involvement of a methyl-CpG binding protein. *Embo J.* 11:327-33.
- Braga, J., J.M. Desterro, and M. Carmo-Fonseca. 2004. Intracellular macromolecular mobility measured by fluorescence recovery after photobleaching with confocal laser scanning microscopes. *Mol Biol Cell.* 15:4749-60.
- Brero, A., H.P. Easwaran, D. Nowak, I. Grunewald, T. Cremer, H. Leonhardt, and M.C. Cardoso. 2005. Methyl CpG-binding proteins induce large-scale chromatin reorganization during terminal differentiation. *J Cell Biol.* 169:733-43.

- Brown, D.D., and J.B. Gurdon. 1964. Absence of Ribosomal Rna Synthesis in the Anucleolate Mutant of *Xenopus Laevis*. *Proc Natl Acad Sci U S A*. 51:139-46.
- Brown, K.E., S.S. Guest, S.T. Smale, K. Hahm, M. Merckenschlager, and A.G. Fisher. 1997. Association of transcriptionally silent genes with Ikaros complexes at centromeric heterochromatin. *Cell*. 91:845-54.
- Bullock, K.E., S.T. Gammon, S. Violini, A.M. Prantner, V.M. Villalobos, V. Sharma, and D. Piwnicka-Worms. 2006. Permeation peptide conjugates for in vivo molecular imaging applications. *Mol Imaging*. 5:1-15.
- Cardoso, M.C., C. Joseph, H.P. Rahn, R. Reusch, B. Nadal-Ginard, and H. Leonhardt. 1997. Mapping and use of a sequence that targets DNA ligase I to sites of DNA replication in vivo. *J Cell Biol*. 139:579-87.
- Cardoso, M.C., and H. Leonhardt. 1998. Protein targeting to subnuclear higher order structures: a new level of regulation and coordination of nuclear processes. *J Cell Biochem*. 70:222-30.
- Carmo-Fonseca, M., L. Mendes-Soares, and I. Campos. 2000. To be or not to be in the nucleolus. *Nat Cell Biol*. 2:E107-12.
- Carrero, G., D. McDonald, E. Crawford, G. de Vries, and M.J. Hendzel. 2003. Using FRAP and mathematical modeling to determine the in vivo kinetics of nuclear proteins. *Methods*. 29:14-28.
- Catez, F., H. Yang, K.J. Tracey, R. Reeves, T. Misteli, and M. Bustin. 2004. Network of dynamic interactions between histone H1 and high-mobility-group proteins in chromatin. *Mol Cell Biol*. 24:4321-8.
- Chen, D., M. Dundr, C. Wang, A. Leung, A. Lamond, T. Misteli, and S. Huang. 2005. Condensed mitotic chromatin is accessible to transcription factors and chromatin structural proteins. *J Cell Biol*. 168:41-54.
- Cheutin, T., A.J. McNairn, T. Jenuwein, D.M. Gilbert, P.B. Singh, and T. Misteli. 2003. Maintenance of stable heterochromatin domains by dynamic HP1 binding. *Science*. 299:721-5.
- Cheutin, T., M.F. O'Donohue, A. Beorchia, M. Vandelaer, H. Kaplan, B. Defever, D. Ploton, and M. Thiry. 2002. Three-dimensional organization of active rRNA genes within the nucleolus. *J Cell Sci*. 115:3297-307.
- Chevalier, S., and J.J. Blow. 1996. Cell cycle control of replication initiation in eukaryotes. *Curr Opin Cell Biol*. 8:815-821.
- Chow, C.M., A. Georgiou, H. Szutorisz, A. Maia e Silva, A. Pombo, I. Barahona, E. Dargelos, C. Canzonetta, and N. Dillon. 2005. Variant histone H3.3 marks promoters of transcriptionally active genes during mammalian cell division. *EMBO Rep*. 6:354-60.
- Collas, P., K. Le Guellec, and K. Tasken. 1999. The A-kinase-anchoring protein AKAP95 is a multivalent protein with a key role in chromatin condensation at mitosis. *J Cell Biol*. 147:1167-80.
- Contreras, A., T.K. Hale, D.L. Stenoien, J.M. Rosen, M.A. Mancini, and R.E. Herrera. 2003. The dynamic mobility of histone H1 is regulated by cyclin/CDK phosphorylation. *Mol Cell Biol*. 23:8626-36.
- Corona, D.F., G. Langst, C.R. Clapier, E.J. Bonte, S. Ferrari, J.W. Tamkun, and P.B. Becker. 1999. ISWI is an ATP-dependent nucleosome remodeling factor. *Mol Cell*. 3:239-45.
- Cremer, T., M. Cremer, S. Dietzel, S. Muller, I. Solovei, and S. Fakan. 2006. Chromosome territories--a functional nuclear landscape. *Curr Opin Cell Biol*. 18:307-16.
- Cremer, T., and C. Cremer. 2001. Chromosome territories, nuclear architecture and gene regulation in mammalian cells. *Nat Rev Genet*. 2:292-301.
- Cremer, T., G. Kreth, H. Koester, R.H. Fink, R. Heintzmann, M. Cremer, I. Solovei, D. Zink, and C. Cremer. 2000. Chromosome territories, interchromatin domain compartment, and nuclear matrix: an integrated view of the functional nuclear architecture. *Crit Rev Eukaryot Gene Expr*. 10:179-212.
- Cronshaw, J.M., A.N. Krutchinsky, W. Zhang, B.T. Chait, and M.J. Matunis. 2002. Proteomic analysis of the mammalian nuclear pore complex. *J Cell Biol*. 158:915-27.

- Crosio, C., G.M. Fimia, R. Loury, M. Kimura, Y. Okano, H. Zhou, S. Sen, C.D. Allis, and P. Sassone-Corsi. 2002. Mitotic phosphorylation of histone H3: spatio-temporal regulation by mammalian Aurora kinases. *Mol Cell Biol.* 22:874-85.
- Daban, J.R. 2003. High concentration of DNA in condensed chromatin. *Biochem Cell Biol.* 81:91-9.
- Dang, C.V., and W.M. Lee. 1989. Nuclear and nucleolar targeting sequences of c-erbA, c-myb, N-myc, p53, HSP70, and HIV tat proteins. *J Biol Chem.* 264:18019-23.
- Davis, L.I. 1995. The nuclear pore complex. *Annu Rev Biochem.* 64:865-96.
- Davis, S.K., and C.J. Bardeen. 2003. Cross-linking of histone proteins to DNA by UV illumination of chromatin stained with Hoechst 33342. *Photochem Photobiol.* 77:675-9.
- Dehghani, H., G. Dellaire, and D.P. Bazett-Jones. 2005. Organization of chromatin in the interphase mammalian cell. *Micron.* 36:95-108.
- Dellaire, G., R. Nisman, and D.P. Bazett-Jones. 2004. Correlative light and electron spectroscopic imaging of chromatin in situ. *Methods Enzymol.* 375:456-78.
- Dellino, G.I., Y.B. Schwartz, G. Farkas, D. McCabe, S.C. Elgin, and V. Pirrotta. 2004. Polycomb silencing blocks transcription initiation. *Mol Cell.* 13:887-93.
- Derenzini, M., G. Pasquinelli, M.F. O'Donohue, D. Ploton, and M. Thiry. 2006. Structural and functional organization of ribosomal genes within the mammalian cell nucleolus. *J Histochem Cytochem.* 54:131-45.
- Dillon, N. 2004. Heterochromatin structure and function. *Biol Cell.* 96:631-7.
- Dimitri, P., N. Corradini, F. Rossi, and F. Verni. 2005. The paradox of functional heterochromatin. *Bioessays.* 27:29-41.
- Dirks, R.W., and S. Snaar. 1999. Dynamics of RNA polymerase II localization during the cell cycle. *Histochem Cell Biol.* 111:405-10.
- Dorigo, B., T. Schalch, A. Kulangara, S. Duda, R.R. Schroeder, and T.J. Richmond. 2004. Nucleosome arrays reveal the two-start organization of the chromatin fiber. *Science.* 306:1571-3.
- Duchardt, F., M. Fotin-Mleczek, H. Schwarz, R. Fischer, and R. Brock. 2007. A comprehensive model for the cellular uptake of cationic cell-penetrating peptides. *Traffic.* 8:848-66.
- Dundr, M., and T. Misteli. 2001. Functional architecture in the cell nucleus. *Biochem J.* 356:297-310.
- Durand, R.E., and P.L. Olive. 1982. Cytotoxicity, Mutagenicity and DNA damage by Hoechst 33342. *J Histochem Cytochem.* 30:111-6.
- Easwaran, H.P., L. Schermelleh, H. Leonhardt, and M.C. Cardoso. 2004. Replication-independent chromatin loading of Dnmt1 during G2 and M phases. *EMBO Rep.* 5:1181-6.
- Easwaran, H.P., H. Leonhardt, and M.C. Cardoso. 2005. Cell cycle markers for live cell analyses. *Cell Cycle.* 4:453-5.
- Ellenberg, J., E.D. Siggia, J.E. Moreira, C.L. Smith, J.F. Presley, H.J. Worman, and J. Lippincott-Schwartz. 1997. Nuclear membrane dynamics and reassembly in living cells: targeting of an inner nuclear membrane protein in interphase and mitosis. *J Cell Biol.* 138:1193-206.
- Eskiw, C.H., G. Dellaire, J.S. Mymryk, and D.P. Bazett-Jones. 2003. Size, position and dynamic behavior of PML nuclear bodies following cell stress as a paradigm for supramolecular trafficking and assembly. *J Cell Sci.* 116:4455-66.
- Fawell, S., J. Seery, Y. Daikh, C. Moore, L.L. Chen, B. Pepinsky, and J. Barsoum. 1994. Tat-mediated delivery of heterologous proteins into cells. *Proc Natl Acad Sci U S A.* 91:664-8.
- Felsenfeld, G., and M. Groudine. 2003. Controlling the double helix. *Nature.* 421:448-53.
- Fischle, W., B.S. Tseng, H.L. Dormann, B.M. Ueberheide, B.A. Garcia, J. Shabanowitz, D.F. Hunt, H. Funabiki, and C.D. Allis. 2005. Regulation of HP1-chromatin binding by histone H3 methylation and phosphorylation. *Nature.*
- Francis, N.J., R.E. Kingston, and C.L. Woodcock. 2004. Chromatin compaction by a polycomb group protein complex. *Science.* 306:1574-7.

- Franke, W. 1988. Matthias Jacob Schleiden and the definition of the cell nucleus. *Eur J Cell Biol.* 47:145–156.
- Fretz, M.M., N.A. Penning, S. Al-Taei, S. Futaki, T. Takeuchi, I. Nakase, G. Storm, and A.T. Jones. 2007. Temperature-, concentration- and cholesterol-dependent translocation of L- and D-octa-arginine across the plasma and nuclear membrane of CD34+ leukaemia cells. *Biochem J.* 403:335–42.
- Fujita, M., Y. Ishimi, H. Nakamura, T. Kiyono, and T. Tsurumi. 2002. Nuclear organization of DNA replication initiation proteins in mammalian cells. *J Biol Chem.* 277:10354–61.
- Fujita, N., S. Watanabe, T. Ichimura, S. Tsuruzoe, Y. Shinkai, M. Tachibana, T. Chiba, and M. Nakao. 2003. Methyl-CpG binding domain 1 (MBD1) interacts with the Suv39h1-HP1 heterochromatic complex for DNA methylation-based transcriptional repression. *J Biol Chem.* 278:24132–8.
- Fuks, F., W.A. Burgers, A. Brehm, L. Hughes-Davies, and T. Kouzarides. 2000. DNA methyltransferase Dnmt1 associates with histone deacetylase activity. *Nat Genet.* 24:88–91.
- Gallinari, P., S. Di Marco, P. Jones, M. Pallaoro, and C. Steinkuhler. 2007. HDACs, histone deacetylation and gene transcription: from molecular biology to cancer therapeutics. *Cell Res.* 17:195–211.
- Garagna, S., M. Zuccotti, E. Capanna, and C.A. Redi. 2002. High-resolution organization of mouse telomeric and pericentromeric DNA. *Cytogenet Genome Res.* 96:125–9.
- Georgel, P.T., R.A. Horowitz-Scherer, N. Adkins, C.L. Woodcock, P.A. Wade, and J.C. Hansen. 2003. Chromatin compaction by human MeCP2. Assembly of novel secondary chromatin structures in the absence of DNA methylation. *J Biol Chem.* 278:32181–8.
- Gilbert, N., S. Gilchrist, and W.A. Bickmore. 2005. Chromatin organization in the mammalian nucleus. *Int Rev Cytol.* 242:283–336.
- Gilbert, S.L., J.R. Pehrson, and P.A. Sharp. 2000. XIST RNA associates with specific regions of the inactive X chromatin. *J Biol Chem.* 275:36491–4.
- Görisch, S.M., K. Richter, M.O. Scheuermann, H. Herrmann, and P. Lichter. 2003. Diffusion-limited compartmentalization of mammalian cell nuclei assessed by microinjected macromolecules. *Exp Cell Res.* 289:282–94.
- Görisch, S.M., M. Wachsmuth, C. Itrich, C.P. Bacher, K. Rippe, and P. Lichter. 2004. Nuclear body movement is determined by chromatin accessibility and dynamics. *Proc Natl Acad Sci U S A.* 101:13221–6.
- Görisch, S.M., M. Wachsmuth, K.F. Toth, P. Lichter, and K. Rippe. 2005. Histone acetylation increases chromatin accessibility. *J Cell Sci.*
- Gottesfeld, J.M., and D.J. Forbes. 1997. Mitotic repression of the transcriptional machinery. *Trends Biochem Sci.* 22:197–202.
- Goulian, M., and S.M. Simon. 2000. Tracking single proteins within cells. *Biophys J.* 79:2188–98.
- Gregory, R.I., T.E. Randall, C.A. Johnson, S. Khosla, I. Hatada, L.P. O'Neill, B.M. Turner, and R. Feil. 2001. DNA methylation is linked to deacetylation of histone H3, but not H4, on the imprinted genes Snrpn and U2af1-rs1. *Mol Cell Biol.* 21:5426–36.
- Grunwald, D., R.M. Martin, V. Buschmann, D.P. Bazett-Jones, H. Leonhardt, U. Kubitscheck, and M.C. Cardoso. 2008. Probing intranuclear environments at the single-molecule level. *Biophys J.* 94:2847–58.
- Grunwald, D., B. Spottke, V. Buschmann, and U. Kubitscheck. 2006. Intranuclear binding kinetics and mobility of single native U1 snRNP particles in living cells. *Mol Biol Cell.* 17:5017–27.
- Hallbrink, M., J. Oehlke, G. Papsdorf, and M. Bienert. 2004. Uptake of cell-penetrating peptides is dependent on peptide-to-cell ratio rather than on peptide concentration. *Biochim Biophys Acta.* 1667:222–8.
- Hammermann, M., K. Toth, C. Rodemer, W. Waldeck, R.P. May, and J. Langowski. 2000. Salt-dependent compaction of di- and trinucleosomes studied by small-angle neutron scattering. *Biophys J.* 79:584–94.

- Hancock, R. 2000. A new look at the nuclear matrix. *Chromosoma*. 109:219-25.
- Handwerger, K.E., J.A. Cordero, and J.G. Gall. 2004. Cajal Bodies, Nucleoli, and Speckles in the *Xenopus* Oocyte Nucleus Have a Low Density, Sponge-like Structure. *Mol Biol Cell*. 16:202-211.
- Handwerger, K.E., and J.G. Gall. 2006. Subnuclear organelles: new insights into form and function. *Trends Cell Biol*. 16:19-26.
- Hatanaka, M. 1990. Discovery of the nucleolar targeting signal. *Bioessays*. 12:143-8.
- Heitz, E. 1928. Das Heterochromatin der Moose. I. *Jahrbücher für wissenschaftliche Botanik*. 69:762-818.
- Heitz, E. 1929. Heterochromatin, Chromocentren, Chromomeren. *Ber. der Deutschen Bot. Gesellsch.* XLVII:274-284.
- Hendrich, B., and A. Bird. 1998. Identification and Characterization of a Family of Mammalian Methyl-CpG Binding Proteins. *Mol. Cell. Biol.* 18:6538-6547.
- Heng, H.H., S. Goetze, C.J. Ye, G. Liu, J.B. Stevens, S.W. Bremer, S.M. Wykes, J. Bode, and S.A. Krawetz. 2004. Chromatin loops are selectively anchored using scaffold/matrix-attachment regions. *J Cell Sci*. 117:999-1008.
- Henikoff, S. 2008. Nucleosome destabilization in the epigenetic regulation of gene expression. *Nat Rev Genet*. 9:15-26.
- Henikoff, S., and K. Ahmad. 2005. Assembly of variant histones into chromatin. *Annu Rev Cell Dev Biol*. 21:133-53.
- Hernandez-Verdun, D. 2006. Nucleolus: from structure to dynamics. *Histochem Cell Biol*. 125:127-37.
- Higashi, T., S. Matsunaga, K. Isobe, A. Morimoto, T. Shimada, S. Kataoka, W. Watanabe, S. Uchiyama, K. Itoh, and K. Fukui. 2007. Histone H2A mobility is regulated by its tails and acetylation of core histone tails. *Biochem Biophys Res Commun*. 357:627-32.
- Hirano, T., R. Kobayashi, and M. Hirano. 1997. Condensins, chromosome condensation protein complexes containing XCAP-C, XCAP-E and a *Xenopus* homolog of the *Drosophila* Barren protein. *Cell*. 89:511-21.
- Hirota, T., J.J. Lipp, B.H. Toh, and J.M. Peters. 2005. Histone H3 serine 10 phosphorylation by Aurora B causes HP1 dissociation from heterochromatin. *Nature*.
- Huang, D.Y., and M.B. Prystowsky. 1996. Identification of an essential cis-element near the transcription start site for transcriptional activation of the proliferating cell nuclear antigen gene. *J Biol Chem*. 271:1218-1225.
- Iborra, F.J., A. Pombo, D.A. Jackson, and P.R. Cook. 1996. Active RNA polymerases are localized within discrete transcription "factories" in human nuclei. *J Cell Sci*. 109:1427-1436.
- Isogai, Y., and R. Tjian. 2003. Targeting genes and transcription factors to segregated nuclear compartments. *Curr Opin Cell Biol*. 15:296-303.
- Jacobs, G.A., J.A. Smith, R.A. Watt, and J.M. Barry. 1976. Ion binding and chromatin condensation. *Biochim Biophys Acta*. 442:109-15.
- Jiang, T., E.S. Olson, Q.T. Nguyen, M. Roy, P.A. Jennings, and R.Y. Tsien. 2004. Tumor imaging by means of proteolytic activation of cell-penetrating peptides. *Proc Natl Acad Sci U S A*. 101:17867-72.
- Johnson, T.C., and J.J. Holland. 1965. Ribonucleic acid and protein synthesis in mitotic HeLa cells. *J Cell Biol*. 27:565-74.
- Joseph, A., A.R. Mitchell, and O.J. Miller. 1989. The organization of the mouse satellite DNA at centromeres. *Exp Cell Res*. 183:494-500.
- Kanda, T., K.F. Sullivan, and G.M. Wahl. 1998. Histone-GFP fusion protein enables sensitive analysis of chromosome dynamics in living mammalian cells. *Curr Biol*. 8:377-385.
- Karymov, M.A., M. Tomschik, S.H. Leuba, P. Caiafa, and J. Zlatanova. 2001. DNA methylation-dependent chromatin fiber compaction in vivo and in vitro: requirement for linker histone. *Faseb J*. 15:2631-41.
- Kimura, H., and P.R. Cook. 2001. Kinetics of core histones in living human cells: little exchange of H3 and H4 and some rapid exchange of H2B. *J Cell Biol*. 153:1341-53.

- Kimura, K., V.V. Rybenkov, N.J. Crisona, T. Hirano, and N.R. Cozzarelli. 1999. 13S condensin actively reconfigures DNA by introducing global positive writhe: implications for chromosome condensation. *Cell*. 98:239-48.
- Kireeva, N., M. Lakonishok, I. Kireev, T. Hirano, and A.S. Belmont. 2004. Visualization of early chromosome condensation: a hierarchical folding, axial glue model of chromosome structure. *J Cell Biol*. 166:775-85.
- Klose, R.J., K. Yamane, Y. Bae, D. Zhang, H. Erdjument-Bromage, P. Tempst, J. Wong, and Y. Zhang. 2006. The transcriptional repressor JHDM3A demethylates trimethyl histone H3 lysine 9 and lysine 36. *Nature*. 442:312-6.
- Kourmouli, N., P. Jeppesen, S. Mahadevhaiah, P. Burgoyne, R. Wu, D.M. Gilbert, S. Bongiorno, G. Pranter, L. Fanti, S. Pimpinelli, W. Shi, R. Fundele, and P.B. Singh. 2004. Heterochromatin and tri-methylated lysine 20 of histone H4 in animals. *J Cell Sci*. 117:2491-501.
- Kourmouli, N., Y.M. Sun, S. van der Sar, P.B. Singh, and J.P. Brown. 2005. Epigenetic regulation of mammalian pericentric heterochromatin in vivo by HP1. *Biochem Biophys Res Commun*. 337:901-7.
- Kouzarides, T. 2007. Chromatin modifications and their function. *Cell*. 128:693-705.
- Kubitscheck, U., O. Kückmann, T. Kues, and R. Peters. 2000. Imaging and tracking of single GFP molecules in solution. *Biophys J*. 78:2170-9.
- Lam, Y.W., L. Trinkle-Mulcahy, and A.I. Lamond. 2005. The nucleolus. *J Cell Sci*. 118:1335-7.
- Lamond, A.I., and D.L. Spector. 2003. Nuclear speckles: a model for nuclear organelles. *Nat Rev Mol Cell Biol*. 4:605-12.
- Lang, I., M. Scholz, and R. Peters. 1986. Molecular mobility and nucleocytoplasmic flux in hepatoma cells. *J Cell Biol*. 102:1183-1190.
- Lehnertz, B., Y. Ueda, A.A. Derijck, U. Braunschweig, L. Perez-Burgos, S. Kubicek, T. Chen, E. Li, T. Jenuwein, and A.H. Peters. 2003. Suv39h-mediated histone H3 lysine 9 methylation directs DNA methylation to major satellite repeats at pericentric heterochromatin. *Curr Biol*. 13:1192-200.
- Leonhardt, H., A.W. Page, H.U. Weier, and T.H. Bestor. 1992. A targeting sequence directs DNA methyltransferase to sites of DNA replication in mammalian nuclei. *Cell*. 71:865-73.
- Leonhardt, H., H.P. Rahn, P. Weinzierl, A. Spörl, T. Cremer, D. Zink, and M.C. Cardoso. 2000. Dynamics of DNA replication factories in living cells. *J Cell Biol*. 149:271-80.
- Leung, A.K., and A.I. Lamond. 2003. The dynamics of the nucleolus. *Crit Rev Eukaryot Gene Expr*. 13:39-54.
- Levine, A., A. Yeivin, E. Ben-Asher, Y. Aloni, and A. Razin. 1993. Histone H1-mediated inhibition of transcription initiation of methylated templates in vitro. *J Biol Chem*. 268:21754-21759.
- Lewis, J., and A. Bird. 1991. DNA methylation and chromatin structure. *FEBS Lett*. 285:155-9.
- Lewis, J.D., R.R. Meehan, W.J. Henzel, I. Maurer-Fogy, P. Jeppesen, F. Klein, and A. Bird. 1992. Purification, sequence, and cellular localization of a novel chromosomal protein that binds to methylated DNA. *Cell*. 69:905-914.
- Lopez-Larraz, D.M., J. Padron, N.E. Ronci, and L.A. Vidal Rioja. 2006. Chromatin condensation and differential sensitivity of mammalian and insect cells to DNA strand breaks induced by bleomycin. *Mutat Res*. 600:93-101.
- Lu, Z., C. Zhang, and Z. Zhai. 2005. Nucleoplasmin regulates chromatin condensation during apoptosis. *Proc Natl Acad Sci U S A*. 102:2778-83.
- Luger, K., A.W. Mader, R.K. Richmond, D.F. Sargent, and T.J. Richmond. 1997. Crystal structure of the nucleosome core particle at 2.8 Å resolution. *Nature*. 389:251-60.
- Lyon, C.E., K. Bohmann, J. Sleeman, and A.I. Lamond. 1997. Inhibition of protein dephosphorylation results in the accumulation of splicing snRNPs and coiled bodies within the nucleolus. *Exp Cell Res*. 230:84-93.

- Maddox, P.S., N. Portier, A. Desai, and K. Oegema. 2006. Molecular analysis of mitotic chromosome condensation using a quantitative time-resolved fluorescence microscopy assay. *Proc Natl Acad Sci U S A*. 103:15097-102.
- Mais, C., and U. Scheer. 2001. Molecular architecture of the amplified nucleoli of *Xenopus* oocytes. *J Cell Sci*. 114:709-18.
- Maison, C., and G. Almouzni. 2004. HP1 and the dynamics of heterochromatin maintenance. *Nat Rev Mol Cell Biol*. 5:296-305.
- Maison, C., D. Bailly, A.H. Peters, J.P. Quivy, D. Roche, A. Taddei, M. Lachner, T. Jenuwein, and G. Almouzni. 2002. Higher-order structure in pericentric heterochromatin involves a distinct pattern of histone modification and an RNA component. *Nat Genet*. 30:329-34.
- Maldonado-Codina, G., and D.M. Glover. 1992. Cyclins A and B associate with chromatin and the polar regions of spindles, respectively, and do not undergo complete degradation at anaphase in syncytial *Drosophila* embryos. *J Cell Biol*. 116:967-976.
- Marshall, W.F., A. Straight, J.F. Marko, J. Swedlow, A. Dernburg, A. Belmont, A.W. Murray, D.A. Agard, and J.W. Sedat. 1997. Interphase chromosomes undergo constrained diffusional motion in living cells. *Curr Biol*. 7:930-9.
- Martin, R.M., H. Leonhardt, and M.C. Cardoso. 2005. DNA labeling in living cells. *Cytometry A*. 67:45-52.
- Martin, R.M., G. Tunnemann, H. Leonhardt, and M.C. Cardoso. 2007a. Nucleolar marker for living cells. *Histochem Cell Biol*. 127:243-51.
- Martin, R.M., S.M. Gorisch, H. Leonhardt, and M.C. Cardoso. 2007b. An Unexpected Link Between Energy Metabolism, Calcium, Chromatin Condensation and Cell Cycle. *Cell Cycle*. 6.
- Martin, R.M., and M.C. Cardoso. 2008. Chromatin condensation modulates access and binding of nuclear proteins. *submitted at JMB*.
- Martinez-Balbas, M.A., A. Dey, S.K. Rabindran, K. Ozato, and C. Wu. 1995. Displacement of sequence-specific transcription factors from mitotic chromatin. *Cell*. 83:29-38.
- Marvin, K.W., P. Yau, and E.M. Bradbury. 1990. Isolation and characterization of acetylated histones H3 and H4 and their assembly into nucleosomes. *J Biol Chem*. 265:19839-47.
- Matarazzo, M.R., S. Boyle, M. D'Esposito, and W.A. Bickmore. 2007. Chromosome territory reorganization in a human disease with altered DNA methylation. *Proc Natl Acad Sci U S A*. 104:16546-51.
- Mayer, R., A. Brero, J. von Hase, T. Schroeder, T. Cremer, and S. Dietzel. 2005. Common themes and cell type specific variations of higher order chromatin arrangements in the mouse. *BMC Cell Biol*. 6:44.
- McCusker, C.T., Y. Wang, J. Shan, M.W. Kinyanjui, A. Villeneuve, H. Michael, and E.D. Fixman. 2007. Inhibition of experimental allergic airways disease by local application of a cell-penetrating dominant-negative STAT-6 peptide. *J Immunol*. 179:2556-64.
- McKittrick, E., P.R. Gafken, K. Ahmad, and S. Henikoff. 2004. Histone H3.3 is enriched in covalent modifications associated with active chromatin. *Proc Natl Acad Sci U S A*. 101:1525-30.
- Mekhail, K., M. Khacho, A. Carrigan, R.R. Hache, L. Gunaratnam, and S. Lee. 2005. Regulation of ubiquitin ligase dynamics by the nucleolus. *J Cell Biol*. 170:733-44.
- Mi, Z., J. Mai, X. Lu, and P.D. Robbins. 2000. Characterization of a class of cationic peptides able to facilitate efficient protein transduction in vitro and in vivo. *Mol Ther*. 2:339-47.
- Miller, O.J., W. Schnedl, J. Allen, and B.F. Erlanger. 1974. 5-Methylcytosine localised in mammalian constitutive heterochromatin. *Nature*. 251:636-7.
- Misteli, T. 2001. Protein dynamics: implications for nuclear architecture and gene expression. *Science*. 291:843-7.
- Mitchell, A.R. 1996. The mammalian centromere: its molecular architecture. *Mutat Res*. 372:153-62.

- Mito, Y., J.G. Henikoff, and S. Henikoff. 2007. Histone replacement marks the boundaries of cis-regulatory domains. *Science*. 315:1408-11.
- Mortusewicz, O., L. Schermelleh, J. Walter, M.C. Cardoso, and H. Leonhardt. 2005. Recruitment of DNA methyltransferase I to DNA repair sites. *Proc Natl Acad Sci U S A*. 102:8905-9.
- Mozziconacci, J., C. Lavelle, M. Barbi, A. Lesne, and J.M. Victor. 2006. A physical model for the condensation and decondensation of eukaryotic chromosomes. *FEBS Lett*. 580:368-72.
- Muchardt, C., M. Guilleme, J.-S. Seeler, D. Trouche, A. Dejean, and M. Yaniv. 2002. Coordinated methyl and RNA binding is required for heterochromatin localization of mammalian HP1{alpha}. *EMBO Reports*:kvf194.
- Muller, W.G., D. Walker, G.L. Hager, and J.G. McNally. 2001. Large-scale chromatin decondensation and recondensation regulated by transcription from a natural promoter. *J Cell Biol*. 154:33-48.
- Nagahara, H., A.M. Vocero-Akbani, E.L. Snyder, A. Ho, D.G. Latham, N.A. Lissy, M. Becker-Hapak, S.A. Ezhevsky, and S.F. Dowdy. 1998. Transduction of full-length TAT fusion proteins into mammalian cells: TAT-p27Kip1 induces cell migration. *Nat Med*. 4:1449-52.
- Nan, X., F.J. Campoy, and A. Bird. 1997. MeCP2 is a transcriptional repressor with abundant binding sites in genomic chromatin. *Cell*. 88:471-81.
- Nan, X., H.H. Ng, C.A. Johnson, C.D. Laherty, B.M. Turner, R.N. Eisenman, and A. Bird. 1998. Transcriptional repression by the methyl-CpG-binding protein MeCP2 involves a histone deacetylase complex. *Nature*. 393:386-9.
- Nan, X., P. Tate, E. Li, and A. Bird. 1996. DNA methylation specifies chromosomal localization of MeCP2. *Mol Cell Biol*. 16:414-21.
- Ng, H.H., Y. Zhang, B. Hendrich, C.A. Johnson, B.M. Turner, H. Erdjument-Bromage, P. Tempst, D. Reinberg, and A. Bird. 1999. MBD2 is a transcriptional repressor belonging to the MeCP1 histone deacetylase complex. *Nat Genet*. 23:58-61.
- Nguyen, C.T., F.A. Gonzales, and P.A. Jones. 2001. Altered chromatin structure associated with methylation-induced gene silencing in cancer cells: correlation of accessibility, methylation, MeCP2 binding and acetylation. *Nucleic Acids Res*. 29:4598-606.
- Nielsen, A.L., M. Oulad-Abdelghani, J.A. Ortiz, E. Remboutsika, P. Chambon, and R. Losson. 2001. Heterochromatin formation in mammalian cells: interaction between histones and HP1 proteins. *Mol Cell*. 7:729-39.
- Nielsen, P.R., D. Nietlispach, H.R. Mott, J. Callaghan, A. Bannister, T. Kouzarides, A.G. Murzin, N.V. Murzina, and E.D. Laue. 2002. Structure of the HP1 chromodomain bound to histone H3 methylated at lysine 9. *Nature*. 416:103-7.
- Nolden, L., F. Edenhofer, S. Haupt, P. Koch, F.T. Wunderlich, H. Siemen, and O. Brustle. 2006. Site-specific recombination in human embryonic stem cells induced by cell-permeant Cre recombinase. *Nat Methods*. 3:461-7.
- Ogg, S.C., and A.I. Lamond. 2002. Cajal bodies and coilin--moving towards function. *J Cell Biol*. 159:17-21.
- Ohtani-Fujita, N., T. Fujita, A. Aoike, N.E. Osifchin, P.D. Robbins, and T. Sakai. 1993. CpG methylation inactivates the promoter activity of the human retinoblastoma tumor-suppressor gene. *Oncogene*. 8:1063-1067.
- Okuwaki, M., K. Kato, H. Shimahara, S. Tate, and K. Nagata. 2005. Assembly and disassembly of nucleosome core particles containing histone variants by human nucleosome assembly protein I. *Mol Cell Biol*. 25:10639-51.
- Olson, M.O., and M. Dundr. 2005. The moving parts of the nucleolus. *Histochem Cell Biol*. 123:203-16.
- Paschal, B.M. 2002. Translocation through the nuclear pore complex. *Trends Biochem Sci*. 27:593-6.
- Peaston, A.E., B.B. Knowles, and K.W. Hutchison. 2007. Genome plasticity in the mouse oocyte and early embryo. *Biochem Soc Trans*. 35:618-22.
- Pederson, T. 2000. Half a century of "the nuclear matrix". *Mol Biol Cell*. 11:799-805.
- Pederson, T. 2001. Protein mobility within the nucleus--what are the right moves? *Cell*. 104:635-8.

- Perry, R.P. 1962. The Cellular Sites of Synthesis of Ribosomal and 4s Rna. *Proc Natl Acad Sci U S A*. 48:2179-86.
- Peters, A.H., S. Kubicek, K. Mechtler, R.J. O'Sullivan, A.A. Derijck, L. Perez-Burgos, A. Kohlmaier, S. Opravil, M. Tachibana, Y. Shinkai, J.H. Martens, and T. Jenuwein. 2003. Partitioning and plasticity of repressive histone methylation states in mammalian chromatin. *Mol Cell*. 12:1577-89.
- Peters, A.H., D. O'Carroll, H. Scherthan, K. Mechtler, S. Sauer, C. Schofer, K. Weipoltshammer, M. Pagani, M. Lachner, A. Kohlmaier, S. Opravil, M. Doyle, M. Sibilia, and T. Jenuwein. 2001. Loss of the Suv39h histone methyltransferases impairs mammalian heterochromatin and genome stability. *Cell*. 107:323-37.
- Phair, R.D., S.A. Gorski, and T. Misteli. 2004. Measurement of dynamic protein binding to chromatin in vivo, using photobleaching microscopy. *Methods Enzymol*. 375:393-414.
- Phair, R.D., and T. Misteli. 2000. High mobility of proteins in the mammalian cell nucleus. *Nature*. 404:604-9.
- Pikaart, M.J., F. Recillas-Targa, and G. Felsenfeld. 1998. Loss of transcriptional activity of a transgene is accompanied by DNA methylation and histone deacetylation and is prevented by insulators. *Genes Dev*. 12:2852-62.
- Poglitsch, C.L., G.D. Meredith, A.L. Gnatt, G.J. Jensen, W.H. Chang, J. Fu, and R.D. Kornberg. 1999. Electron crystal structure of an RNA polymerase II transcription elongation complex. *Cell*. 98:791-8.
- Politz, J.C., I. Polena, I. Trask, D.P. Bazett-Jones, and T. Pederson. 2005. A nonribosomal landscape in the nucleolus revealed by the stem cell protein nucleostemin. *Mol Biol Cell*. 16:3401-10.
- Politz, J.C., R.A. Tuft, and T. Pederson. 2003. Diffusion-based transport of nascent ribosomes in the nucleus. *Mol Biol Cell*. 14:4805-12.
- Politz, J.C., R.A. Tuft, T. Pederson, and R.H. Singer. 1999. Movement of nuclear poly(A) RNA throughout the interchromatin space in living cells. *Curr Biol*. 9:285-91.
- Politz, J.C., R.A. Tuft, K.V. Prasanth, N. Baudendistel, K.E. Fogarty, L.M. Lifshitz, J. Langowski, D.L. Spector, and T. Pederson. 2006. Rapid, diffusional shuttling of poly(A) RNA between nuclear speckles and the nucleoplasm. *Mol Biol Cell*. 17:1239-49.
- Poot, R.A., L. Bozhenok, D.L. van den Berg, S. Steffensen, F. Ferreira, M. Grimaldi, N. Gilbert, J. Ferreira, and P.D. Varga-Weisz. 2004. The Williams syndrome transcription factor interacts with PCNA to target chromatin remodelling by ISWI to replication foci. *Nat Cell Biol*.
- Prymakowska-Bosak, M., T. Misteli, J.E. Herrera, H. Shirakawa, Y. Birger, S. Garfield, and M. Bustin. 2001. Mitotic phosphorylation prevents the binding of HMGN proteins to chromatin. *Mol Cell Biol*. 21:5169-78.
- Quina, A.S., M. Buschbeck, and L. Di Croce. 2006. Chromatin structure and epigenetics. *Biochem Pharmacol*. 72:1563-9.
- Raska, I., K. Koberna, J. Malinsky, H. Fidlerova, and M. Masata. 2004. The nucleolus and transcription of ribosomal genes. *Biol Cell*. 96:579-594.
- Regha, K., M.A. Sloane, R. Huang, F.M. Pauler, K.E. Warczok, B. Melikant, M. Radolf, J.H. Martens, G. Schotta, T. Jenuwein, and D.P. Barlow. 2007. Active and repressive chromatin are interspersed without spreading in an imprinted gene cluster in the mammalian genome. *Mol Cell*. 27:353-66.
- Reik, W., W. Dean, and J. Walter. 2001. Epigenetic reprogramming in mammalian development. *Science*. 293:1089-93.
- Rice, J.C., and B.W. Futscher. 2000. Transcriptional repression of BRCA1 by aberrant cytosine methylation, histone hypoacetylation and chromatin condensation of the BRCA1 promoter. *Nucleic Acids Res*. 28:3233-9.
- Richard, J.P., K. Melikov, E. Vives, C. Ramos, B. Verbeure, M.J. Gait, L.V. Chernomordik, and B. Lebleu. 2003. Cell-penetrating peptides. A reevaluation of the mechanism of cellular uptake. *J Biol Chem*. 278:585-90.
- Richards, E.J., and S.C. Elgin. 2002. Epigenetic codes for heterochromatin formation and silencing: rounding up the usual suspects. *Cell*. 108:489-500.

- Roberge, M. 1992. Checkpoint controls that couple mitosis to completion of DNA replication. *Trends Cell Biol.* 2:277-281.
- Robertson, K.D., S. Ait-Si-Ali, T. Yokochi, P.A. Wade, P.L. Jones, and A.P. Wolffe. 2000. DNMT1 forms a complex with Rb, E2F1 and HDAC1 and represses transcription from E2F-responsive promoters. *Nat Genet.* 25:338-42.
- Robinson, P.J., L. Fairall, V.A. Huynh, and D. Rhodes. 2006. EM measurements define the dimensions of the "30-nm" chromatin fiber: evidence for a compact, interdigitated structure. *Proc Natl Acad Sci U S A.* 103:6506-11.
- Rydberg, B., W.R. Holley, I.S. Mian, and A. Chatterjee. 1998. Chromatin conformation in living cells: support for a zig-zag model of the 30 nm chromatin fiber. *J Mol Biol.* 284:71-84.
- Sadoni, N., K.F. Sullivan, P. Weinzierl, E.H. Stelzer, and D. Zink. 2001. Large-scale chromatin fibers of living cells display a discontinuous functional organization. *Chromosoma.* 110:39-51.
- Scheer, U., and R. Hock. 1999. Structure and function of the nucleolus. *Curr Opin Cell Biol.* 11:385-90.
- Scheer, U., B. Xia, H. Merkert, and D. Weisenberger. 1997. Looking at Christmas trees in the nucleolus. *Chromosoma.* 105:470-80.
- Schmiedeberg, L., K. Weissart, S. Diekmann, G. Meyer Zu Hoerste, and P. Hemmerich. 2004. High- and low-mobility populations of HP1 in heterochromatin of mammalian cells. *Mol Biol Cell.* 15:2819-33.
- Schneider, R., and R. Grosschedl. 2007. Dynamics and interplay of nuclear architecture, genome organization, and gene expression. *Genes Dev.* 21:3027-43.
- Schotta, G., M. Lachner, K. Sarma, A. Ebert, R. Sengupta, G. Reuter, D. Reinberg, and T. Jenuwein. 2004. A silencing pathway to induce H3-K9 and H4-K20 trimethylation at constitutive heterochromatin. *Genes Dev.* 18:1251-62.
- Segil, N., S.B. Roberts, and N. Heintz. 1991. Mitotic phosphorylation of the Oct-1 homeodomain and regulation of Oct-1 DNA binding activity. *Science.* 254:1814-6.
- Seksek, O., J. Biwersi, and A.S. Verkman. 1997. Translational diffusion of macromolecule-sized solutes in cytoplasm and nucleus. *J Cell Biol.* 138:131-42.
- Shahbazian, M.D., and M. Grunstein. 2007. Functions of site-specific histone acetylation and deacetylation. *Annu Rev Biochem.* 76:75-100.
- Shao, L., B. Isaac, S. Uzawa, D.A. Agard, J.W. Sedat, and M.G. Gustafsson. 2008. 15S: Widefield Light Microscopy with 100-nm-scale Resolution in Three Dimensions. *Biophys J.*
- Shav-Tal, Y., J. Blechman, X. Darzacq, C. Montagna, B.T. Dye, J.G. Patton, R.H. Singer, and D. Zipori. 2005. Dynamic sorting of nuclear components into distinct nucleolar caps during transcriptional inhibition. *Mol Biol Cell.* 16:2395-413.
- Shav-Tal, Y., X. Darzacq, S.M. Shenoy, D. Fusco, S.M. Janicki, D.L. Spector, and R.H. Singer. 2004. Dynamics of single mRNPs in nuclei of living cells. *Science.* 304:1797-800.
- Singh, P.B., and S.D. Georgatos. 2002. HP1: facts, open questions, and speculation. *J Struct Biol.* 140:10-6.
- Sleeman, J., C.E. Lyon, M. Platani, J.P. Kreivi, and A.I. Lamond. 1998. Dynamic interactions between splicing snRNPs, coiled bodies and nucleoli revealed using snRNP protein fusions to the green fluorescent protein. *Exp Cell Res.* 243:290-304.
- Smallwood, A., P.O. Esteve, S. Pradhan, and M. Carey. 2007. Functional cooperation between HP1 and DNMT1 mediates gene silencing. *Genes Dev.* 21:1169-78.
- Spector, D.L. 2001. Nuclear domains. *J Cell Sci.* 114:2891-3.
- Spector, D.L. 2006. SnapShot: Cellular bodies. *Cell.* 127:1071.
- Sporbert, A., A. Gahl, R. Ankerhold, H. Leonhardt, and M.C. Cardoso. 2002. DNA polymerase clamp shows little turnover at established replication sites but sequential de novo assembly at adjacent origin clusters. *Mol Cell.* 10:1355-65.
- Stein, R., Y. Gruenbaum, Y. Pollack, A. Razin, and H. Cedar. 1982. Clonal inheritance of the pattern of DNA methylation in mouse cells. *Proc Natl Acad Sci U S A.* 79:61-65.

- Stern, S., T. Dror, E. Stolovicki, N. Brenner, and E. Braun. 2007. Genome-wide transcriptional plasticity underlies cellular adaptation to novel challenge. *Mol Syst Biol.* 3:106.
- Stoffler, D., B. Feja, B. Fahrenkrog, J. Walz, D. Typke, and U. Aepli. 2003. Cryo-electron tomography provides novel insights into nuclear pore architecture: implications for nucleocytoplasmic transport. *J Mol Biol.* 328:119-30.
- Strick, R., P.L. Strissel, K. Gavrilov, and R. Levi-Setti. 2001. Cation-chromatin binding as shown by ion microscopy is essential for the structural integrity of chromosomes. *J Cell Biol.* 155:899-910.
- Struhl, K. 2007. Transcriptional noise and the fidelity of initiation by RNA polymerase II. *Nat Struct Mol Biol.* 14:103-5.
- Sun, J.M., Z. Ali, R. Lurz, and A. Ruiz-Carrillo. 1990. Replacement of histone H1 by H5 in vivo does not change the nucleosome repeat length of chromatin but increases its stability. *Embo J.* 9:1651-8.
- Sutherland, H.G., G.K. Mumford, K. Newton, L.V. Ford, R. Farrall, G. Dellaire, J.F. Caceres, and W.A. Bickmore. 2001. Large-scale identification of mammalian proteins localized to nuclear sub-compartments. *Hum Mol Genet.* 10:1995-2011.
- Taddei, A., C. Maison, D. Roche, and G. Almouzni. 2001. Reversible disruption of pericentric heterochromatin and centromere function by inhibiting deacetylases. *Nat Cell Biol.* 3:114-20.
- Taddei, A., D. Roche, J.B. Sibarita, B.M. Turner, and G. Almouzni. 1999. Duplication and maintenance of heterochromatin domains. *J Cell Biol.* 147:1153-66.
- Tanabe, H., F.A. Habermann, I. Solovei, M. Cremer, and T. Cremer. 2002. Non-random radial arrangements of interphase chromosome territories: evolutionary considerations and functional implications. *Mutat Res.* 504:37-45.
- Taverna, S.D., H. Li, A.J. Ruthenburg, C.D. Allis, and D.J. Patel. 2007. How chromatin-binding modules interpret histone modifications: lessons from professional pocket pickers. *Nat Struct Mol Biol.* 14:1025-40.
- Terranova, R., S. Sauer, M. Merkenschlager, and A.G. Fisher. 2005. The reorganisation of constitutive heterochromatin in differentiating muscle requires HDAC activity. *Exp Cell Res.* 310:344-56.
- Thiry, M. 1992. New data concerning the functional organization of the mammalian cell nucleolus: detection of RNA and rRNA by in situ molecular immunocytochemistry. *Nucleic Acids Res.* 20:6195-200.
- Tremethick, D.J. 2007. Higher-order structures of chromatin: the elusive 30 nm fiber. *Cell.* 128:651-4.
- Tunnemann, G., R.M. Martin, S. Haupt, C. Patsch, F. Edenhofer, and M.C. Cardoso. 2006. Cargo-dependent mode of uptake and bioavailability of TAT-containing proteins and peptides in living cells. *Faseb J.* 20:1775-84.
- Tunnemann, G., G. Ter-Avetisyan, R.M. Martin, M. Stockl, A. Herrmann, and M.C. Cardoso. 2008. Live-cell analysis of cell penetration ability and toxicity of oligo-arginines. *J Pept Sci.* 14:469-76.
- Tyagi, M., M. Rusnati, M. Presta, and M. Giacca. 2001. Internalization of HIV-1 tat requires cell surface heparan sulfate proteoglycans. *J Biol Chem.* 276:3254-61.
- Varga-Weisz, P.D., M. Wilm, E. Bonte, K. Dumas, M. Mann, and P.B. Becker. 1997. Chromatin-remodelling factor CHRAC contains the ATPases ISWI and topoisomerase II. *Nature.* 388:598-602.
- Verkman, A.S. 2002. Solute and macromolecule diffusion in cellular aqueous compartments. *Trends Biochem Sci.* 27:27-33.
- Verreault, A., P.D. Kaufman, R. Kobayashi, and B. Stillman. 1996. Nucleosome assembly by a complex of CAF-1 and acetylated histones H3/H4. *Cell.* 87:95-104.
- Verschure, P.J., I. Van Der Kraan, E.M. Manders, D. Hoogstraten, A.B. Houtsmuller, and R. Van Driel. 2003. Condensed chromatin domains in the mammalian nucleus are accessible to large macromolecules. *EMBO Rep.* 4:861-866.
- Vives, E., J.P. Richard, C. Rispal, and B. Lebleu. 2003. TAT peptide internalization: seeking the mechanism of entry. *Curr Protein Pept Sci.* 4:125-32.
- Voliotis, M., N. Cohen, C. Molina-Paris, and T.B. Liverpool. 2008. Fluctuations, pauses, and backtracking in DNA transcription. *Biophys J.* 94:334-48.

- Wachsmuth, M., T. Weidemann, G. Muller, U.W. Hoffmann-Rohrer, T.A. Knoch, W. Waldeck, and J. Langowski. 2003. Analyzing intracellular binding and diffusion with continuous fluorescence photobleaching. *Biophys J.* 84:3353-63.
- Wadia, J.S., and S.F. Dowdy. 2002. Protein transduction technology. *Curr Opin Biotechnol.* 13:52-6.
- Weinert, T.A., G.L. Kiser, and L.H. Hartwell. 1994. Mitotic checkpoint genes in budding yeast and the dependence of mitosis on DNA replication and repair. *Genes Dev.* 8:652-665.
- Weisenberger, D., and U. Scheer. 1995. A possible mechanism for the inhibition of ribosomal RNA gene transcription during mitosis. *J Cell Biol.* 129:561-575.
- Wissmann, M., N. Yin, J.M. Muller, H. Greschik, B.D. Fodor, T. Jenuwein, C. Vogler, R. Schneider, T. Gunther, R. Buettner, E. Metzger, and R. Schule. 2007. Cooperative demethylation by JMJD2C and LSD1 promotes androgen receptor-dependent gene expression. *Nat Cell Biol.* 9:347-53.
- Woodcock, C.L., and S. Dimitrov. 2001. Higher-order structure of chromatin and chromosomes. *Curr Opin Genet Dev.* 11:130-5.
- Xin, H., H.G. Yoon, P.B. Singh, J. Wong, and J. Qin. 2003. Components of a pathway maintaining histone modification and HP1 binding at the pericentric heterochromatin in mammalian cells. *J Biol Chem.*
- Xu, E.Y., X. Bi, M.J. Holland, D.E. Gottschling, and J.R. Broach. 2005. Mutations in the nucleosome core enhance transcriptional silencing. *Mol Cell Biol.* 25:1846-59.
- Yu, F., J. Thiesen, and W.H. Stratling. 2000. Histone deacetylase-independent transcriptional repression by methyl-CpG-binding protein 2. *Nucleic Acids Res.* 28:2201-6.
- Yu, F.L. 1993. A hypothesis for chemical carcinogen induced chromatin condensation. *Carcinogenesis.* 14:1969-70.
- Zhang, Z., K. Shibahara, and B. Stillman. 2000. PCNA connects DNA replication to epigenetic inheritance in yeast. *Nature.* 408:221-5.

6 Annex

6.1 Abbreviations

5mC	-	5-methyl cytosine
CAF	-	chromatin assembly factor
CENP	-	centromere binding protein
CPP	-	cell penetrating peptide
DFC	-	dense fibrillar component
DNA	-	deoxyribonucleic acid
DRAQ5	-	deep red fluorescing anthraquinone Nr. 5
EM	-	electron microscopy
ESI	-	electron spectroscopic imaging
ER	-	endoplasmatic reticulum
FC	-	fibrillar center
FITC	-	fluorescein isothiocyanate
GC	-	granular component
GFP	-	green fluorescent protein
HIV	-	human immunodeficiency virus
HMGN	-	high-mobility group nucleosome binding protein
hnRNP	-	heterogeneous nuclear ribonucleoprotein particles
HP1	-	heterochromatin protein 1
mRFP	-	monovalent red fluorescent protein
mRNA	-	messenger RNA
MBD	-	methyl cytosine binding domain proteins
MeCP2	-	methyl cytosine binding protein 2
MW	-	molecular weight
NLS	-	nuclear localization sequence
TAT	-	HIV transactivator of transcription
PBD	-	PCNA binding domain
pc	-	phase contrast
PCNA	-	proliferating cell nuclear antigen
PI	-	propidium iodide
PML	-	promyelocytic leukemia
S	-	Swedberg sedimentation unit
SMT	-	single molecule tracking
UV	-	ultra violet

6.2 Publications

Martin, R. M., Leonhardt, H., and Cardoso, M. C. (2005). DNA labeling in living cells. *Cytometry A* 67, 45-52.

Walther W., Minow T., **Martin R.**, Fichtner I., Schlag P.M., Stein U. (2006). Uptake, biodistribution, and time course of naked plasmid DNA trafficking after intratumoral in vivo jet injection. *Human Gene Therapy* 17:1–14

Tunnemann, G., **Martin, R. M.**, Haupt, S., Patsch, C., Edenhofer, F., and Cardoso, M. C. (2006). Cargo-dependent mode of uptake and bioavailability of TAT-containing proteins and peptides in living cells. *FASEB J* 20, 1775-1784.

Martin, R. M., Tunnemann, G., Leonhardt, H., and Cardoso, M. C. (2007). Nucleolar marker for living cells. *Histochem Cell Biol* 127, 243-251.

Martin, R. M., Gorisch, S. M., Leonhardt, H., and Cardoso, M. C. (2007). An unexpected link between energy metabolism, calcium, chromatin condensation and cell cycle. *Cell Cycle* 6-19, 2422-24.

Tunnemann, G., Ter-Avetisyan, G., **Martin, R. M.**, Stockl, M., Herrmann, A., and Cardoso, M. C. (2007). Live-cell analysis of cell penetration ability and toxicity of oligo-arginines. *J Pept Sci.* 14:469-76.

Grunwald, D., **Martin, R. M.**, Buschmann, V., Bazett-Jones, D. P., Leonhardt, H., Kubitscheck, U., and Cardoso, M. C. (2008). Probing intranuclear environments at the single molecule level. *Biophys J.* 94:2847-58

Martin R.M., Cardoso M.C. (2008). Chromatin condensation modulates access and binding of nuclear proteins
Manuscript submitted at JMB

6.3 Conference contributions

- | | |
|-----------|---|
| Nov 2004 | Oral presentation at the Max-Delbrück-Center for Molecular Medicine (MDC) Cardiovascular Retreat, Gross Dölln |
| Sept 2005 | Oral presentation at the Max-Delbrück-Center for Molecular Medicine (MDC) & Leibniz-Institut für Molekulare Pharmakologie (FMP) PhD-Retreat, Strausberg |
| Nov 2005 | Oral presentation “DNA Labeling in Living Cells”, CenTech, Münster |
| Dec 2005 | Oral & poster presentation at Graduate biophysics program; Workshop on Cell Biology and Microscopy, Altleiningen |
| July 2006 | Poster presentation, International symposium “Optical analysis of biomolecular machines”, Berlin |
| Sept 2006 | Oral presentation at the Max-Delbrück-Center for Molecular Medicine (MDC) & Leibniz-Institut für Molekulare Pharmakologie (FMP) PhD-Retreat, Motzen |
| Dec 2006 | Poster presentation at “Chromatin structure and function” conference, Punta Cana, Dom. Rep. |
| Aug 2007 | Oral presentation at Wilhelm Bernhard Workshop on the Cell Nucleus, St. Andrews, UK |

6.4 Acknowledgments and declaration of own contributions

Acknowledgments

The projects of this thesis would not have been possible without the help of many people. Most of them are listed as coauthors in the publications above. Here I would like to express my grateful thanks especially to M. Cristina Cardoso for all the guidance and support over the years with enthusiasm and patience in scientific working as well as for fruitful and inspiring discussions. Together with Cristina I have to thank here Heinrich Leonhardt for the supervision of the thesis in all steps and his help and support during all the experimental work and preparation of figures and manuscripts. Both of them as single persons and as a team have encouraged me to appreciate and invest in my work and enjoy all about science.

The nice atmosphere in the Cardoso Lab has encouraged me to a motivated work and in this way I wanted to thank and appreciate all former and present members of this lab. Some of them I wanted to mention explicitly for their support in the daily live in the lab, namely the irreplaceable Petra, Marion and Ingrid. I also thank Anje for introducing me to confocal microscopy and being there in case of problems, questions and discussions.

Special thanks I owe to the people I have worked with in close collaboration during the different projects. First of all it is David Grünwald whom I thank for the excellent cooperation, very inspiring discussions and making my visits in Münster a delight. I would like to thank Volker Buschmann for his advice and cooperation as a colleague while joining the Cardoso Lab and beyond for nice times outside of the lab. I greatly appreciate the team in Munich and especially Kourosh and Oliver for creating a cheerful and pleasant atmosphere during the 'Illuminati' meetings as well as in workshops and meetings

Finally I would like to thank my Family who accompanied me in all the years with support, help and patience in all aspects of live. Additional thanks go out to Lars and Olaf for having nice times and support on hard days, the exchange of ideas and just being real friends.

*Declaration of contributions:**Chapter 3.1 DNA labeling in living cells*

This project was started already 2002 during my diploma thesis in the group of M. Cristina Cardoso at the Max-Delbrück-Center in Berlin, Germany. The comparison of DNA dyes in Fig. 1 and the linescan analysis of DRAQ5 with histone GFP labeled chromatin in Fig. 2 are part of the Diploma thesis. All following experiments were performed, designed, analyzed and evaluated by me, except for FACS experiments at the core facility at the MDC-Berlin, performed by Hans-Peter Rahn. The manuscript including the figures was written and designed by me with the help and advice of M. Cristina Cardoso and Heinrich Leonhardt.

Chapter 3.2 Nucleolar marker for living cells

The project to develop and use cell penetrating peptides as nucleolar marker for living cells was initiated by me. The experiments for this project were designed, performed and analyzed by me, excluding the uptake of the nucleolar marker into live rat cardiomyocytes performed by Gisela Tünnemann. The manuscript was written and prepared by me with the helpful advice of M. Cristina Cardoso and proofreading by G. Tünnemann.

Chapter 3.3 Cargo-dependent mode of uptake and bioavailability of TAT-containing proteins and peptides in living cells.

For this project I performed together with Gisela Tünnemann the cell cycle progression assay and contributed with the design and performance of the FRAP and transduction experiments. Simone Haupt, Cristoph Patsch and Frank Edenhofer provided the reporter cell line (3T3-FDR1.2 cells) and fluorescently labeled TAT-Cre protein as well as performed the respective experiments. The manuscript and figures were prepared by Gisela Tünnemann and me, supported by M. Cristina Cardoso with scientific advice and discussion of the results.

Chapter 3.4 Live cell analysis of cell penetration ability and toxicity of oligo-arginines

This project was initiated by M. Cristina Cardoso, Gisela Tünnemann and me after discussing our results on cell penetrating peptides and the nucleolar marker. Gohar Ter-Avetisyan performed, evaluated and illustrated all transduction experiments. I supported the initial experiments with supervision and help during the performance and contributed unpublished experimental data. Martin Stöckl analyzed the transduction frequency of NBD-labeled peptides in large unilamellar vesicles (LUV) by spectrophotometry. Andreas Herrman provided expertise and equipment for the LUV experiments and M. Cristina Cardoso accompanied all stages of the experimental part and the manuscript preparation with scientific and practical advice. Gisela Tünnemann performed evaluated and illustrated experiments in Fig. 2/ Fig. 3. and wrote the manuscript. My part during the manuscript preparation was the help in analyzing and displaying the data, preparing the supplementary movie and scientific proofreading of the manuscript.

Chapter 3.5 An unexpected link between energy metabolism, calcium, chromatin condensation and cell cycle

The concept of the project layout was done together with M. Cristina Cardoso and Sabine M. Görisch. The experiments were designed and performed by me, including the data analysis. Further I wrote the paper manuscript and prepared the figures with supportive advice and fruitful discussions with M. Cristina Cardoso and Heinrich Leonhardt. Tony J. Collins (McMaster University, Hamilton, Canada) made helpful comments on the manuscript.

Chapter 3.6 Chromatin condensation modulates access and binding of nuclear proteins

All experiments in this manuscript were developed, performed and analyzed by me including the writing of the manuscript and preparation of the figures with support by M. Cristina Cardoso.

Chapter 3.7 Probing intranuclear environments at the single molecule level.

My contribution to this project was the design and performance of the experimental live cell work together with David Grünwald, who has built the single molecule microscope setup.

In addition my part was the design and performance of the FRAP and FLIP control experiments as well as the testing of plasmid constructs, microinjection and confocal microscopy localization studies. The evaluation of the FRAP and FLIP experiments was supported by Volker Buschmann, who also contributed importantly to the analysis of the single molecule data. During the work for the manuscript my part was the preparation of figures, contribution to the text, discussion of the results and editing of the final manuscript with the help and advice of M. Cristina Cardoso.

Declaration according to the "Promotionsordnung der LMU München für die Fakultät Biologie"

Betreuung: Hiermit erkläre ich, dass die vorgelegte Arbeit an der LMU von Herrn Prof. Dr. Heinrich Leonhardt betreut wurde.

Anfertigung: Hiermit versichere ich ehrenwörtlich, dass die Dissertation von mir selbstständig und ohne unerlaubte Hilfsmittel angefertigt wurde. Über Beiträge, die im Rahmen der kumulativen Dissertation in Form von Manuskripten und Publikationen in der Dissertation enthalten sind, wurde im Kapitel 6.4 Rechenschaft abgelegt und die eigenen Leistungen wurden aufgelistet.

Prüfung: Hiermit erkläre ich, dass die Dissertation weder als ganzes noch in Teilen an einem anderen Ort einer Prüfungskommission vorgelegt wurde. Weiterhin habe ich weder an einem anderen Ort eine Promotion angestrebt oder angemeldet oder versucht eine Doktorprüfung abzulegen.

München, den _____

(Robert Martin)

6.5 Curriculum Vitæ

Personal details

Name: Martin
First names: Robert Manfred
Born: 06 October 1976 in Dresden, Germany

Contact information

E-mail: Robertmartin@freenet.de
Postal: Gruenberger Strasse 37, 10245 Berlin, Germany

Education

1996 Allgemeine Hochschulreife (grade 2.0)
Alexander von Humboldt Gymnasium
Eberswalde, Germany
1997 – 1999 Intermediate diploma biology
University of Rostock, Germany
1999 – 2003 Diploma in biology (grade 1.4)
Humboldt University Berlin, Germany
2003 – 2008 PhD student in biology
Max-Delbrueck-Center for Molecular Medicine, Berlin
Ludwig Maximilians University, Munich

Positions

2002 Student assistant in the group of Prof. H. Leonhardt
2006 Co-supervision of the project study of Franziska Witzel

Additional skills

Languages: German (native)
English (fluently spoken & written)
Russian

7 Index of electronic supplementary material CD

1-Dissertation PDF: Mobility and distribution of proteins in the nucleus of living cells

2-Figures in this thesis

- ↳ Cover Figure
- ↳ Fig 1
- ↳ Fig 2
- ↳ Fig 3
- ↳ Fig 4
- ↳ Fig 5
- ↳ Fig 6
- ↳ Fig 7
- ↳ Fig 8

3-Publication PDF & online supplementary material

- ↳ **3-1** DNA labeling in living cells
- ↳ **3-2** Nucleolar marker for living cells
 - ↳ Fig S1 *The nucleolar marker is not removed by fixation*
 - ↳ Movie 1 *Kinetics of FITC-R10 uptake into living C2C12 cells*
- ↳ **3-3** Cargo-dependent mode of uptake and bioavailability of TAT-containing proteins and peptides in living cells
- ↳ **3-4** Live-cell analysis of cell penetration ability and toxicity of oligo-arginines
 - ↳ Cover Figure
 - ↳ Fig S1 *Penetration of artificial membranes by oligo-arginines*
 - ↳ Movie 1 *Simultaneous uptake of D- and L-R9 into live cells*
- ↳ **3-5** An unexpected link between energy metabolism, calcium, chromatin condensation and cell cycle
 - ↳ Cover Figure
 - ↳ Fig S1 *Effect of different cations combined with digitonin permeabilization on chromatin condensation*
 - ↳ Fig S2 *Extracellular calcium influx triggered by ionomycin causes chromatin condensation.*
 - ↳ Fig S3 *NaN₃ induces chromatin condensation independent of extracellular calcium.*
- ↳ **3-6** Probing intranuclear environments at the single molecule level
 - ↳ Cover Figure
 - ↳ Movie 1 *Probing mammalian nuclear compartments with single streptavidin molecules.*
 - ↳ Tab S1 *Quantitative analysis of the nuclear distribution of NLS-SAv-Cy5.*
 - ↳ Fig S1 *Steady state distribution of NLS-SAv-Cy5 complexes in nuclear subcompartments.*
 - ↳ Fig S2 *NLS-SAv-Cy5 complexes do not form aggregates and are completely mobile within the nucleus and cytoplasm.*
 - ↳ Fig S3 *Temporal stability of trapping sites in the nucleoplasm.*
 - ↳ Fig S4 *Streptavidin can cross compartment borders without hindrance.*
- ↳ **3-7** Chromatin condensation modulates access and binding of nuclear proteins
 - ↳ Fig S1 *Effect of chromatin condensation state on accessibility of nucleoplasmic proteins of different size*